REGULATORY ROLE OF p38γ AND p38δ IN INFLAMMATION AND CARDIOVASCULAR SYSTEM IN HOMEOSTASIS AND DISEASE

BÁRBARA GONZÁLEZ TERÁN

INTERNATIONAL THESIS

Madrid, 2016

UNIVERSIDAD AUTÓNOMA DE MADRID

DEPARTAMENTO DE BIOQUÍMICA

UNIVERSIDAD AUTÓNOMA DE MADRID

DEPARTAMENTO DE BIOQUÍMICA

Tesis Doctoral

REGULATORY ROLE OF p38γ AND p38δ IN INFLAMMATION AND CARDIOVASCULAR SYSTEM IN HOMEOSTASIS AND DISEASE

BÁRBARA GONZÁLEZ TERÁN ©

Madrid, 2016

UNIVERSIDAD AUTÓNOMA DE MADRID-UAM

DEPARTAMENTO DE BIOQUÍMICA

FACULTAD DE MEDICINA

REGULATORY ROLE OF p38γ AND p38δ IN INFLAMMATION AND CARDIOVASCULAR SYSTEM IN HOMEOSTASIS AND DISEASE

Tesis doctoral presentada por:

Bárbara González Terán

Licenciada en Biología por la Universidad Complutense de Madrid (UCM)

Máster en Biomedicina Molecular por la Universidad Autónoma de Madrid (UAM)

Bajo la dirección de la Doctora:

Guadalupe Sabio Buzo

GRUPO DE PAPEL DE QUINASAS ACTIVADAS POR ESTRÉS

CENTRO NACIONAL DE INVESTIGACIONES CARDIOVASCULARES (CNIC)

UT Southwestern Medical Center

Eric N. Olson, Ph.D.
Professor and Chair
Department of Molecular Biology
The Robert A. Welch Distinguished Chair in Science
Annie and Willie Nelson Professorship in Stem Cell Research
Pogue Distinguished Chair in Research on Cardiac Birth Defects

Director
Hamon Center for Regenerative Science and Medicine

April 25, 2016

Greetings:

I have read the Doctoral Thesis of Dr. Barbara Gonzalez Teran entitled "Regulatory Role of p38γ and p38δ in Inflammation and Cardiovascular System in Homeostasis and Disease". This is an extremely comprehensive and impressive body of work that will guide the field for many years to come. Indeed, I have rarely, if ever, seen a PhD thesis that resulted in such a large number of major publications in top tier journals.

Dr. Teran's discovery of the signal transductions systems involved in pathological cardiac remodeling as well as signaling from the heart to the liver to control metabolism are truly ground-breaking.

Dr. Teran's thesis represents a unique and visionary contribution to the field. I am pleased to offer my strong support for her graduation.

Sincerely

Location: 6000 Harry Hines Blvd., Dallas, Texas 75390-9148 Ph: (214) 648-1187 Eric.Olson@utsouthwestern.edu

hhmi | Howard Hughes Medical Institute

April 22, 2016

Dear Sir or Madam:

I have read Bárbara Gonzalez-Teran's Doctoral Thesis entitled "Regulatory Role of p38gamma and delta in inflammation and cardiovascular system in homeostasis and disease" and I believe this research study on stress kinase signalling is very interesting.

Activation of p38 MAPK pathway helps the cell to respond to the stimuli. Thus, it is an important regulator of several cell functions. There are 4 different isoforms of p38s kinases, p38α and p38β that have been well studied and the alternatives p38s, p38γ and p38δ, whose function was almost completely unknown. With this work Bárbara has made several contributions to the field.

Bárbara has studied the role of p38γ and p38δ in inflammation using a model of LPS-induced hepatitis. She has shown for the first time that these kinases are potential therapeutic targets for the treatment of liver diseases with a great inflammatory component. This work has been published in *JCI*.

She also evaluated the role of p38γ and p38δ in the development of liver steatosis and insulin resistance. In her thesis, Bárbara shows that p38γ and p38δ in neutrophils play a key role in the development of steatohepatitis. This worked was published in *EMBO J*.

To evaluate the role of p38γ and p38δ in hearth growth, she has used total and conditional mice as well as adeno-associated virus that overexpress the active form of these kinases specifically in the cardiomyocytes. She has demonstrated that p38γ and p38δ are essential in cardiomyocytes for a normal cardiac hypertrophic growth during postnatal development. These kinases control cardiac hypertrophy through the phosphorylation of the mTOR inhibitory protein, DEPTOR, which induces its degradation and the activation of the mTOR pathway. Likewise, the lack of these kinases protects against cardiac overload induced hypertrophy with normal systolic function, indicating that p38γ and p38δ are possible targets for the treatment of cardiac hypertrophy. This work has been published in *Nature Communications*.

Finally, she describes how MKK3 and MKK6 regulate the different p38s in cardiomyocytes and how this regulation could affect cardiac growth. This study is not published, but it is expected to reach the same quality of journal as the previous articles.

In summary, she described that these kinases are involved in several physiological processes. The function of these alternative p38 isoforms was uncertain and this thesis elucidates some of the functions of these signalling pathways - opening a new research area. This is an outstanding research thesis.

Sincerely

Roger J. Davis, Ph.D., F.R.S.
Investigator

University of Massachusetts Medical School
Program in Molecular Medicine
373 Plantation Street, Suite 309, Worcester, Massachusetts 01605
508.856.6054 • Fax 508.856.3210 • roger.davis@umassmed.edu

La presente Tesis Doctoral se realizó en el Centro Nacional de Investigaciones Cardiovasculares (CNIC) de Madrid entre los años 2011 y 2016 bajo la supervisión de la Dra. Guadalupe Sabio Buzo.

Las siguientes becas, ayudas y proyectos han permitido la realización de esta Tesis Doctoral:

- Beca CNIC-FPI Severo Ochoa (Convocatoria 2013) del Ministerio de Economía y Competitividad. Periodo 2014-2016. Ref: SVP-2013-067639.

- Beca Estancias Cortas FPI del Ministerio de Economía y Competitividad (Convocatoria 2014) para visitar el laboratorio de Eric Olson en UT Southwestern Medical Center, Dallas, Texas. Periodo Junio - Octubre 2015. Ref: EEBB-I-15-10000.

- EMBO Short Term Fellowship para visitar el laboratorio de Eric Olson en UT Southwestern Medical Center, Dallas, Texas. Periodo Octubre - Diciembre 2015. Ref: EMBO ASTF 558-2015.

- Proyecto (260464_OBECAN) ERC Starting Grant de la Comunidad Europea dirigido por la Dra. Guadalupe Sabio Buzo. Periodo 2011-2016.

A mis padres.

"No es el conocimiento, sino el acto de aprendizaje, y no la posesión,
sino el acto de llegar allí, que concede el mayor disfrute."

"It is not knowledge, but the act of learning, not possession
but the act of getting there, which grants the greatest enjoyment."

— Carl Friedrich Gauss.

ACKNOWLEDGEMENTS

Empiezo a escribir el último apartado de mi tesis y aún no puedo creer lo rápido que ha pasado el tiempo. Siento que fue ayer el día en el que entraba en el CNB por pimera vez desorientada, llena de ilusión pero al mismo tiempo nerviosa por conocer el laboratorio en el que iba a tener mi primera experiencia de investigación fuera de la universidad gracias a una beca de verano. Siempre quise dedicarme a la investigación, desde muy pequeñita. El primer recuerdo que tengo es de cuando tenía 10 años que cuando mis padres me preguntaban a dónde me gustaría ir de vacaciones les decía que quería ir al Polo a ver a los científicos. ¿Por qué exactamente al Polo? No lo tengo claro aún… Lo que sí que tenía muy claro y, como sabéis, soy de ideas bastante fijas, era que quería ser investigadora aunque en ese momento no supiese bien lo que aquello significaba. Muchos años han pasado llenos de ilusiones y decepciones, grandes esfuerzos, muchas personas y grandes amigos, torbellinos de sensaciones, cientos de experimentos fallidos y algunos exitosos, años llenos de vivencias durante los que he sido muy feliz. Hasta hoy, que aquí estoy, escribiendo estas ultima páginas, un pasito más cerca de alcanzar mis sueños.

Es muy dificil de transmitir en un par de páginas el agradecimiento que siento hacia toda la gente que me ha acompañado en este camino de maduración personal y profesional, y que han contribuido en mayor o menor parte a formarme, a convertirme en lo que soy hoy en día.

En primer lugar quiero dar las gracias a **Guadalupe** por creer en mí cuando aún ni había terminado la universidad y haberme adoptado como tu primera estudiante. Por transmitirme tu pasión por el laboratorio e invertir desinteresadamente un sifín de horas en enseñarme a pensar y razonar de forma científca. Gracias por valorar mis opiniones y apoyarme en mis decisiones. Te estaré eternamente agradecida.

Mi primera experiencia en un laboratorio fuera de la uni fue bajo la tutela de **Ana Cuenda** en el CNB. Gracias por ofrecerme la oportunidad de conocer cómo es la ciencia fuera de la universidad. Gracias también por haberme puesto a trabajar junto a Guadalupe, y por tu apoyo todos estos años. Así mismo, agradecer al resto del grupo, en su mayoría extremeño, que acogió a esta madrileña con tanto cariño y me enseñó tantas cosas. **Maribel**, **Paloma**, **Ana** y **Fran**, gracias por transmitirme la energía positiva que me reafirmó en mi idea de dedicarme a la ciencia.

Otro grupo de gente muy importante para mí en estos 5 últimos años, son mis compañeros de laboratorio: **Elisa**, **Luis**, **Edgar**, **Valle**, **Toñi**, **Nuria**, **Ivana**, **Victor**, **Leti** y **Elena**. Con los que he compartido más tiempo que con ningún otro, nos hemos apoyado en los momentos difíciles y celebrado los momentos buenos, hemos aprendido los unos de los otros y crecido juntos como personas y como científicos.

Mi estancia en Dallas ha sido otro perido corto de mi vida, de tan sólo 6 meses, pero muy intenso. En el que he conocido gente que me ha marcado para siempre, muy buenos amigos y mentores, de los que de cada uno me he llevado un trocito conmigo.

I cannot start without thanking the person who gave me the oportunity to visit "The Best Lab of the World", as he calls it, and to have such an amazing experience. Thank you **Dr. Eric Olson** for making me feel as a member of your lab from the very begining, for your time, guideness and mentorship. In your lab I learned that science is all about passion and hard work, but also the importance of a happy and unified group. Now I know how I would like to manage my lab if one day I have the oportunity. Thanks for making it happen. Thanks also to **Rhonda**, because she was the person who made fit all the pieces of the puzzle to make it work.

To all the people from **Eric Olson lab**, who were my international big family in Dallas. Because y'all took care of me from the first day, you help me to survive in Texas without a car, allways willing to help me. Thanks for all the late nights in the lab, the long conversations about science and about things that are not scientific at all, the Happy Hours, the pool parties, the "Buenos dias" in the mornings… Thank you for being as you are, please do not ever change. Thanks especially to all the people in the "Fun Room", my room, for making me feel at home.

A **mis padres**, porque me habéis ofrecido una vida llena de posibilidades, siempre me habéis apoyado incondicionalmente y guiado en las decisiones más complicadas para ayudarme a conseguir mis objetivos. Mis logros siempre serán vuestros logros. **A mi padre**, por ser un ejemplo de que con pasión y esfuerzo uno puede dedicarse y vivir de lo que más le gusta y por inculcarme que en todo lo que haga debo ser la mejor versión de mí misma. **A mi madre**, que desde muy pequeña me enseñó a no desistir y seguir andando en la dirección elegida a pesar de estar cansada, a que granito a granito uno puedo construir una montaña del tamaño que quiera. Ahora ya sé que eso es la perseverancia y que es una de las cualidades más útiles en la vida. A ambos os debo el

respeto y la curiosidad por lo desconocido, así como el amor por viajar, cuyas bases las fundaron todos esos viajes que hemos hecho a distintas partes del mundo desde muy pequeños. Gracias de corazón por lo que me habéis enseñado y lo que me enseñaréis.

A **mi hermano**, compañero de expediciones, peleas, gamberradas y demás chiquilladas. Por quererme, aguantarme y cuidarme todos estos años.

A **Samu**, por ser mi pilar de apoyo, mi fuente de equilibrio y desconexión. Porque siempre me haces reir cuando más lo necesito y me comprendes cuanto estoy estresada y de mal humor. Gracias por todos esos días que me has traido o recogido del laboratorio incluyendo fines de semana o altas horas de la madrugada. Admiro el gran esfuerzo que haces para enterder mis proyectos, incluso para darme ideas y enseñarme a explicarlos de forma menos técnica. Te agradezco muchísimo que me apoyases con mi estancia en Dallas a pesar de que fuese una situación difícil y dura para ambos. Gracias por creer en lo que hago y por esar dispuesto a dejarlo todo para intentar perseguir mis sueños, nuestros sueños. En resumen, gracias por hacerme feliz.

Finalmente agradecer al Ministerio de Economía y Competitividad y a EMBO por finarciar mi formación durante estos años y por promover el nacimiento de nuevas generaciones de científicos en nuesro país. Aunque sinceramente creo que hace falta ir más allá, y no ser tan sólo un país formador de gandres talentos, sino convertirnos en un país en el que sus garndes talentos y los de todo el mundo tengan cabida y un futuro por delante. Yo, al menos, lucharé por ello.

Gracias a todas aquellas personas que, de en un modo u otro, hayan formado parte de esta etapa tan bonita de mi vida.

Bárbara

RESUMEN/ABSTRACT

Las células reconocen y responden a estímulos extracelulares mediante la activación de diferentes procesos intracelulares como puden ser las cascadas de señalización que llevan a la activación de las proteinas quinasas activadas por mitógenos (MAPKs). Las células eucariotas tienen múltiples cascadas de señalización MAPKs involucradas en la regulación de diversos procesos celulares. En mamíferos se han descrito cinco subgrupos de MAPKs, ERK1/2, JNK, p38 and ERK5. Esta tesis se centra en las p38 MAPKs, también conocidas como proteínas quinasas activadas por estrés (SAPKs) junto a las JNK puesto que son activadas por estímulos de estrés. Esta subfamilia comprende 4 isoformas de p38: p38α, p38β, p38γ y p38δ. Debido a la disponibilidad de inhibidores específicos y de modelos de ratón deficientes para p38α y p38β, la función de estas dos isoformas ha sido ampliamente estudiada. Sin embargo, se conoce mucho menos sobre las implicaciones fisiológicas de p38γ y p38δ.

El objetivo principal de este trabajo es ampliar el conocimiento actual sobre las funciones de las proteínas quinasa p38γ y p38δ en homeostasis y en el desarrollo de enfermedades inflamatorias y cardiovasculares. Para ello se emplearon modelos de ratón deficientes en las quinasas en todo el organismo y modelos condicionales de tejido. En combinación, se emplearon técnicas básicas bioquímicas y estudios *in vitro*, para poder dilucidar los mecanismos moleculares mediante los cuales p38γ y p38δ ejercen su función biológica. Nuestros estudios muestran que las distintas isoformas de p38 se regulan de forma diferente por las quinasas activadoras MKK3 y MKK6. Esta regulación diferencial es específica de tejido. Además, p38γ y p38δ presentan un patrón de expresión muy característico, diferente entre sí y que difiere completamente de la expresión ubicua que muestran las quinasas p38α y p38β. Aquí demostramos que p38γ y p38δ son esenciales para la regulación de la respuesta inflamatoria. Además, juegan un papel clave en el desarrollo de enfermedades hepáticas con un fuerte componente inflamatorio como son la hepatitis aguda o la esteatosis. En este contexto, p38γ y p38δ tienen papeles parcialmente redundantes, por lo que es necesaria la inhibición de ambas quinasas para prevenir el daño hepático. Asimismo, mostramos que p38γ y p38δ son fundamentales en el control del crecimiento cardiaco hipertrófico tanto fisiológico como patológico. En este caso, ambas quinasas interaccionan y cooperan en la regulación del crecimiento del corazón. Nuestros resultados indican que p38γ y p38δ son potenciales dianas terapéuticas para el tratamiento de enfermedades hepáticas e hipertrofia cardiaca.

Cells recognize and respond to extracellular stimuli by engaging different intracellular programs, such as the signaling cascade that leads to the activation of the mitogen activated protein kinases (MAPKs). All eukaryotic cells posses multiple MAPK pathways, which regulate a diverse array of cellular processes. In mammals four distinct subgroups have been described (1) extracellular signal-regulated kinases 1/2 (ERKs), (2) c-jun N-terminal or stress-activated protein kinases (JNK/SAPK), (3) the p38 group of protein kinases and (4) ERK5. The focus of this thesis is the p38 kinases, also called stress-activated protein kinases (SAPKs) together with the JNKs, because are activated by environmental and genotoxic stresses. This subfamily comprises four different p38 isoforms: p38α, p38β, p38γ and p38δ. Due to the availability of specific inhibitors and animal models for p38α and p38β, the role of these two kinases has been broadly studied. However, much less is known about the physiological implications of p38γ and p38δ.

The main objective of this thesis is to broaden our knowledge about the functions of p38γ and p38δ, also called alternative p38s, in homeostasis and disease, taking advantage of full knockout or conditional knockout mice for these kinases. Besides, to better understand their biological implications at the molecular level we used *in vitro* models and basic biochemistry. Our data shows that the p38 MAPK isoforms are differentially regulated by their up-stream kinases, MKK3 and MKK6 in a tissue-specific manner. Besides, the p38γ and p38δ isoforms have very distinctive expression patterns in comparison with the ubiquitous expression of p38α and p38β, which suggests highly specialized cellular functions for these p38 isoforms. We demonstrate that p38γ and p38δ are essential in the regulation of inflammatory responses and key players in the development of liver inflammatory-mediated diseases such as acute hepatitis and steatosis. In these contexts, they play partially redundant roles, and the inhibition of both kinases is necessary to protect against the disease progression. Moreover, p38γ and p38δ are also involved in the control of cardiac growth and in the development of cardiomyopathies. We have shown that their expression and activation in the heart are developmentally upregulated during early postnatal stages of cardiac development. Besides, we report for the first time that p38γ and p38δ interact and cooperate in the regulation of both physiological and pathological cardiac hypertrophic growth. Our findings indicate that p38γ and p38δ are potential targets for the treatment of liver inflammatory-mediated diseases and cardiac hypertrophy.

INDEX

ABBREVIATIONS

ALI: Acute lung injury

ANG-II: Angiotensin- II

ANP: Atrial natriuteric peptide

ARDS: Acute respiratory distress syndrome

ATF: Activating transcription factor

ATP: Adenosine triphosphate

BNP: Brain natriuteric peptide

CFLAR: CASP8 and FADD-Like Apoptosis Regulator

CMGC: including CDK, MAPK, GSK3 and CLK families

Co-IP: Co-Immunoprecipitation

COPS: Chronic obstructive pulmonary syndrome

COX: Cyclooxygenase

CREB: cAMP response element-binding

DMEM: Dulbecco's Modified Eagle's Medium

DNA: Deoxyribonucleic acid

DUSP: Dual specificity phosphatase

ECG: Electrocardiogram

eEF2K: Eukaryotic elongation factor 2 kinase

EF: Ejection Fraction

EGFR: Epidermal growth factor receptor

eIF4: Eukaryotic initiation factor 4

ePK: Eukaryotic protein kinase

ERK: Extracellular signal-regulated kinases

FGFR: Fibroblast growth factor receptor

FS: Fractional shortening

GLUT4: Glucose transporter 4

GTT: Glucose tolerance test

HEK-293: Human Embryonic Kidney 293 cells

H&E: Hematoxiline and eosine

HCM: Hypertrophic cardiomyopathy

HFD: High fat diet

HFF: High fat and fructose diet

HMGN: High Mobility Group Nucleosome-binding

IKK: IκB kinase

IL-1: Interleukin 1

IL-17: Interleukin 17

IL-6: Interleukin 6

INFγ: Interferon-gamma

IP: Immunoprecipitation

ITT: Insulin tolerance test

IVS: Inter-ventricular septum

JIP: JNK interacting protein

JNK: c-Jun N-terminal kinase

LPS: lipopolysaccharide

LV: Left ventricle

LVID: Left ventricle internal diameter

LVPW: Left ventricle posterior wall

MAPK: Mitogen-activated protein kinases

MAPKAPK: MAP Kinase Activated Protein Kinase

MCD: Methionine and choline deficient diet

MEF: Mouse embryonic fibroblasts

MEF2: Myocyte Enhancer Factor 2

MIP: Macrophage inflammatory protein

MKK: Mitogen-activated protein kinase kinase

MKP: Mitogen-activated protein kinase phosphatase

mRNA: Messenger ribonucleic acid

mTOR: Mammalian target of Rapamycin

NAFLD: Non-alcoholic liver disease

NES: Nuclear export signal

NLS: Nuclear localization signal

OA: Okadaic acid

PBS: Phosphate-buffered saline

PKA: Protein kinase A

PKC: Protein kinase C

PKD1: Protein kinase D1

PP2A: Protein phosphatase 2A

PP2C: Protein phosphatase 2C

PTEN: Phosphatase and tensin homolog

PTP: Protein-tyrosine phosphatase

RA: Reumatoid Arthritis

RNA: Ribonucleic acid

RPS6KA: Ribosomal protein S6 kinase alpha

SAPK: Stress-activated protein kinase

STAT: Signal transducer and activator of transcription

TAB: TAK1-binding p Trotein 1

TAC: Transverse aortic constriction

TAK: Transforming Growth Factor-Beta-Activated Kinase 1

TGFβ: Transforming Growth Factor-Beta

TNF: Tumor necrosis factor

TPA: 12-O-Tetradecanoylphorbol-13-Acetate

TPL2: Tumor progression locus 2

TSC1/2: Tuberous Sclerosis 1/2

VCAM: Vascular Cell Adhesion Molecule

WGA: Wheat-germ agglutinin

INTRODUCTION

1. General aspects of cell communication

Cells need to perceive and correctly respond to the continuous changes that occur in the physical and chemical properties of the surrounding environment to survive. Therefore, cells do not live in isolation and are continuously communicating with its environment and with itself. Besides, cells can also communicate directly with one another and change their own internal machinery in response by way of a variety of chemical and mechanical signals.

Cell signaling is part of a complex system of communication that governs basic cellular activities and coordinates cell actions. [22]. A proper cellular communication is the basis of development, tissue repair, and immunity as well as normal tissue homeostasis. Errors in cellular information processing are responsible for diseases such as cancer, autoimmunity, and cardiovascular diseases [153, 167, 168]. Understanding of cell signaling will help to the treatment of diseases.

1.1 Cell Signaling

Cell signaling (or signal transduction) involves the detection of a stimulus that can be soluble factors generated locally (for example, synaptic transmission) or distantly (hormones or growth factors), ligands present on the surface of another cell, a molecule present in the surrounding environment or mechanical forces [118]. To achieve this, cells maintain a diversity of receptors on their surface that respond specifically to individual stimuli. These signals have been classically categorized based on the distance between signaling and responder cells. Signaling within, between, and among cells is subdivided into the following classifications [22]:

·*Intracrine* signals are produced by the target cell and stay within the target cell.

·*Autocrine* signals are produced by the target cell, are secreted, and affect the target cell itself via receptors.

·*Juxtacrine* is a cell contact-dependent signaling and therefore occurs in short distance. These signals are transmitted along cell membranes via protein or lipid components integral to the membrane and are capable of affecting either the emitting cell or cells immediately adjacent.

·*Paracrine* signaling molecules are released from paracrine cells and diffuse locally through the extracellular fluid, targeting cells that are nearby, thus acting as local mediators.

·*Endocrine* signaling involves sending a signal throughout the whole body by secreting hormones into the bloodstream. The cells that produce hormones are called endocrine cells.

Once the signaling molecule activates a specific receptor located on the cell surface or inside the cells, the signal transduction occurs, triggering a biochemical chain of events inside the cell to

create a cellular response. The signal can be amplified at any step. Thus, one single molecule can cause many responses.

There are different mechanistic principles that are used to initiate and transmit receptor-activated signals in the cytoplasm and down a signaling pathway. Every protein typically changes the conformation of the next down the path by post-translational modifications such as phosphorylation, ubiquitination, acetylation, SUMOylation, glycosylation, by calcium mobilization, lipid-derived second messengers, protein-protein interactions, Cyclic Nucleotides, and G proteins. The final effect is to trigger a cell response, such as the activation of gene transcription [48].

Protein phosphorylation and dephosphoylation by kinases or phosphatases, respectively, is the main regulatory mechanism through which protein activity is regulated in eukaryotic cells [29].

2. Protein kinases

Protein kinases are important players in almost every signaling pathway involved in normal development and disease. The transduction, amplification and integration of intracellular and intercellular processes need a specific regulation made, often, by protein phosphorylation [32].

It is predicted that vertebrate genome might encode as many as 1001 protein kinases, and that more than 30% of intracellular proteins can be phosphorylated at one or more residues. Protein phosphorylation not only regulates enzymatic activity through inducing conformational changes or through direct steric effects, but also modulates the function of structural proteins through conformational changes or charge effects. The different classes of protein kinases are classified by nature of the amino acid that is phosphorylated. The two mayor classes of protein kinases are the Serine/Threonine kinases and the Tyrosine kinases, but the phosphorylation in other amino acids has been described in prokaryotes and eukaryotes [18].

2.1 Serine/Threonine and tyrosine kinases

Most of the **eukaryotic protein kinases** belong to a superfamily of kinases. This superfamily comprises serine/threonine-, tyrosine-specific and dual specificity protein kinases that share a conserved catalytic domain. Ser/Thr kinases are found in all eukaryotes and function in a broad range of signaling pathways. Tyrosine kinases appear later in evolution and are predominately found in multicellular animals, were they play very important roles in intracellular signaling [76].

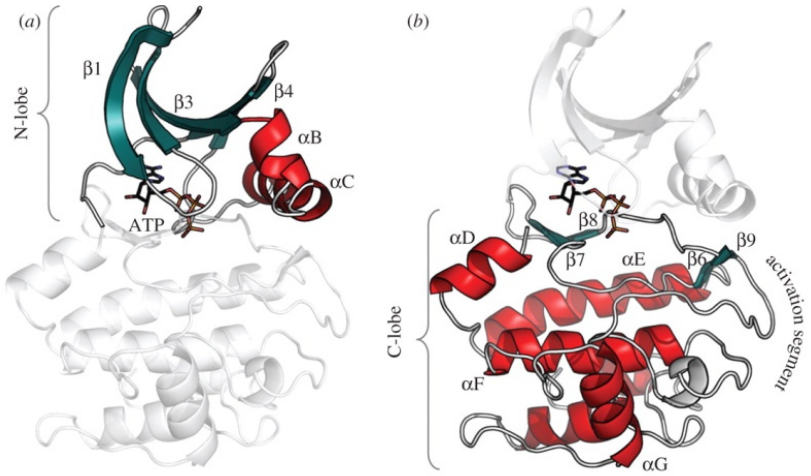

Figure 1. Conserved core of the eukaryotic protein kinases. Functional motifs in the N-lobe (*a*) and the C-lobe (*b*) using PKA as a prototype for the ePK family. Helices are shown in red; β-strands in teal. (*a*) The N-lobe contains five β -strands and a large αC-helix. (*b*) The C-lobe is mostly helical with a large activation segment. A four-stranded β-sheet rests on the helical core and forms one surface of the active site cleft. ATP is bound in the cleft between the two lobes [163]

Their catalytic domains consist of N-terminal and C-terminal lobes connected by a hinge. ATP binds the active site cleft between the lobes, forming critical contacts with residues and motifs that are conserved among kinases. The activation loop in the C-terminal lobe of the kinase forms contacts with the substrate. It is a flexible segment that can rearrange substantially and is often the location for regulatory phosphorylation [181]. The structure of Ser/Thr and Tyrosine kinases is very similar in the active state. In contrast, the mechanisms by which these kinases are inhibited are numerous, leading to different conformations in the inactive state [18]. Therefore, we could take advantage from these differences in inactivated kinase structure, to design specific small-molecule inhibitors of kinase function.

2.2 Atypical kinases

A much smaller number of protein kinases do not share this catalytic domain with other kinases, and are often collectively called **atypical kinases** [117]. In addition to Ser, Thr and Tyr, several other amino acids in proteins can be phosphorylated, including Lys, Arg and His, but in most cases remains unclear the provenance of the respective protein kinases.

Histidine Kinases phosphorylate themselves (autophosphorylate) on Histidine, before transferring that phosphate to an Aspartate on a substrate protein (so they are more correctly called Histidine-Aspartate Kinases). This type of protein kinases is common in prokaryotes and lower eukaryotes, but it was believed that regulatory histidine phosphorylation was of minor importance in vertebrates and that histidine kinases were not found in mammals [91, 157]. However, recent research provided evidence for a regulatory role of histidine phosphorylation in mammals with the identification of the ubiquitously expressed histidine kinase nucleoside

diphosphate kinase (NDPK) and its specific counteracting phosphatase (PHPT-1), what gives rise to the assumption that there is more to be detected [8].

A wide variety of other kinases phosphorylate various small molecules, including those involved in metabolism, such as glycolysis or nucleotide metabolism. These come from a wide variety of different structures, distinct from that of protein kinases. One notable exception is the phosphatidyl inositol 3' kinases (PI3K). These are structurally related to protein kinases, and a subset of PI3K, known as PIKK, do phosphorylate proteins rather than small molecules.

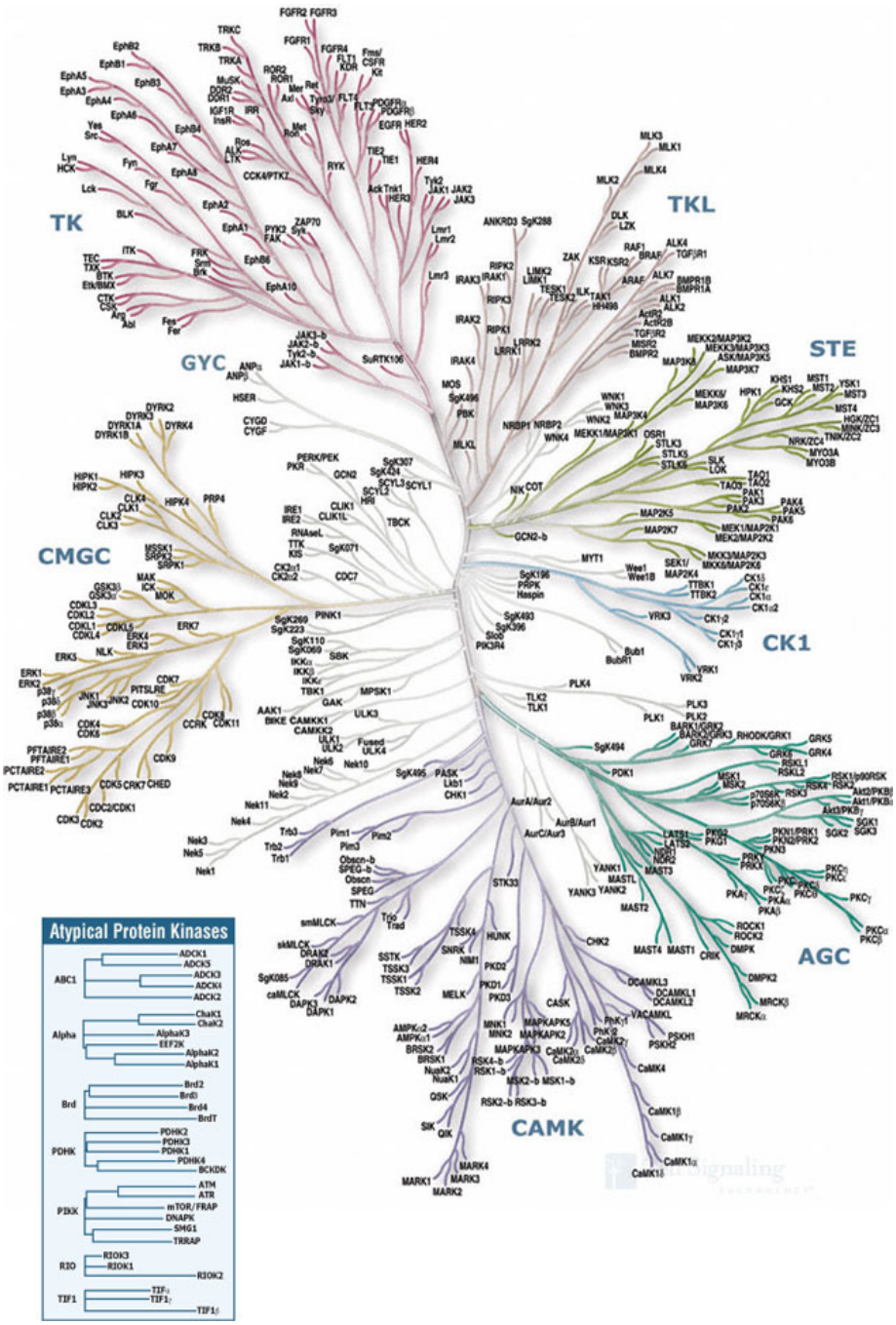

Figure 2. The Human Kinome. This phylogenetic tree depicts the relationships between members of the complete superfamily of human protein kinases. The inset diagram shows trees for seven atypical protein kinase families. (Courtesy of Cell Signaling Technology, Inc. (www.cellsignal.com))

3. The MAP Kinase Family

The Mitogen –activated protein kinases are Ser/Thr kinases that belong to the CMGC group (CDK, MAPK, GSK3, CLK group) within the Eukaryotic Protein Kinase Superfamily. The CMGC group also includes cyclin-dependent kinases (CDKs), glycogen synthase kinases (GSK) and CDK-like kinases [17].

MAPK cascades are evolutionarily conserved in all eukaryotes and play a key role in the regulation of a diverse array of cellular programs, participate extensively in the control of cell fate decisions such as proliferation, differentiation and death, as well as in the regulation of stress responses and inflammation in all eukaryotic phyla and in all tissues of metazoans [24, 183].

MAPK activity is regulated through three-tiered cascades composed of a MAPK, MAPK kinase (MAPKK, MKK or MEK) and a MAPKK kinase or MEK kinase (MAPKKK or MEKK) [6, 26, 36]. Transmission of signals is achieved by sequential phosphorylation and activation of the components specific to a respective cascade. The MAPKs are activated upon dual phosphorylation of tyrosine and threonine residues in a conserved Thr–Xaa–Tyr motif (where Xaa is any amino acid) in the activation loop of kinase subdomain VIII. Phosphorylation of MAPKs is catalyzed by the dual specificity kinases, MKKs, which are in turn activated upon phosphorylation of Ser/ Thr residues, and are highly selective in phosphorylating specific MAPKs. This specificity is in part conferred by the phosphorylation motif and by the interaction on the N-terminal region on the MKK with different docking sites on the MAPK. The activation of these kinases is tightly regulated by a group of MAPK phosphatases that return the MAPK into the inactive state by the phosphorylation [26, 144].

To date, four distinctly regulated groups of MAPKs have been described to be express in mammals, extracellular signal-related kinases (ERK)-1/2, Jun amino-terminal kinases (JNK1/2/3), p38 proteins (p38α/β/γ/δ) and ERK5. Each of these groups is activated by dual phosphorylation on their conserved motif in which Xaa is Glu in ERKs, Pro in JNKs and Gly in p38s. Besides, the different MAPK subfamilies are activated by specific MAPKKs; MEK1/2 for ERK1/2, MKK3/6 for the p38s, MKK4/7 (JNKK1/2) for the JNKs, and MEK5 for ERK5. Each MAPKK, however, can be activated by more than one MAPKKK, in a stimulus-dependent manner, increasing the complexity and diversity of MAPK signaling. Having in mind that *Saccharomyces Cerevisiae* possesses six different MAPKs, and the relative complexity of the human genome, its plausible thinking that there are probably several additional vertebrate MAPK subfamilies [142].

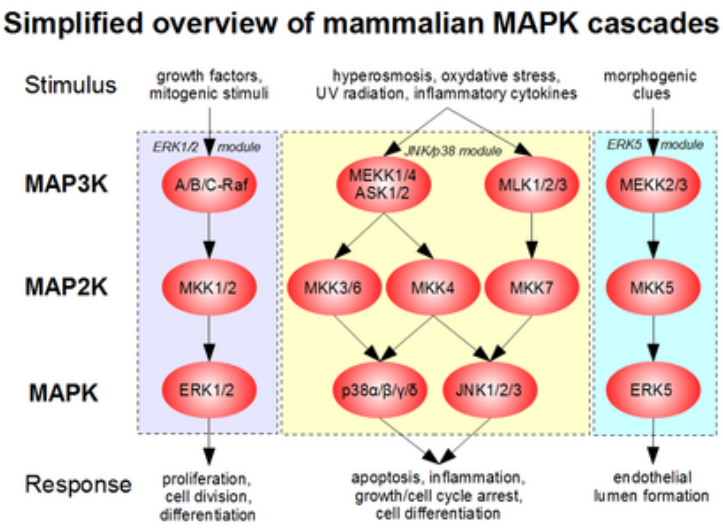

Figure 3. A simplified overview of MAPK pathways in mammals organized into three main signaling modules (ERK1/2, JNK/p38 and ERK5); (From Wikipedia).

The most extensively studied groups of vertebrate MAPKs to date are the ERK1/2, JNKs, and p38 kinases. Although, these MAPK groups can be activated by a wide variety of different stimuli, in general, ERK1 and ERK2 are preferentially activated in response to growth factors and phorbol esters. While the JNK and p38 kinases are more responsive to stress stimuli ranging from osmotic shock and ionizing radiation to cytokine stimulation, and therefore are called Stress Protein Kinases (SAPKs) [24].

Once activated, MAPKs mediate a wide range of functions through phosphorylation of several substrates, including phospholipases, transcription factors, and cytoskeletal proteins as well as the phosphorylation and activation of other protein kinases, termed MAPK-activated protein kinases (MKs) such as RSKs, MSKs or MNKs, which mediate a wide range of biological functions in response to mitogens and stress stimuli [24, 26].

4. The p38 MAP Kinases

The p38 MAPKs were cloned for the first time in 1994 (Han et al, 1994), identified as a 38 kDa polypeptide that undergoes tyrosine phosphorylation in response to LPS treatment and hyperosmolarity shock, and that shares high sequence homology with HOG1 from *Saccharomyces Cerevisae*. p38α is the mammalian MAPK orthologue of HOG1. In parallel, two other groups independently identified p38α as a kinase activated by stress (also called Reactivating Kinase, RK) and IL-1 (named p40) that can directly phosphorylate and activate MAPKAP-K2 [41].

A few years after the identification of p38α, three additional isoforms were described: p38β [83], p38γ (also called SAPK3 and ERK6) [110] and p38δ (also called SAPK4) [84]. Different

genes encode the p38 isoforms, located tandemly in two chromosomes, with p38β (*Mapk11*) and p38γ (*Mapk12*) genes in one chromosome (15 in mice and 22 in humans), and p38δ (*Mapk13*) and p38α (*Mapk14*) genes in other chromosome (17 in mice and 6 in humans). It has been proposed that *Mapk12* arise from a tandem duplication of *Mapk11*, and that the *Mapk13-Mapk14* unit comes from a segmental duplication of the *Mapk11-Mapk12* gene unit [108].

Although p38 isoforms are widely expressed, p38α and p38β are considered ubiquitous, while p38γ is most significantly expressed in skeletal muscle [110], and p38δ is mainly found in testis, pancreas, kidney, lung, small intestine and neutrophils [81, 84]. According to the Human protein atlas, the expression at the protein level of the different p38 isoforms in human cells is very similar to the mouse pattern [166].

The p38 MAPK family can be further subdivided into two subsets, with p38α and p38β in one group and p38γ and p38δ in the other. This is first evident from their amino acid sequence identity; p38α and p38β are 75% identical, whereas p38γ and p38δ are 62% and 61% identical to p38α, respectively. Of note, p38γ and p38δ are more identical (70%) to each other. Moreover, they present differential susceptibility to inhibition by certain compounds; *In vitro* and *in vivo* assays demonstrated that only p38α and p38β are inhibited by pyridinyl imidazoles (SB202190 and SB203580) inhibitors, whereas p38γ and p38δ were completely unaffected by the drugs. A third difference between these two subgroups of p38MAPKs is with regard to substrate selectivity of these kinases. For example, microtubule-associated protein Tau is a better *in vitro* substrate for p38γ and p38δ than p38α and p38β [58, 69], and this is also true for the scaffold proteins α1-syntrophin, SAP90/PSD95 and SAP97/hDlg [77, 143, 145]. Conversely, MAPKAP-K2 and MAPKAPK3 are better phosphorylated by p38α and p38β than p38γ and p38δ [145].

4.1 Subcellular localization

With the apparent complexity of p38 MAPK signaling pathway and the identification of multiple targets and effectors which include both nuclear and cytoplasmic proteins, there is increasing interest in the spatio-temporal organization of these signaling cascades. Despite the number of studies showing activation of p38 MAPK in response to different stimuli, their intracellular distribution remains unclear. Unlike other MAPKs, p38s have no nuclear localization signal, but they have been shown to be distributed throughout the cytosol and nucleus. Furthermore, not direct interaction has been reported between importins or exportins and p38 MAPKs. Thus, the translocation across the nuclear membrane most likely occurs through interactions with NES- and NLS-containing proteins. p38α is exported from the nucleus to the cytoplasm in response to hyper-osmotic stimuli in a complex with the NLS-containing protein, MAPKAP kinase-2 in a phosphorylation dependent manner of MAPKAP kinase-2 by p38α [14]. Other groups have reported a selective nuclear accumulation of p38α MAPK in

response to DNA damage [177]. Although several studies have been performed on p38α cellular localization, there are only a few reports about the other p38 isoforms. It has been shown in cardiomyocytes that p38α and p38β are localized in the nucleus and the cytoplasm while p38γ is only present in the cytoplasm, probably reflecting specialized functions for the different isoforms [34]. According to the Human Proteome Atlas, p38α and p38γ are localized to the nucleus but excluded from the nucleoli in both human and mouse cells; in contrast, p38δ is mainly localized to the nucleus and nucleoli, and in addition localized to the cytoplasm. However, p38β seems to be localized to the mitochondria in human cells. It is possible that the intracellular distribution of p38 MAPK is associated with its substrate specificity and determined by the nature of the stimuli.

4.2 Structure

p38 MAPKs contain little more than the kinase catalytic domain. The short N- and C-terminal extensions bear little homology to other known proteins except the related p38 family members and JNK isoforms. The structures of unphosphorylated and phosphorylated p38s have been solved by X-ray crystallography, providing insight into the mechanism controlling activation and substrate specificity [164, 173-176, 190].

The fold and topology of p38 MAPKs is similar to that of ERK2, despite significant differences in the conformation of the activation loop. The phosphorylation lip sequence in p38 MAPKs is six residues shorter than in ERK2, placing the Thr and Tyr phosphorylation sites in distinct positions. In p38 isoforms, as in JNK3, this sequence is folded up between the two domains. The Gly residue in the Thr-Gly-Tyr (TGY) dual-phosphorylation motif, as well as the length of the loop, contributes to p38 substrate specificity. The P+1 specificity pocket is blocked by the C-terminus of the lip in p38. The length of the activation loop also plays an important role in controlling autophosphorylation, yet modifications of the loop structure do not result in any change in the selection of p38 by MKKs [85]. p38 specificity is also influenced by docking sites within various substrates as described for ERK2 [82, 184].

A surprising observation is that, despite a high degree of sequence similarity in the p38 MAPK family, different residues are utilized to carry out the coordination of the phosphate groups in the different p38 MAPKs [190].

4.3 Regulation of the p38 MAPK signaling module

4.3.1 Dual phosphorylation by MKKs

The p38 MAPKs are strongly activated in response to various physical and chemical stresses, such as oxidative stress, UV irradiation, hypoxia, ischemia, and various cytokines, including interleukin-1 (IL-1) and tumor necrosis factor alpha (TNFα) [28]. The canonical activation of

p38 MAPKs occurs via dual phosphorylation of their Thr–Gly–Tyr motif, in the activation loop, by MKK3 (MEK3) and MKK6 (MEK6). These two upstream kinases show a high degree of specificity for p38 MAPK isoforms, as they do not activate ERK1/2 or JNK. MKK4 (also known as MEK4 and Sek1) is a known JNK kinase that possesses some MAPKK activity toward p38α, suggesting that MKK4 represents a site of integration for the p38 and JNK pathways [19]. Upon activation, the dually phosphorylated p38 MAPK undergoes global conformational changes that alter the alignment of the kinase lobes (N-terminal and C-terminal domains) of the folded protein and enhances access to substrate, which together increases enzymatic activity.

The physiological relevance of these two MKKs comes from knockout studies, where mice lacking both MKK3 and MKK6 are not viable, dying in mid-gestation due to placental defects and altered development of the embryonic vasculature [19]. This observation indicates that MKK3 and MKK6 have some redundant roles, because loss of either gene alone yields healthy mice [113, 160, 179].

Specificity of p38 MAPK signaling has been reported in studies of the MAPK kinases (MAPKKs) that activate the p38 MAPK isoforms [136]. However, the mechanism that accounts for signaling specificity by the p38 MAPK pathway is not well understood. Previously, it has been demonstrated *in vitro* that MKK6 is a common activator of p38α, p38β, p38γ and p38δ MAPK, while MKK3 activates only p38α, p38γ and p38δ MAPK [38, 54, 68, 83, 170]. This selectivity of p38 MAPK activation by MKK3 and MKK6 may contribute to the specificity of signal transduction by the p38 MAPK pathway. The specificity in p38 activation is thought to result from the formation of functional complexes between MKK3/6 and different p38 isoforms and the selective recognition of the activation loop (T-loop) of individual p38 MAPK isoforms by the MKKs. Furthermore, the tissue-specific expression of the MKKs and p38s, will add another layer of complexity to the signaling specificity. Although MKK6 is present in various forms in multiple tissues, tissue-specific splice forms of MKK6 have been described in skeletal muscle and heart [74]. Given the distinct expression patterns of MKKs and p38s, it is likely that these MKK act as a regulators of p38 activation depending on expression in a given tissue and/or cell type. For instance, MKK3 has been shown to be the major p38 activator in mesangial cells stimulated by transforming growth factor [169], while MKK6 appears to be the predominant isoform in thymocytes [160]. Other factor that could contribute to the specificity of the p38 MAPK activation is the presence of scaffold molecules that mediate the interaction between the MKKs and the different p38 isoforms and regulate the activation of the pathway. Although a number of scaffold proteins have been implicated in the regulation of different MAPK signaling modules, not many have been found to participate in the p38 MAPK cascade. Examples are JIP-2 and JIP-4 that mediate the interaction between MKK3 and different p38 isoforms. These scaffold proteins could be express in a tissue-specific manner and promote the

interaction of a specific MKK with and particular p38 isoform, contributing to the specificity of p38 MAPK activation.[119, 147, 148].

4.3.2 Autophosphorylation

Although the canonical p38 MAPK pathway regulation is by MKKK–MKK pathway in mammalian cells, two other possible mechanisms of activating p38α have been proposed. In a yeast two-hybrid screen TAB1 (Transforming growth factor-β-activated protein 1 (TAK1)-binding protein 1) was identified to bind to p38α MAPK, but not to interact with other p38 family members. TAB1 binding to p38α induces its autophosphorylation and activation. This MKK-independent activation of p38α has been implicated in the ischemic heart and immunological processes [65, 161]. Furthermore, this mechanism appears to be involved in the AMPK activation of p38α in ischemic heart [107].

Another MKK-independent mechanism of activation of p38α has been observed in T cells stimulated through the T cell antigen receptor (TCR). In this system, p38α is activated by an alternative mechanism in which TCR-mediated stimulation activates proximal tyrosine kinases that results in the phosphorylation of p38α on a non-canonical activating residue, Tyr323, and subsequently to its autophosphorylation on its Thr–Gly–Tyr motif (Thr180 and Tyr182) [146].

On the other hand, autophosphorylation activity has been detected in intrinsically active p38α, p38β, p38γ mutants, no such mechanism has been observed to activate the endogenous kinases but on p38α. [7, 9]. This mechanism may be reflecting a natural activation mechanism of the endogenous kinases.

4.3.3 Dimerization

Many protein kinase functions, including autophosphorylation in trans, require dimerization, possibly by activation segment exchange. Such dimers have been reported for autophosphorylating protein kinases, but only a few for mitogen-activated protein kinases (MAPKs). The fact that activation of p38α MAPK proceeds not only via the well-characterized action of dual T/Y specificity MKKs, but also via a non-canonical activation involving autophosphorylation, open the possibility that certain stimuli could induce dimerization of p38α. It was found that p38 dimers created *in vitro* by cysteine oxidation, were more active than p38 monomers, establishing that dimerization could indeed affect catalytic activity. Recently, it has been shown that p38α forms a homodimer upon phosphorylation on Tyr323. In the dimer, a structural unit containing Tyr323 is formed at a dimerization contact region that stabilizes the HRD catalytic loop in a unique inactive geometry [140]. The dimer explains the regulation properties of p38α non-canonical autoactivation. However, no dimerization has been reported to the date for other p38 isoforms.

4.3.4 Downregulation of p38 MAPK pathway

The magnitude and duration of p38 MAPK signal transduction are critical determinants of its biological effects. Activation of p38 MAPK occurs within minutes in response to most stimuli and is transient.

MAP kinase phosphatases (MKPs) catalyze dephosphorylation of activated MAP kinase (MAPK) molecules and deactivate them, playing an important role in determining the magnitude and duration of MAPK activities. The MKP family members share the sequence homology and the preference for MAPK molecules, but they are different in substrate specificity among MAPK molecules, tissue distribution, subcellular localization and induction by extracellular stimuli.

In mammalian cells, several protein phosphatases interact with and inactivate p38 MAPK pathway. MKP-1, the firstly discovered MKP, is induced rapidly after exposure to growth factors, heat shock and oxidative stress and seems to act on JNK and p38 rather than ERK1/2 [60]. Besides, both PP2C (Ser/Thr phosphatase) and PTP (Tyr phosphatase) have been shown to regulate p38 MAPKs [158, 159]. Moreover, another family of dual-specificity phosphatases plays a key role in the regulation of these MAPKs, since, for example, the M3/6 and MKP-7 phosphatases regulate JNK and p38 MAPKs, but not ER1/2 [93, 162].

5. p38 MAPK pathway Inhibitors

Pyridinyl imidazole compounds are the best-characterized inhibitors of the p38 pathway. Several compounds that belong to this group have been described SB203580, SB203590 or SB220025, SKF86002. The pyridinyl imidazoles only inhibit p38α and p38β isoforms, but not p38γ ad p38δ. These inhibitors bind in an extended pocket in the ATP binding site, preventing ATP to bind, and the subsequent kinase activity [57, 71, 176, 189].

SB203580 is the most commonly used compound to inhibit p38α and p38β. Although it has beneficial effects in several inflammatory diseases or in Ischemia/Reperfusion injury, it cannot be used clinically due to liver toxicity [27, 39, 71, 105]. However, several analogues have been developed during the last years that are more potent and with reduced toxicity (SB220025, ML3403 or SB239063) [40, 121]. Among them, SB239063 that can readily be used *in vivo* has demonstrated beneficial effects in the infract rat model of Ischemia/Reperfusion injury [64].

Despite the diverse compounds developed to specifically inhibit p38α and p38β, no highly specific inhibitors for p38γ and p38δ have been described, but BIRB796 that is a pan-p38 MAPK inhibitor [126]. p38γ and p38δ inhibition occurs at higher BIRB796 concentrations than those that inhibit p38α and p38β, and at lower concentrations than those that inhibit the activation of JNK isoforms.

Pirfenidone (5-methyl-1-phenyl-2-[1H]-pyridone) is an FDA-approved compound in Europe for

the treatment of the debilitating and fatal lung disease idiopathic pulmonary fibrosis (IPF) under the name of *Esbriet,* which has been shown to exert its protective effects through the inhibition of p38γ [10, 101, 125]. Moreover, the interaction of p38γ interaction with its PDZ containing substrates and their subsequent activation can be blocked with a small PDZ peptide [143, 145].
The recent observation that the residues that carry out the coordination of the phosphate groups are different in the four p38 isoforms, suggests that the inhibition of specific p38 MAPKs may be accomplished by targeting the non-conserved residues that are critical for stabilizing the active form of the kinase. The design and development of small molecules that selectively inhibit the p38 MAPK isoforms is still a challenge within the industry.

6. p38 MAPK pathway Substrate Specificity

6.1 Docking Motifs

The different MAPK subfamilies phosphorylate a distinct set of protein substrates. These substrates act as the critical effectors that enable cells to mount the appropriate responses to varied stimuli. A common phosphorylation site motif has been defined for MAPK family members, consisting of a Serine or a Threonine followed by a Proline in the position P+1. Besides, this motif includes a weak preference for aliphatic residues at the P+2 [150]. Therefore, although phosphorylation site motifs likely serve to direct the MAPK to phosphorylate a specific serine or threonine residue within a protein, the specificity in protein substrate recognition of the different MAPK subgroups cannot be directed by this sequence. It is true that mechanisms such as subcellular localization and the use of scaffolding proteins can contribute to kinase substrate targeting *in vivo*, however, MAPKs also exhibit a high degree of target specificity *in vitro*.
Mutagenesis experiments with MAPKs have shown that residues downstream the phosphorylation site, are important for substrate recognition. These sequence motifs in the substrate interact with regions of the kinase outside the active site, called docking motifs [15, 70].
Two types of docking motifs have been described in MAPKs and their substrates that serve to enhance affinity and specificity. The best-characterized docking site utilized by MAPKs is the D-site (also referred to as the D-domain), which consists of two or more basic residues followed by a short linker (LXL) and a cluster of hydrophobic residues [23]. D-domains can show specificity for families of MAPKs [63, 185]. Some D-domains show specificity within the p38MAPK family [63]. The D-domain can be positioned either N- or C-terminal to the phosphorylation site [12, 149, 162, 186]. The second major MAPK docking site, known as the DEF site (docking site for ERK FXF, also called the F-site), has been identified in a number of ERK substrates. DEF sites are generally characterized as an FX(F/Y)P sequence, typically

located between 6 and 20 amino acids C-terminal to the phosphorylation site. Although initially DEFs sites were described in ERK substrates, divergent DEF docking sites have been described to be recognized by other MAPKs. While p38α and p38β have a very similar DEF domain to ERK, with a high preference for aromatic residues at P+1 and P+3, p38γ and p38δ DEFs domains strikingly preferred aliphatic residues (Ile, Leu, Pro, and Val). This dramatic difference between the different p38 isoforms, could account, in part, for their substrate specificity.

6.2 Protein Domains

A feature that makes p38γ unique among the p38 MAPKs is its short C-terminal sequence KETXL, an amino acid sequence ideal for binding PDZ domains in proteins. SAPK3/p38γ binds to a variety of these proteins, such as alpha1-syntrophin, SAP90/PSD95 and SAP97/hDlg, and under stress conditions is able to phosphorylate them and modulate their activity [77, 143, 145]. These PDZ domain-containing proteins are scaffold proteins usually targeted to the plasma membrane cytoskeleton at specialized sites such as the neuromuscular junction and gap junctions through protein-protein interactions. In the case of SAP97/hDlg its phosphorylation by p38γ provides a mechanism of dissociating it from the cytoskeleton [143], which indicates a role of this p38MAPK isoform in modulation of cytoskeletal organization. Although p38γ can also phosphorylate typical p38 MAPK substrates, the PDZ domain confers part of its substrate specificity.

7. Downstream targets

p38 isoforms are present in the nuclei and cytoplasm of quiescent cells and have been shown to accumulate in the nuclei of cells subjected to certain stresses [135]. Upon stimulation, p38 isoforms phosphorylate a large number of substrates in many cellular compartments, including the cytoplasm (cPLA2, MNK1/2, MK2/3, HuR, Bax, and Tau) and the nucleus (ATF1/2/6, MEF2, Elk-1, GADD153, Ets1, p53, and MSK1/2) [99, 142]. Although the substrate specificity of all p38 MAPK isoforms is known to overlap, there are some differences between the two subgroups of p38 MAPKs with regard to substrate selectivity of these kinases, such as particular protein domains or docking sites, described above.

7.1 p38α and p38β substrates

p38α and p38β physiological substrates include other protein kinases, transcription factors, and other proteins such as metabolic enzymes or phospholipases. p38β functions are mostly redundant with those of p38α. p38α MAPK is essential for embryonic development and it regulates different cellular functions such as proliferation, differentiation, cell death, adhesion, migration, as well as the response to stress and many metabolic pathways, among others. It does

so through regulation of transcription, mRNA stability, chromatin remodeling, protein synthesis, etc. [151].

Cytoplasmic Substrates. Some of the p38α and p38β targets are downstream kinases, which are activated through phosphorylation and further phosphorylate additional targets. RPS6KA5/MSK1 and RPS6KA4/MSK2 can directly phosphorylate and activate transcription factors such as CREB1, ATF1, the NF-kappa-B isoform RELA/NFKB3, STAT1 and STAT3, but can also phosphorylate histone H3 and the nucleosomal protein HMGN1. RPS6KA5/MSK1 and RPS6KA4/MSK2 play important roles in the rapid induction of immediate-early genes in response to stress or mitogenic stimuli, either by inducing chromatin remodeling or by recruiting the transcription machinery [131]. On the other hand, two other kinase targets, MAPKAPK2/MK2 and MAPKAPK3/MK3, participate in the control of gene expression mostly at the post-transcriptional level, by phosphorylating ZFP36 (tristetraprolin) and ELAVL1, and by regulating eEF2K, which is important for the elongation of mRNA during translation [38, 61, 141]. MKNK1/MNK1 and MKNK2/MNK2, two other kinases activated by p38 MAPKs, regulate protein synthesis by phosphorylating the initiation factor EIF4E2 [43, 102].

In the cytoplasm, the p38α and p38β MAPK is an important regulator of protein turnover. For example, CFLAR is an inhibitor of TNFα-induced apoptosis whose proteasome-mediated degradation is regulated by p38 MAPK phosphorylation. Ectodomain shedding of transmembrane proteins is regulated by p38 MAPKs as well. In response to inflammatory stimuli, p38 MAPKs phosphorylate the membrane-associated metalloprotease ADAM17. Such phosphorylation is required for ADAM17-mediated ectodomain shedding of TGF-α family ligands, which results in the activation of EGFR signaling and cell proliferation [182]. Additional examples of p38 MAPK substrates are the FGFR1. FGFR1 can be translocated from the extracellular space into the cytosol and nucleus of target cells, and regulates processes such as rRNA synthesis and cell growth. FGFR1 translocation requires p38 MAPK activation [154].

Nuclear Substrates. In the nucleus, many transcription factors are phosphorylated and activated by p38 MAPKs in response to different stimuli. Classical examples include ATF1, ATF2, ATF6, ELK1, PTPRH, DDIT3, TP53/p53 and MEF2C and MEF2A [54, 184]. The p38 MAPKs are emerging as important modulators of gene expression by regulating chromatin modifiers and remodelers. The promoters of several genes involved in the inflammatory response, such as IL6, IL8 and IL12B, display a p38 MAPK-dependent enrichment of histone H3 phosphorylation on Ser-10 (H3S10ph) in LPS-stimulated myeloid cells. This phosphorylation enhances the accessibility of the cryptic NF-kappa-B-binding sites marking promoters for increased NF-kappa-B recruitment [89, 94].

7.2 p38γ and p38δ substrates

Although p38γ and p38δ can also phosphorylate typical p38 MAPK substrates such as the transcription factors ATF2, Elk-1 or SAP1, they cannot phosphorylate MAPKAPK2 or MAPKAPK3, which are good substrates for other p38 MAPK isoforms [38, 68]. p38γ only weakly phosphorylates the p38α and p38β substrates MEF2A, MEF2C and MEF2D *in vitro* and barely stimulates their transcriptional activities *in vivo*, whereas p38δ does not phosphorylate any of them [116, 178].

PDZ domain containing proteins may be specific substrates for p38γ, such as SAP90/PSD95, the first physiological substrate described for this kinase [145] or SAP97/hDlg [143]. Nevertheless, p38γ and p38δ share many substrates that do not require PDZ domain binding interactions like the microtubule-associated protein Tau [58]. Tau function is modulated by phosphorylation, and its ability to bind and stabilize microtubules correlates inversely with its phosphorylation which may facilitate its self-assembly. It has been reported that p38δ phosphorylates Tau *in vivo* on Thr 50 which is phosphorylated in Alzheimer disease [58].

In correlation with p38γ high expression in skeletal muscle in comparison to other tissues, it has been reported that this kinase plays a fundamental role in skeletal muscle differentiation. Thus, endogenous p38γ protein levels increase when myoblast differentiate into myotubes [37, 165]. Moreover, it has been shown that over-expression of p38γ in skeletal muscle cells leads to differentiation from myoblast to myotubes, and that a dominant-negative mutant of p38γ prevented this differentiation process [103]. Furthermore, p38γ phosphorylates the transciption factor MyoD, one of the earliest markers of myogenic commitment, which results in a decrease in its transcriptional activity [67]. This MyoD repression plays a cardinal role in blocking the premature differentiation of skeletal muscle stem cells, the satellite cells. Additionally, p38γ regulates mitochondrial biogenesis and angiogenesis, and it is required for endurance exercise-induced skeletal muscle adaptation [133].

p38δ has been associated with the cytoskeleton regulation as it has been reported to phosphorylate the cytoplasmic protein stathmin and Tau, which control microtubule dynamics [58, 69, 127, 188]. In addition, p38δ plays a role in the regulation of protein elongation by phosphorylating and inactivating the eukaryotic elongation factor 2 (eEF2) kinase [95, 96]. p38δ also regulates insulin secretion as well as in the survival of pancreatic beta cells, through an inhibitory phosphorylation of the protein kinase D1 (PKD1), which controls insulin exocytosis in pancreatic beta cells [156]. Furthermore, through the phosphorylation of the same protein and regulation of PTEN activity in neutrophils, p38δ controls neutrophil migration in an acute lung injury model [81]. p38δ has been suggested to play an important role in inducing keratinocyte differentiation by regulating the expression of Involucrin, which is a protein expressed during

keratinocyte differentiation [50]. Activation of exogenously expressed p38δ by differentiation-inducing agents such as a bioactive green tea polyphenol (EGCG), okadaic acid (OA) or the phorbol ester TPA, correlated with increased Involucrin promoter activity in keratinocytes via increased activity at AP1, Sp1 and C/EBP sites [11, 51]. The mechanisms by which p38δ may regulates keratinocyte differentiation is still unknown, although it has been reported that in keratinocytes expressing exogenous p38δ, this forms a complex with ERK1/ERK2 [51]. Additional data supporting the idea that p38δ may play a role in keratinocyte differentiation come from a study carried out in lesional psoriasis skin [86]. It has been shown that the activity of p38α, p38β and p38δ is augmented in lesional psoriasis skin compared with non-lesional psoriasis skin [86]. Alternatively, it has been also claimed that p38δ may have a dual role in keratinocytes contributing not only to the differentiation process, but also to their apoptosis in a PKCδ dependent manner, and in response to OA or hydrogen peroxide (H_2O_2) [52, 98].

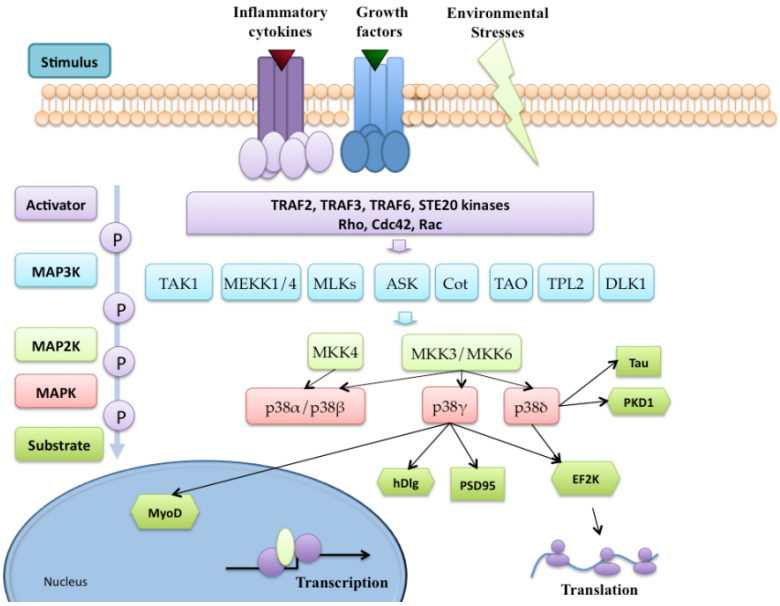

Figure 4. The p38γ and p38δ MAPK pathway. Different stimuli such as growth factors, inflammatory cytokines or a wide variety of environmental stresses can activate p38 MAPKs. A number of representative downstream targets, including protein kinases, cytosolic substrates and transcription factors, are shown [36].

8. Crosstalk with other signaling pathways

Crosstalk between signaling pathways is very common in cell regulation, which usually depends on cell context and plays an important role in fine-tuning biological responses. There are many examples of crosstalk among different MAPK pathways.

p38 inhibits ERK signaling in non-transformed cells. Generally, ERK activity promotes survival. The suppression of this activity by p38 is critical for induction of apoptosis in non-transformed cells. p38 induces PP2A expression, and it dephosphorylates MEK to reduce ERK pathway activation [87]. Furthermore, p38α mediates a feedback control of TAK1 in macrophages upon LPS stimulation through TAB1 regulation, which not only limits the

activation of p38α but also synchronizes its activity with other signaling pathways that lie downstream of TAK1 (JNK and IKK) [30].

JNK can also inhibit p38α, as JNK activity inhibited both ERK and p38 signaling in mouse cardiomyocytes [128] and c-Jun deficient hepatocytes showed increased phosphorylation of p38α [155]. The JNK-ERK/p38 crosstalk may involve a p53-DUSP2 dependent pathway, as the c-Jun mediated inhibition of p38α observed in hepatocytes was p53 dependent [155] and DUSP2 was identified as a transcriptional target of p53 in mouse embryonic fibroblast and breast cancer cell lines [187].

Cell growth pathways and stress-sensing pathways are tightly regulated through signaling crosstalk. When faced with cellular damage or stress, cells can respond by shutting down cell growth, allowing repair to take place until the cell commits to further growth and division. Or alternatively, cells can promote growth and translation, presumably in order to promote the synthesis of stress response proteins and the turnover of damaged molecules. Therefore, there is a close relationship in between the master regulator of cell growth, mTOR pathway, and the p38 MAPKs stress signaling pathway. For example, UV radiation, which activates stress pathways such as p38 and JNK through the induction of DNA damage, activates TORC1 in a number of cell types [21, 134, 192]. Besides, in mammalian and Drosophila tissue culture, as well as in Drosophila ovaries *ex vivo*, p38β can activate mTOR pathway in response to H_2O_2 and anisomycin [42].

The crosstalk between mTOR and p38 has been shown as well in the mammalian heart. In Ischemia/reperfusion, cardiac p38α promotes mTOR activation in response to oxidant stress to promote cell survival. p38α induces the decline of REDD1 protein levels, promoting the interaction of Tsc2 with 14-3-3 proteins, which dissociates from mTOR leading to its activation [79].

Besides, both *in vitro* and *in vivo* experiments demonstrate that the p38-activated kinase MK2 (also known as MAPKAPK2) also regulates mTOR activation, by the direct phosphorylation of Ser1210 on TSC2. Phosphorylation of TSC2 by MK2 creates a 14-3-3 binding site and thus, releasing mTOR from the TSC2 inhibition [109].

9. p38 MAPK Physiological Functions

Knockout mice for p38α have been generated, but they die at midgestation due to placental defects and abnormal angiogenesis in the yolk sac [1, 120]. Whereas tissue-specific knockouts have implicated p38α in controlling inflammation, as well as the proliferation, differentiation and survival of different cell types [75, 123]. Recently, p38β, p38γ and p38δ and double

p38γ/p38δ knockout mice have also been generated, which are viable and fertile [13, 143]. Functional redundancy of all four p38MAPKs may contribute, at least in part, to the lack of evident phenotype of these mice [44]. Nonetheless, there are recent reports showing the implication of p38γ and p38δ in tissue regeneration, cancer, and metabolic diseases, further strengthening the interest of these pathways for the development of new therapeutic strategies.

9.1 Role of p38MAPK Pathway in inflammation

Inflammatory response is a basic protective immune process of the organism to defend our body from pathogens. Diseases induced by chronic inflammation damage millions of people's health every year. Moreover, there is growing evidence that inflammation is a critical initiation factor inducing a variety of other major diseases such as cancer, atherosclerosis, Alzheimer's disease, cardiovascular disease, neurological disorders, and pulmonary diseases [59, 106, 180]. Therefore, understanding better the molecular mechanisms and signaling pathways that regulate inflammation, could lead to the discovery of new therapeutic targets for the treatment of inflammatory-associated diseases.

There is *in vivo* and *in vitro* evidence linking p38 MAPK signaling to the production of inflammatory mediators and pro-inflammatory cytokines in several cell types via transcriptional and post-transcriptional mechanisms [41, 137].

Myeloid- and epithelial cell- specific p38α knockout mice have been use to demonstrate the implication of this pathway in inflammatory responses *in vivo*. p38α has been involved in the regulation of cytokine production (TNFα, IL-1β, Il6, COX-2, IL-17, etc.) at transcriptional and post-transcriptional levels [100]. Moreover, p38α can regulate the production of endothelial vascular cell adhesion molecule-1 (VCAM-1), which participates in cell proliferation and differentiation of the immune response [4, 132]. p38α has also been implicated in the survival promotion of double-negative T cells [47].

Furthermore, p38α is associated with various inflammatory diseases, such as septic shock induced by LPS, collagen-induced arthritis, multiple sclerosis, diabetes, and acute lung inflammation, as well as joint diseases, including synovial inflammation, cartilage damage, and bone loss [72].

In contrast, p38β knockout mice present normal T-cell development and responses to TNFα and LPS in the immune system. The production of TNFα, IL-1β, IL-6 and MIP1 was not compromised in $p38\beta^{-/-}$ mice or in LPS stimulated macrophages derived from these mice. Consistent with this outcome, p38β deficiency did not affect the development of arthritis or inflammatory bowel disease, suggesting that p38β is not critical for these functions [13]. Nevertheless, p38β has been involved in the regulation of TPA-induced skin inflammation and tumor development [112].

On the other hand, mice lacking p38γ and p38δ present reduced inflammatory responses.

Besides, myeloid cells deficient in p38γ and p38δ are impaired in the LPS-induced production of several cytokines, which has been suggested to correlate with reduced levels of the MAPK kinase kinase (MAP3K) TPL-2 and extracellular signal-regulated kinase (ERK)1/2 signaling [138]. Interestingly, p38α activation does not appear to be affected by p38γ and p38δ downregulation [138]. This suggests that they regulate the inflammatory response by distinct mechanisms.

A study of p38δ MAPK knockout (KO) mice as well as myeloid-restricted deletion of p38δ MAPK in mice has shown that p38δ is required for the recruitment of neutrophils to sites of inflammation. PKD1 phosphorylation by p38δ MAPK regulates PTEN activity to control neutrophil extravasation and chemotaxis in a model of inflammation-induced acute lung injury (ALI), which can cause acute respiratory distress syndrome (ARDS), a condition with a high mortality rate. Therefore, abnormal p38δ -PKD1 signaling may play an important role in both ALI and ARDS in humans [81].

p38γ and p38δ have been also involved in rheumatoid arthritis (RA). In RA patients, both kinases are expressed in the synovium. Moreover mice lacking p38γ and p38δ displayed reduced arthritis severity compared to control mice. The protection observed was associated with a lower expression of IL-1β and TNFα, as well as a reduction in T-cell proliferation, INFγ and IL-17 production [35].

Recently, p38δ MAPK has been implicated in the signaling pathway responsible for controlling IL-13 driven excess mucus production. This pathway is hyperactivated in patients that suffer from chronic obstructive pulmonary disease (COPD). In correlation with a possible role of p38δ in the disease, lungs from COPD patients present high p38δ expression levels [3].

9.2 Role of p38MAPK pathway in diabetes and obesity

Inflammation and cellular dysfunction are features of obesity, diabetes and diabetic nephropathy, which are associated with intracellular activation of mitogen-activated protein kinase (MAPK) signaling pathways. Levels of activated p38α are elevated in the skeletal muscle, adipose tissue and kidneys of diabetic patients [2, 25, 97], suggesting that some p38 responses may be important for the pathogenesis of diabetes and its complications.

Several recent studies have shown that inhibition of p38α in p38β with SB203580 improves glucose transport in L6 and 3T3L1, myoblast and preadipocyte cell lines. These results correlate with the study of Carlson et al. (2003) showing that p38 activity participates in a downregulation of GLUT4 protein levels and is significantly higher in isolated adipocytes from type-2 diabetes patients [25].

Furthermore, *in vitro* experiments have shown a positive role of p38α in adipogenesis. Most studies were performed in 3T3-L1 preadipocyte cell lines and used pyridinyl imidazole

inhibitors such as SB203580 to inhibit p38 activation [53]. More recently, Hata et al. demonstrated that Bone Morphogenic Protein-2 (BMP-2) oriented pluripotent mesenchymal cell lines C3H10T1/2 into the adipocyte lineage through activation of p38α/β [78].

In contrast, p38 activation is strongly reduced in the liver of obese mice and its activation leads to improved glucose metabolism and reduces hepatic ER stress. This beneficial effect is achieved through the phosphorylation of XBP1 that enhances its nuclear localization [104].

Recent reports have highlighted the implication of p38δ and p38γ in metabolic diseases [114]. Sumara G., et al (2009) has reported that p38δ regulates insulin secretion as well as survival of pancreatic β-cells. Mice lacking p38δ display improved glucose tolerance due to enhanced insulin secretion from pancreatic β-cells, associated with a strong reduction in PKD inhibitory phosphorylation by p38δ. Besides, these mice are protected against high-fat-feeding-induced insulin resistance and oxidative stress-mediated β-cell failure. This regulation takes place through the inhibitory phosphorylation by p38δ of PKD [156].

9.3 Role of p38MAPK pathway in cardiovascular physiology and dysfunction

While p38 has been shown to have a key role in skeletal muscle development [92], its function in cardiac development has not been as extensively studied. Recent studies point to a possible role for p38 in cardiac development. For example, p38α activity is required for cardiomyocyte differentiation of P19CL6 cells, and this is mediated via its activation of the transcription factor AP-1 [55]. Further evidence of the importance of p38 in cardiomyocyte differentiation comes from the discovery that p38α promotes cardiogenesis over neurogenesis in ES cells [5].

Unfortunately, while cell culture studies have strongly implicated p38α as an important player in cardiogenesis, there is little to no *in vivo* data supporting this hypothesis. As mentioned previously, $p38\alpha^{-/-}$ embryos are embryonic lethal due to defects in placental angiogenesis. However, cardiac-specific deletion of p38α results in normal development of the heart [66].

The role of p38 MAPK pathway in cardiac pathology has been much more extensively studied. Cardiovascular mortality is one of the most important health problems in human populations nowadays. Two leading causes of cardiac morbidity are pressure overload cardiac hypertrophy resulting from hypertension and cardiomyocyte apoptosis and necrosis following ischemic injuries.

p38α MAPK activation has been described upon ischemia/reperfusion in mice and in humans failing hearts secondary to ischemic heart disease [16, 33]. Shear stress from pressure overload can also activate stress-activated protein kinases pathways [172]. Moreover, p38α has been

shown to be activated in cultured neonatal cardiomyocytes by hypertrophic stimulation [31, 122] and in mouse hearts in response to pressure overload [171].

Although the four p38 MAPKs are expressed in the heart, p38α and p38γ are the predominant isoforms. Studies have proposed both a protective and damaging roles of p38MAPK in the stressed myocardium. This seemed to be dependent in part in the system studied.

The role of p38 MAPKs in cardiac hypertrophy has been suggested in first place by studies using over-expressed active forms of their upstream activators MKK3 and MMK6 in cardiomyocytes. In these studies it was found that the active mutants induced characteristic hypertrophic responses [172, 191]. Moreover, over-expression of MKK3 in cardiomyocytes leads to an increase in apoptosis [172]. Interestingly, the differences between MKK3 and MKK6 can point out distinct roles of p38 isoforms. Furthermore, p38 MAPK pathway is activated in cardiomyocytes upon hypertrophic stimuli, and the inhibition of p38α/β with SB203580 is sufficient to block the hypertrophic growth [191]. One year after, Yibin Wang et al. (1998) reported that forced activation of p38β activity in culture cardiomyocytes results in characteristic features of hypertrophy, whereas the activation of p38α activity leads to the induction of myocyte apoptosis. According with this result, the p38α cardiac-specific knockout mice showed that p38α plays a critical role in the cardiomyocyte survival pathway in response to pressure overload, while cardiac hypertrophic growth is unaffected despite its dramatic down-regulation [123]. Although some groups have reported a role of p38α in the regulation of cardiac hypertrophy, most of the studies were performed by overexpressing the dominant-negative p38α, a non-physiological method, or by indirect strategies that could be altering the function of other p38 isoforms [20, 130].

Due to the lack of pharmacological inhibitors, p38γ and p38δ have been far less extensively studied. There is only one study that reported on the role of these kinases in cardiac hypertrophy. Dharmendra Dingar et al. (2010) characterized the expression and subcellular localization in cardiomyocytes of the p38 MAPK isoforms in physiological conditions and in response to chronic pressure overload. Chronic pressure overload induced by transverse aorta constriction (TAC) does not induce changes in quantity of p38α mRNA. In contrast, p38β and p38δ mRNA increased within 1 day of pressure overload and remained elevated whereas p38γ mRNA showed an initial increase but had returned to basal levels by day 7. However, although increases in mRNA abundance were observed for p38β, p38γ, and p38δ, the protein level of each isoform was unaltered. Confocal immunofluorescence studies revealed p38α and p38γ in both the cytoplasm and nucleus. After chronic pressure overload, p38γ accumulated in the nucleus whereas the distribution of p38α remained unaffected. These differences in localization would result in access to different substrates and hence distinct functional effects [49].

OBJECTIVES

Since the discovery of the first p38 isoform, more than 15 years ago, the p38 MAPK family has been implicated in the regulation of a diverse array of cellular processes. However, most of the reports refer to p38α and p38β isoforms, which have been extensively characterized thanks to the availability of highly specific inhibitors and knockout mouse models. Nonetheless, we still know very little about the role of the alternative p38 MAPKs, p38γ and p38δ. Thus, the main objective of this thesis is to understand deeper the importance of p38γ and p38δ in homeostasis and disease.

Study the implication of p38 MAPK pathway, specifically of p38γ and p38δ, in acute inflammatory responses.

1.1. To study the role of the up-stream kinases MKK3 and MKK6 using LPS-induced acute hepatitis as a model of acute inflammatory response.
1.2. To assess the implication of the different p38 isoforms in LPS-induced acute hepatitis.
1.3. To unveil the specific cell types in which p38γ and p38δ are expressed and important for LPS-induced acute hepatitis.
1.4. To understand the molecular mechanism through which p38 MAPKs regulate this process.

Address the role of p38γ and p38δ in chronic inflammatory responses associated to metabolic alterations.

1.1. To analyze the expression levels of p38γ and p38δ in patients suffering from Non-Alcoholic Fatty Liver Disease (NAFLD).
1.2. To study if the mouse model of steatosis induced by MCD diet could replicate the changes observed in human NAFLD patients.
1.3. To unveil the role of p38γ and p38δ in chronic inflammation associated to steatosis and its impact in the disease progression.
1.4. To assess the role of p38γ and p38δ in chronic inflammation associated to obesity and its impact in the disease progression.

Understand the role and regulation of p38γ and p38δ the heart.

1.5. To analyze the cardiac expression and activation levels of these kinases during postnatal stages of cardiac development.
1.6. To address the role of p38γ and p38δ in postnatal cardiac growth.
1.7. To investigate the role of p38γ and p38δ in cardiac-overload induced hypertrophy.
1.8. To address the molecular mechanism through which these p38 isoforms control cardiac growth.
1.9. To understand their regulation by upstream MKKs in postnatal cardiac growth.

RESULTS

ARTÍCULO 1: Eukaryotic elongation factor 2 controls TNF-α translation in LPS-induced hepatitis.

Autores: González-Terán B, Cortés JR, Manieri E, Matesanz N, Verdugo Á, Rodríguez ME, González-Rodríguez Á, Valverde ÁM, Martín P, Davis RJ, Sabio G.

Publicado en *Journal of Clinical Investigations*. 2013 Jan;123(1):164-78.

doi: 10.1172/JCI65124.

RESUMEN

Las infecciones y el daño tisular desencadenan una respuesta inflamatoria para contener o eliminar el agente causante del daño. La producción controlada de citoquinas por los leucocitos regula la respuesta inmunitaria. Sin embargo, su producción exacerbada puede causar más daño que el agente patógeno inicial, como ocurre en la sepsis o hepatitis aguda. El lipopolisacárido bacteriano (LPS) ha sido implicado en la patogénesis de la hepatitis aguda a través de la inducción de la citoquina pro-inflamatoria TNF-α. Los niveles de TNF-α se consideran un determinante crítico en el inicio y la progresión de la disfunción hepatica. Un posible mecanismo de control de los niveles de TNF-α es a nivel de su elongación proteica, puesto que permitiría una adaptación rápida a las necesidades fisiológicas. Sin embargo, no se conocen bien los mecanismos que controlan la fase de elongación durante el proceso de traducción . En este estudio mostramos que p38γ y p38δ son necesarias en macrógafos y células de kupffer para una correcta síntesis de TNFα en respuesta a LPS. La vía de señalización MKK3/6-p38γ/δ media la fosforilación inhibitoria de la quinasa del factor de elongación eucariótico 2 (eEF2K), lo que lleva a la activación del factor de elongación eucariótico 2 (eEF2) y a la subsiguiente elongación de la proteína TNF-α en respuesta a LPS. Estos resultados muestran un nuevo mecanismo molecular para la regulación de la producción de TNF-α y sugieren nuevas potenciales dianas terapéuticas para el tratamiento de enfermedades mediadas por esta citoquina pro-inflamatoria.

Aportación Personal al trabajo: He participado tanto en el diseño experimental, como en la realización de los experimentos y en la escritura del artículo.

Eukaryotic elongation factor 2 controls TNF-α translation in LPS-induced hepatitis

Bárbara González-Terán,[1] José R. Cortés,[1] Elisa Manieri,[1,2] Nuria Matesanz,[1] Ángeles Verdugo,[1,2] María E. Rodríguez,[1] Águeda González-Rodríguez,[3,4] Ángela Valverde,[3,4] Pilar Martín,[1] Roger J. Davis,[5] and Guadalupe Sabio[1]

[1]Department of Vascular Biology and Inflammation, Fundación Centro Nacional de Investigaciones Cardiovasculares Carlos III, Madrid, Spain. [2]Department of Immunology and Oncology, Centro Nacional de Biotecnología/CSIC, Campus de Cantoblanco, Madrid, Spain. [3]Institute of Biomedicine Alberto Sols (CSIC/UAM), Madrid, Spain. [4]Centro de Investigación Biomédica en Red de Diabetes y Enfermedades Metabólicas Asociadas, CIBERDEM, ISCIII, Spain. [5]Howard Hughes Medical Institute and Program in Molecular Medicine, University of Massachusetts Medical School, Worcester, Massachusetts, USA.

Bacterial LPS (endotoxin) has been implicated in the pathogenesis of acute liver disease through its induction of the proinflammatory cytokine TNF-α. TNF-α is a key determinant of the outcome in a well-established mouse model of acute liver failure during septic shock. One possible mechanism for regulating TNF-α expression is through the control of protein elongation during translation, which would allow rapid cell adaptation to physiological changes. However, the regulation of translational elongation is poorly understood. We found that expression of p38γ/δ MAPK proteins is required for the elongation of nascent TNF-α protein in macrophages. The MKK3/6-p38γ/δ pathway mediated an inhibitory phosphorylation of eukaryotic elongation factor 2 (eEF2) kinase, which in turn promoted eEF2 activation (dephosphorylation) and subsequent TNF-α elongation. These results identify a new signaling pathway that regulates TNF-α production in LPS-induced liver damage and suggest potential cell-specific therapeutic targets for liver diseases in which TNF-α production is involved.

Introduction

Infection and tissue injury trigger a protective inflammatory response that mobilizes a variety of effector mechanisms to contain and eliminate the injurious agent (1). Hepatic and circulating inflammatory cytokines initiate a positive feedback loop on the innate immune system (2); although cytokine production protects against pathogenic stimuli, it can cause more damage than the initiating event if its magnitude and duration are not strictly controlled by intrinsic negative regulators (1).

The cytokine TNF-α has been identified as a key regulator of the inflammatory response in animal models of fulminant hepatitis (3). Elevated concentrations of this proinflammatory cytokine are also found in acute and chronic inflammatory conditions, including trauma, sepsis, and rheumatoid arthritis (4). Upon binding to its receptors, TNF-α initiates several intracellular signaling cascades that influence cell survival, death, differentiation, proliferation, and migration (5, 6).

TNF-α signaling is particularly important in the liver. While it mediates hepatocyte survival and proliferation, it is also implicated in liver failure, since it triggers hepatocyte apoptosis and leads to upregulation of key adhesion molecules and chemokines involved in leukocyte migration and infiltration (6, 7). A well-established mouse model of acute liver failure and septic shock is the in vivo administration of bacterial LPS and D-galactosamine (D-gal), which strongly induce endogenous TNF-α and other cytokines that cause liver damage (8, 9).

TNF-α signaling can be mediated by protein kinases and phosphatases, in particular the MAPK family members ERK, JNK, and p38 MAPK. The p38 MAPK pathway transduces a variety of extracellular signals regulating cellular responses to stress, being implicated in cell proliferation, differentiation, and apoptosis (10, 11). Four p38 MAPK family members have been identified: p38α, p38β, p38γ, and p38δ, also known as stress-activated kinase 2 a (SAPK2a), SAPK2b, SAPK3, and SAPK4 (10, 12, 13). The p38 MAPK family can be further divided into 2 subsets, with p38α and p38β in one group and p38γ and p38δ in the other. All these kinases are activated by double phosphorylation mediated by the upstream kinases MKK3 and MKK6 (14, 15). To date, the best-characterized p38 isoform is p38α. This isoform is required for macrophage inflammatory responses (1), but in hepatocytes prevents endotoxin-induced liver damage (16, 17). Studies using inhibitors suggested that p38α and p38β cooperate in inflammatory processes; however, p38β-knockout mice show no differences in several in vivo and in vitro models of inflammation (18). Less is known about the role of the p38γ and p38δ MAPK. p38δ is known to phosphorylate eukaryotic elongation factor 2 (eEF2) kinase (eEF2K), inhibiting its activity (19). eEF2K blocks mRNA translation into protein through an inhibitory phosphorylation of eEF2.

The rate-limiting step in mRNA translation is thought to be the initiation step; however, far less is known about the regulation of the elongation step of protein biosynthesis (20). The process of peptide-chain elongation is at least partially regulated by eEF2 phosphorylation/dephosphorylation events induced by diverse stimuli (21). Moreover, the phosphorylation state of the upstream kinase eEF2K can be modulated by signaling molecules that regulate the activity of this factor, such as mTOR and MAPKs, including p38 kinases (19, 21–23). Because these kinases are activated by different stimuli, it is expected that the regulation of eEF2 will be important in cell adaptation to different physiological states. Here, we show that p38δ and p38γ expressed in myeloid cells promote eEF2 activity and, in consequence, TNF-α production and the inflammatory response. By blocking p38γ/δ activity in myeloid macrophages, we were able to suppress hepatitis caused by LPS-induced TNF-α expression.

Conflict of interest: The authors have declared that no conflict of interest exists.
Citation for this article: *J Clin Invest.* 2013;123(1):164–178. doi:10.1172/JCI65124.

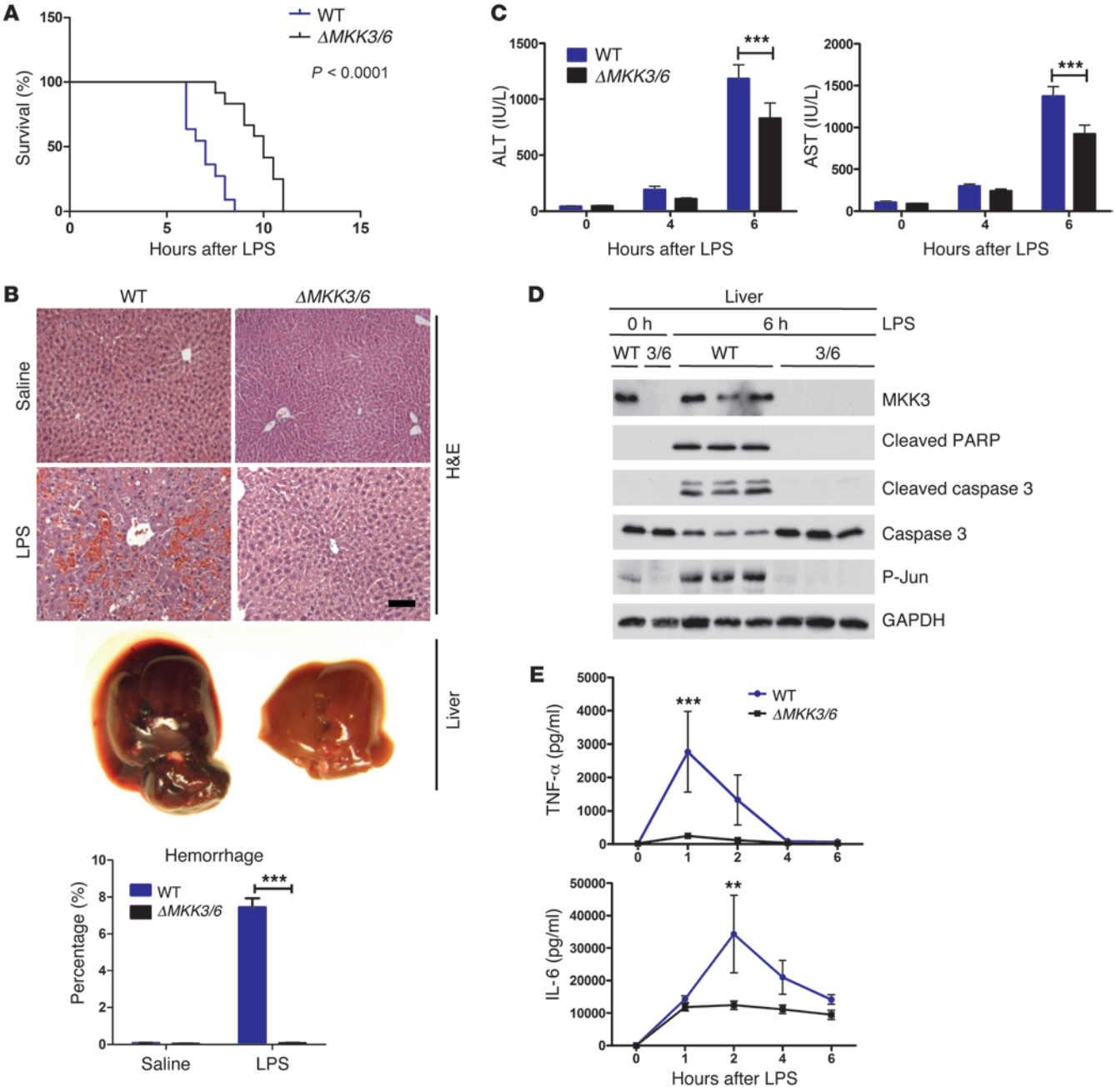

Figure 1

Δ*MKK3/6* mice are protected against LPS-induced liver damage. WT and *Mkk3*$^{-/-}$*Mkk6*$^{-/+}$ mice (Δ*MKK3/6*) were treated with D-gal+LPS or saline. (**A**) Survival curves after D-gal+LPS injection (n = 21). Survival curves were created with the Kaplan-Meier method and compared by log-rank (Mantel-Cox) test. (**B**) Livers were removed at 6 hours after injection. Panels show representative H&E-stained liver sections and livers. The chart presents hemorrhagic area as a percentage of the total area (n = 6–8). Scale bar: 50 μm. (**C**) Serum transaminase activity at 4 and 6 hours after injection (n = 10). (**D**) Liver extracts were examined by immunoblot with antibodies to cleaved PARP, cleaved caspase 3, caspase 3, phospho-Jun and GAPDH (n = 6–8). (**E**) ELISA analysis of serum TNF-α and IL-6 at different times after injection (n = 16). Data are means ± SD. $^{**}P < 0.01$; $^{***}P < 0.001$ (2-way ANOVA coupled to Bonferroni's post tests).

Results

MKK3 and MKK6 collaborate in LPS-induced hepatitis. To study the role of p38 MAPK signaling in hepatitis, we examined the effect of D-gal+LPS treatment on mice deficient for the upstream kinases MKK3 and MKK6. No differences in mortality where detected in *Mkk3*$^{-/-}$ or *Mkk6*$^{-/-}$ mice compared with WT animals (Supplemental Figure 1A; supplemental material available online with this article; doi:10.1172/JCI65124DS1). However, *Mkk3*$^{-/-}$ mice present less severe liver hemorrhage (Supplemental Figure 1B) and *Mkk6*$^{-/-}$ liver apoptosis was significantly reduced (Supplemental

Figure 1C). Levels of alanine transaminase (ALT) and aspartate aminotrasferase (AST), 2 well-established markers of hepatic necrosis, were not altered in *Mkk3*$^{-/-}$ mice, but were significantly reduced in *Mkk6*$^{-/-}$ mice, thus showing an effect on liver necrosis (Supplemental Figure 1D).

The p38 MAPK pathway is a key regulator of the expression of inflammatory cytokines, including IL-6 and TNF-α, the main determinant of LPS-stimulated liver damage (24–27). Circulating levels of TNF-α and IL-6 after D-gal+LPS injection did not differ between WT mice and the *Mkk3*$^{-/-}$ or *Mkk6*$^{-/-}$ mice (Supplemental Figure 2A). In vitro stimulation of isolated BM macrophages from these mice with LPS also revealed no differences in proliferation rate or released TNF-α and IL-6 levels (Supplemental Figure 2, B and C). Moreover, supernatants from WT, *Mkk3*$^{-/-}$, and *Mkk6*$^{-/-}$ macrophages induce apoptosis similarly in cultured hepatocytes (not shown), thus indicating that the partial protection against LPS-induced liver apoptosis was not due to circulating macrophages.

Neutrophil infiltration can cause mild to severe liver damage (28), and p38α was recently shown to control neutrophil cytokine production (29). We examined liver myeloid leukocytes based on CD11b, Gr-1, F4/80, and Ly6C markers (Supplemental Figure 2D and ref. 30). Analysis of liver cell populations revealed that D-gal+LPS injection increased liver infiltration by neutrophils (CD11b^{+}Gr-1^{hi}) in WT mice, but this effect was impaired in *Mkk3*$^{-/-}$ and *Mkk6*$^{-/-}$ mice (Supplemental Figure 1E). To investigate the potential involvement of liver neutrophils and macrophages in the protection detected in *Mkk3*$^{-/-}$ and *Mkk6*$^{-/-}$ mice, we isolated leukocytes from the livers of WT, *Mkk3*$^{-/-}$, and *Mkk6*$^{-/-}$ mice and stimulated them with LPS. Whereas the percentage of neutrophils expressing TNF-α was the same in all genotypes, the percentage of monocytes (CD11b^{+}Gr-1^{intermediate}) expressing TNF-α was higher in WT mice than in *Mkk3*$^{-/-}$ and *Mkk6*$^{-/-}$ mice (Supplemental Figure 1F), indicating that the protection against LPS-induced liver apoptosis could be mediated by liver inflammatory monocytes.

Mkk3$^{-/-}$*Mkk6*$^{-/+}$ *mice are protected against LPS-induced liver failure*. MKK3 and MKK6 show functional redundancy in the activation of p38 MAPK (14), and while single mutants are viable, doubly deficient *Mkk3*$^{-/-}$*Mkk6*$^{-/-}$ and *Mkk3*$^{-/+}$*Mkk6*$^{-/-}$ mice die early in embryogenesis. To minimize interference from redundant actions, we used *Mkk3*$^{-/-}$ *Mkk6*$^{-/+}$ (ΔMKK3/6) mice, which are viable (14). As expected, ΔMKK3/6 mice were protected against LPS-induced hepatotoxicity, showing milder hemorrhage and better survival than WT mice (Figure 1, A and B). Immunoblot analysis demonstrated that D-gal+LPS injection activated caspase 3 and PARP cleavage in WT liver but not in ΔMKK3/6 livers (Figure 1D). Moreover, circulating transaminases were reduced in ΔMKK3/6 mice, indicating a reduction in liver necrosis (Figure 1C). These data demonstrate that MKK3/6 deficiency severely limits LPS-stimulated hepatic apoptosis. Examination of serum TNF-α after D-gal+LPS injection revealed that the marked increase in TNF-α concentration observed in WT and singly deficient mice was not detected in ΔMKK3/6 mice (Figure 1E). Serum IL-6 was also lower in ΔMKK3/6 mice (Figure 1E). The loss of LPS-stimulated TNF-α expression in ΔMKK3/6 mice might account for the finding that LPS activation of JNK pathway in the livers of WT mice was not seen in ΔMKK3/6 mice (Figure 1D).

MKK3 and MKK6 are required for neutrophil migration after LPS injection. The lower TNF-α production in ΔMKK3/6 mice could be a consequence of the lower leukocyte infiltration in liver. To address this, we analyzed myeloid cell migration after D-gal+LPS injection. Quantification of liver chemokines showed that in WT mice, LPS treatment increased mRNA expression of molecules important for migration of macrophages (MCP1 and ICAM) and neutrophils (KC, MIP2), whereas induction of these chemokines and adhesion molecules was decreased in the livers of ΔMKK3/6 mice (Figure 2A). Phenotypic characterization of liver-infiltrating leukocytes from control and D-gal+LPS–treated livers revealed a significant increase in neutrophils in the inflammatory cell infiltrate of WT mice that was impaired in ΔMKK3/6 mice (Figure 2B), consistent with the reduced disease severity (28). However, the percentages of macrophages and monocytes did not differ between genotypes (Figure 2B). These findings correlated with lower RNA expression of neutrophil markers (*Elastase 2*, *Ly6G*) in the livers of LPS-injected ΔMKK3/6 mice (Supplemental Figure 3A).

The reduced liver neutrophil infiltration in ΔMKK3/6 mice could be due either to impaired neutrophil release from BM or to a defect in cell migration. The levels of circulating neutrophils after LPS injection showed a sharp increase in WT mice that was absent in ΔMKK3/6 mice (Figure 2C). These data show that the reduced neutrophil infiltration in liver is in part caused by lowered neutrophil mobilization from the BM. To investigate whether the low circulating levels of TNF-α in ΔMKK3/6 mice might be responsible for this alteration, we injected TNF-α+D-gal into WT and ΔMKK3/6 mice, resulting in increased circulating neutrophil levels in both genotypes (Supplemental Figure 3B). These data indicate that the defect in migration is secondary to the low production of TNF-α in ΔMKK3/6 mice.

MKK3 and MKK6 regulate TNF-α production by macrophages. To investigate the molecular mechanism underlying reduced circulating TNF-α in ΔMKK3/6 mice, we treated BM-derived macrophages from WT and ΔMKK3/6 mice with LPS. Whereas treatment of WT macrophages with LPS activated JNK, ERK, and p38 MAPK, in ΔMKK3/6 macrophages the activation of p38 MAPK was impaired (Supplemental Figure 3C). The ΔMKK3/6 macrophages also secreted markedly reduced amounts of TNF-α and IL-6 compared with WT macrophages, confirming that MKK3/6 deficiency causes major defects in TNF-α production (Supplemental Figure 3D). Further analysis showed that neutrophils and Kupffer cells, 2 other myeloid cell types implicated in liver damage, also secreted reduced amounts of TNF-α and IL-6 (Supplemental Figure 3, E and F). However, in vivo analysis indicated that although the percentage of liver neutrophils expressing TNF-α after D-gal+LPS injection was the same in both genotypes, the percentage of monocytes and macrophages expressing TNF-α was higher in WT livers (Figure 2D).

To confirm that reduced cytokine production by liver macrophages is responsible for the protection against hepatocyte apoptosis in ΔMKK3/6 mice, we stimulated primary hepatocytes with conditioned medium from LPS-treated BM-derived macrophages. Conditioned medium from LPS-treated WT macrophages increased hepatocyte apoptosis, measured by cleavage of caspase 3 and PARP, whereas conditioned medium from LPS-treated ΔMKK3/6 macrophages had no effect (Supplemental Figure 3G).

MKK3 and MKK6 are not required for TNF-α–induced liver damage. Our results so far show that MKK3/6 deficiency causes decreased TNF-α production in a TNF-α–dependent hepatitis model. This implies that ΔMKK3/6 mice are defective for TNF-α secretion, but not TNF-α responsiveness. To test this, we treated mice with TNF-α, finding that TNF-α caused similar mortality and liver damage in

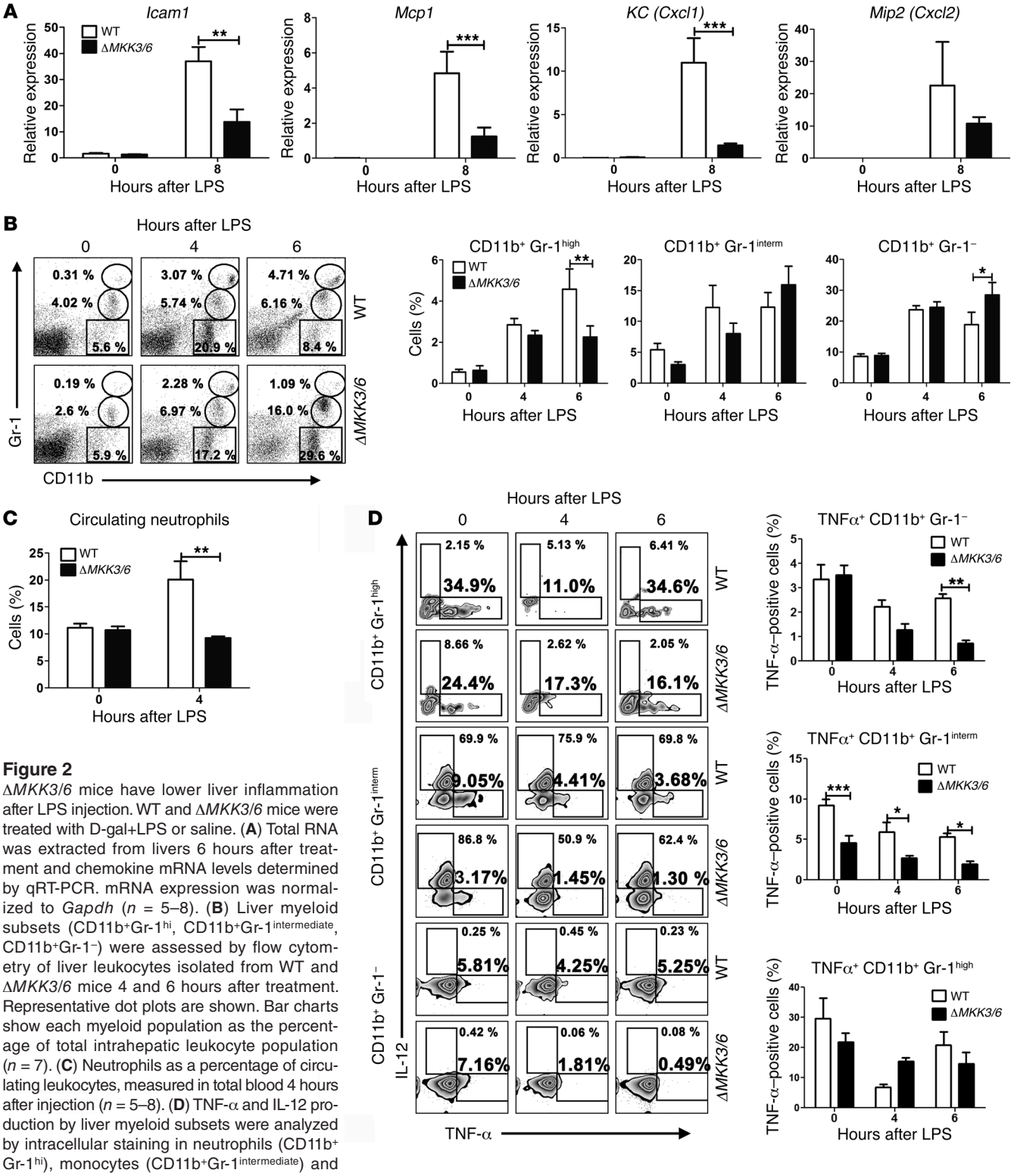

Figure 2

Δ*MKK3/6* mice have lower liver inflammation after LPS injection. WT and Δ*MKK3/6* mice were treated with D-gal+LPS or saline. (**A**) Total RNA was extracted from livers 6 hours after treatment and chemokine mRNA levels determined by qRT-PCR. mRNA expression was normalized to *Gapdh* (n = 5–8). (**B**) Liver myeloid subsets (CD11b$^+$Gr-1^{hi}, CD11b$^+$Gr-1^{intermediate}, CD11b$^+$Gr-1$^-$) were assessed by flow cytometry of liver leukocytes isolated from WT and Δ*MKK3/6* mice 4 and 6 hours after treatment. Representative dot plots are shown. Bar charts show each myeloid population as the percentage of total intrahepatic leukocyte population (n = 7). (**C**) Neutrophils as a percentage of circulating leukocytes, measured in total blood 4 hours after injection (n = 5–8). (**D**) TNF-α and IL-12 production by liver myeloid subsets were analyzed by intracellular staining in neutrophils (CD11b$^+$ Gr-1^{hi}), monocytes (CD11b$^+$Gr-1^{intermediate}) and CD11b$^+$Gr-1$^-$ myeloid cells isolated from WT and Δ*MKK3/6* mice 4 and 6 hours after injection. Representative dot plots are shown for all treatment groups, and bar charts show TNF-α–positive cells as the percentage of each myeloid population (n = 7). Data are means ± SD. $^*P < 0.05$; $^{**}P < 0.01$; $^{***}P < 0.001$ (2-way ANOVA coupled to Bonferroni's post tests).

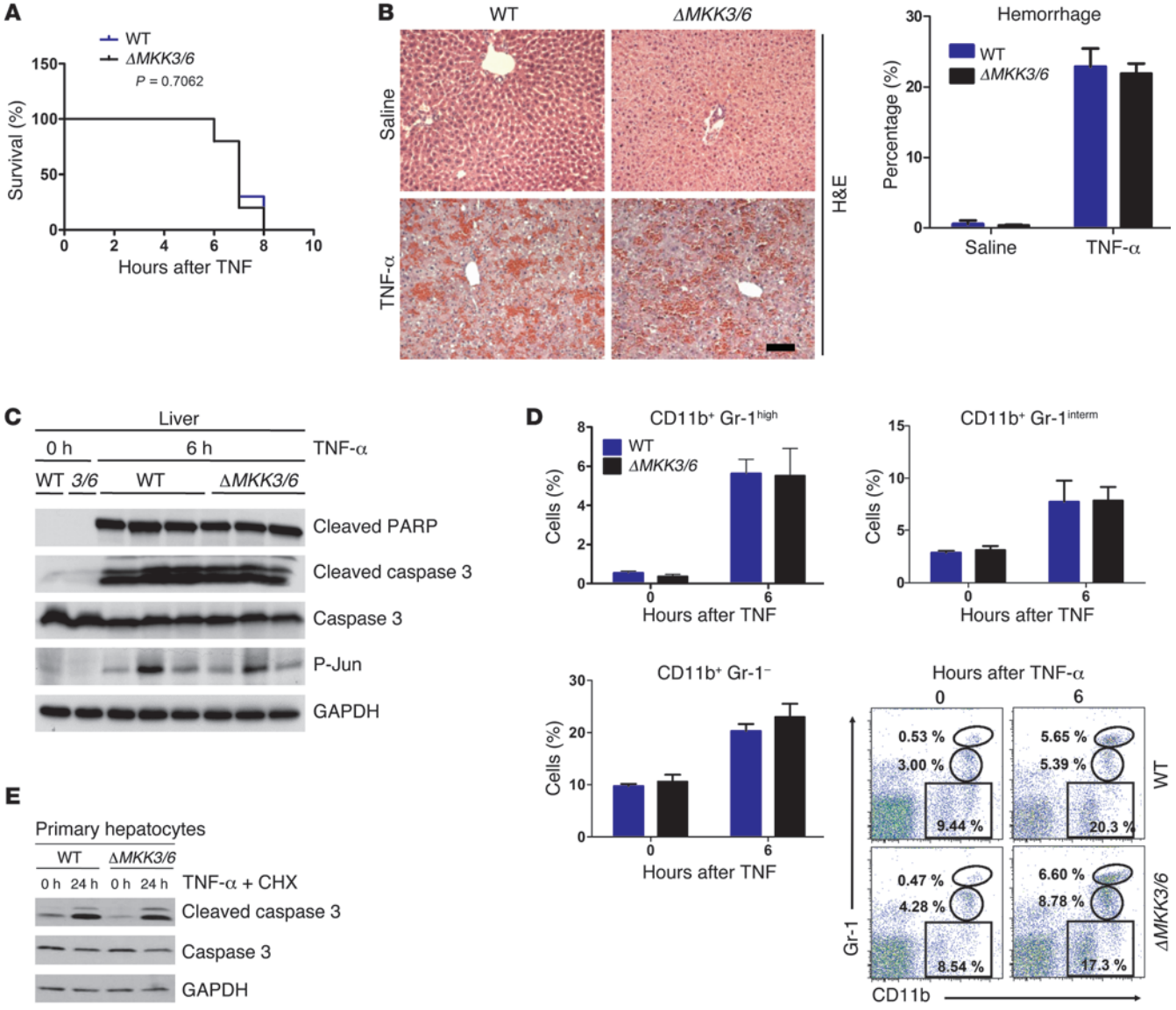

Figure 3

Δ*MKK3/6* mice are not protected against TNF-α–induced liver damage. WT and Δ*MKK3/6* mice were i.v. injected with 10 μg/kg TNF-α plus 1 g/kg D-gal (TNF-α/Gal) or with saline. (**A**) Survival curves after TNF-α/Gal injection (n = 13). Survival curves were created with the Kaplan-Meier method and compared by log-rank (Mantel-Cox) test. (**B**) Representative H&E-stained sections of livers extracted 6 hours after injection. The chart presents hemorrhagic area as a percentage of the total area (n = 8). Scale bar: 50 μm. (**C**) Liver extracts were examined by immunoblot analysis for cleaved PARP, cleaved caspase 3, caspase 3, phospho-Jun, and GAPDH (n = 6–8). (**D**) Liver myeloid subsets (CD11b$^+$Gr-1^{hi}, CD11b$^+$Gr-1^{intermediate}, CD11b$^+$Gr-1$^-$) were assessed by flow cytometry of liver leukocytes isolated from WT and Δ*MKK3/6* mice 4 and 6 hours after treatment. Representative dot plots are shown. Bar charts show each myeloid subset as a percentage of the total intrahepatic leukocyte population (n = 4–6). (**E**) Immunoblot of cleaved caspase 3, caspase 3, and GAPDH in WT and Δ*MKK3/6* primary hepatocytes treated with TNF-α (20 ng/ml) plus CHX (100 μg/ml). Data are means ± SD. No significant differences were found (2-way ANOVA coupled to Bonferroni's post tests).

WT and ΔMKK3/6 mice (Figure 3, A and B). Immunoblot analysis demonstrated that TNF-α stimulated a similar degree of caspase 3 and PARP cleavage (Figure 3C). Moreover, TNF-α induced the same levels of neutrophil liver infiltration in both genotypes (Figure 3D). To confirm that the protection was due to defective cytokine production and not to a protective loss of responsiveness to TNF-α, we treated primary hepatocytes from WT or ΔMKK3/6 mice with TNF-α and the protein synthesis inhibitor cycloheximide (CHX). Both hepatocyte populations presented the same level of apoptosis (Figure 3E). These data demonstrate that ΔMKK3/6 mice do not exhibit resistance to TNF-α–induced hepatitis and indicate that the primary protection against LPS-induced hepatitis in these mice is due to an inability to produce TNF-α.

MKK3 and MKK6 are required in the hematopoietic compartment for LPS-induced liver damage. The source of TNF-α in mouse models of hepatitis is the hematopoietic compartment (31, 32). There-

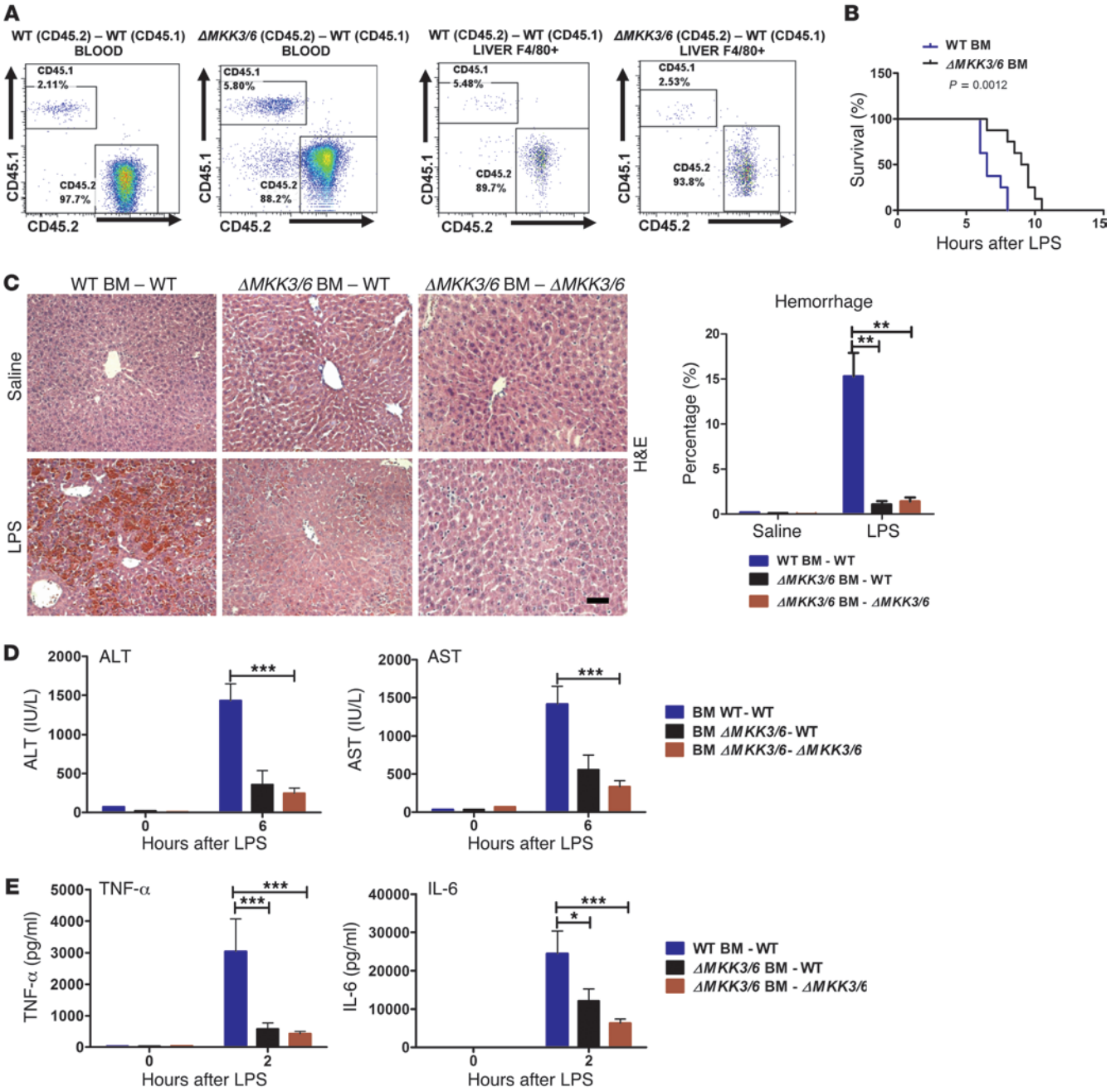

Figure 4

Δ*MKK3/6* hematopoietic cells protect mice against hepatitis. Lethally irradiated WT mice were reconstituted with BM from WT or Δ*MKK3/6* mice. Mice were treated with D-gal+LPS 2 months after transplantation. (**A**) 2×10^7 freshly prepared CD45.2 whole BM mononuclear cells were transplanted into lethally irradiated B6.SJL (CD45.1) mice, and engraftment by CD45.2 cells (%) was analyzed by antibody staining and FACS of peripheral blood after 4 months. Left panels: representative FACS dot plot of CD45.1 and CD45.2 expression in cells isolated from the blood of transplanted mice. Right panels: representative FACS dot plot of CD45.1 and CD45.2 expression in F4/80-positive cells isolated from the liver of transplanted mice ($n = 3$). (**B**) Survival curves after D-gal+LPS injection ($n = 10$). Survival curves were created with the Kaplan-Meier method and compared by log-rank (Mantel-Cox) test. (**C**) Representative H&E-stained sections of livers extracted 6 hours after injection. The chart presents hemorrhagic area as a percentage of the total area ($n = 5–8$). Scale bar: 50 μm. (**D**) Serum transaminase activity at 4 and 6 hours after injection ($n = 5–8$). (**E**) ELISA of serum TNF-α and IL-6 at different times after injection ($n = 5–8$). Data are means ± SD. $^*P < 0.05$; $^{**}P < 0.01$; $^{***}P < 0.001$ (2-way ANOVA coupled to Bonferroni's post tests).

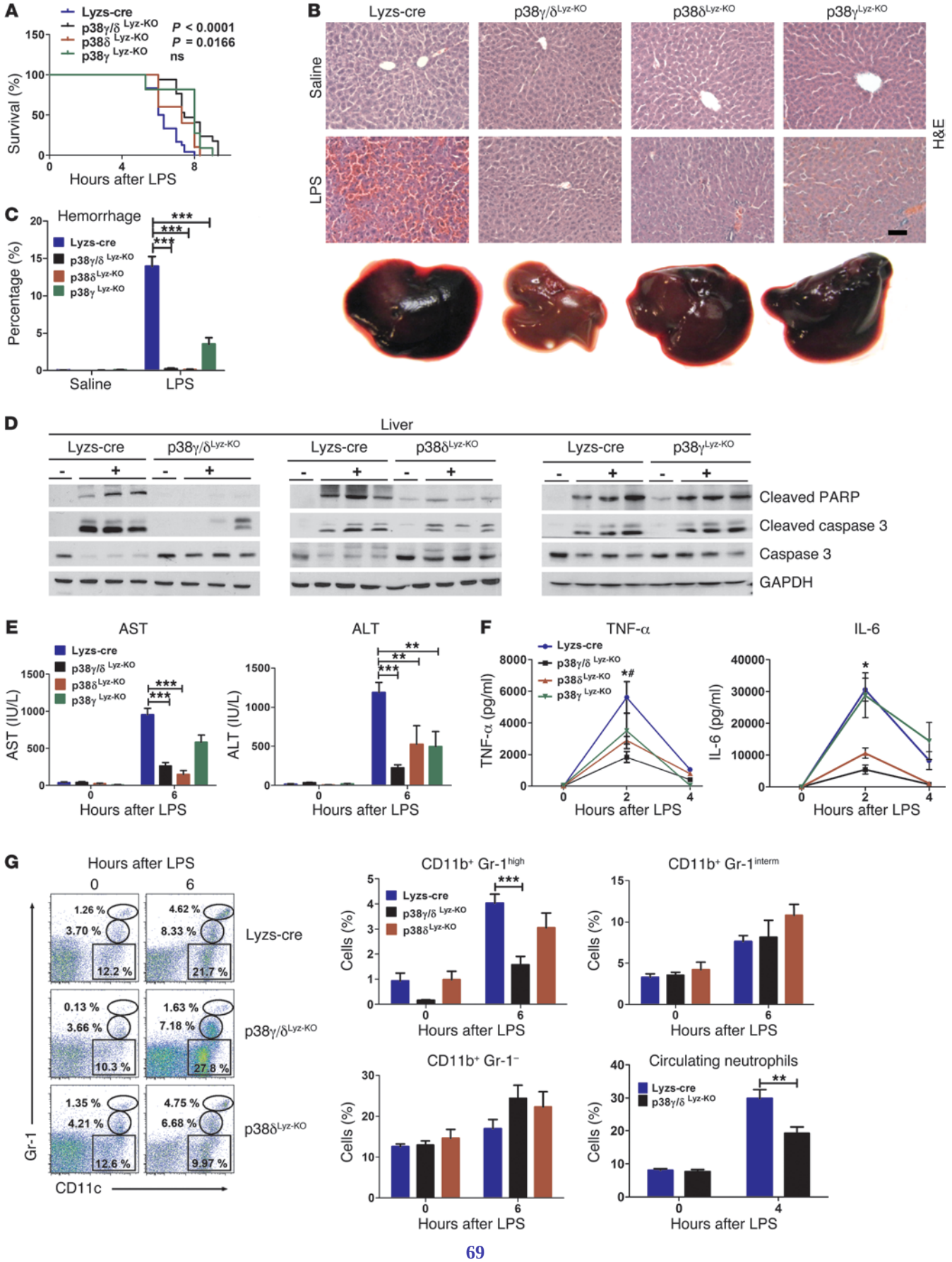
A
Lyzs-cre
p38γ/δ Lyz-KO
p38δ Lyz-KO
p38γ Lyz-KO
P < 0.0001
P = 0.0166
ns
Survival (%)
Hours after LPS
B
Lyzs-cre
p38γ/δLyz-KO
p38δLyz-KO
p38γLyz-KO
Saline
LPS
H&E
C
Hemorrhage
Percentage (%)
Saline
LPS
D
Liver
Cleaved PARP
Cleaved caspase 3
Caspase 3
GAPDH
E
AST
ALT
AST (IU/L)
ALT (IU/L)
Hours after LPS
F
TNF-α
IL-6
TNF-α (pg/ml)
IL-6 (pg/ml)
Hours after LPS
G
Hours after LPS
1.26 %
3.70 %
12.2 %
4.62 %
8.33 %
21.7 %
0.13 %
3.66 %
10.3 %
1.63 %
7.18 %
27.8 %
1.35 %
4.21 %
12.6 %
4.75 %
6.68 %
9.97 %
Gr-1
CD11c
CD11b+ Gr-1high
CD11b+ Gr-1interm
CD11b+ Gr-1−
Circulating neutrophils
Cells (%)
Hours after LPS

Figure 5
p38γ/δ$^{Lyz\text{-}KO}$ mice are protected against LPS-induced liver damage. p38γ$^{Lyz\text{-}KO}$, p38δ$^{Lyz\text{-}KO}$, p38γ/δ$^{Lyz\text{-}KO}$, and control Lyzs-cre transgenic mice were injected with D-gal+LPS or saline. (**A**) Mouse survival after D-gal+LPS injection (n = 14). Survival curves were created with the Kaplan-Meier method and compared by log-rank (Mantel-Cox) test. (**B**) Livers were removed at 6 hours after injection. Panels show representative H&E-stained liver sections and livers (n = 5–8). Scale bar: 50 μm. (**C**) Hemorrhagic area as a percentage of the total area on H&E-stained liver sections (n = 5–8). (**D**) Immunoblot analysis of liver extracts (n = 5–8). (**E**) Serum transaminase activity at 6 hours after injection (n = 8–10). (**F**) ELISA of serum TNF-α and IL-6 at different times after injection (n = 10). $^{\#}P < 0.01$ for Lyzs-cre versus p38δ$^{Lyz\text{-}KO}$ mice in TNF-α; $^{*}P < 0.001$ for Lyzs-cre versus p38γ/δ$^{Lyz\text{-}KO}$ mice for TNF-α and for Lyzs-cre versus p38γ/δ$^{Lyz\text{-}KO}$ or p38δ$^{Lyz\text{-}KO}$ mice in IL-6 (n = 6–8). (**G**) Liver myeloid subsets (CD11b^{+}Gr-1^{hi}, CD11b^{+}Gr-1^{intermediate}, CD11b^{+}Gr-1^{-}) were assessed by flow cytometry of liver leukocytes isolated from p38γ$^{Lyz\text{-}KO}$, p38δ$^{Lyz\text{-}KO}$, p38γ/δ$^{Lyz\text{-}KO}$, and control Lyzs-cre transgenic mice 6 hours after injection. Representative dot plots are shown. Bar charts show each myeloid population as a percentage of the total intrahepatic leukocyte population (mean ± SD; n = 4–6). Circulating neutrophils in total blood were measured as a percentage of circulating leukocytes 4 hours after injection (n = 5–8). Data are means ± SD. $^{**}P < 0.01$; $^{***}P < 0.001$ (2-way ANOVA coupled to Bonferroni's post tests).

fore, if defective TNF-α expression accounts for the protection of ΔMKK3/6 mice against TNF-α–dependent hepatitis, transplantation of the hematopoietic compartment of ΔMKK3/6 mice to immunodeficient donors should confer this protection. To test the role of hematopoietic cells, we constructed radiation chimeras by transplanting BM from WT and ΔMKK3/6 donor mice into lethally irradiated congenic WT and ΔMKK3/6 recipients. Efficient reconstitution of B6.SJL (CD45.1) mice with BM from WT C57BL/6J (CD45.2) or ΔMKK3/6 (CD45.2) mice was confirmed by flow cytometry analysis of peripheral blood leukocytes stained with antibodies to CD45.1/CD45.2. Moreover, analysis of Kupffer cells (F4/80^{+}) in the liver of recipients after transplantation showed that more than 90% of Kupffer cells originated from the donor mice (Figure 4A).

We found that lethally irradiated mice reconstituted with ΔMKK3/6 BM were indeed protected against LPS-induced mortality and exhibited lower levels of LPS-stimulated serum TNF-α and hepatic damage than mice reconstituted with WT BM (Figure 4, B–E). These data confirm that MKK3 and MKK6 expressed in hematopoietic cells play a critical role in the expression of TNF-α that leads to the development of hepatitis.

Inhibition of p38γ and p38δ protects against LPS-induced hepatitis. MKK3 and MKK6 are the main regulators of the α, β, γ, and δ p38 MAPK isoforms. To determine which isoforms mediate MKK3/MKK6-induced TNF-α expression, we analyzed the effect on D-gal+LPS–induced liver damage of 2 inhibitors: SB203580, which inhibits p38α and p38β, and BIRB796, which inhibits all isoforms (33). We treated mice with BIRB796, SB203580, or DMSO prior to LPS injection. We first examined the specific action of these inhibitors on MAPK pathway activity. Both compounds efficiently inhibited p38α/β, as shown by the loss of the phosphorylation of the known p38α substrate HSP27 (Supplemental Figure 4A and ref. 34). In contrast, only BIRB796 was able to inhibit p38δ activation, as indicated by suppression of the phosphorylation of its substrate, eEF2K (19). No changes in ERK or JNK phosphorylation were observed (Supplemental Figure 4A). Injection of BIRB796 into WT mice protected against D-gal+LPS–induced liver damage, whereas SB203580 exacerbated liver damage (hemorrhage, apoptosis, and necrosis) (Supplemental Figure 4, B–D). Injection of BIRB796 also reduced serum levels of IL-6 and TNF-α in D-gal+LPS–treated mice (Supplemental Figure 4E). These results suggest that LPS-induced liver injury might be mediated by p38γ and p38δ.

Myeloid expression of p38γ and p38δ is required for LPS-induced hepatitis. To investigate the role of p38γ and p38δ in LPS-induced hepatitis, we generated mice with myeloid cell–specific ablation of these p38 isoforms, separately and in combination. Mice carrying conditional loxP-flanked alleles for p38γ, p38δ, and p38γ/δ (p38γ^{fl}, p38δ^{fl}, and p38γ/δ^{fl} mice) were crossed with Lyzs-cre transgenic mice (35), yielding p38γ$^{Lyz\text{-}KO}$, p38δ$^{Lyz\text{-}KO}$, and p38γ/δ$^{Lyz\text{-}KO}$ mice. Immunoblot analysis confirmed efficient ablation of the appropriate kinases in macrophages, neutrophils, and Kupffer cells (Supplemental Figure 5, A and B).

Compared with control Lyzs-cre transgenic mice, p38δ$^{Lyz\text{-}KO}$ and p38γ/δ$^{Lyz\text{-}KO}$ mice showed a delay in mortality in response to injection of D-gal+LPS (Figure 5A). These mice were also protected against liver damage and apoptosis, showing milder liver hemorrhaging, reduced serum levels of ALT and AST, and reduced caspase 3 cleavage (Figure 5, B–E). Analysis of cytokines revealed significantly lower circulating TNF-α and IL-6 in LPS-injected p38δ$^{Lyz\text{-}KO}$ and p38γ/δ$^{Lyz\text{-}KO}$ mice than in similarly treated Lyzs-cre controls (Figure 5F). Other chemokines involved in leukocyte migration (MIP1α and MIP1β) were also reduced (Supplemental Figure 6). In contrast, p38γ$^{Lyz\text{-}KO}$ mice presented only a modest effect on circulating TNF-α levels and no differences in the levels of other cytokines (Figure 5F and Supplemental Figure 6).

The phenotype found in p38γ/δ$^{Lyz\text{-}KO}$ mice might reflect the function of these kinases in several myeloid cell populations implicated in D-gal+LPS damage (such as neutrophils, Kupffer cells, and macrophages). Analysis of these cell types in Lyzs-cre mice revealed expression of p38γ and p38δ in macrophages, predominant expression of p38δ in neutrophils, and exclusive expression of p38γ in Kupffer cells (Supplemental Figure 5A). Moreover, p38γ is strongly activated in Kupffer cells by LPS or TNF-α treatment (Supplemental Figure 5B), as judged by the impaired p38 phosphorylation observed by FACS in Kupffer cells from p38γ/δ$^{Lyz\text{-}KO}$ mice. Furthermore, analysis of phospho-p38 by Western blot confirmed that p38γ was the isoform activated in these cells after LPS treatment (Supplemental Figure 5C). LPS and TNF-α also activated p38γ and p38δ in macrophages (Figure 6), while in neutrophils, p38α was the only isoform activated after either stimulus (Supplemental Figure 5, B and D). Since neutrophils, Kupffer cells, and macrophages express p38γ, p38δ, or both isoforms, any of these cell populations could have a role in the protection observed in p38γ/δ$^{Lyz\text{-}KO}$ mice. We therefore analyzed the different leukocyte populations that infiltrated the liver after D-gal+LPS injection. Analysis of liver-infiltrating leukocytes showed lower numbers of neutrophils in LPS-injected p38γ/δ$^{Lyz\text{-}KO}$ mice than in similarly treated Lyzs-cre mice. However, this reduction was not significant in LPS-injected p38δ$^{Lyz\text{-}KO}$ mice (Figure 5G). None of the myeloid-specific p38-deficient mice showed alterations in the percentages of infiltrated macrophages or monocytes. Collectively, these data show that p38γ/δ$^{Lyz\text{-}KO}$ mice are more strongly affected than either of the single conditional knockouts; however, p38δ$^{Lyz\text{-}KO}$ animals have a stronger phenotype than p38γ$^{Lyz\text{-}KO}$ mice, indicating partial

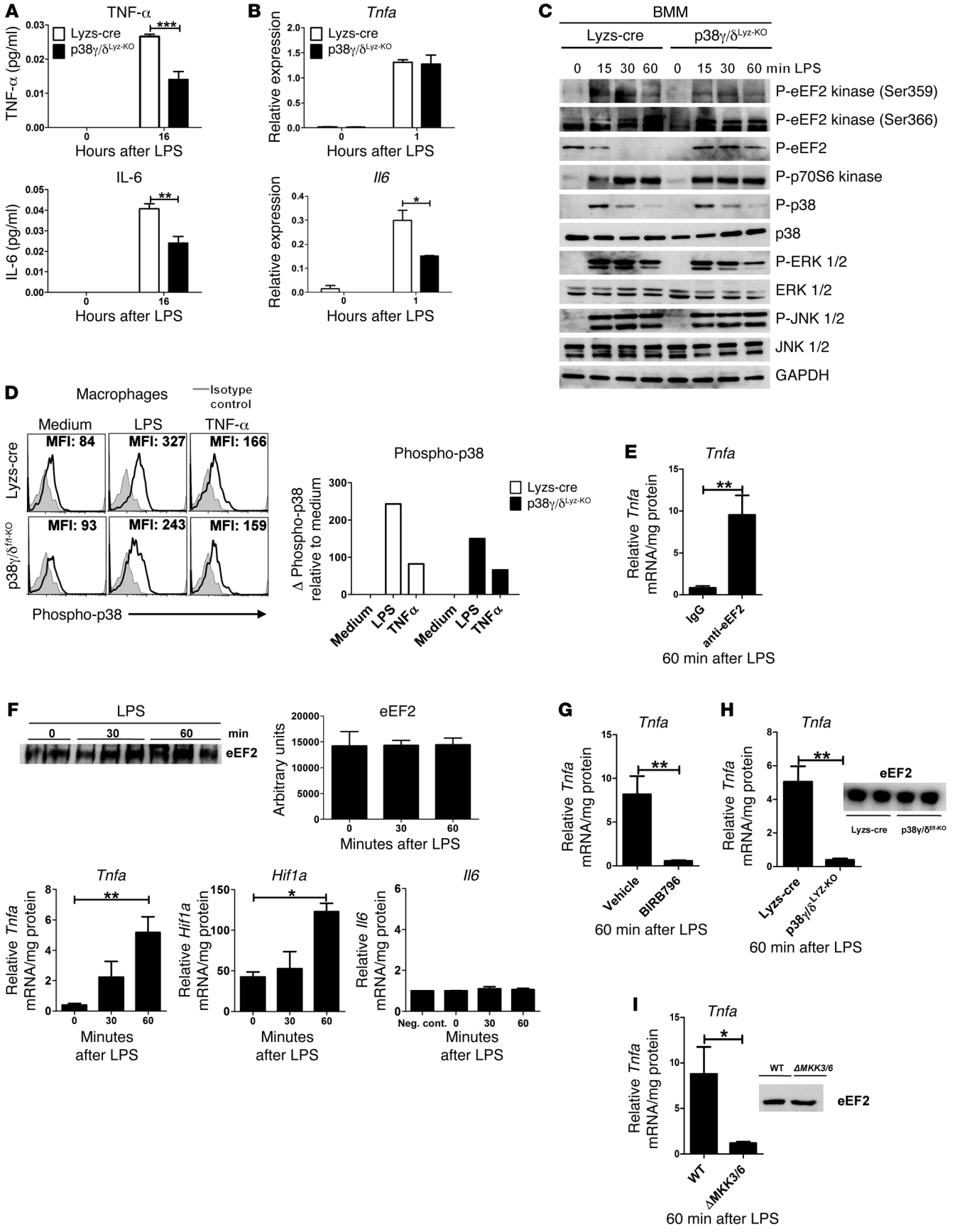
A
TNF-α
Lyzs-cre
p38γ/δLyz-KO
TNF-α (pg/ml)
Hours after LPS
IL-6
IL-6 (pg/ml)
B
Tnfa
Relative expression
Il6
C
BMM
Lyzs-cre
p38γ/δLyz-KO
0 15 30 60 0 15 30 60 min LPS
P-eEF2 kinase (Ser359)
P-eEF2 kinase (Ser366)
P-eEF2
P-p70S6 kinase
P-p38
p38
P-ERK 1/2
ERK 1/2
P-JNK 1/2
JNK 1/2
GAPDH
D
Macrophages
Isotype control
Medium
LPS
TNF-α
Lyzs-cre
p38γ/δf/f-KO
MFI: 84
MFI: 327
MFI: 166
MFI: 93
MFI: 243
MFI: 159
Phospho-p38
Δ Phospho-p38 relative to medium
E
Tnfa
Relative Tnfa mRNA/mg protein
IgG
anti-eEF2
60 min after LPS
F
LPS
min
eEF2
Arbitrary units
Minutes after LPS
Hif1a
Il6
Neg. cont.
G
Vehicle
BIRB796
H
Lyzs-cre
p38γ/δLYZ-KO
I
WT
ΔMKK3/6

Figure 6
p38γ/δ$^{Lyz\text{-}KO}$ macrophages promote TNF-α translation through phosphorylation of eEF2 kinase. (**A**–**D**) BM-derived macrophages from p38γ/δ$^{Lyz\text{-}KO}$ and Lyzs-cre mice were treated with LPS (10 μg/ml) or TNF-α (20 ng/ml). Data were analyzed by 2-way ANOVA coupled to Bonferroni's post tests. (**A**) ELISA of TNF-α and IL-6 in supernatants. (**B**) qRT-PCR of *Tnfa* and *Il6* mRNA normalized to *Gapdh*. (**C**) Immunoblot of BM-derived macrophage (BMM) lysates. (**D**) Flow cytometry of phospho-p38 in BM-derived macrophages stimulated with LPS and TNF-α for 30 minutes. Intracellular phospho-p38 is depicted in black; gray corresponds to the isotype control. (**E**–**I**) Cells were treated with LPS. *Tnfa* mRNA was detected by qRT-PCR in immunoprecipitates (1 mg protein) obtained with anti-eEF2. mRNA amounts are expressed relative to the amount detected in control IgG immunoprecipitates. Data were analyzed by Student's *t* test unless otherwise indicated. (**E**) *Tnfa* mRNA in RAW 264.7 cell immunoprecipitates. (**F**) *Tnfa*, *Hif1a*, and *Il6* mRNA in RAW 264.7 cell immunoprecipitates. The presence of eEF2 was determined by immunoblot (upper panel) and quantified with ImageJ (1-way ANOVA coupled to Bonferroni's post tests). (**G**) RAW 264.7 cells were pretreated with DMSO or BIRB796 (10 μM) for 30 minutes before stimulation with LPS (60 minutes). *Tnfa* mRNA was measured in immunoprecipitates. (**H** and **I**) *Tnfa* mRNA in immunoprecipitates of BM-derived macrophages from Lyzs-cre and 38γ/δ$^{Lyz\text{-}KO}$ mice (**H**) or WT or ΔMKK3/6 mice (**I**) after stimulation (60 minutes). eEF2 in immunoprecipitates was detected by immunoblot (upper panel). Data are means ± SD (n = 4). *P < 0.05; **P < 0.01; ***P < 0.001.

redundancy between p38γ and p38δ, with a predominant role of p38δ. This overlapping action has been shown before and might account for the limited protection observed in single conditional knockouts (36, 37). We therefore used p38γ/δ$^{Lyz\text{-}KO}$ mice for further experiments. Further studies showed that the reduced neutrophil infiltration in liver is, in part, caused by lowered neutrophil mobilization from the BM (Figure 5G), probably due to the defective production of TNF-α. Furthermore, measurement of TNF-α–stimulated chemotaxis in a chamber assay revealed a slightly lower-than-control mobility in p38γ/δ$^{Lyz\text{-}KO}$ neutrophils (Supplemental Figure 8A), and this effect was not increased by stimulation with a cytokine cocktail (Supplemental Figure 8B). Neutrophils produce several cytokines, and this function can be controlled by p38α (29). Examination of cytokine production in our system showed that p38γ/δ$^{Lyz\text{-}KO}$ neutrophils express slightly reduced levels of TNF-α and IL-6 after LPS treatment, but not sufficient to explain the phenotype observed (Supplemental Figure 8C).

To investigate whether the lower neutrophil infiltration in the livers of p38γ/δ$^{Lyz\text{-}KO}$ mice could account for the protection observed, we investigated whether neutrophil-specific depletion in Lyzs-cre mice results in milder liver damage upon D-gal+LPS treatment, similar to the phenotype of p38γ/δ$^{Lyz\text{-}KO}$ mice. GR1 is highly expressed on neutrophils, and anti-GR1 antibody treatment has been shown to specifically deplete neutrophils (38). Treatment of mice with anti-GR1 one day before D-gal+LPS injection completely depleted Gr1$^+$ neutrophils (Supplemental Figure 8D). Neutrophil depletion did not affect liver damage in Lyzs-cre mice, and neither did it abolish the protection observed in p38γ/δ$^{Lyz\text{-}KO}$, as assessed by the levels of ALT and AST, cleaved caspase 3, and PARP, or liver damage observed in H&E-stained sections (Supplemental Figure 8, E–G).

These data indicate that neutrophils do not play a dominant role in the protection against D-gal+LPS–stimulated hepatic damage observed in p38γ/δ$^{Lyz\text{-}KO}$ mice and therefore indicate that a different myeloid cell type underlies this phenotype. Available evidence suggests an involvement of cytokine and chemokine production by activated Kupffer cells and infiltrated macrophages in the pathogenesis of liver damage (39). We therefore examined cytokine production by macrophages and Kupffer cells upon LPS treatment. ELISA analysis demonstrated that LPS-induced production of TNF-α and IL-6 was lower in p38γ/δ$^{Lyz\text{-}KO}$ macrophages and Kupffer cells than in Lyzs-cre control cells (Figure 6A and Supplemental Figure 7C). Moreover, only the supernatant from macrophages of p38γ/δ$^{Lyz\text{-}KO}$ animals was unable to induce apoptosis in primary hepatocytes (Supplemental Figure 7A), and analysis of this supernatant indicated a defect in cytokine production (Figure 6A and Supplemental Figure 7B). Similarly, induction of apoptosis by supernatant from control Lyzs-cre macrophages was blocked by addition of anti–TNF-α antibody, resulting in a protection similar to that obtained with p38γ/δ$^{Lyz\text{-}KO}$ supernatant (Supplemental Figure 7C). This finding thus indicates that the low TNF-α levels in p38γ/δ$^{Lyz\text{-}KO}$ macrophages and Kupffer cells could account for the protection against D-gal+LPS–induced liver damage.

p38γ and p38δ mediate TNF-α translation in myeloid cells by phosphorylating eEF2K. p38 MAPK can promote cytokine expression at the level of transcription, after transcription (by promoting mRNA stability), and translation (27, 40). *Il6* mRNA expression was reduced in p38γ/δ$^{Lyz\text{-}KO}$ macrophages, but levels of *Tnfa* mRNA were comparable to those in Lyzs-cre macrophages (Figure 6B). The stability of *Tnfa* mRNA also showed no difference between the 2 genotypes (Supplemental Figure 7F). The translational action of p38δ has been linked to eEF2 kinase, the enzyme that inactivates eEF2. This kinase is inhibited by p38δ-mediated phosphorylation on Ser359 and also by ribosomal protein S6 kinase–mediated phosphorylation on Ser366 (19, 23). Since little is known about the regulation of eEF2K in macrophages, we investigated the effect of p38γ/δ deletion on the phosphorylation of eEF2K and its downstream substrate eEF2. LPS stimulation of Lyzs-cre macrophages induced eEF2K phosphorylation on Ser359, but this was markedly impaired in p38γ/δ$^{Lyz\text{-}KO}$ macrophages (Figure 6C). This observation was also corroborated in Kupffer cells (Supplemental Figure 7D). eEF2K phosphorylation in Lyzs-cre macrophages correlated with dephosphorylation of eEF2, implying activation of elongation. In contrast, p38γ/δ$^{Lyz\text{-}KO}$ macrophages sustained high levels of eEF2 phosphorylation after the stimulus, suggesting that elongation is abolished.

To assess whether eEF2 controls TNF-α elongation, we examined the binding of eEF2 to *Tnfa* mRNA in immunoprecipitates of mRNA-eEF2 complexes in RAW cells. RAW extracts were incubated with anti-eEF2 or an isotype control antibody, and the presence of *Tnfa* mRNA in the immunoprecipitates was examined by quantitative (q) real-time PCR. High relative levels of *Tnfa* mRNA were detected in the anti-eEF2 immunoprecipitate, and this association was increased by LPS treatment (Figure 6, E and F). High mRNA levels for *Hif1a*, a known eEF2 target, were also detected in the anti-eEF2 immunoprecipitate (Figure 6F). In contrast, *Il6* mRNA levels did not differ between the anti-eEF2 and isotype control immunoprecipitates (Figure 6F). Pretreatment of RAW cells with BIRB796 abolished the association of eEF2 with *Tnfa* mRNA (Figure 6G). Moreover, *Tnfa* mRNA was detected in anti-eEF2 immunoprecipitates from LPS-treated Lyzs-cre or WT BM–derived macrophages but not in immunoprecipitates from similarly treated p38γ/δ$^{Lyz\text{-}KO}$ or ΔMKK3/6 macrophages (Figure 6, H and I). Together, our data indicate that *Tnfa* mRNA is a selective target of eEF2 and that

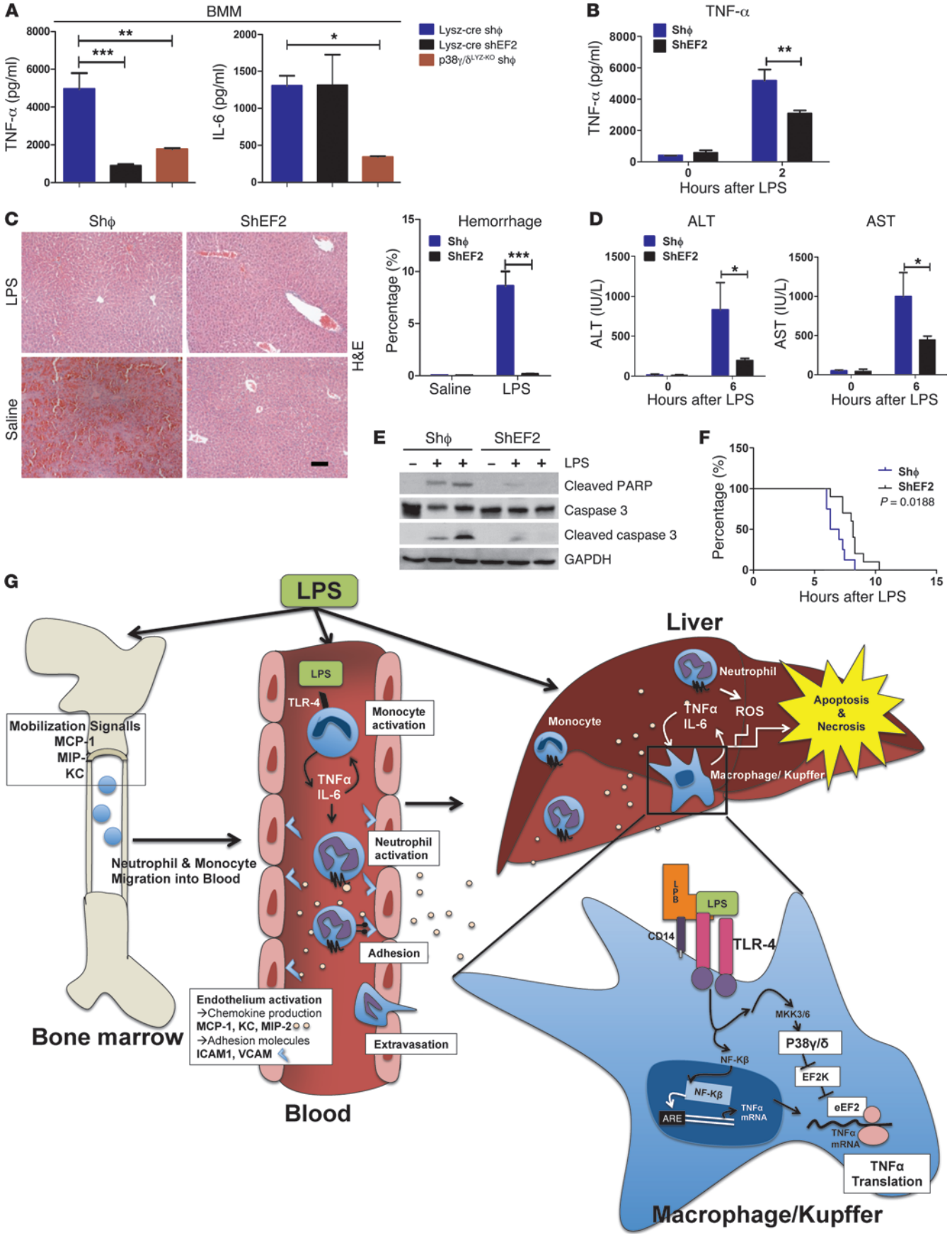
A
BMM
TNF-α (pg/ml)
IL-6 (pg/ml)
Lysz-cre shϕ
Lysz-cre shEF2
p38γ/δ LYZ-KO shϕ
B
TNF-α
Shϕ
ShEF2
TNF-α (pg/ml)
Hours after LPS
C
Shϕ
ShEF2
LPS
Saline
H&E
Hemorrhage
Percentage (%)
Saline
LPS
D
ALT
AST
ALT (IU/L)
AST (IU/L)
Hours after LPS
E
Shϕ
ShEF2
LPS
Cleaved PARP
Caspase 3
Cleaved caspase 3
GAPDH
F
Shϕ
ShEF2
P = 0.0188
Percentage (%)
Hours after LPS
G
LPS
Liver
Neutrophil
Monocyte
TNFα
IL-6
ROS
Apoptosis & Necrosis
Macrophage/ Kupffer
Mobilization Signalls
MCP-1
MIP-2
KC
Neutrophil & Monocyte Migration into Blood
TLR-4
Monocyte activation
Neutrophil activation
Adhesion
Extravasation
Endothelium activation
→Chemokine production
MCP-1, KC, MIP-2
→Adhesion molecules
ICAM1, VCAM
Bone marrow
Blood
LPB
CD14
MKK3/6
P38γ/δ
NF-Kβ
EF2K
eEF2
ARE
TNFα mRNA
TNFα Translation
Macrophage/Kupffer

Figure 7
eEF2 controls TNF-α elongation, and its gene silencing protects against LPS-induced liver damage. (**A**) BM-derived macrophages from Lyzs-cre and p38γ/δ$^{Lyz\text{-}KO}$ mice were transduced with GFP$^+$ lentivirus expressing eEf2 shRNA (shEF2) or with empty vector (shΦ). ELISA of TNF-α and IL-6 in culture supernatants was performed 16 hours after LPS (10 μg/ml) stimulation. One-way ANOVA coupled to Bonferroni's post tests (n = 6). (**B**–**F**) WT mice were i.v. injected with shEF2 or shΦ GFP$^+$ lentiviral vectors. After 7 days, mice were injected with D-gal+LPS or saline. Data are means ± SD. *P < 0.05; **P < 0.01; ***P < 0.001 (2-way ANOVA coupled to Bonferroni's post tests). (**B**) ELISA of TNF-α and IL-6 in mouse serum 6 hours after treatment (n = 6). (**C**) Representative livers and H&E-stained sections after removal at 6 hours after injection The chart presents hemorrhagic area as a percentage of the total area (n = 6). Scale bar: 50 μm. (**D**) Serum transaminase activity at 6 hours after injection (n = 6). (**E**) Immunoblot analysis of liver extracts (n = 6). (**F**) Mouse survival after D-gal+LPS injection (n = 10). Survival curves were created with the Kaplan-Meier method and compared by log-rank (Mantel-Cox) test. (**G**) The MKK3/6-p38γ/δ-eEF2K pathway is necessary for LPS-induced hepatitis. LPS induces leukocyte egress from BM and cytokine/chemokine production in peripheral blood and by Kupffer cells. This leads to massive leukocyte infiltration in the liver and hepatocellular injury. TNF-α plays a dominant role in LPS-induced liver injury. Activation of the MKK3/6-p38γ/δ-eEF2K pathway in macrophages/Kupffer cells controls TNF-α production at the mRNA elongation level in acute inflammatory responses to LPS.

the MKK3/6-p38γ/δ pathway, by releasing eEF2K-mediated inhibition of eEF2 activity, promotes the translational elongation of TNF-α in macrophages.

eEF2 controls TNF-α translation elongation. To confirm eEF2 control of TNF-α translation elongation, we used a recombinant lentivirus expressing an eEF2 shRNA (shEF2), which causes robust eEF2 knockdown in RAW cells (Supplemental Figure 9A). In macrophages, shEF2-mediated loss of eEF2 caused a decrease in TNF-α production of a magnitude similar to that caused by loss of p38γ/δ (Figure 7A). In contrast, p38γ/δ-dependent IL-6 production was eEF2 independent (Figure 7A). These data indicate that the expression of TNF-α is controlled by eEF2, while the reduced IL-6 production in p38γ/δ$^{Lyz\text{-}KO}$ mice is caused by a different mechanism, most likely the loss of p38γ/δ-regulated *Il6* gene transcription.

To test the role of eEF2 in vivo, we injected mice with the shEF2 lentivirus or control shRNA lentivirus 1 week before exposure to D-gal+LPS. Blood levels of TNF-α were strongly reduced by the shEF2-injected mice compared with controls (Figure 7B). Moreover, this reduction in TNF-α was associated with protection against hepatic cell death, measured by cleavage of caspase 3 and PARP and protection against hepatic necrosis, and measured by liver hemorrhage and blood levels of ALT and AST (Figure 7, C–E). Collectively, these data indicate that p38γ/δ MAPK proteins are required for the translation elongation of TNF-α in macrophages mediated by phosphorylation of eEF2K and the activation of eEF2.

Discussion

In this study,we show that protein kinases p38γ/δ mediate the development of LPS-induced acute hepatitis by acting within a protein kinase signaling network that regulates the production of TNF-α by hematopoietic cells. MKK3 and MKK6 activate p38γ/δ (14, 15), which in turn phosphorylate and inactivate eEF2 kinase (41). Once eEF2K is inactivated, eEF2 is dephosphorylated and activated, allowing the translational elongation of nascent TNF-α. To our knowledge, this is the first report that eEF2 or p38γ/δ control cytokine production in myeloid cells. Our findings raise 3 key areas of interest: the specific role of myeloid cells, the involvement of p38γ/δ compared with that of the other kinases of the same family, and how acute inflammatory responses can be controlled through tight regulation of translational elongation.

Myeloid cells such as Kupffer cells and other macrophages are well known to be a critical source of TNF-α in LPS-induced hepatitis (14, 32). This specific role of hematopoietic cells is consistent with our finding that the protective effects of MKK3/6 deficiency are also present in irradiated WT mice reconstituted with ΔMKK3/6 BM (Figure 5). Furthermore, this protection was also observed in mice specifically lacking p38γ/δ in the myeloid compartment (Figure 6). Two cell types of special relevance in acute hepatitis are neutrophils and monocytes/macrophages (including Kupffer cells), and both of these BM-derived cell populations are essential for the innate immune response (42). Monocytes/macrophages bind to microbial constituents (such as LPS and cell wall constituents of Gram-positive bacteria), producing large amounts of pro- and antiinflammatory cytokines (3). Neutrophil recruitment and activation occur through TNF-α–mediated chemokine production (3). This is evidenced by our finding that low expression of TNF-α in ΔMKK3/6 or p38γ/δ$^{Lyz\text{-}KO}$ mice results in decreased chemokine production and neutrophil migration, an effect reversed by injection with TNF-α. We did not find, however, any evidence for a role of p38γ/δ in neutrophil migration, and we found only a minor effect on cytokine expression. This contrasts with the recent finding that p38α can control cytokine production by neutrophils (29), illustrating the different roles and clinical potential of p38 kinase isoforms as targets for preventing LPS-induced damage.

Previous reports have identified p38α as a key kinase involved in TNF-α production (43). p38α MAPK deficiency in macrophages results in decreased TNF-α production, with a modest effect on IL-6 expression (44). However, specific inhibition of this kinase has been shown to be hepatotoxic, hindering its clinical use. For example, the p38α inhibitor AMG 548 showed more than 85% inhibition of ex vivo LPS-induced TNF-α in healthy males, but its production and clinical use were suspended due to random liver enzyme elevations that were not dose or exposure dependent (45). Our results show that specific inhibition of p38α/β with SB203580 intensifies D-gal+LPS–induced liver damage, whereas BIRB796, which inhibits all 4 p38 isoforms (α/β/γ/δ) improves liver condition, including a reduction in apoptosis and necrosis. The toxicity associated with SB203580 might be caused by inhibition of p38α in hepatocytes, since mice with specific p38α deficiency in hepatocytes have increased JNK activity and increased susceptibility to liver damage (17, 43). In clinical use, BIRB796 also produces some liver enzyme elevations (46), most likely because of inhibition of p38. Our findings indicate that the generation of inhibitors that specifically target p38γ/δ kinases might avoid the adverse effects found with p38α inhibitors.

Our results further show that p38γ/δ control macrophage production of TNF-α by promoting protein elongation during translation by eEF2. Protein synthesis is tightly regulated at transcriptional and posttranscriptional levels. Owing to the relatively long life time of mRNA transcripts, transcriptional regulation is commonly involved in slow, long-term cell responses, whereas immediate cell responses require posttranscriptional regulation of mRNA stability or translation. Two physiological situations requiring rapid regulation of protein synthesis are starvation and inflam-

matory conditions. In starvation conditions, mTOR stops protein synthesis at the elongation step — the step that consumes most metabolic energy — by inhibiting eEF2, thereby preventing cell energy depletion. Less is known about the mechanisms involved in the termination of the inflammatory response once it has achieved its goal. This process needs to be rapidly regulated in order to avoid more tissue damage. Our results suggest that control of protein elongation might be an important mechanism by which cells rapidly shut down production of proinflammatory proteins that could extend tissue damage in the body, such as TNF-α during an inflammatory response. This might be an important mechanism by which cells tightly regulate cytokine production induced by stress kinases activated during inflammation.

In summary, we conclude that p38γ/δ in myeloid cells promote TNF-α production by activating its translation without changes in mRNA levels. This is achieved by phosphorylation of eEF2K, releasing the inhibitory action of this kinase on eEF2. This post-transcriptional regulation might be an important mechanism regulating cytokine secretion during the innate immune response and provides potential targets for the treatment of liver diseases.

Methods

Mice. *Mkk3*$^{-/-}$ (B6.129-*Map2k3*^{tm1Flv}) (47, 48) and *Mkk6*$^{-/-}$ (B6.129-*Map2k6*^{tm1Flv}) mice (49) were as previously described (14). p38γ (B6.129-*Mapk12*^{tm1}) and p38δ (B6.129-*Mapk13*^{tm1}) mice were crossed with B6.129P2-*Lyz2tm1(cre)Ifo*/J and backcrossed for 10 generations to the C57BL/6J background (Jackson Laboratory) and genotyped by PCR analysis of genomic DNA. Radiation chimeras were generated by exposing recipient mice to 2 doses of ionizing radiation (525 Gy) and reconstituting them with 2 × 10^7 donor BM cells by injection into the tail vein. Hepatitis was induced by i.p. injection with 50 μg/kg *E. coli* 0111:B LPS (Sigma-Aldrich) plus 1 g/kg D-gal (Sigma-Aldrich) or by i.v. injection with 10 μg/kg TNF-α (R&D Systems) plus 1 g/kg GalN. When required, inhibitors were administered by i.p. injection at 15 mg/kg as previously reported (50, 51). For in vivo neutrophil depletion, 300 μg/mouse of anti-Gr1 or the same volume of saline were i.v. injected 24 hours before challenge with LPS. Specificity of the depletion of cell populations was determined by flow cytometry of blood samples collected during the experiment.

Lentivirus vector production and infection of mice. Lentiviruses were produced as described (52). Transient calcium phosphate cotransfection of HEK-293 cells was done with the pGIZP empty vector or pGIZP.shEF2 vector (Thermo Scientific) together with pΔ8.9 and pVSV-G. The supernatants containing the LV particles were collected 48 and 72 hours after removal of the calcium phosphate precipitate and were centrifuged at 700 *g* at 4°C for 10 minutes and concentrated (×165) by ultracentrifugation for 2 hours at 121 986 *g* at 4°C (Ultraclear Tubes, SW28 rotor and Optima L-100 XP Ultracentrifuge; Beckman). Viruses were collected by adding cold sterile PBS and were titrated by qPCR.

Mice were injected in the tail vein with 200 μl lentiviral particles suspended in PBS. Seven days after infection, mice were injected with LPS+D-gal.

Cell culture. Primary BM-derived macrophages were prepared and cultured as described previously (53). To isolate primary Kupffer cells from mouse livers, we performed collagenase perfusion and differential centrifugation using Percoll (Pharmacia) as described previously (54). BM neutrophils were purified by positive selection using biotinylated GR-1 (BD Biosciences — Pharmingen) and MACS streptavidin microbeads (Miltenyi Biotec). Neutrophil purity was 95% or greater, as assessed by flow cytometry (55). Cytokines in the culture medium were measured by multiplexed ELISA using a Luminex 200 analyzer (Millipore) and a mouse cytokine kit (Millipore). For primary hepatocyte isolation, liver parenchymal cells were prepared from 8- to 12-week-old anesthetized mice by in situ collagenase perfusion of the liver (56). Primary monolayer cultures were established by plating 1.5 × 10^5 viable cells/cm^2 in 6-well collagen IV–coated plates. After 16 hours, primary hepatocytes were stimulated for 24 hours with TNF-α (20 ng/ml) plus CHX (100 μg/ml) or with 500 μl of macrophage-conditioned medium for 12 hours. Neutrophil migration assays were performed using BD Falcon FluoroBlok 96 Multi-Well insert systems. Neutrophils were stained for 1 hour with 1.5 μM calcein AM. Then, 1 × 10^5 cells were plated per well in the upper chamber in 50 μl of culture medium without FBS. Lower chambers contained 200 μl of culture medium alone or supplemented with the chemoattractant (20 ng/ml TNF-α or 1/10 cytokine cocktail). Fluorescence emission was measured at different time points with a fluorescent plate reader with bottom-reading capability (Fluoroskan Ascent; Thermo Scientific).

Serum analysis. Serum activities of ALT and AST were measured using the ALT and AST Reagent Kit (Biosystems Reagents) with a Benchmark Plus Microplate Spectrophotometer. Serum concentrations of cytokines were measured by multiplexed ELISA with a Luminex 200 analyzer (Millipore).

Biochemical analysis. Tissue extracts were prepared using Triton lysis buffer (20 mM Tris [pH 7.4], 1% Triton X-100, 10% glycerol, 137 mM NaCl, 2 mM EDTA, 25 mM β-glycerophosphate, 1 mM sodium orthovanadate, 1 mM phenylmethylsulfonyl fluoride, and 10 μg/ml aprotinin and leupeptin). Extracts (30 μg protein) and immunoprecipitates (prepared from 2 mg protein) were examined by protein immunoblot analysis with antibodies to ERK1/2, phospho-ERK1/2, phospho-MKK3/6, p38α MAPK, phospho-p38, phospho-hsp27, phospho-JNK1/2, JNK1/2, caspase 3, cleaved caspase 3, cleaved PARP, and phospho-eEF2 kinase (Ser366), all from Cell Signaling and MKK3 (BD Biosciences — Pharmingen), MKK6 (Stressgen), and GAPDH and eEF2 (Santa Cruz Biotechnology Inc.). The anti-p38γ and p38δ antibodies were raised against the peptides PPRQLGARVPKETAL and PIARKDSRRRSGMKL, respectively, which correspond to the C termini of the proteins.

Immunohistochemistry. Livers were fixed in 4% paraformaldehyde, processed, and embedded in paraffin. Sections (5 μm) were stained with H&E.

Isolation of liver-infiltrating mononuclear leukocytes. Mouse livers were collected, and a single-cell suspension was obtained and passed through a 70-μm strainer. Leukocytes were collected from the interphase of centrifuged Ficoll gradients. Cells were counted with a CASY Cell Counter (57). Then 10^6 Cells were labeled by surface staining (PE-conjugated anti-CD11b and PerCP-conjugated anti–Gr-1; Invitrogen), and another 10^6 cells were stimulated in vitro with LPS (10 μg/ml) plus brefeldin A,which inhibits protein transport from ER to Golgi, leading to the accumulation of protein inside the ER (BD GolgiPlug) (1:1000) for 2 hours. The LPS-stimulated cells were then labeled by surface staining (PE-conjugated anti-CD11b and PerCP-conjugated anti–Gr-1; Invitrogen), fixed, permeabilized, and stained for intracellular TNF-α (APC-conjugated anti–TNF-α from BD Biosciences) and IL-12 (PE-conjugated anti–IL-12 from BD Biosciences). Flow cytometry was performed with a FACScan cytofluorometer (FACS Canto BD), and data were examined using FlowJo software.

Phospho-p38 FACS analysis. Primary myeloid cells were isolated (neutrophils, BM macrophages, and Kupffer cells) and stimulated for 30 minutes with LPS (10 μg/ml). Cells were fixed overnight in 70% methanol at –20°C and stained with anti–phospho-p38 antibody (Cell Signaling) or control rabbit IgG followed by FITC–anti-rabbit IgG. Signal was detected by flow cytometry.

RNA-immunoprecipitation assay. RAW 264.7 cells (mouse leukemic monocyte macrophage cell line) were stimulated with LPS (10 μg/ml) and RNA-immunoprecipitation assays (RIPs) were performed using antibodies against eEF2 (Santa Cruz Biotechnology Inc.). The efficiency of immunoprecipitation was checked by immunoblot analysis. RNA was isolated from the input lysate, isotype control immunoprecipitate, and the anti-eEF2 immunoprecipitate. After reverse transcription, the levels of

TNF-α mRNA were determined by qRT-PCR. Relative mRNA levels were calculated by subtracting background from the level of the target mRNA and then using the standard $\Delta\Delta C_T$ formula.

qRT-PCR. The expression of mRNA was examined by qRT-PCR using a 7900 Fast Real Time thermocycler and FAST SYBR GREEN assays (Applied Biosystems). Relative mRNA expression was normalized to *Gapdh* mRNA measured in each sample. *Hif-1α*, *Gr-1*, *KC* (*Cxcl1*), *Mip-2* (*Cxcl2*), *Mcp-1*, and *Icam-1* were amplified using the primers shown in Supplemental Table 1.

Statistics. Differences between groups were examined for statistical significance using 2-tailed Student's *t* test or ANOVA coupled to Bonferroni's post-test. Kaplan-Meier analysis of survival was performed using the log-rank test.

Study approval. Animal studies were approved by the local ethics committee and by the IACUC of the University of Massachusetts Medical School. All animal procedures conformed to EU Directive 86/609/EEC and Recommendation 2007/526/EC regarding the protection of animals used for experimental and other scientific purposes, enacted under Spanish law 1201/2005.

Acknowledgments

We thank J.M. Vazquez and E. Calvo for the proteomic analysis; T. Barrett and L.G. Leiva for technical assistance; S. Bartlett for English editing; and M. Rincón and F. Sanchez-Madrid for kindly revising and critically reading the article. Phospho-eEF2K (Ser359) antibody was provided by the Division of Signal Transduction Therapy (DSTT), University of Dundee, Dundee, United Kingdom. pΔ8.9 and pVSV-G were kindly provided by Katia Urso and Juan Miguel Redondo (Centro Nacional de Investigaciones Cardiovasculares, Spain). FACS cytometry was conducted at the CNIC-Cellomics Unit. G. Sabio is an investigator of the Ramón y Cajal Program and a recipient of a Principe de Girona Impulsa award. R.J. Davis is an investigator of the Howard Hughes Medical Institute. Á. Verdugo is a recipient of a Madrid Regional Government fellowship. E. Manieri is a fellow of the La Caixa Foundation. Á. González-Rodríguez was supported by CIBERDEM (ISCIII, Spain). This work was funded by the following grants: ERC 260464, EFSD 2030, MICINN SAF2010-19347, and Comunidad de Madrid S2010/BMD-2326 (to G. Sabio:); MICINN SAF2011-27330 (to P. Martin); and MICINN SAF2012-3328 (to Á. Valverde). The CNIC is supported by the Ministry of Economy and Competitiveness and the Pro-CNIC Foundation.

Received for publication May 31, 2012, and accepted in revised form October 4, 2012.

Address correspondence to: Guadalupe Sabio, Vascular Biology and Inflammation, Centro Nacional de Investigaciones Cardiovasculares Carlos III, C/ Melchor Fernández Almagro, 3, 28029 Madrid, Spain. Phone: 34.91453.12.00, ext. 2004; Fax: 34.91.453.12.45; E-mail: gsabio@cnic.es.

1. Kim C, et al. The kinase p38 alpha serves cell type-specific inflammatory functions in skin injury and coordinates pro- and anti-inflammatory gene expression. *Nat Immunol*. 2008;9(9):1019–1027.
2. Wu Z, Han M, Chen T, Yan W, Ning Q. Acute liver failure: mechanisms of immune-mediated liver injury. *Liver Int*. 2010;30(6):782–794.
3. Antoniades CG, Berry PA, Wendon JA, Vergani D. The importance of immune dysfunction in determining outcome in acute liver failure. *J Hepatol*. 2008;49(5):845–861.
4. Popa C, Netea MG, van Riel PL, van der Meer JW, Stalenhoef AF. The role of TNF-alpha in chronic inflammatory conditions, intermediary metabolism, and cardiovascular risk. *J Lipid Res*. 2007;48(4):751–762.
5. Wajant H, Pfizenmaier K, Scheurich P. Tumor necrosis factor signaling. *Cell Death Differ*. 2003;10(1):45–65.
6. Bradley JR. TNF-mediated inflammatory disease. *J Pathol*. 2008;214(2):149–160.
7. Schwabe RF, Brenner DA. Mechanisms of Liver Injury. I. TNF-alpha-induced liver injury: role of IKK, JNK, and ROS pathways. *Am J Physiol Gastrointest Liver Physiol*. 2006;290:G583–G589.
8. Pfeffer KD, Hueckstedt TP, Hoidal JR. Expression and regulation of tumor necrosis factor in macrophages from cystic fibrosis patients. *Am J Respir Cell Mol Biol*. 1993;9(5):511–519.
9. Pasparakis M, Alexopoulou L, Douni E, Kollias G. Tumour necrosis factors in immune regulation: everything that's interesting is...new! *Cytokine Growth Factor Rev*. 1996;7(3):223–229.
10. Nebreda AR, Porras A. p38 MAP kinases: beyond the stress response. *Trends Biochem Sci*. 2000; 25(6):257–260.
11. Schieven GL. The biology of p38 kinase: a central role in inflammation. *Curr Top Med Chem*. 2005;5(10):921–928.
12. Cuenda A, Rousseau S. p38 MAP-kinases pathway regulation, function and role in human diseases. *Biochim Biophys Acta*. 2007;1773(8):1358–1375.
13. Kyriakis JM, Avruch J. Mammalian mitogen-activated protein kinase signal transduction pathways activated by stress and inflammation. *Physiol Rev*. 2001;81(2):807–869.
14. Brancho D, et al. Mechanism of p38 MAP kinase activation in vivo. *Genes Dev*. 2003;17(16):1969–1978.
15. Remy G, et al. Differential activation of p38 MAPK isoforms by MKK6 and MKK3. *Cell Signal*. 2010;22(4):660–667.
16. Heinrichsdorff J, Luedde T, Perdiguero E, Nebreda AR, Pasparakis M. p38 alpha MAPK inhibits JNK activation and collaborates with IkappaB kinase 2 to prevent endotoxin-induced liver failure. *EMBO Rep*. 2008;9(10):1048–1054.
17. Hui L, et al. p38alpha suppresses normal and cancer cell proliferation by antagonizing the JNK-c-Jun pathway. *Nat Genet*. 2007;39(6):741–749.
18. Beardmore VA, et al. Generation and characterization of p38beta (MAPK11) gene-targeted mice. *Mol Cell Biol*. 2005;25(23):10454–10464.
19. Knebel A, Morrice N, Cohen P. A novel method to identify protein kinase substrates: eEF2 kinase is phosphorylated and inhibited by SAPK4/p38delta. *EMBO J*. 2001;20(16):4360–4369.
20. Jung GA, et al. Methylation of eukaryotic elongation factor 2 induced by basic fibroblast growth factor via mitogen-activated protein kinase. *Exp Mol Med*. 2011;43(10):550–560.
21. Browne GJ, Proud CG. Regulation of peptide-chain elongation in mammalian cells. *Eur J Biochem*. 2002;269(22):5360–5368.
22. Wang L, Wang X, Proud CG. Activation of mRNA translation in rat cardiac myocytes by insulin involves multiple rapamycin-sensitive steps. *Am J Physiol Heart Circ Physiol*. 2000;278(4):H1056–H1068.
23. Knebel A, Haydon CE, Morrice N, Cohen P. Stress-induced regulation of eukaryotic elongation factor 2 kinase by SB 203580-sensitive and -insensitive pathways. *Biochem J*. 2002;367(pt 2):525–532.
24. Ono K, Han J. The p38 signal transduction pathway: activation and function. *Cell Signal*. 2000;12(1):1–13.
25. Mahtani KR, Brook M, Dean JL, Sully G, Saklatvala J, Clark AR. Mitogen-activated protein kinase p38 controls the expression and posttranslational modification of tristetraprolin, a regulator of tumor necrosis factor alpha mRNA stability. *Mol Cell Biol*. 2001;21(19):6461–6469.
26. Turpeinen T, Nieminen R, Moilanen E, Korhonen R. Mitogen-activated protein kinase phosphatase-1 negatively regulates the expression of interleukin-6, interleukin-8, and cyclooxygenase-2 in A549 human lung epithelial cells. *J Pharmacol Exp Ther*. 2010;333(1):310–318.
27. Nagaleekar VK, et al. Translational control of NKT cell cytokine production by p38 MAPK. *J Immunol*. 2011;186(7):4140–4146.
28. Kotlyarov A, et al. MAPKAP kinase 2 is essential for LPS-induced TNF-alpha biosynthesis. *Nat Cell Biol*. 1999;1(2):94–97.
29. Ramaiah SK, Jaeschke H. Role of neutrophils in the pathogenesis of acute inflammatory liver injury. *Toxicol Pathol*. 2007;35(6):757–766.
30. Alagbala Ajibade A, et al. TAK1 negatively regulates NF-kappaB and p38 MAP kinase activation in Gr-1(+)CD11b(+) neutrophils. *Immunity*. 2012;36(1):43–54.
31. Xia S, Sha H, Yang L, Ji Y, Ostrand-Rosenberg S, Qi L. Gr-1+ CD11b+ myeloid-derived suppressor cells suppress inflammation and promote insulin sensitivity in obesity. *J Biol Chem*. 2011;286(26):23591–23599.
32. Dong Z, Wei H, Sun R, Tian Z. The roles of innate immune cells in liver injury and regeneration. *Cell Mol Immunol*. 2007;4(4):241–252.
33. Kuma Y, Sabio G, Bain J, Shpiro N, Marquez R, Cuenda A. BIRB796 inhibits all p38 MAPK isoforms in vitro and in vivo. *J Biol Chem*. 2005;280(20):19472–19479.
34. Cuenda A, et al. SB 203580 is a specific inhibitor of a MAP kinase homologue which is stimulated by cellular stresses and interleukin-1. *FEBS Lett*. 1995;364(2):229–233.
35. Clausen BE, Burkhardt C, Reith W, Renkawitz R, Forster I. Conditional gene targeting in macrophages and granulocytes using LysMcre mice. *Transgenic Res*. 1999;8(4):265–277.
36. Sabio G, et al. Stress- and mitogen-induced phosphorylation of the synapse-associated protein SAP90/PSD-95 by activation of SAPK3/p38gamma and ERK1/ERK2. *Biochem J*. 2004;380(pt 1):19–30.

37. Sabio G, et al. p38gamma regulates the localisation of SAP97 in the cytoskeleton by modulating its interaction with GKAP. *EMBO J*. 2005;24(6):1134–1145.
38. Jonsson F, et al. Mouse and human neutrophils induce anaphylaxis. *J Clin Invest*. 2011;121(4):1484–1496.
39. Kolios G, Valatas V, Kouroumalis E. Role of Kupffer cells in the pathogenesis of liver disease. *World J Gastroenterol*. 2006;12(46):7413–7420.
40. Noubade R, et al. Activation of p38 MAPK in CD4 T cells controls IL-17 production and autoimmune encephalomyelitis. *Blood*. 2011;118(12):3290–3300.
41. Kotlyarov A, Gaestel M. Is MK2 (mitogen-activated protein kinase-activated protein kinase 2) the key for understanding post-transcriptional regulation of gene expression? *Biochem Soc Trans*. 2002;30(pt 6):959–963.
42. Shi C, et al. Bone marrow mesenchymal stem and progenitor cells induce monocyte emigration in response to circulating toll-like receptor ligands. *Immunity*. 2011;34(4):590–601.
43. Lee JC, et al. A protein kinase involved in the regulation of inflammatory cytokine biosynthesis. *Nature*. 1994;372(6508):739–746.
44. Kang YJ, et al. Macrophage deletion of p38alpha partially impairs lipopolysaccharide-induced cellular activation. *J Immunol*. 2008;180(7):5075–5082.
45. Lee MR, Dominguez C. MAP kinase p38 inhibitors: clinical results and an intimate look at their interactions with p38alpha protein. *Curr Med Chem*. 2005;12(25):2979–2994.
46. Schreiber S, et al. Oral p38 mitogen-activated protein kinase inhibition with BIRB 796 for active Crohn's disease: a randomized, double-blind, placebo-controlled trial. *Clin Gastroenterol Hepatol*. 2006;4(3):325–334.
47. Wysk M, Yang DD, Lu HT, Flavell RA, Davis RJ. Requirement of mitogen-activated protein kinase kinase 3 (MKK3) for tumor necrosis factor-induced cytokine expression. *Proc Natl Acad Sci U S A*. 1999;96(7):3763–3768.
48. Lu HT, et al. Defective IL-12 production in mitogen-activated protein (MAP) kinase kinase 3 (Mkk3)-deficient mice. *EMBO J*. 1999;18(7):1845–1857.
49. Tanaka N, et al. Differential involvement of p38 mitogen-activated protein kinase kinases MKK3 and MKK6 in T-cell apoptosis. *EMBO Rep*. 2002;3(8):785–791.
50. Chopra P, et al. Pharmacological profile of AW-814141, a novel, potent, selective and orally active inhibitor of p38 MAP kinase. *Int Immunopharmacol*. 2010;10(4):467–473.
51. Sukhtankar D, et al. Inhibition of p38-MAPK signaling pathway attenuates breast cancer induced bone pain and disease progression in a murine model of cancer-induced bone pain. *Mol Pain*. 2011;7:81.
52. Urso K, et al. NFATc3 regulates the transcription of genes involved in T-cell activation and angiogenesis. *Blood*. 2011;118(3):795–803.
53. Kim L, Butcher BA, Denkers EY. Toxoplasma gondii interferes with lipopolysaccharide-induced mitogen-activated protein kinase activation by mechanisms distinct from endotoxin tolerance. *J Immunol*. 2004;172(5):3003–3010.
54. Kuboki S, et al. Hepatocyte NF-kappaB activation is hepatoprotective during ischemia-reperfusion injury and is augmented by ischemic hypothermia. *Am J Physiol Gastrointest Liver Physiol*. 2007;292(1):G201–G207.
55. Partida-Sanchez S, et al. Chemotaxis of mouse bone marrow neutrophils and dendritic cells is controlled by adp-ribose, the major product generated by the CD38 enzyme reaction. *J Immunol*. 2007;179(11):7827–7839.
56. Mayoral R, Valverde AM, Llorente Izquierdo C, Gonzalez-Rodriguez A, Bosca L, Martin-Sanz P. Impairment of transforming growth factor beta signaling in caveolin-1-deficient hepatocytes: role in liver regeneration. *J Biol Chem*. 2010;285(6):3633–3642.
57. Cruz-Adalia A, et al. CD69 limits the severity of cardiomyopathy after autoimmune myocarditis. *Circulation*. 2010;122(14):1396–1404.

Supplemental Data

eEF2 controls TNFα translation in LPS-induced hepatitis

Bárbara González-Terán[1], José R. Cortés[1], Elisa Manieri[2,1], Nuria Matesanz[1], Ángeles Verdugo[2,1], María E. Rodriguez[1], Águeda González-Rodríguez[3,4], Ángela Valverde[3,4], Pilar Martín[1], Roger J. Davis[5] and Guadalupe Sabio[1]*

Figure S1

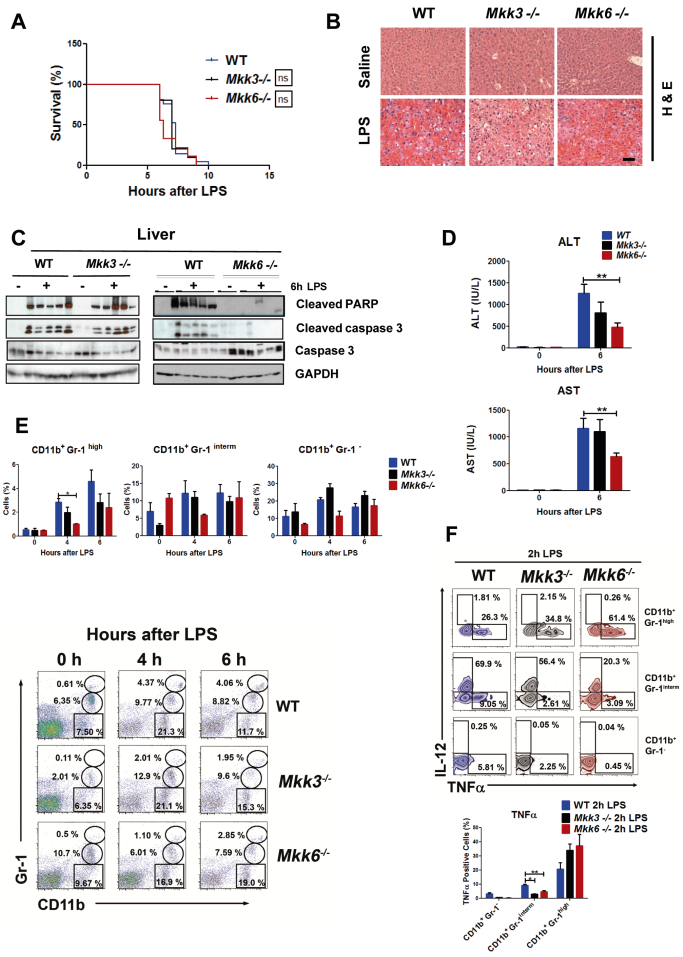

Figure S1. *Mkk3*$^{-/-}$ and *Mkk6*$^{-/-}$ mice are partially protected against LPS-induced liver damage.

Wild-type (WT), *Mkk3*$^{-/-}$ and *Mkk6*$^{-/-}$ mice were treated by intraperitoneal (i.p.) injection with 50 µg/kg LPS plus 1g/kg D-Gal (D-Gal+LPS) or saline.

(A) Survival curves after D-Gal+LPS injection (n=10). Survival curves were created with the Kaplan-Meier method and compared with Log-rank (Mantel-Cox) test.

(B) Livers were removed at 6 h post-injection. Panels show representative H&E-stained liver sections (scale bar 50µm) and livers (n= 6).

(C) Liver extracts were examined by immunoblot with antibodies to cleaved PARP, cleaved caspase 3, caspase 3 and GAPDH (n=6).

(D) Serum transaminase activity at 4 and 6 h post injection (n=6)

(E) Liver myeloid subsets (CD11b^{+} Gr-1^{high}, CD11b^{+} Gr-1^{intermediate}, CD11b^{+} Gr-1^{-}) were characterized by flow cytometry of leukocytes isolated from WT, *Mkk3*$^{-/-}$ and *Mkk6*$^{-/-}$ livers at 4 and 6 h after treatment. Bar charts show each myeloid population as a percentage of the total intra-hepatic leukocyte population; representative dot plots are shown below (n=4-7).

(F) TNFα and IL-12 production by liver myeloid populations was analyzed by intracellular staining in neutrophils (CD11b^{+} Gr-1^{high}), monocytes (CD11b^{+} Gr-1^{interm}) and CD11b^{+} Gr-1^{-} myeloid cells isolated from WT, *Mkk3*$^{-/-}$ and *Mkk6*$^{-/-}$ livers and treated in vitro with LPS (10 µg/ml) plus brefeldin A (1:1000) for 2 h. Representative dot plots are shown, and the bar charts show the percentages of TNFα-positive cells in each myeloid population. (n=4-7).

Data are means ± SD (n= 5-10). *P < 0.05; **P<0.01 (Two-way ANOVA coupled to Bonferroni post-test).

Figure S2

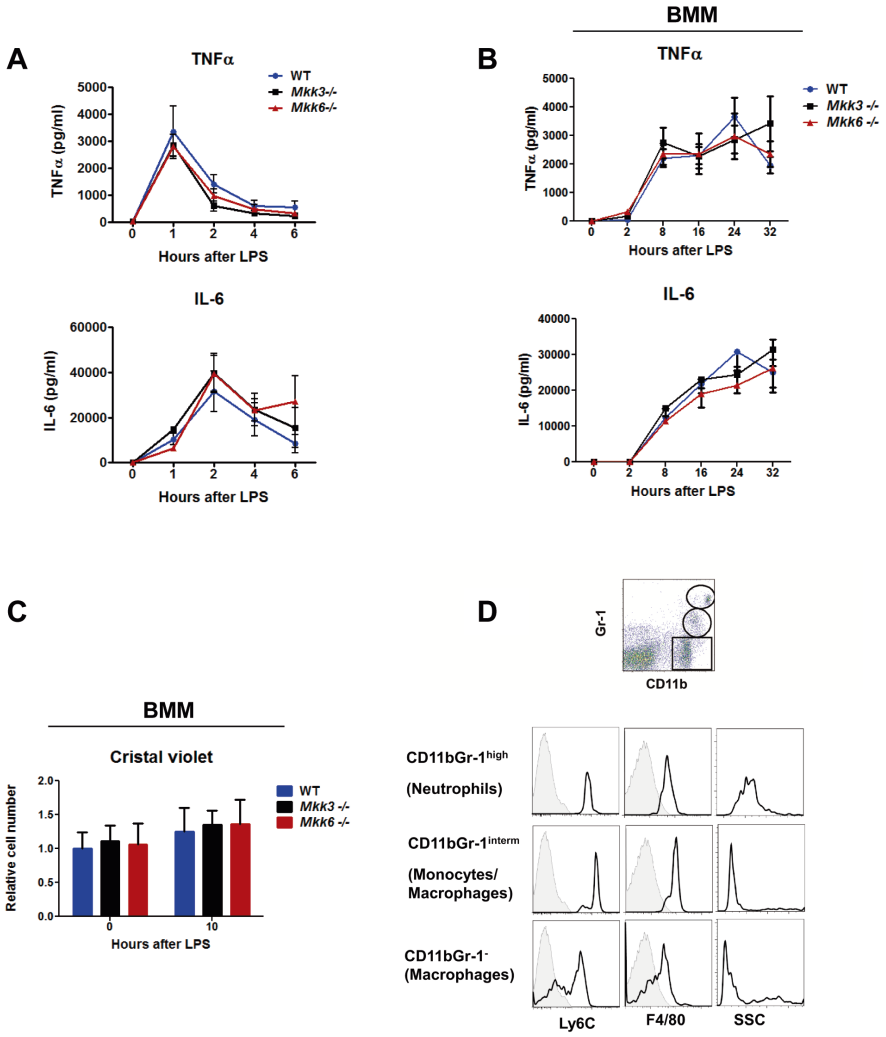

Figure S2. ***Mkk3-/-*** **and** ***Mkk6-/-*** **mice have normal levels of TNFα**

(A) Mice were treated by intraperitoneal (i.p.) injection with D-Gal+LPS (LPS/Gal), and serum cytokines (TNFα & IL-6) were measured at different times after injection by multiplexed ELISA (n = 10).

(B) Primary bone marrow macrophages from Mkk3-/-, Mkk6 -/- and WT mice were treated with LPS (10 µg/ml) in culture. The concentration of TNFα and IL-6 in the tissue culture medium was measured by ELISA (n = 4).

(C) Proliferation of Mkk3-/-, Mkk6-/- and WT bone marrow macrophages (BMM) was assayed by crystal violet staining after LPS stimulation.

(D) Representative images of flow cytometry analysis of leucocytes from WT liver based on CD11b+ and Gr-1expression levels. Three distinct populations are shown: $Cd11b^{+}$ $Gr\text{-}1^{high}$ (neutrophils), $Cd11b^{+}$ $Gr\text{-}1^{intermediate}$ (monocytes/ macrophages) and $Cd11b^{+}$ $Gr\text{-}1^{-}$ (macrophages). The $Cd11b^{+}$ subsets from WT livers were triple-stained for Cd11b, Gr-1 and indicated markers (black), and gated for SSC. Gray histograms indicate isotype control (n=7).

Data are means ± SD. No significant differences were found (Two-way ANOVA coupled to Bonferroni post-test).

Figure S3

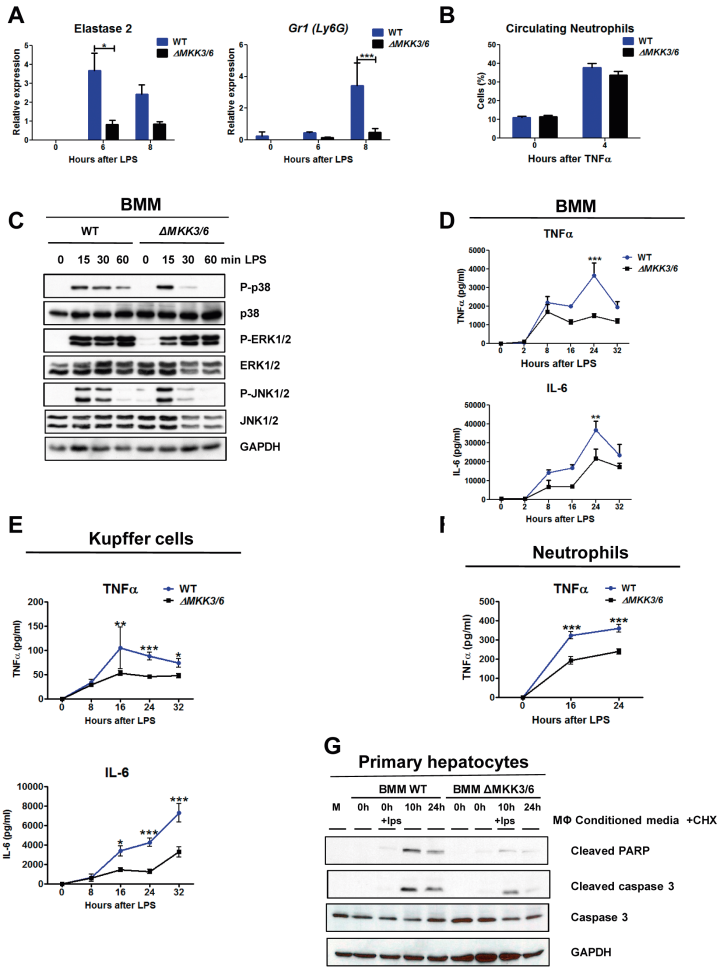

Figure S3. *ΔMKK3/6* mice show defective TNFα production and neutrophil migration

(A) WT and MKK3/6-deficient mice were injected with LPS/Gal or saline. After 6 h, liver RNA was extracted, and neutrophil marker mRNAs were determined by quantitative real-time PCR. mRNA expression was normalized to the amount of *Gapdh* mRNA (n = 8).

(B) Neutrophils were measured as the percentage of circulating leukocytes in total blood collected from WT and MKK3/6-deficient mice 4 h after TNF/Gal treatment.

(C) Primary BMM from WT and *ΔMKK3/6* mice were treated with LPS (10µg/ml) in culture for the times indicated. Cell lysates were examined by immunoblot (n= 5).

(D) ELISA analysis of the concentrations of TNFα and IL-6 in the culture medium of WT and *Mkk3*$^{-/-}$ *Mkk6*$^{-/+}$ deficient macrophages (n = 6).

(E) ELISA analysis of the concentrations of TNFα and IL-6 in the culture medium of WT and Mkk3-/- Mkk6-/+ deficient liver-isolated Kupffer cells (n = 6).

(F) ELISA analysis of the concentrations of TNFα and IL-6 in the culture medium of WT and Mkk3-/- Mkk6-/+ deficient BM- isolated neutrophils (n=6).

(G) Primary bone marrow macrophages from WT and Δ*MKK3/6* mice were treated with LPS (10µg/ml) for the times indicated. The macrophage-conditioned culture medium was collected, filtered and used to stimulate primary WT hepatocytes (12 h) in combination with cycloheximide (100µg/ml). As a control, LPS was added directly to hepatocytes treated with culture medium from untreated macrophages. Hepatocyte lysates were examined by immunoblot (n=5).

Data are means ± SD. *P < 0.05; **P<0.01; ***P<0.001 (Two-way ANOVA coupled to Bonferroni post-test).

Figure S4

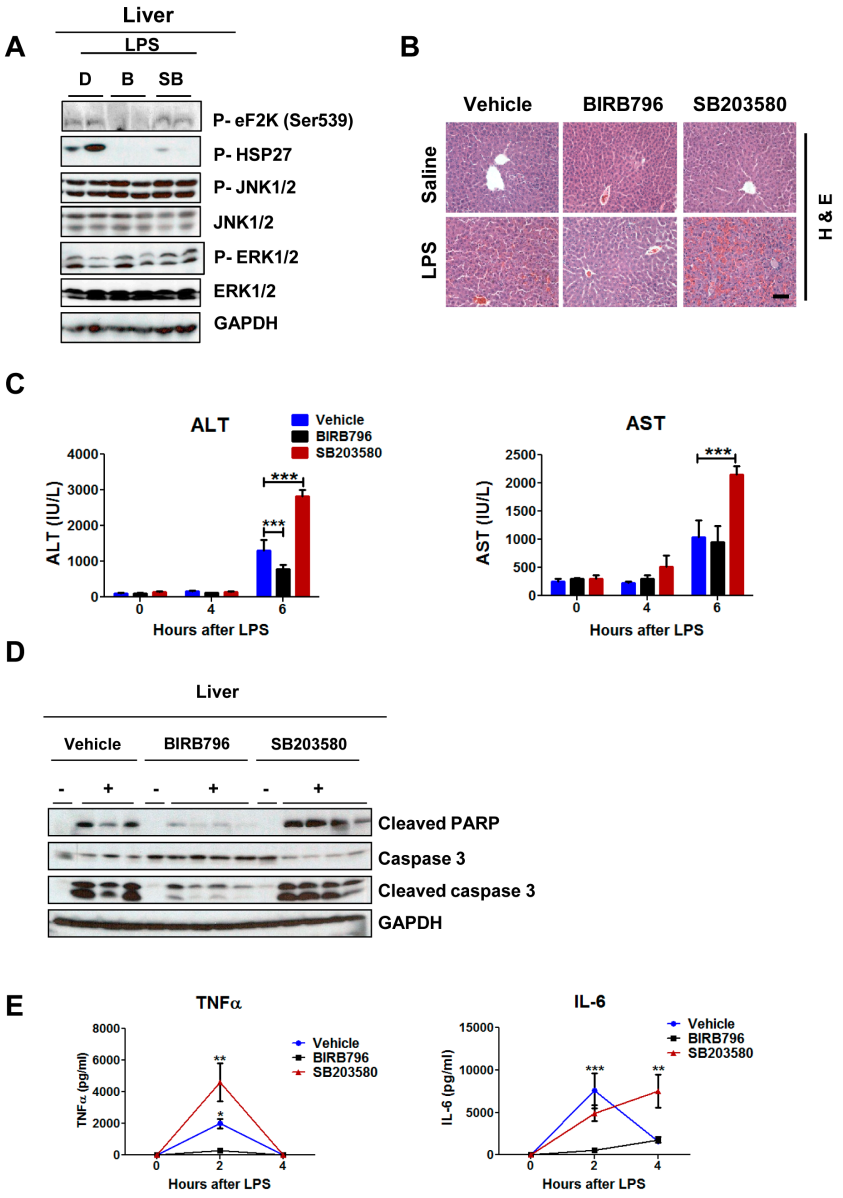

Figure S4. BIRB796 protects mice against D-Gal+LPS-induced hepatitis

Mice were i.p. injected with DMSO, BIRB796 (15mg/kg) or SB 203580 (15mg/kg). After 30min, mice were i.p. injected with D-Gal+LPS.

(A) Liver extracts were examined by immunoblot with antibodies to phospho-HSP27, phospho-EF2K (Ser359), phospho-JNK1/2, JNK1/2, phospho-ERK1/2, ERK1/2. D = DMSO; B = BIRB796; SB = SB203580, (n=8).

(B) Representative H&E-stained liver sections at 6 h after treatment. Scale bar 50µm (n=8).

(C) Serum transaminase activity at 6 h after treatment (n = 10).

(D) Liver extracts (6 h) were examined by immunoblot with antibodies to cleaved PARP, cleaved caspase 3, caspase 3 and GAPDH (n=8).

(E) Serum cytokines (TNFα, IL6) were measured at different times post-injection by multiplexed ELISA (n = 8).

Data are means ± SD. *P < 0.05; **P<0.01; ***P<0.001 (Two-way ANOVA coupled to Bonferroni post-test).

Figure S5

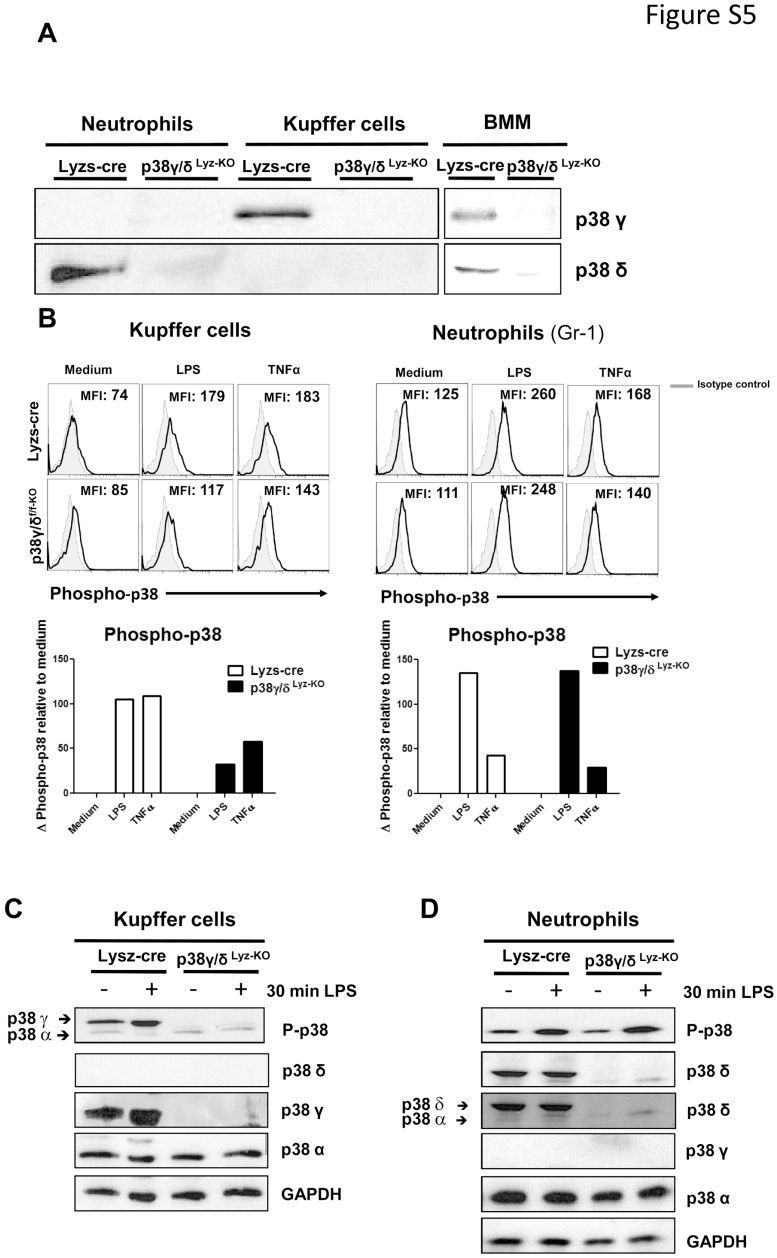

Figure S5. Myeloid expression and activation of p38γ and δ.

(A) p38γ protein expression was analyzed by immunoprecipitation of cell extracts from bone marrow-isolated neutrophils (300µg protein) or BM-derived macrophages (800µg protein), or by immunoblot of cell extracts from liver-isolated Kupffer cells (20µg protein). p38δ protein expression was analyzed by immunoprecipitation of cell extracts from bone marrow-isolated neutrophils, liver-isolated Kupffer cells (300µg protein) and BM-derived macrophages (800µg protein).

(B-C) BM-isolated neutrophils and Kupffer cells isolated from the liver of Lysz-cre mice and p38γ/$\delta^{Lyz\text{-}KO}$ transgenic mice were stimulated with LPS or TNFα for 30 min.

(B) After stimulation, cells were fixed, permeabilized, and stained for phospho-p38. Signal was detected by flow cytometry. Histograms depict intracellular phospho-p38 expression (blue histogram). Red line represents the isotype control.

(C) Cell lysates were examined by immunoblot with antibodies to phospho-p38, p38 delta, p38 gamma, p38 alpha and GAPDH.

Figure S6

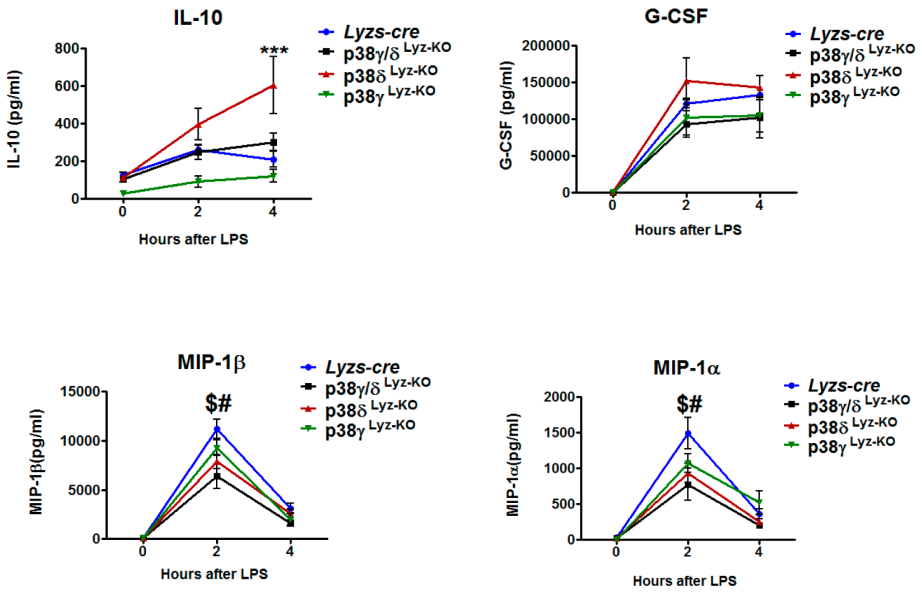

Figure S6. *p38*δ$^{Lyz\text{-}KO}$ and *p38*γ/δ$^{Lyz\text{-}KO}$ mice show defective chemokine production

*p38*γ$^{Lyz\text{-}KO}$, *p38*δ$^{Lyz\text{-}KO}$, *p38*γ/δ$^{Lyz\text{-}KO}$ and control *Lyzs-cre* transgenic mice were injected with D-Gal+LPS or vehicle.

(A) Serum cytokines and chemokines were measured at different times post-injection by multiplexed ELISA (mean ± SD; n = 10). *P < 0.05; ***P<0.001 for between-group differences in IL-10 and G-CSF. Statistically significant differences in MIP-1α and MIP-1β levels are indicated as $P < 0.001 (*Lyz-cre* versus *p38*γ/δ$^{Lyz\text{-}KO}$ mice) and #P < 0.01 (*Lyz-cre* versus *p38*δ$^{Lyz\text{-}KO}$ mice).

Figure S7

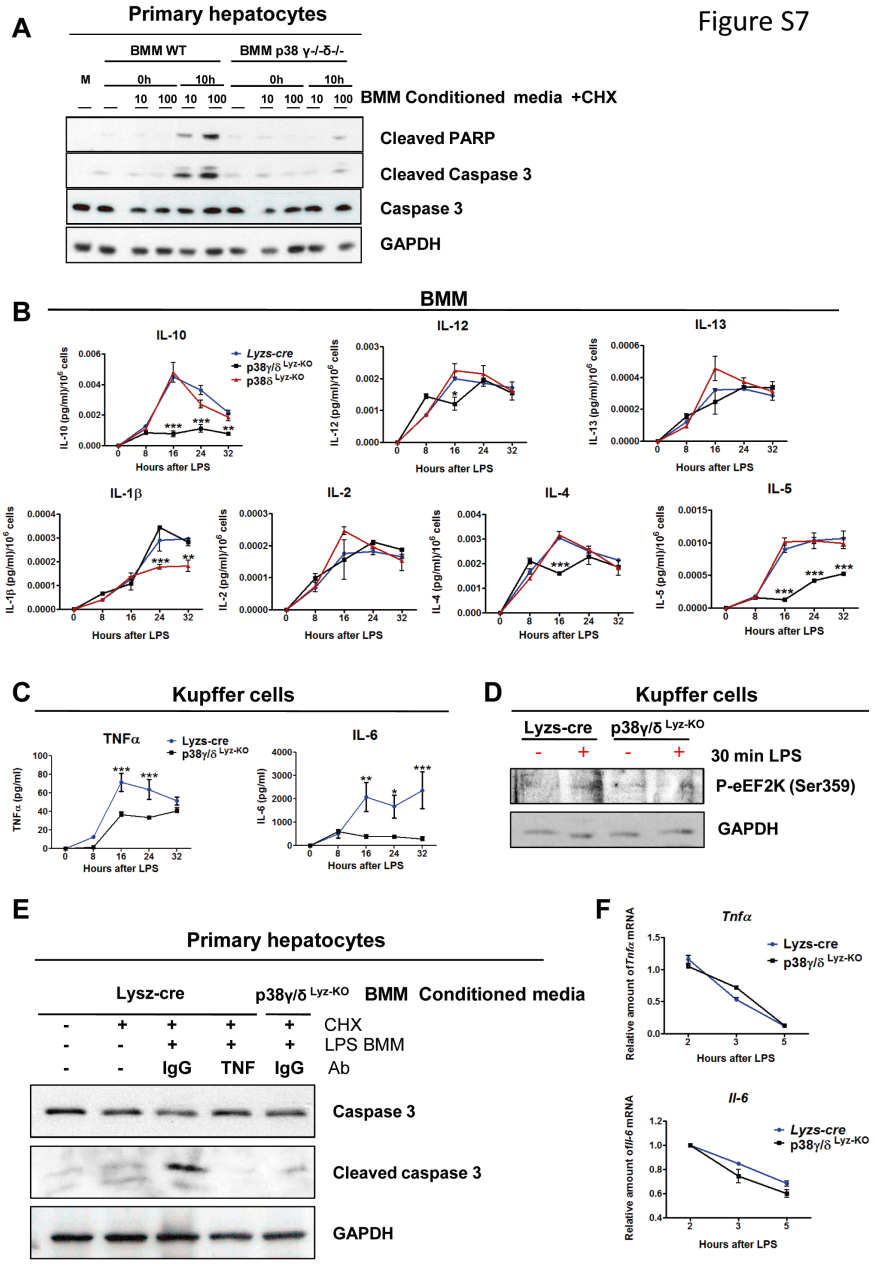

Figure sup 7. *p38*δ$^{Lyz\text{-}KO}$ and *p38*γ/δ$^{Lyz\text{-}KO}$ macrophages show defects in cytokine production

(A) *Lyzs-cre* and *p38*γ/δ deficient bone marrow macrophages were treated with LPS (10 or 100µg/ml) for 10 h. Macrophage-conditioned culture medium was collected, filtered and used to stimulate primary WT hepatocytes (12 h) in combination with cyclohexamide (100µg/ml). As a control, LPS (10 or 100µg/ml) was added directly to hepatocytes treated with culture medium from unstimulated macrophages. Hepatocyte lysates were examined by immunoblot (n=5).The concentration of cytokines in the culture medium of *Lyzs-cre*, *p38*γ/δ and *p38*δ deficient bone marrow macrophages was measured by ELISA (n=6).

(B) ELISA analysis of the concentration of cytokines in the culture medium of *Lyzs-cre*, *p38*γ/δ and *p38*δ deficient bone marrow macrophages (n = 6).

(C) Kupffer cells from the liver of Lysz-cre mice and p38γ/δ$^{Lyz\text{-}KO}$ transgenic mice were stimulated with LPS (10µg/ml) for 30 min.

(D) Cell lysates were examined by immunoblot with antibodies to phospho-eEF2K (serine 359) and GAPDH.

(E) Primary bone marrow macrophages from Lysz-cre and p38γ/δ$^{Lyz\text{-}KO}$ mice were treated with LPS (10 µg/ml) for 10 h. The macrophage-conditioned culture medium was collected, filtered and then incubated for 1 h with cycloheximide (100µg/ml) plus TNFα blocking antibodies or IgG antibodies, in the combinations indicated in the figure. The conditioned media was then used to stimulate primary WT hepatocytes for 12 h. Hepatocyte lysates were examined by immunoblot (n=5).

(F) To analyze TNFα and IL6 mRNA stability, *Lyzs-cre* and *p38*γ/δ deficient bone marrow macrophages were stimulated with LPS (10µg/ml), and actinomycin (10µg/ml) was added 1 h later. mRNA was isolated at the times indicated, and analyzed by quantitative real-time PCR. mRNA expression was normalized to the amount of *Gapdh* mRNA (n = 4).

Data are means ± SD. **P<0.01; ***P<0.001 (Two-way ANOVA coupled to Bonferroni post-test).

Figure S8

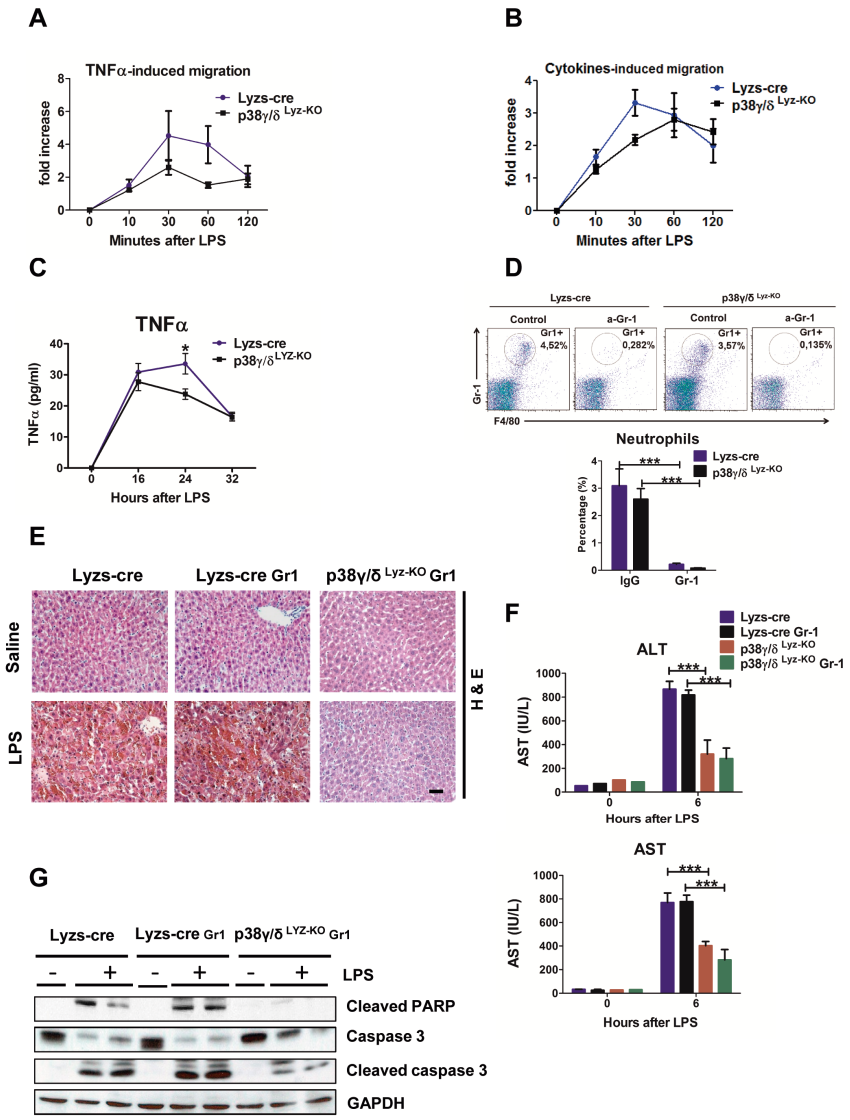

Figure S8. Role of p38γ/δ in neutrophils and LPS-induced liver injury

(A-C) Neutrophils were isolated from the bone marrow of Lysz-cre and p38γ/$\delta^{Lyz\text{-}KO}$ transgenic mice and stimulated with LPS for the indicated times. Data are means ± SD. **P<0.01; ***P<0.001 (Two-way ANOVA coupled to Bonferroni post-test).

(A) TNFα induced chemotaxis and cytokine cocktail-induced chemotaxis (B) in neutrophils. (A-B) Cells pre-labeled with 1.5 µM calcein AM were incubated with 20ng/ml TNFα or culture medium alone for 2 h using the BD FluoroBlok multiwell insert system. Fluorescence was measured at the indicated times after the addition of the chemoatractant using a Thermo Scientific Fluoroskan Ascent reader. TNFα-induced chemotaxis is expressed as the fold increases in fluorescence compared with cells treated with culture medium alone. Data are represented as mean ± SD of six replicate wells.

(C) ELISA analysis of the concentrations of TNFα and IL-6 in the culture medium of Lysz-cre and p38γ/δ deficient bone marrow-isolated neutrophils (n = 6).

(D-G) Neutrophil depletion with Gr-1 mAb does not alter LPS-induced liver injury. Lysz-cre and p38γ/$\delta^{Lyz\text{-}KO}$ mice were injected i.v. with PBS or Gr-1 mAb (250 µg) and after 24 h were injected i.p. with LPS+D-Gal or saline.

(D) The percentage of neutrophils ($Cd11b^{+}Gr\text{-}1^{high}$) in the peripheral blood of Lysz-cre mice

injected with Gr-1 mAb or saline was determined by FACS after staining with Cd11b and Gr-1 antibodies.

(E) Livers were removed at 6 h post-LPS injection. Panels show representative H&E-stained liver sections (scale bar 50μm) and livers (n= 4-8).

(F) Serum transaminase activity at 6 h after LPS treatment (n = 4-8). Data are means ± SD. ***P<0.001 (Two-way ANOVA coupled to Bonferroni post-test).

(G) Liver extracts (6 h) were examined by immunoblot with antibodies to cleaved PARP, cleaved caspase 3, caspase 3 and GAPDH (n=4-8).

Figure S9

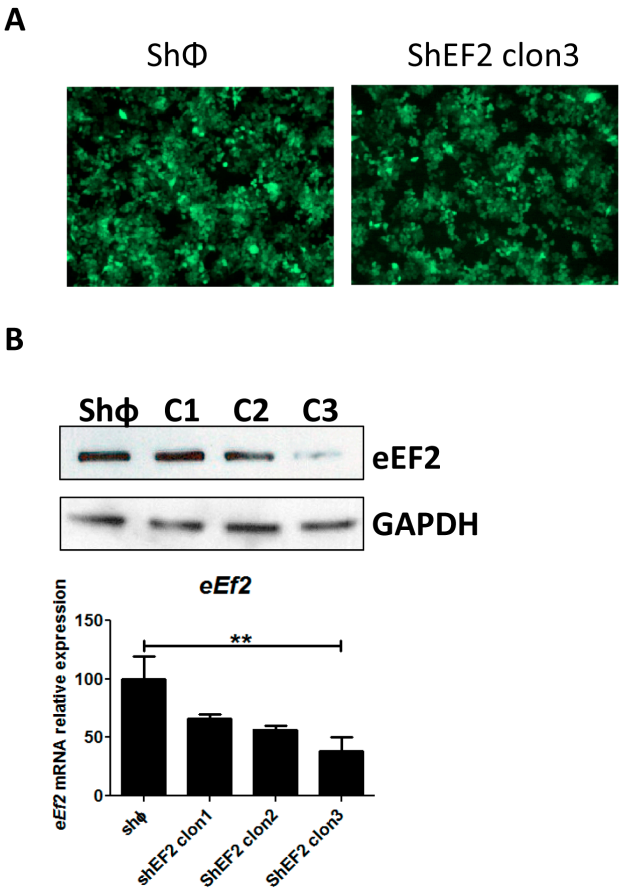

Figure S9. eEf2 silencing by lentiviral transduction of mouse BM-derived macrophage cultures.

(A) GFP expression by RAW 264.7 cells transduced with GFP$^+$ lentivirus expressing shRNA against eEf2 (shEF2 clon3) or with empty vector (ShΦ) by fluorescence microscopy. Magnification 10x.

(B) RAW 264.7 cells were transduced with three different lentiviruses, each one expressing a different shRNA clone against eEf2. Gene silencing efficiency was determined by immunoblot of cell extracts (top) and by qRT-PCR of eEf2 mRNA (bottom). mRNA expression was normalized to the amount of *Gapdh* mRNA. Data are means ± SD. **P<0.01 (One-way ANOVA coupled to Bonferroni post-test).

Supplemental Experimental Procedures

Tissue culture.

Conditioned medium from bone marrow-derived macrophages was obtained after stimulation of cells on day 7 of differentiation with LPS (10µg/ml) for 10 or 24 h The collected medium was sterile filtered to eliminate BM macrophages and frozen (-20ºC) until use. Primary hepatocytes were treated with the conditioned medium for 13 h.

qRT-PCR primers.

Primers were purchased from Sigma Aldrich.

Hif-1 α	Forward Primer	ACCTTCATCGGAAACTCCAAAG
	Reverse Primer	CTGTTAGGCTGGGAAAAGTTAGG
Gr-1	Forward Primer	GACTTCCTGCAACACAACTACC
	Reverse Primer	ACAGCATTACCAGTGATCTCAGT
KC	Forward Primer	CTGGGATTCACCTCAAGAACATC
	Reverse Primer	CAGGGTCAAGGCAAGCCTC
Mip-2	Forward Primer	CCAACCACCAGGCTACAGG
	Reverse Primer	GCGTCACACTCAAGCTCTG
Mcp-1	Forward Primer	TTAAAAACCTGGATCGGAACC
	Reverse Primer	GCATTAGCTTCAGATTTACGG
Icam-1	Forward Primer	GTGATGCTCAGGTATCCATCC
	Reverse Primer	CACAGTTCTCAAAGCACAGCG
Tnfα	Forward Primer	CCCTCACACTCAGATCATCTT
	Reverse Primer	GCTACGACGTGGGCTACAG
Il-6	Forward Primer	TAGTCCTTCCTACCCCAATTT
	Reverse Primer	TTGGTCCTTAGCCACTCCTTC

Statistical analysis.

Differences between groups were examined for statistical significance using Student's t-test, analysis of variance (ANOVA) coupled to the Bonferroni post-test, or the log-rank test.

ARTÍCULO 2: p38γ and p38δ reprogram liver metabolism by modulating neutrophil infiltration.

Autores: González-Terán B*, Matesanz N*, Nikolic I*, Verdugo MA, Sreeramkumar V, Hernández-Cosido L, Mora A, Crainiciuc G, Sáiz ML, Bernardo E, Leiva-Vega L, Rodríguez E, Bondía V, Torres JL, Perez-Sieira S, Ortega L, Cuenda A, Sanchez-Madrid F, Nogueiras R, Hidalgo A, Marcos M, Sabio G.

*Equal contribution.

Publicado en *EMBO Journal*, 2016 Mar 1;35(5):536-52.

doi: 10.15252/embj.201591857.

RESUMEN

La esteatosis, la acumulación excesiva de grasa en el hígado que causa inflamación y daño hepático, es una de las enfermedades más comunes en las sociedades desarrolladas. Está asociada a la obesidad o la ingesta excesiva de alcohol, y puede tener consecuencias muy graves como el desarrollo de cirrosis, diabetes o cáncer hepático. Sin embargo, hoy en día no existen tratamientos efectivos para la esteatosis. p38γ y p38δ han sido involucradas en el desarrollo de diferentes enfermedades con un fuerte componente inflamatorio. En este estudio mostramos que pacientes con enfermedad de hígado graso no alcohólica (NAFLD) presentan en el hígado niveles elevados de p38δ. Además, ratones deficientes en estas quinasas específicamente en células mieloides están protegidos frente al desarrollo de esteatosis y complicaciones asociadas. Este efecto protector es debido a una migración deficiente de los neutrófilos carentes en p38γ/δ al hígado dañado. Así mismo, este trabajo resalta la importancia de los neutrófilos en el inicio y progresión de la esteatosis a través de la inflamación generada y la inducción de cambios en el metabolismo hepático. Por tanto, sugerimos que p38γ y p38δ en células mieloides constituyen potenciales dianas terapéuticas para el tratamiento de la esteatosis hepática.

Aportación Personal al trabajo: He participado tanto en el diseño experimental, como en la realización de los experimentos y en la escritura del artículo.

Published online: February 3, 2016

Article

TRANSPARENT PROCESS

THE EMBO JOURNAL

p38γ and p38δ reprogram liver metabolism by modulating neutrophil infiltration

Bárbara González-Terán[1,†], Nuria Matesanz[1,†], Ivana Nikolic[1,†], María Angeles Verdugo[1,2], Vinatha Sreeramkumar[1], Lourdes Hernández-Cosido[3,4], Alfonso Mora[1], Georgiana Crainiciuc[1], María Laura Sáiz[1], Edgar Bernardo[1], Luis Leiva-Vega[1], Elena Rodríguez[1], Victor Bondía[1], Jorge L Torres[5,6], Sonia Perez-Sieira[7,8], Luis Ortega[3,4], Ana Cuenda[2], Francisco Sanchez-Madrid[1], Rubén Nogueiras[7,8], Andrés Hidalgo[1], Miguel Marcos[5,6] & Guadalupe Sabio[1,*]

Abstract

Non-alcoholic fatty liver disease (NAFLD) is a major health problem and the main cause of liver disease in Western countries. Although NAFLD is strongly associated with obesity and insulin resistance, its pathogenesis remains poorly understood. The disease begins with an excessive accumulation of triglycerides in the liver, which stimulates an inflammatory response. Alternative p38 mitogen-activated kinases (p38γ and p38δ) have been shown to contribute to inflammation in different diseases. Here we demonstrate that p38δ is elevated in livers of obese patients with NAFLD and that mice lacking p38γ/δ in myeloid cells are resistant to diet-induced fatty liver, hepatic triglyceride accumulation and glucose intolerance. This protective effect is due to defective migration of p38γ/δ-deficient neutrophils to the damaged liver. We further show that neutrophil infiltration in wild-type mice contributes to steatosis development by means of inflammation and liver metabolic changes. Therefore, p38γ and p38δ in myeloid cells provide a potential target for NAFLD therapy.

Keywords diabetes; inflammation; obesity; steatosis; stress kinases
Subject Categories Immunology; Metabolism; Molecular Biology of Disease
DOI 10.15252/embj.201591857 | Received 20 April 2015 | Revised 18 December 2015 | Accepted 22 December 2015

Introduction

Non-alcoholic fatty liver disease (NAFLD) is the leading cause of chronic liver disease in Western countries and estimates of its worldwide prevalence range from 6 to 35% (Vernon *et al*, 2011). NAFLD refers to a wide spectrum of liver damage, ranging from simple steatosis caused by intracellular triglyceride accumulation to inflammation (non-alcoholic steatohepatitis [NASH]), fibrosis, and cirrhosis (Marchesini *et al*, 2003). NAFLD is a main cause of cryptogenic cirrhosis and may also predispose to hepatocarcinoma (Farrell & Larter, 2006).

The pathogenesis of NAFLD is strongly associated with insulin resistance, obesity and type 2 diabetes (Fabbrini *et al*, 2010). However, the mechanisms involved in the accumulation of triglycerides in the liver and subsequent hepatocellular damage are multifactorial and not completely understood. Metabolic deregulation and hepatic steatosis have been linked to stress signaling (Sabio & Davis, 2010; Sabio *et al*, 2010), and the activation of stress kinases in steatosis and obesity suggests a role for these proteins in this disease (Sabio & Davis, 2010). The stress-activated protein kinase group consists of two subfamilies: p38 mitogen-activated kinases (p38 MAPKs) and c-Jun N-terminal kinases (JNKs). While the role of JNKs in the development of steatosis has been widely studied (Sabio *et al*, 2008, 2009), less is known about the role of the p38 MAPK signaling pathway. In mammals, four p38 MAPK isoforms have been identified: p38α, -β, -γ, and -δ. Despite biochemical evidence of specific roles for the individual isoforms, redundancy and embryonic lethality have impeded attempts to establish their distinct functions *in vivo* (Sabio & Davis, 2014). Embryos lacking p38α die due to defects in placental development (Adams *et al*, 2000; Allen *et al*, 2000; Tamura *et al*, 2000), but mice lacking p38β, -γ, and -δ are viable without any obvious defects under basal conditions (Beardmore *et al*, 2005; Sabio *et al*, 2005). Kinases p38γ and -δ were recently shown to control inflammation by regulating

1 Fundación Centro Nacional de Investigaciones Cardiovasculares Carlos III, Madrid, Spain
2 Department of Immunology and Oncology, Centro Nacional de Biotecnología/CSIC, Madrid, Spain
3 Bariatric Surgery Unit, Department of General Surgery, University Hospital of Salamanca, Salamanca, Spain
4 Department of Surgery, University of Salamanca, Salamanca, Spain
5 Department of Internal Medicine, University Hospital of Salamanca-IBSAL, Salamanca, Spain
6 Department of Medicine, University of Salamanca, Salamanca, Spain
7 Department of Physiology, CIMUS, University of Santiago de Compostela-Instituto de Investigación Sanitaria, Santiago de Compostela, Spain
8 CIBER Fisiopatología de la Obesidad y Nutrición (CIBERobn), Santiago de Compostela, Spain
*Corresponding author. Tel: +34 91453 12 00; E-mail: guadalupe.sabio@cnic.es
†These authors contributed equally to this work

© 2016 The Authors

macrophage production of tumor necrosis factor (TNF)-α (Risco *et al*, 2012; Gonzalez-Teran *et al*, 2013) and T-cell activation (Criado *et al*, 2014); moreover, p38δ also influences neutrophil inflammatory responses in the lung (Ittner *et al*, 2012).

Since chronic inflammation is central to the progression of NAFLD, we aimed to define the role of p38γ and p38δ in the development of this disorder. We detected elevated liver expression of p38δ in a cohort of obese patients with NAFLD and found that p38γ and p38δ are responsible for the development of steatosis and NASH in three animal models of NAFLD: mice fed a high-fat diet (HFD), mice fed a high-fat fructose diet (HFF), and mice fed a methionine–choline-deficient (MCD) diet. Lack of p38γ and p38δ in myeloid cells impaired neutrophil migration to the liver and thus protected against steatosis and further hepatic damage. These results highlight the importance of p38 kinases and neutrophils in NAFLD and open a new avenue for the treatment of this disease.

Results

p38γ and p38δ are overexpressed in NAFLD

Analysis of liver biopsies from obese NAFLD patients (body mass index [BMI] > 35 kg/m^2) revealed elevated mRNA expression of *MAPK13* (p38delta) compared with non-obese individuals without NAFLD, and a similar tendency was detected for *MAPK12* (p38gamma) (Fig 1A). Further, among individuals with a BMI < 35 kg/m^2, hepatic *MAPK12* and *MAPK13* mRNA was elevated in individuals with liver steatosis compared with control individuals without liver disease (Fig 1B). Western blot analysis confirmed higher liver expression of p38δ protein in obese individuals with steatosis (Fig 1C). To corroborate these results in a mouse model of steatosis, we studied the expression and activation of p38γ and p38δ in livers from mice fed a methionine–choline-deficient (MCD) diet, which induces macrovesicular steatosis and is widely used in NASH research (Anstee & Goldin, 2006). MCD diet increased the mRNA expression of p38δ (Fig 1D) and induced the activation of p38γ and p38δ after 1 week (Fig 1E). This activation remained high during the 3 weeks of the diet (Fig 1E and F). These results indicate a possible role of p38γ and p38δ in the development of steatosis.

Mice lacking p38γ and p38δ are protected against MCD-induced steatosis

To study how these kinases affect the development of fatty liver, we fed a MCD diet to WT mice and mice lacking p38γ (p38γ$^{-/-}$), p38δ (p38δ$^{-/-}$), and both p38γ and p38δ (p38γ/δ$^{-/-}$). Compared with MCD-diet WT mice, MCD-diet p38γ$^{-/-}$ and p38δ$^{-/-}$ mice showed only a slightly milder liver steatosis as evaluated by H&E and Oil Red staining (Appendix Fig S1A); in contrast, the development of steatosis and inflammation was strongly attenuated in p38γ/δ$^{-/-}$ mice (Fig 2A and Appendix Fig S2A). These findings were confirmed by biochemical analysis of hepatic triglyceride content (Fig 2B and Appendix Fig S1B). Moreover, whereas MCD diet increased serum levels of alanine transaminase (ALT) in WT, p38γ$^{-/-}$, and p38δ$^{-/-}$ mice, the level in p38γ/δ$^{-/-}$ mice was significantly lower, indicating milder liver necrosis (Fig 2C and Appendix Fig S1C). The appearance of steatosis protection only in mice doubly deficient for p38γ and p38δ probably reflects the previously described partial functional redundancy between the two isoforms (Risco *et al*, 2012; Gonzalez-Teran *et al*, 2013).

An early event in MCD-induced choline deficiency is the appearance in liver of oxidized lipids, DNA, and proteins. Assay of thiobarbituric acid reactive substances in the livers of MCD-fed animals detected lower oxidized lipid content in p38γ/δ$^{-/-}$ mice than in WT animals, correlating with lower levels of hydrogen peroxide in the double-knockout mice (Fig 2D). Liver fibrosis is a hallmark of NASH. Livers of MCD-diet WT mice expressed higher levels of *Col1a1* and *Acta2* than MCD-diet p38γ/δ$^{-/-}$ mice (Fig 2E), correlating with higher Masson's trichrome staining (Fig 2F). These results demonstrate that p38γ/δ$^{-/-}$ mice are protected against MCD-diet-induced steatosis and NASH.

Inflammation plays a key role in the pathogenesis of NAFLD, and the development of hepatic steatosis is associated with increased liver infiltration by myeloid cells (Tiniakos *et al*, 2010). p38γ/δ kinases regulate inflammation through the control of TNF-α production in macrophages and Kupffer cells (Risco *et al*, 2012; Gonzalez-Teran *et al*, 2013), and p38δ modulates neutrophil motility in lung disease (Ittner *et al*, 2012), prompting us to examine the mRNA expression levels of myeloid cell markers and pro-inflammatory cytokines in mice fed the MCD diet. Liver expression

Figure 1. p38γ and p38δ are up-regulated in NAFDL.

A Left: qRT–PCR analysis of mRNA expression of *MAPK12* (p38gamma) and *MAPK13* (p38delta) in liver extracts prepared from obese patients with alcoholic fatty liver disease (NAFLD) and control individuals without NAFLD. mRNA expression was normalized to the amount of *Gapdh* mRNA (n = 11–74). Right: representative H&E-stained liver sections. Scale bar: 50 μm.

B Left: qRT–PCR analysis of mRNA expression of *MAPK12* (p38gamma) and *MAPK13 (*p38delta) in liver extracts prepared from control patients with NAFLD/non-alcoholic steatohepatitis (NASH) and control individuals without NAFLD/NASH. mRNA expression was normalized to the amount of *Gapdh* mRNA (n = 9–11). Right: representative H&E-stained liver sections. Scale bar: 50 μm.

C Quantification of immunoblot analysis of p38δ expression in liver extracts prepared from obese patients with NAFLD and individuals without NAFLD. Representative blots are shown (n = 7–40).

D qRT–PCR analysis of *Mapk12* (p38gamma) and *Mapk13 (*p38delta) mRNA expression in liver extracts prepared from wild-type mice (WT) fed a diet deficient in methionine and choline (MCD) or control diet (ND) for 3 weeks; mRNA expression was normalized to the amount of *Gapdh* mRNA (n = 5–10).

E Immunoprecipitation analysis of activation and protein levels of p38γ and p38δ isoforms in liver extracts prepared from WT fed a MCD or ND diet for the times indicated.

F Immunoprecipitation analysis of activation and protein levels of p38γ and p38δ isoforms in liver extracts prepared from WT fed a MCD or ND for 3 weeks (n = 5). Western blot against vinculin was used to assay the protein amount in the total lysate (TL) used for each IP. Protein expression was normalized to vinculin.

Data information: Data are means ± SEM. *P < 0.05; **P < 0.01. Statistical significance by two-tailed Student's t-test. Characteristics of patients and controls were compared by means of χ^2 or Mann–Whitney U-tests.

© 2016 The Authors

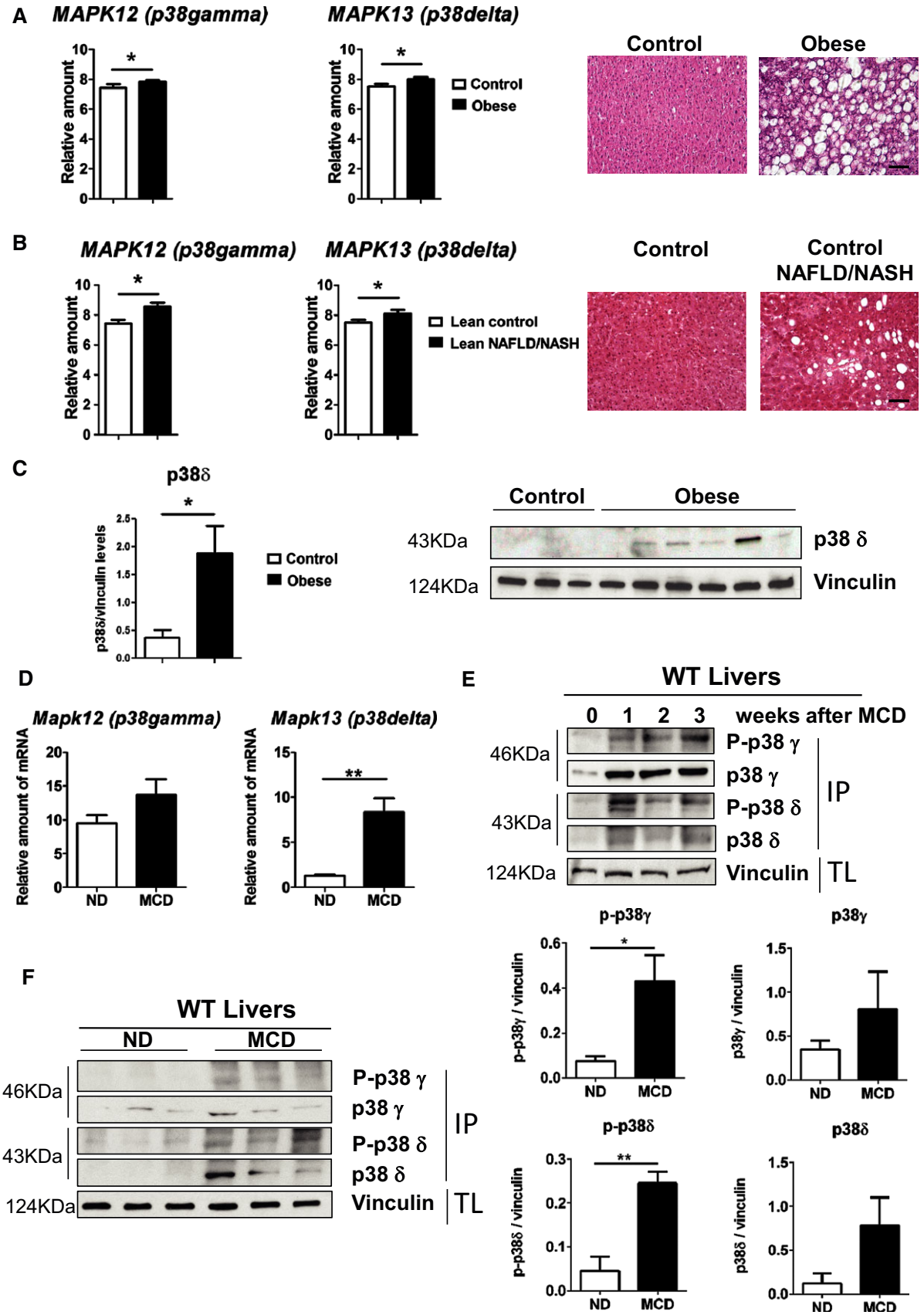

Figure 1.

© 2016 The Authors

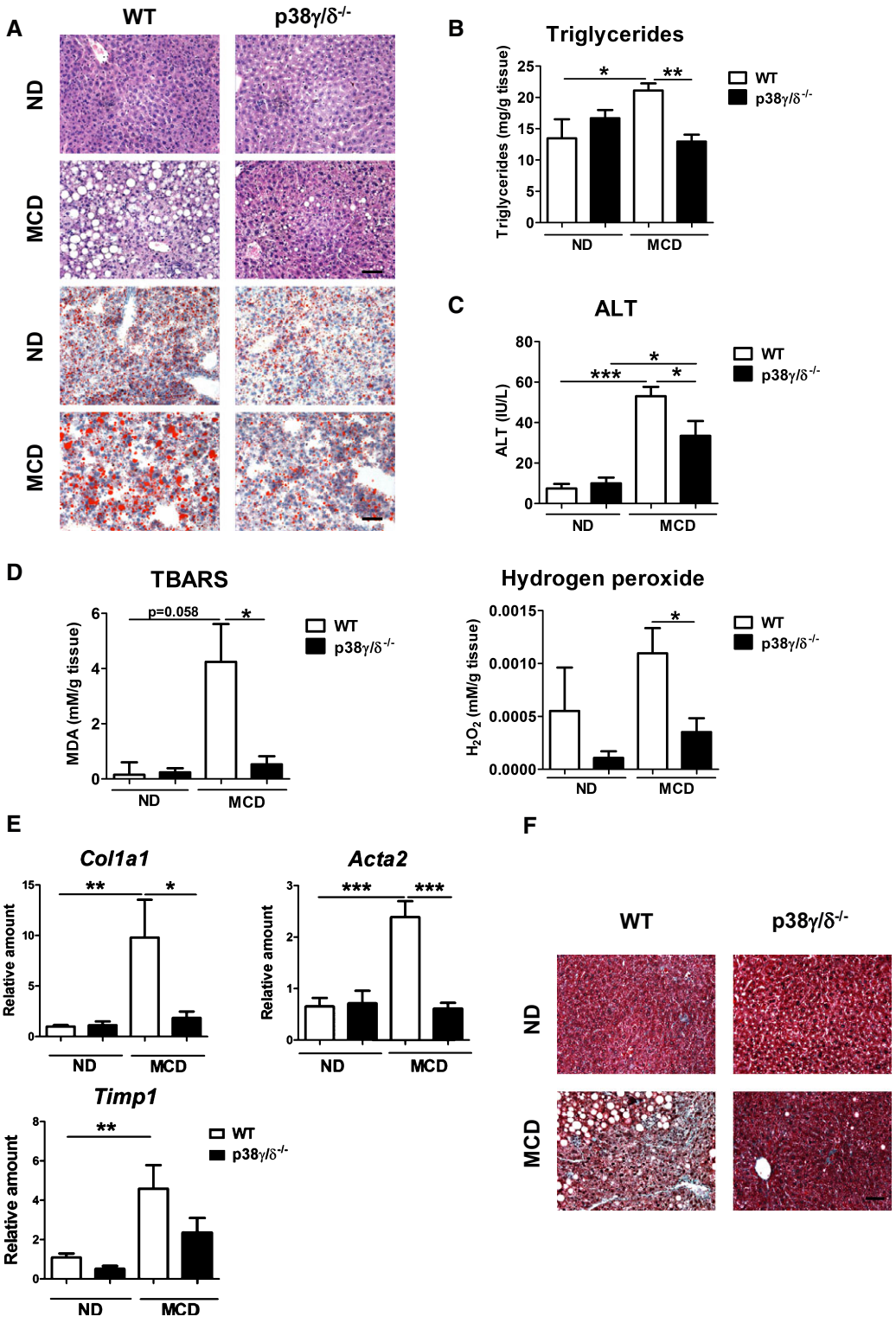

Figure 2. p38γ/δ$^{-/-}$ mice are protected against steatohepatitis and fibrosis.

A Representative H&E- and Oil Red-stained liver sections prepared from WT and p38γ/δ$^{-/-}$ mice fed a ND or the MCD diet for 3 weeks. Scale bar: 50 μm.

B, C Liver triglycerides (B) and plasma transaminase activity (ALT) (C) measured in WT and p38γ/δ$^{-/-}$ mice after 3 weeks of MCD diet.

D TBARS and hydrogen peroxide detected in liver samples from mice fasted overnight after the 3-week MCD diet.

E qRT–PCR analysis of *Col1a1*, *Acta2*, and *Timp1* mRNA expression. mRNA expression was normalized to the amount of *Gapdh* mRNA.

F Representative Masson's trichrome-stained liver sections prepared from WT and p38γ/δ$^{-/-}$ mice fed a ND or the MCD diet for 3 weeks. Scale bar: 50 μm.

Data information: Data are means ± SEM (n = 5–10). *P < 0.05; **P < 0.01; ***P < 0.001 (one-way ANOVA coupled to Bonferroni's post-tests).

© 2016 The Authors

levels of the myeloid cell marker *F4/80* and the cytokines *Tnfa* and *Il6* were significantly lower in p38γ/δ$^{-/-}$ mice than in WT mice (Appendix Fig S2B). However, analysis of M1 and M2 macrophage-differentiation markers revealed no differences in M1 (*Ifng*, *Il23)* and M2 markers (*Il10, Il13* or *Arg)* between WT and p38γ/δ$^{-/-}$ mice (Appendix Fig S2C).

Effect of myeloid cell expression of p38γ and p38δ on MCD-induced steatosis

To elucidate the role of myeloid-expressed p38γ/δ in the development of steatosis, we analyzed mice lacking p38γ/δ in myeloid cells. These mice have complete deletion of p38γ and p38δ in macrophages, and neutrophils infiltrated in liver and spleen while only partial deletion of p38δ was observed in dendritic cells (Appendix Fig S3A). Control mice expressing Cre recombinase (Lyzs-Cre mice) developed the typical hepatic steatosis in response to the MCD diet, with associated liver accumulation of triglycerides and hepatocyte necrosis indexed by serum ALT (Fig 3A–C). In contrast, the response of p38γ/δ$^{Lyzs\text{-}KO}$ mice to the MCD diet was milder for all three parameters (Fig 3A–C), demonstrating a protection similar to that seen in global p38γ/δ$^{-/-}$ mice. The p38γ/δ$^{Lyzs\text{-}KO}$ mice also had lower circulating levels of TNF-α and IL-6 than Lyzs-Cre mice after the MCD diet (Fig 3D), and gene expression analysis revealed significantly lower levels of the pro-inflammatory and myeloid cell markers *Il6, Gr1, Lyzs*, and *F4/80* (Fig 3E). In contrast, there were no between-genotype differences in the M1/M2 polarization of liver-infiltrated macrophages (Fig 3F).

Myeloid-specific p38γ and p38δ deficiencies do not affect diet-induced obesity, but protect against steatosis and diabetes

To confirm that the protection against liver steatosis in MCD-diet p38γ/δ$^{Lyzs\text{-}KO}$ mice was independent of the model used to induce the disease, we fed Lyzs-Cre and p38γ/δ$^{Lyzs\text{-}KO}$ mice with a high-fat diet (HFD). Weight gain was the same in p38γ/δ$^{Lyzs\text{-}KO}$ and Lyzs-Cre mice (Fig 4A), consistent with their similar lean and fat mass (Fig 4B). Liver mass was slightly lower in p38γ/δ$^{Lyzs\text{-}KO}$ mice (Fig 4C), while white adipose tissue mass was similar in both genotypes (Fig 4D). Histological analysis revealed less severe liver HFD-induced steatosis in the p38γ/δ$^{Lyzs\text{-}KO}$ mice (Fig 5A and B), correlating with lower circulating ALT levels (Fig 5C). We found higher energy expenditure in p38γ/δ$^{Lyzs\text{-}KO}$ animals with no differences in the respiratory exchange quotient [VCO_2]/[VO_2] between p38γ/δ$^{Lyzs\text{-}KO}$ and Lyzs-Cre mice (Fig 4E).

To study whether the protection against steatosis ameliorates HFD-induced diabetes, we performed a glucose tolerance test (GTT). HFD-fed p38γ/δ$^{Lyzs\text{-}KO}$ mice showed significantly higher glucose tolerance (Fig 5D) and lower fasting glucose (Fig 5E) than age-matched Lyzs-Cre controls on the same diet. These results indicate that the protection against steatosis in mice lacking p38γ/δ in myeloid cells also protects against HFD-induced diabetes.

A diet high in cholesterol, saturated fat, and fructose (HFF) has been found to recapitulate features of metabolic syndrome and NASH better than the traditional HFD (Charlton *et al*, 2011). Histological analysis of p38γ/δ$^{Lyzs\text{-}KO}$ and Lyzs-Cre mice fed a HFF diet revealed less severe liver steatosis in the p38γ/δ$^{Lyzs\text{-}KO}$ mice (Appendix Fig S3B and F), inflammation and fibrosis (Appendix Fig S3F), correlating with lower triglyceride accumulation and circulating ALT levels (Appendix Fig S3C and D). This protection against liver steatosis was associated with an improvement in fasting glucose (Appendix Fig S3E).

p38γ-floxed mice have below-normal expression of p38γ in muscle and fat (data not shown), raising the possibility that this defective expression might contribute to the protection against steatosis. To exclude this, we generated radiation chimeras by transplanting p38γ/δ$^{Lyzs\text{-}KO}$ or Lyzs-Cre bone marrow cells into lethally irradiated WT mice and fed a HFD or MCD diet. Efficient reconstitution of B6.SJL (CD45.1) mice with p38γ/δ$^{Lyzs\text{-}KO}$ or Lyzs-Cre bone marrow from C57BL/6J (CD45.2) mice was confirmed by staining peripheral blood leukocytes and liver-infiltrated leukocytes with antibodies to CD45.1/CD45.2 and analysis by flow cytometry (Fig 6A). Histological analysis showed milder steatosis (Fig 6B and C and Appendix Fig S4A), correlating with lower circulating ALT levels (Fig 6D and Appendix Fig S4B) after MCD or HFD in CX BM p38γ/δ$^{Lyzs\text{-}KO}$ than in the control CX BM Lyzs-Cre mice. Protection against HFD-induced steatosis associated with lower fasting glucose in CX BM p38γ/δ$^{Lyzs\text{-}KO}$ (Fig 6E). These results confirmed that this protection is a specific consequence of the loss of p38γ/δ in bone marrow-derived cells.

p38γ and p38δ control neutrophil infiltration during steatosis by regulating neutrophil adhesion

The protection of p38γ/δ myeloid KO mice against steatosis and liver inflammation, together with the low levels of myeloid cell markers in the livers of these animals suggested a possible effect on liver infiltration in animals fed a MCD diet or HFD. Characterization of liver-infiltrating leukocyte subsets in mice fed either diet revealed that the diet-induced increase in liver-infiltrating neutrophil counts (CD11b^{+}Gr-1^{high}) was significantly bigger in Lyzs-Cre mice than in p38γ/δ$^{Lyzs\text{-}KO}$ mice (Fig 7A), and similar results were observed in radiation chimeras restored by bone marrow from Lyzs-Cre mice versus p38γ/δ$^{Lyzs\text{-}KO}$ mice (Appendix Figs S4C and S5). This result correlated with lower levels of circulating neutrophils in p38γ/δ$^{Lyzs\text{-}KO}$ mice after both diets (Fig 7B and C).

Figure 3. p38γ/δ$^{Lyzs\text{-}KO}$ mice are protected against steatohepatitis induced by MCD diet.
Lyzs-Cre and p38γ/δ$^{Lyzs\text{-}KO}$ mice were fed a ND or a MCD diet for 3 weeks.

A Representative H&E- and Oil Red-stained liver sections. Scale bar: 50 μm.
B, C Liver triglycerides (B) and plasma ALT (C) at the end of the diet period.
D Measurement of plasma TNF-α and IL-6.
E qRT–PCR analysis of myeloid cell markers and cytokine mRNA expression from liver tissue; mRNA expression was normalized to the amount of *Gapdh* mRNA.
F qRT–PCR analysis of M1 and M2 polarization cell markers from liver-infiltrated macrophages. mRNA expression was normalized to the amount of *Gapdh* mRNA.

Data information: Data are means ± SEM (n = 5–10). *P < 0.05; **P < 0.01; ***P < 0.001 (one-way ANOVA coupled to Bonferroni's post-tests).

© 2016 The Authors

Published online: February 3, 2016
The EMBO Journal

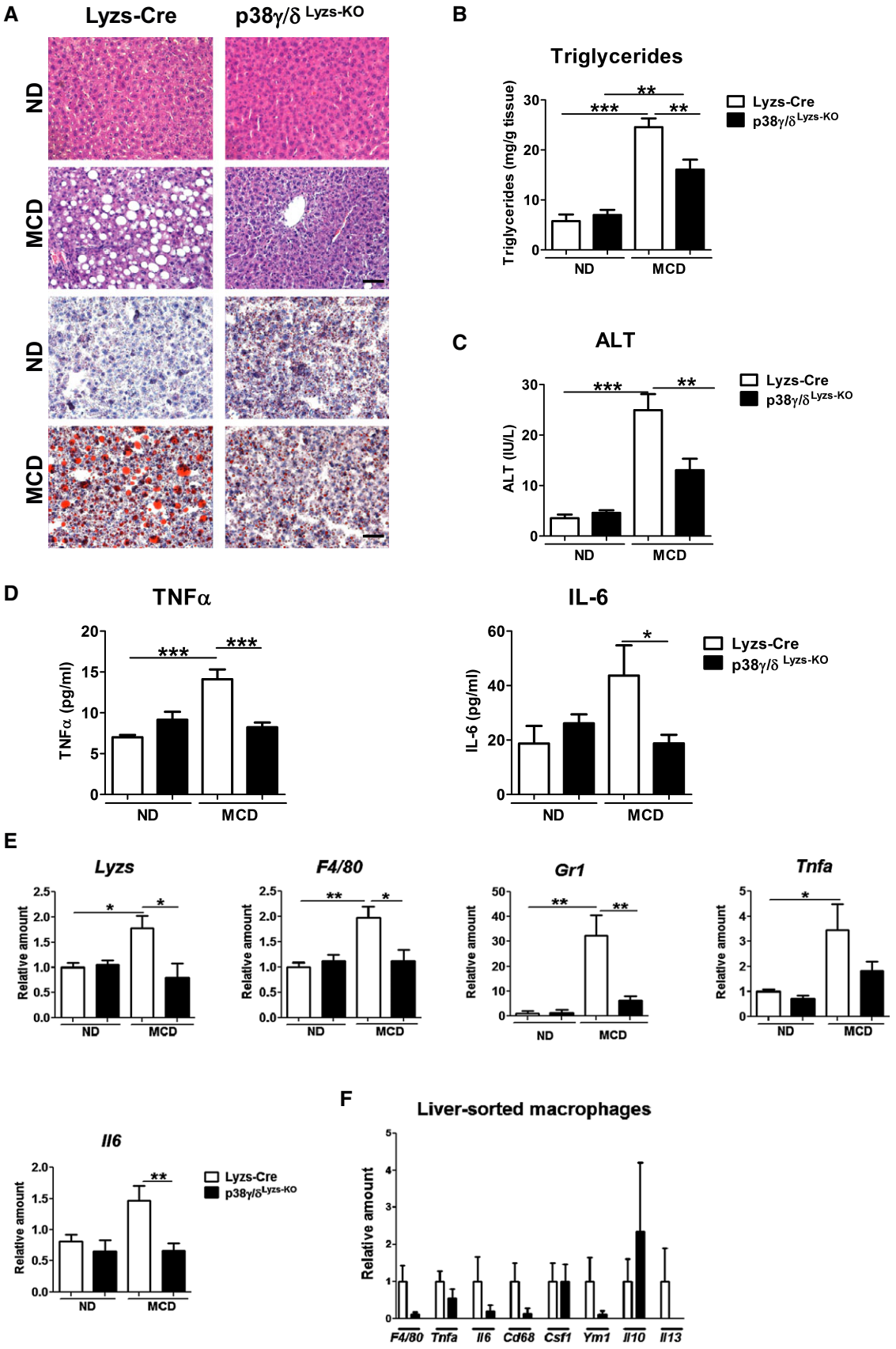

Figure 3.

© 2016 The Authors

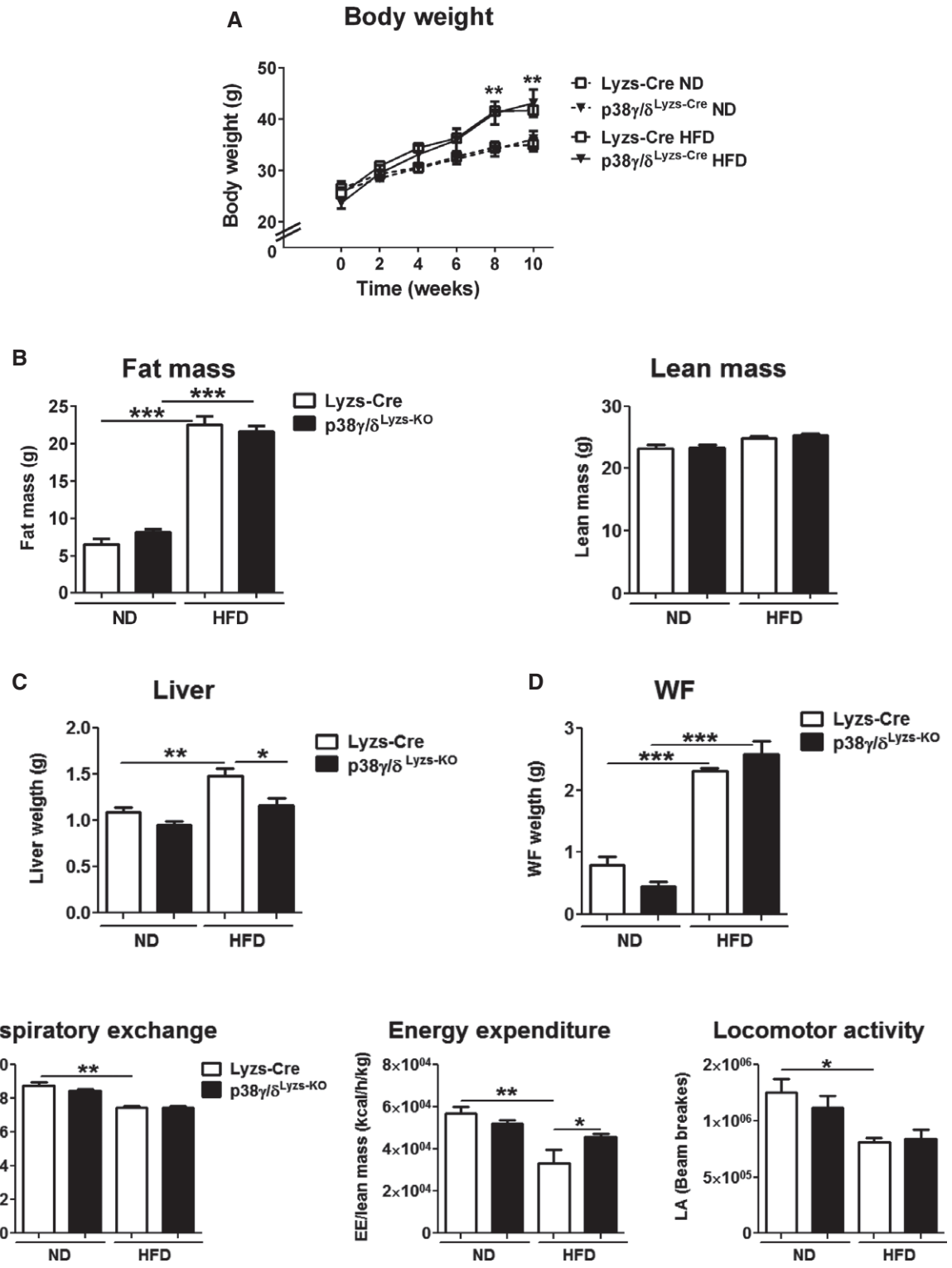

Figure 4. p38γ and p38δ deficiency in myeloid cells improves glucose metabolism in an obesity model.

Lyzs-Cre and p38γ/δ$^{Lyzs-KO}$ mice were fed a ND or a high-fat diet (HFD) for 10 weeks.

A Body weight measured at the indicated times during HFD treatment.

B Fat mass and lean mass determined by MRI at the end of the diet period.

C, D Liver mass and white fat (WF) mass.

E Respiratory exchange quotient, energy expenditure, and locomotor activity, detected in metabolic cages.

Data information: Data are means ± SEM (n = 5–10). *P < 0.05; **P < 0.01; ***P < 0.001 (one-way ANOVA coupled to Bonferroni's post-tests).

© 2016 The Authors

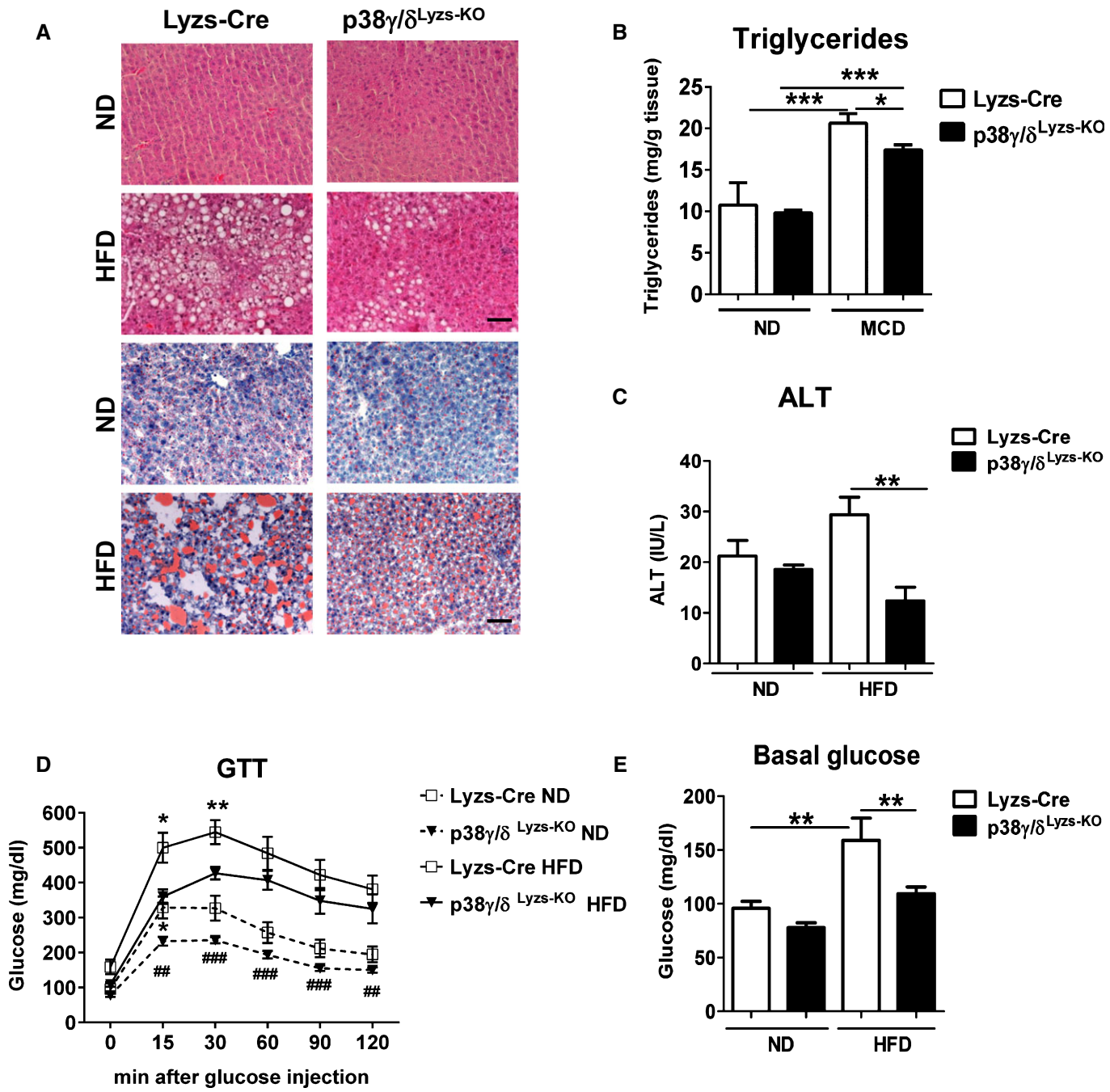

Figure 5. p38γ/δ$^{Lyzs-KO}$ mice are protected against steatohepatitis induced by HFD.
Lyzs-Cre and p38γ/δ$^{Lyzs-KO}$ mice were fed a ND or a HFD for 10 weeks.

A, B Representative H&E- and Oil Red-stained liver sections (scale bar: 50 μm) (A) and liver triglycerides (B).

C Plasma ALT at the end of the diet period.

D Glucose tolerance measured at the end of the diet period. Blood glucose concentration was measured in mice given an intraperitoneal glucose injection (1 g/kg) after overnight fasting.

E Basal blood glucose in overnight-fasted ND and HFD-fed Lyzs-Cre and p38γ/δ$^{Lyzs-KO}$ mice.

Data information: Data are means ± SEM (n = 5–10). *P < 0.05; **P < 0.01; ***P < 0.001 refers to p38γ/δ$^{Lyzs-KO}$ versus Lyzs-Cre; $^{\#\#}P$ < 0.01; $^{\#\#\#}P$ < 0.001 refers to ND versus HFD (one-way ANOVA coupled to Bonferroni's post-tests or Newman–Keuls post-test for liver triglycerides).

Neutrophils are the first immune cell type to respond to inflammation and can induce a chronic inflammatory state by promoting macrophage recruitment and interacting with antigen-presenting cells (Mantovani *et al*, 2011; Talukdar *et al*, 2012). Neutrophil levels by defensin 1–3 and neutrophils activation by nitrotyrosine staining, a measure of NO production, were elevated in the livers of obese

© 2016 The Authors

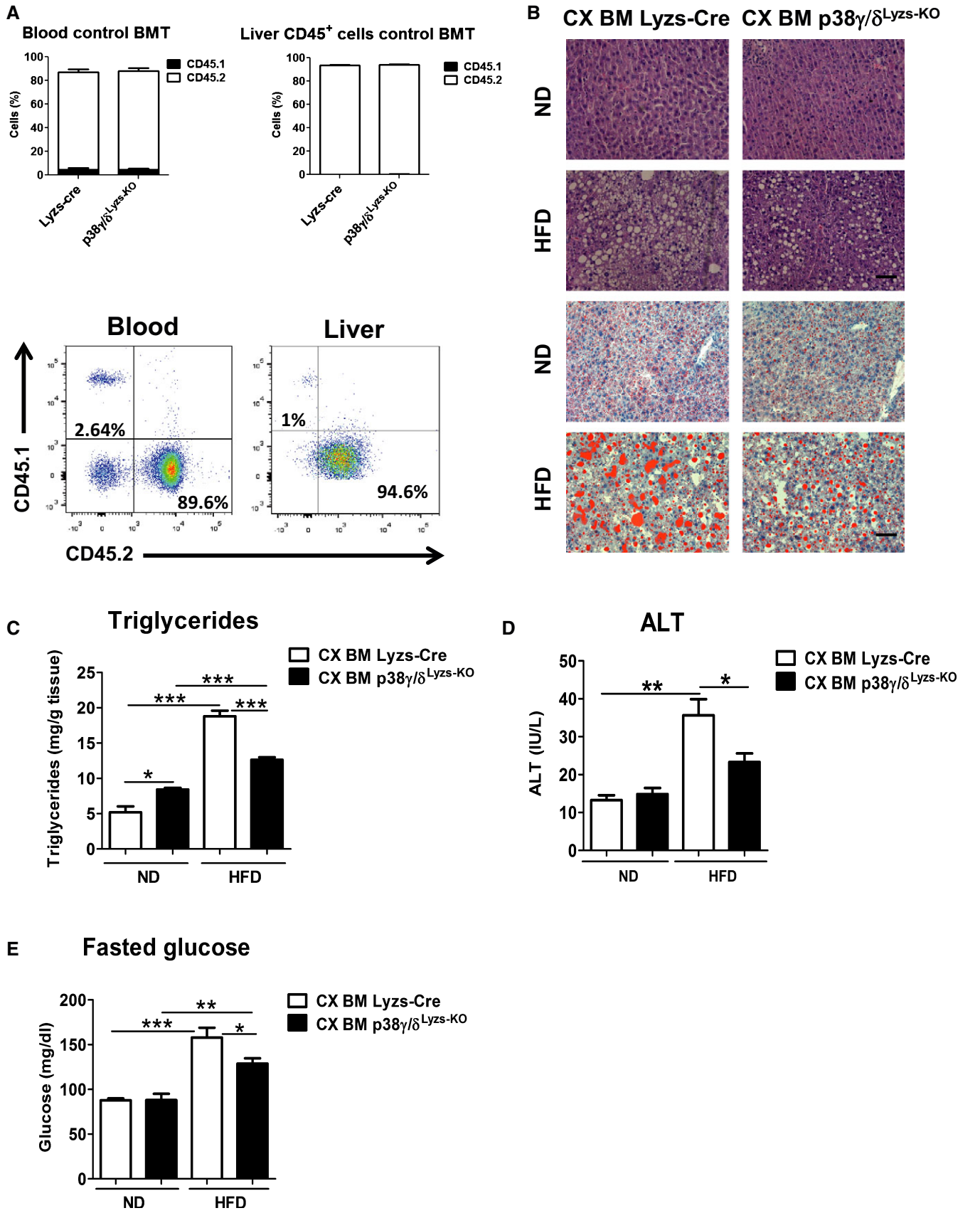

Figure 6.

© 2016 The Authors

Published online: February 3, 2016
The EMBO Journal

Figure 6. p38γ/δ$^{Lyzs\text{-}KO}$ hematopoietic cells protect mice against HFD-induced steatosis.
Lethally irradiated WT mice were reconstituted with BM from Lyzs-Cre (Cx BM Lyzs-Cre) or p38γ/δ$^{Lyzs\text{-}KO}$ mice (Cx BM p38γ/δ$^{Lyzs\text{-}KO}$). Two months after the transplant, mice were fed the HFD for 10 weeks.

A Freshly prepared CD45.2 whole BM mononuclear cells (2×10^7) were transplanted into lethally irradiated B6.SJL (CD45.1) mice, and engraftment by CD45.2 cells (%) was analyzed by antibody staining and FACS of peripheral blood and liver CD45$^+$ cells. Charts show CD45.1 and CD45.2 expression in blood cells (left) and liver cells (right) isolated from transplanted mice (n = 3). Representative FACS dot plots of CD45.1 and CD45.2 expression are shown beneath the charts.

B Representative H&E- and Oil Red-stained liver sections. Scale bar: 50 μm.

C Liver triglyceride content.

D Plasma transaminase ALT activity.

E Fasted glucose, detected at the end of the diet period in overnight-fasted mice.

Data information: Data are means ± SEM (n = 5–10). *P < 0.05; **P < 0.01; ***P < 0.001 (one-way ANOVA coupled to Bonferroni's post-tests).

patients with NAFLD (Appendix Fig S6A and B). To test the possible role of neutrophil p38γ/δ expression in the etiology of inflammation-induced liver steatosis, we first compared the capacity of WT and p38γ/δ-neutrophils to migrate to steatotic liver. For this, we performed a competitive cell migration assay that allows direct and simultaneous comparison of the migration of multiple cell subsets in the same mouse. MCD-diet WT mice were i.v. injected with a 1:1 mix of DiO-labeled WT and DiD-labeled p38γ/δ$^{-/-}$ neutrophils (6×10^6 cells in total). WT neutrophils arrived at the steatotic liver 1 h after injection, but recruitment of p38γ/δ$^{-/-}$ neutrophils was markedly curtailed (Fig 7D and E). The more extensive recruitment of WT neutrophils appear to be not due to better survival since neutrophils from both genotypes showed the same survival ratio; however, we cannot rule out some role of p38γ/δ in neutrophil survival (Appendix Fig S7A).

Using intravital microscopy (IVM), we further quantified TNF-α-stimulated neutrophil migration in the microcirculation of the cremaster muscle of mice reconstituted with bone marrow (BM) from Lyzs-Cre or p38γ/δ$^{Lyzs\text{-}KO}$ mice (Movies EV1 and EV2). Numbers of rolling neutrophils were slightly higher in mice receiving p38γ/δ$^{Lyzs\text{-}KO}$ BM, accompanied by higher rolling velocity and contrasting with lower numbers of adherent neutrophils (Fig 7F). This higher rolling velocity is consistent with increased expression of L-selectin observed in neutrophils lacking p38γ/δ. Moreover, the defective adhesion might be explained by the lower expression in p38γ/δ$^{Lyzs\text{-}KO}$ neutrophils of CD11b, an integrin that regulates neutrophil adhesion and migration (Appendix Fig S7B). These results show that neutrophil adhesion and recruitment are compromised in the absence of p38γ/δ. Neutrophil rolling under flow conditions is mediated by L-selectin (Abbassi *et al*, 1993). To test the involvement L-selectin in the impaired rolling of p38γ/δ$^{Lyzs\text{-}KO}$ neutrophils, we assayed neutrophil migration under flow conditions on plates coated with the CD11b ligand ICAM-1 and the L-selectin ligand E-selectin. Our results indicated that p38γ/δ$^{Lyzs\text{-}KO}$ neutrophils presented a higher rolling velocity than Lyzs-Cre neutrophils (Appendix Fig S7C).

To investigate whether the altered migration capacity of p38γ/δ$^{Lyzs\text{-}KO}$ neutrophils is due to an autonomous effect or a defective production of chemokines, we performed a parabiosis experiment. Efficiency of parabiosis was evaluated by using congenic markers to distinguish blood cells in parabiotic pairs, in which one partner was CD45.1$^+$. Parabiotic exposure of p38γ/δ$^{Lyzs\text{-}KO}$ mice to the circulation of WT (CD45.1) mice, both fed the MCD diet, was enough to worsen the steatosis phenotype of p38γ/δ$^{Lyzs\text{-}KO}$ (Appendix Fig S8A). The exacerbated steatosis correlated with a higher proportion of CD45.1 (WT) neutrophils in p38γ/δ$^{Lyzs\text{-}KO}$ livers compared to the proportion observed in livers from Lyzs-Cre mice (Appendix Fig S8B). There were no differences in macrophage infiltration (Appendix Fig S8B), indicating that the wild-type circulation specifically increases liver neutrophil infiltration in p38γ/δ$^{Lyzs\text{-}KO}$ mice. Neutrophils thus appear to be crucial to the steatosis protection in p38γ/δ$^{Lyzs\text{-}KO}$ mice.

Neutrophil-specific p38δ deficiency protects against steatosis

The most abundant p38 isoform in neutrophils is p38δ (Ittner *et al*, 2012). To test the implication of neutrophil p38δ in liver steatosis, we crossed p38δ-floxed mice with Mrp8-Cre mice (Passegue *et al*, 2004) to generate mice lacking p38δ specifically in neutrophils (p38δ$^{Mrp8\text{-}KO}$ mice; Appendix Fig S9A). H&E and Oil Red staining of liver sections revealed that these mice were partially protected against MCD-induced steatosis (Appendix Fig S9B). Moreover, p38δ$^{Mrp8\text{-}KO}$ mice had below-normal levels of MCD-induced ALT (Appendix Fig S9C). This protection was associated with low

Figure 7. p38γ/δ$^{Lyzs\text{-}KO}$ neutrophils have deficient migration to the liver.

A Flow cytometry analysis of liver myeloid subsets (CD11b$^+$ Gr-1^{high}, CD11b$^+$ Gr-1^{intermediate}, CD11b$^+$ Gr-1$^-$) isolated from Lyzs-Cre and p38γ/δ$^{Lyzs\text{-}KO}$ mice fed a MCD for 3 weeks or HFD for 10 weeks. Representative dot plots are shown, and bar charts show the diet-induced increase in each population as a percentage of the total intrahepatic CD11b$^+$ leukocyte population. Myeloid infiltrating cells isolated from livers were sorted by FACS and stained with H&E. Representative cells are shown next to the appropriate myeloid subsets.

B, C Neutrophils and monocytes as a percentage of total circulating leukocytes, measured in total blood in animals fed the MCD diet for 3 weeks (B) or the HFD for 10 weeks (C).

D, E WT mice fed the MCD diet were i.v. injected with a 1:1 mix of DiO-labeled Lyzs-Cre neutrophils and DiD-labeled p38γ/δ$^{Lyzs\text{-}KO}$ neutrophils (6×10^6 cells in total; n = 10). One hour after injection, liver-infiltrating neutrophils were assessed by flow cytometry (D) and fluorescence micrography on liver sections (E).

F Intravital microscopy quantification of the rolling and adhesion frequencies and rolling velocities of neutrophils recruited to venules irrigating inflamed (TNF-α-injected) cremaster muscle.

Data information: Data are means ± SEM (n = 5–10). *P < 0.05; **P < 0.01; ***P < 0.001 (one-way ANOVA coupled to Bonferroni's post-tests).

© 2016 The Authors

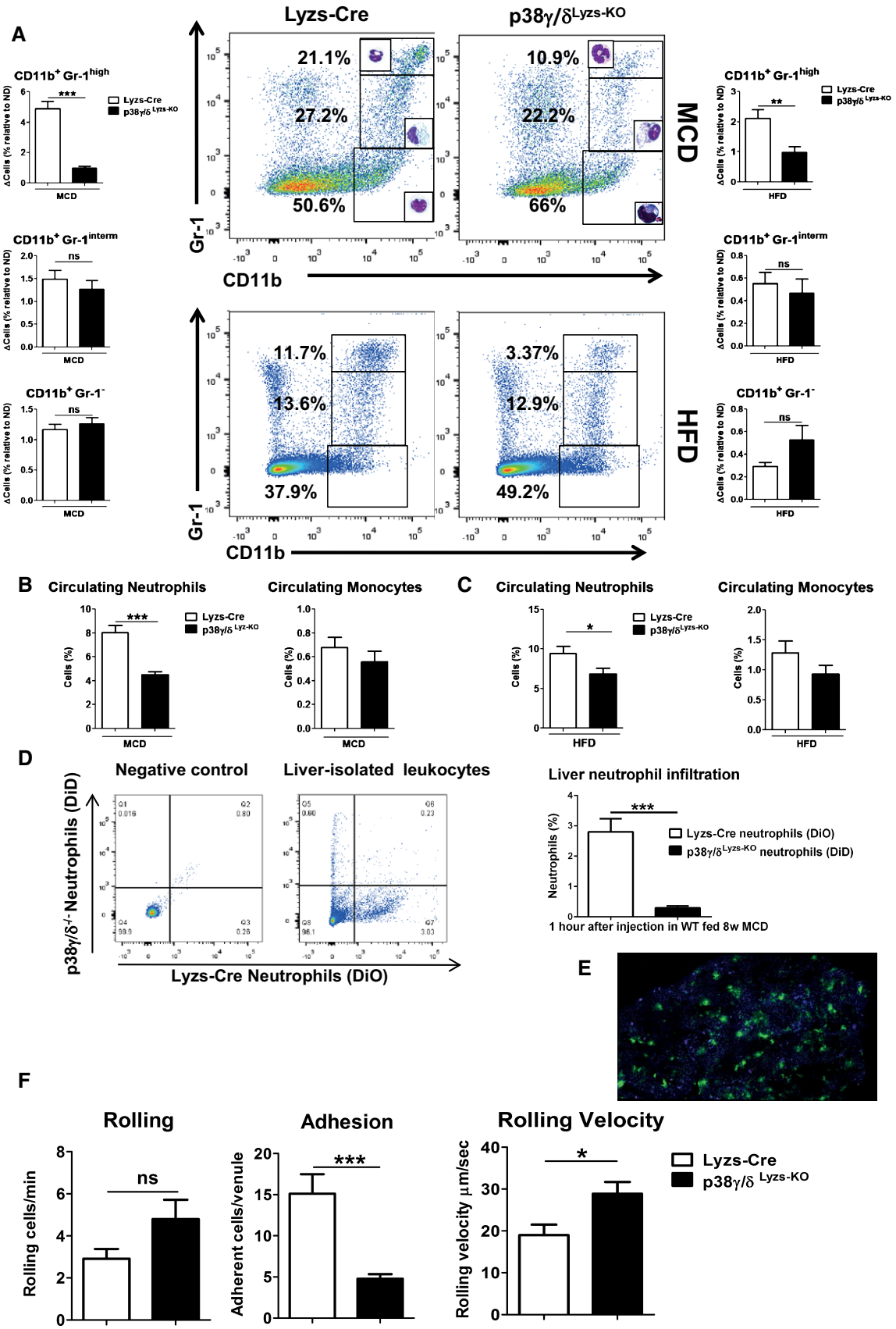

Figure 7.

© 2016 The Authors

Published online: February 3, 2016
The EMBO Journal

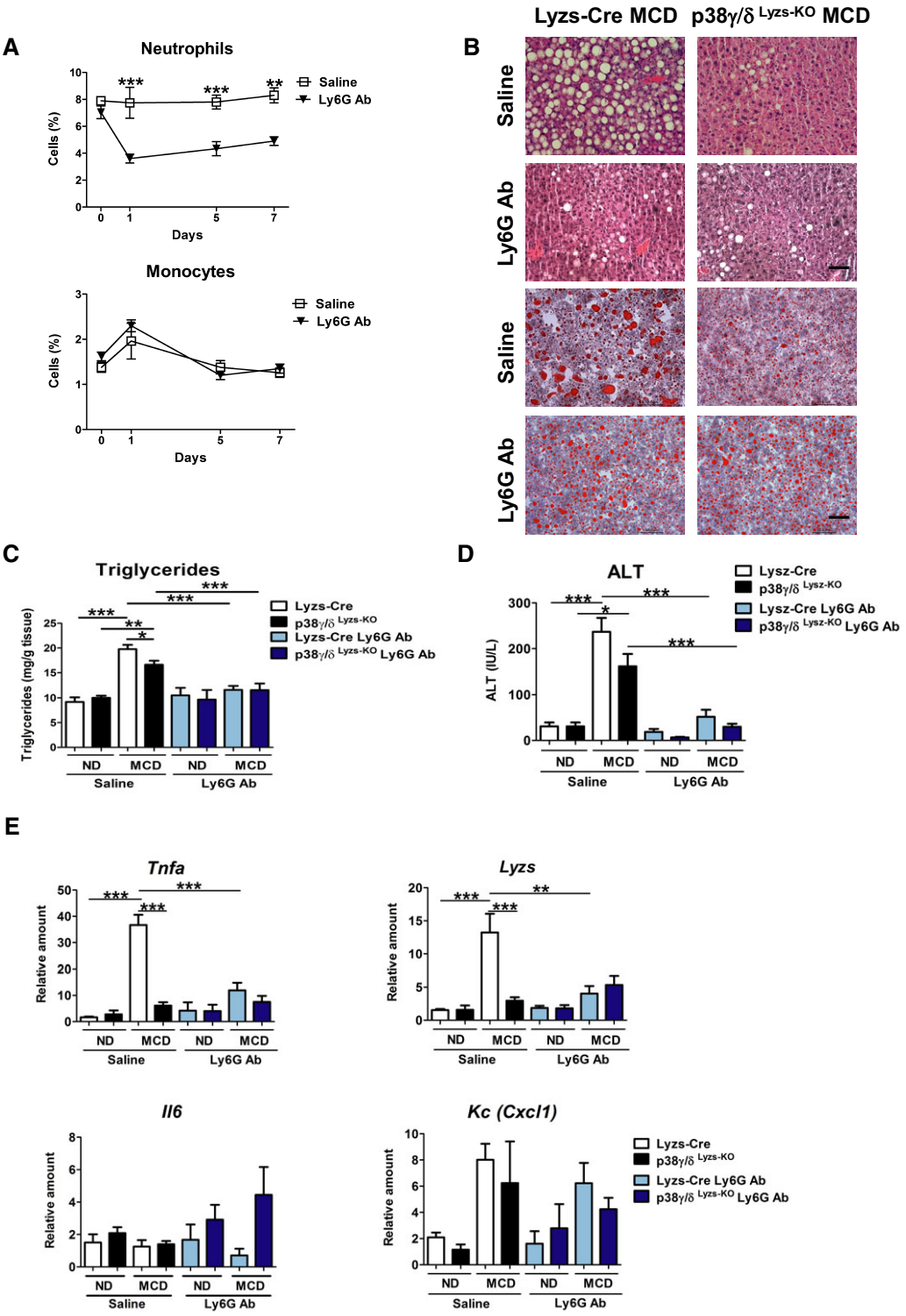

Figure 8. Neutrophil depletion protects against steatosis.

Osmotic minipumps containing saline or Ly6G antibody were implanted subcutaneously in Lyzs-Cre and p38γ/δ$^{Lyzs\text{-}KO}$ mice. These animals were fed a ND or MCD for 3 weeks.

A Neutrophils and monocytes as a percentage of circulating leukocytes, measured in total blood.

B Representative H&E- and Oil Red-stained liver sections after 3 weeks of treatment. Scale bar: 50 μm.

C, D Liver triglyceride (C) and plasma transaminase activity (ALT) (D) at the end of the diet period.

E Total RNA was extracted from livers, and chemokine and cytokine mRNA levels were determined by qRT–PCR. mRNA expression was normalized to the amount of *Gapdh* mRNA.

Data information: Data are means ± SEM (n = 5–10). *P < 0.05; **P < 0.01; ***P < 0.001 (one-way ANOVA coupled to Bonferroni's post-tests).

© 2016 The Authors

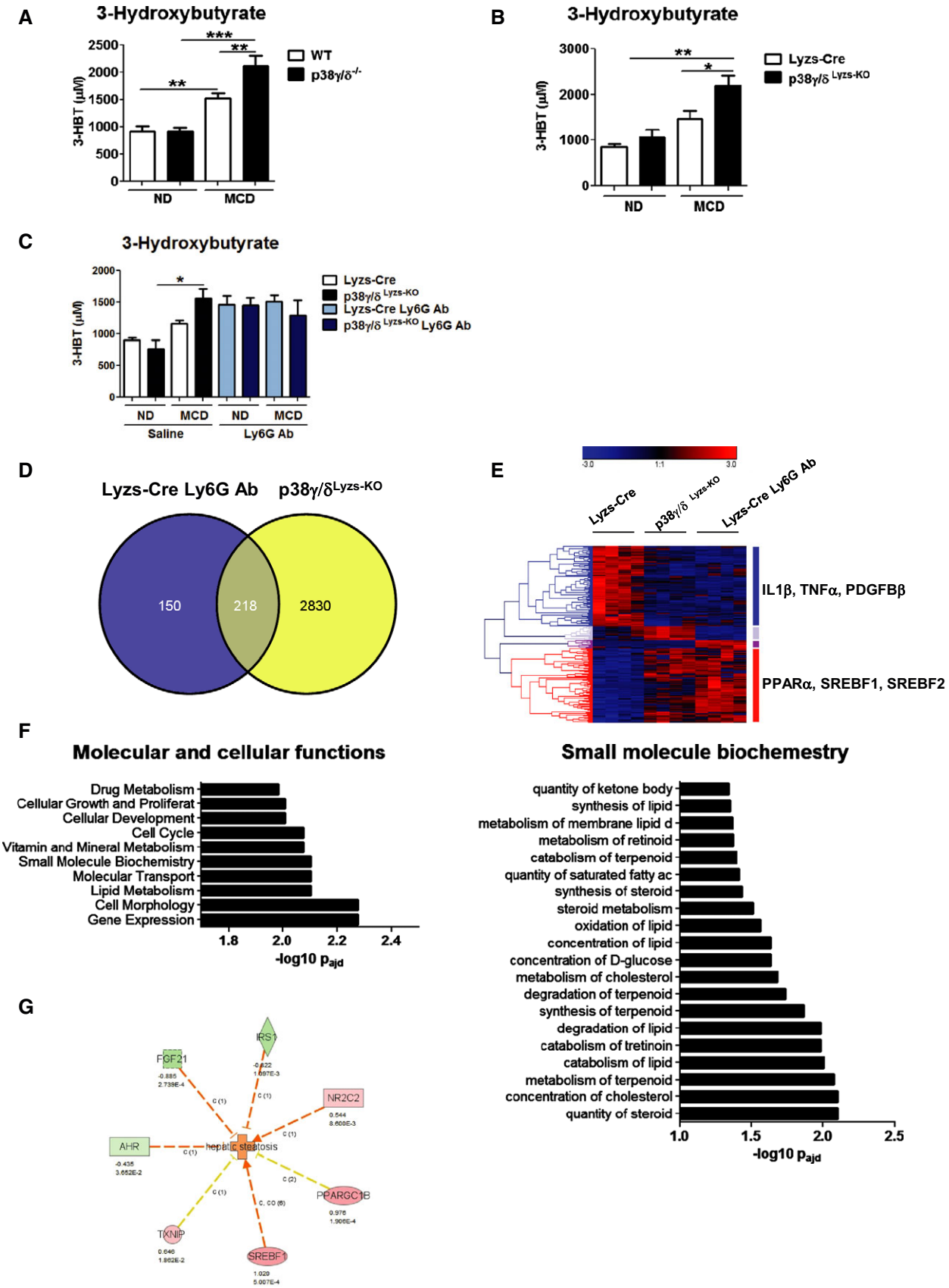

Figure 9.

© 2016 The Authors

neutrophil infiltration of the liver compared with MCD-diet-fed Mrp8-Cre mice (Appendix Fig S9D). These results indicate that the protection against steatosis is at least partially due to the expression of p38δ in neutrophils.

Neutrophil depletion protects against steatosis development

Early neutrophil accumulation triggers monocyte migration and inflammation (Savill *et al*, 1989), and diminished neutrophil accumulation can ameliorate NAFLD (Nathan, 2006). To clarify whether defective neutrophil migration contributes to the milder hepatic steatosis in MCD-diet p38γ/δ$^{Lyzs\text{-}KO}$ mice, we depleted neutrophils in MCD-diet Lyzs-Cre mice by administering anti-Ly6G antibody. Administration of this antibody (0.4 mg/kg per day i.v. for 7 days) reduced the levels of circulating neutrophils without affecting monocytes (Fig 8A), and treatment for 21 days significantly improved liver steatosis and reduced triglyceride accumulation to an extent similar to that observed in the MCD-diet p38γ/δ$^{Lyzs\text{-}KO}$ mice; in contrast, anti-Ly6G treatment of MCD-diet p38γ/δ$^{Lyzs\text{-}KO}$ mice did not appear to provide further benefit (Fig 8B and C). Anti-Ly6G antibody treatment of MCD-diet Lyzs-Cre animals also reduced liver necrosis assessed by serum ALT levels (Fig 8D). Moreover, while liver expression of *Il6* was not affected neutrophil depletion in Lyzs-Cre mice also significantly reduced liver expression of the pro-inflammatory markers *Tnfa* and *Lyzs* (Fig 8E).

Neutrophil depletion protects against steatosis by modulating lipid metabolism

We next measured the fatty-acid oxidation metabolite β-hydroxybutyrate, to investigate whether the improvement in hepatic steatosis in MCD-diet p38γ/δ$^{-/-}$, p38γ/δ$^{Lyzs\text{-}KO}$, and Ly6G-treated mice was linked to an increase in lipid oxidation. p38γ/δ$^{-/-}$, p38γ/δ$^{Lyzs\text{-}KO}$, and Ly6G-treated mice all had higher levels of serum β-hydroxybutyrate than similarly fed WT or Lyzs-Cre mice (Fig 9A–C), and this higher lipid oxidation correlated with the higher energy expenditure observed in p38γ/δ$^{Lyzs\text{-}KO}$ mice (Fig 4E).

To confirm an effect of impaired neutrophil infiltration on liver lipid metabolism, we examined the effect of MCD-diet on hepatic gene expression in Lyzs-Cre, p38γ/δ$^{Lyzs\text{-}KO}$, and anti-Ly6G-treated Lyzs-Cre mice by RNA-seq (Fig 9D–G). Differentially regulated genes that potentially contribute to the hepatic phenotype of the neutrophil-deficient mice were identified by comparing gene expression patterns with MCD-diet-fed Lyzs-Cre mice (Fig 9D–G). Most gene alterations observed in p38γ/δ$^{Lyzs\text{-}KO}$ mice were also detected in anti-Ly6G-treated Lyzs-Cre mice (Fig 9D). Gene ontology analysis of genes that changed in the same manner in both mice identified significant (adjusted $P < 0.001$) association of neutrophil deficiency with elevated oxidative lipid metabolism and decreased inflammation (Fig 9E), including genes regulated by PPAR-α (peroxisome proliferator-activated receptor-alpha) and by IL-2β and TNF-α (Fig 9E). Neutrophil deficiency thus causes increased lipid oxidation and decreased inflammation (Fig 9E–G).

Discussion

The alternative p38 MAPKs p38γ and p38δ regulate inflammatory processes through several mechanisms. Here, we demonstrate that expression of both kinases in myeloid cells is necessary for the development of liver steatosis and inflammation in animal models of NAFLD. Further, these kinases control neutrophil migration to the liver, and hepatic neutrophils contribute to liver steatosis by promoting liver inflammation and lipogenic metabolism. Deletion of p38γ/δ expression in the myeloid compartment curtails neutrophil recruitment to the liver, protecting animals against diet-induced steatosis and associated liver damage, and effect that is also partially mediated by the lack of p38δ in neutrophils. These findings indicate a major role of p38γ/δ in controlling neutrophil recruitment during inflammation and suggest that inhibition of neutrophil trafficking is a potential treatment route for steatosis.

The analysis of NAFLD mouse models clearly demonstrates that the protection in p38γ/δ$^{-/-}$ mice is attributable to the loss of p38γ/δ expression in hematopoietic cells. The bone marrow transfer experiments and conditional KO animal results confirm that p38γ and δ expressions by hematopoietic cells drive steatosis in both diet-induced steatosis models. Neutrophils were recently shown to be important mediators of alcoholic fatty liver disease (Bertola *et al*, 2013), and p38δ is known to control neutrophil inflammatory response in lung by regulating PKD1 activity (Ittner *et al*, 2012). Our analysis shows that loss of p38γ and p38δ in neutrophils might be responsible for the protection observed in the KO animals. Livers from mice lacking p38γ and p38δ had lower neutrophil infiltration, and neutrophils lacking these kinases could not be recruited to the liver in a competition assay, indicating a cell autonomous effect. The low adhesion and higher rolling velocity detected in neutrophils lacking p38γ and p38δ are broadly consistent with previous reports using p38δ$^{-/-}$ animals (Ittner *et al*, 2012). We also observed lower

Figure 9. Neutrophils control liver metabolic changes in steatosis development.

A–C Plasma levels of 3-hydroxybutyrate in WT and p38γ/δ$^{-/-}$ (A), Lyzs-Cre and p38γ/δ$^{Lyzs\text{-}KO}$ mice (B) and Lyzs-Cre Ly6G Ab treated after MCD diet (C) (n = 5–10).

D Overlap of gene expression changes between Lyzs-Cre mice treated with anti-Ly6G and p38γ/δ$^{Lyzs\text{-}KO}$ at the end of the MCD diet period n = 4 (each n is a mix of two different animals).

E Hierarchical clustering of the expression profiles of genes differentially expressed both between p38γ/δ$^{Lyzs\text{-}KO}$ and MCD-diet-fed Lyzs-Cre and between Lyzs-Cre treated with anti-Ly6G and MCD-diet-fed Lyzs-Cre mice. Genes up-regulated in both comparisons (red cluster) were mainly regulated by PPAR-α, SREBF1, and SREBF2, while the enriched upstream regulators of genes down-regulated in both conditions versus the control group (blue cluster) were IL-1β, TNF-α, and PDGFB-β.

F IPA (http://ingenuity.com) functional categories enriched in the set of genes differentially expressed between p38γ/δ$^{Lyzs\text{-}KO}$ and MCD-diet-fed Lyzs-Cre and between Lyzs-Cre treated with anti-Ly6G and MCD-diet-fed Lyzs-Cre mice (n = 4).

G Genes differentially expressed between p38γ/δ$^{Lyzs\text{-}KO}$ and MCD-diet-fed Lyzs-Cre and between Lyzs-Cre treated with anti-Ly6G and MCD-diet-fed Lyzs-Cre mice and involved in liver steatosis according to IPA.

Data information: Data are means ± SEM. *$P < 0.05$; **$P < 0.01$; ***$P < 0.001$ (one-way ANOVA coupled to Bonferroni's post-tests).

© 2016 The Authors

CD11b and higher L-selectin membrane expression, which could account for these defects in adhesion and rolling observed in the neutrophils lacking p38γ and p38δ. Moreover, lack of p38δ alone is insufficient to reduce neutrophil infiltration after the MCD diet and protect against liver steatosis. The ability of p38γ to compensate for the loss of p38δ is somewhat surprising given the low expression level of p38γ in neutrophils (Gonzalez-Teran *et al*, 2013; Han *et al*, 2013). A possible explanation is that $p38\delta^{-/-}$ neutrophils might increase the activation or expression of p38γ as a compensatory mechanism. It is also possible that p38γ in another myeloid cell type (e.g. resident macrophages) contributes to neutrophil migration by controlling cytokine and chemokine production. However, the results of competition migration assays in which resident macrophages are WT, and of the parabiosis experiment, argue against this possibility. Further experiments will be needed to determine the specific roles of p38γ and p38δ in different myeloid subsets and how these two isoforms can compensate each other. However, a role of neutrophils is clear because lack of p38δ only in neutrophils is enough to protect against steatosis.

On the other hand, the fact that neutrophil-specific deletion of p38δ has a more marked effect on phenotype than the whole-body p38δ KO might indicate that p38δ has an opposing role in another tissue and thereby modulates biological actions in a tissue-specific fashion. Opposing effects in different tissues have been shown for the stress kinase JNK: deletion of this kinase in the liver induces steatosis whereas deletion in fat is protective (Sabio *et al*, 2008, 2009).

Our data point out an important role of p38γ/δ in neutrophils. The same level of protection against diet-induced steatosis observed in $p38\gamma/\delta^{Lyzs\text{-}KO}$ mice was also achieved in mice depleted of neutrophils with anti-Ly6G antibody. Moreover, deletion of p38δ in neutrophils reduces hepatic neutrophils infiltration and partially protected against steatosis. These observations strongly suggest that neutrophil recruitment to the liver is essential for the initiation and progression of NAFLD and that neutrophil p38γ/δ expression contributes to the progression of this disease. The central role for neutrophils in NAFLD is consistent with their roles in ethanol-induced liver damage (Bertola *et al*, 2013) and macrophage recruitment to damaged tissue in obesity (Mansuy-Aubert *et al*, 2013) and with the description of neutrophil elastase as an important mediator of obesity-induced diabetes (Talukdar *et al*, 2012; Mansuy-Aubert *et al*, 2013). The importance of infiltrating neutrophils in liver inflammatory responses is also indicated by the underexpression of inflammatory genes in MCD-diet-fed $p38\gamma/\delta^{Lyzs\text{-}KO}$ and neutrophil-depleted mice and by the increased lipid oxidation and reduced lipogenesis in the neutrophil-depleted mice.

The data from mouse models correlate well with the overexpression p38δ and p38γ in livers of individuals with NAFLD, regardless of BMI, which could indicate the involvement of these kinases in the development of steatosis. This elevated p38δ expression could be due to increased neutrophil influx to these livers, as neutrophils are known to express high levels of p38δ (Ittner *et al*, 2012; Gonzalez-Teran *et al*, 2013). Accordingly, we also observed elevated neutrophil activity in the livers of obese patients with NAFLD. It would be interesting to characterize the cell-type contribution to p38δ and p38γ expression in human liver. However, we cannot rule out important roles for p38δ and p38γ expressed in other cell types involved in steatosis development.

In summary, our findings indicate that neutrophil infiltration triggers the development of NAFLD and that p38γ/δ regulate this process by controlling neutrophil infiltration. Therefore, inhibition of p38γ/δ might represent a novel therapeutic target for NAFLD in humans, with the potential to limit injury and possibly prevent progression to NASH and cirrhosis.

Materials and Methods

Study population and sample collection

The study population included a group of obese adult patients with body mass index (BMI) ≥ 35 kg/m^2 and a liver biopsy compatible with NAFLD. Participants were recruited from patients undergoing elective bariatric surgery at the University Hospital of Salamanca. As controls, we included individuals with BMI < 35 kg/m^2 who underwent laparoscopic cholecystectomy for gallstones. These individuals were divided into two groups according to the presence of NAFLD: (i) controls without NALFD ($n = 11$) if they had no laboratory or histopathological evidence of NAFLD or other liver diseases; (ii) controls with NAFLD ($n = 9$) if they had a liver biopsy compatible with NAFLD. Therefore, three groups of subjects were included in the study: obese patients (BMI ≥ 35 kg/m^2) with NAFLD, controls with BMI < 35 without liver disease, and controls with BMI < 35 kg/m^2 and with NAFLD. Baseline characteristics of these groups are listed in Appendix Table S1.

Participants were excluded if they had a history of alcohol use disorders or excessive alcohol consumption (> 30 g/day in men and > 20 g/day in women), chronic hepatitis C or B, or if laboratory and/or histopathological data showed causes of liver disease other than NAFLD. The study was approved by the Ethics Committee of the University Hospital of Salamanca and all subjects provided written informed consent to undergo liver biopsy under direct vision during surgery.

Data were collected on demographic information (age, sex, and ethnicity), anthropomorphic measurements (BMI), smoking and alcohol history, coexisting medical conditions, and medication use. Before surgery, fasting venous blood samples were collected for determination of complete cell blood count, total bilirubin, aspartate aminotransferase (AST), alanine aminotransferase (ALT), total cholesterol, high-density lipoprotein, low-density lipoprotein, triglycerides, creatinine, glucose, and albumin.

A portion of each liver biopsy was fixed in 10% formalin and stained with hematoxylin–eosin and Masson's trichrome for standard histopathological analysis. The remaining portion was stored at −80°C for later protein was extraction. The presence of NAFLD was diagnosed using standard criteria, and severity of the disease was established using the NAFLD activity score (NAS) described by Kleiner (Kleiner *et al*, 2005).

Mice

Mice deficient for p38γ (B6.129-Mapk12tm1) and p38δ (B6.129-Mapk13tm1) were crossed with B6.129P2-Lyz2tm1(cre)Ifo/J mice or with B6.Cg-Tg(S100A8-cre,-EGFP)1Ilw/J mice backcrossed for 10 generations to the C57BL/6J background (Jackson Laboratory). Genotype was confirmed by PCR analysis of genomic DNA.

© 2016 The Authors

Radiation chimeras were generated by exposing recipient mice to 2 doses of ionizing radiation (625 Gy) and reconstituting them with 2×10^7 donor BM cells by injection into the tail vein. Proper reconstitution was checked in B6.SJL (CD45.1) control mice transplanted with CD45.2 BM mononuclear cells by immunostaining and FACS analysis of peripheral blood and liver $CD45^+$ cells. Mice were fed a standard chow diet or a methionine–choline-deficient (MCD) diet for 3 weeks (Research Diets Inc). Alternatively, mice were fed a high-fat diet (HFD) or a high-fat and high-fructose (HFF) diet (Research Diets Inc) for 10 weeks. For neutrophil depletion, mice were treated with anti-Ly6G antibody (0.4 mg/kg per day, 21 days) via subcutaneously implanted mini-osmotic pumps (Alzet); saline was administered as a control. All animal procedures conformed to EU Directive 86/609/EEC and Recommendation 2007/526/EC regarding the protection of animals used for experimental and other scientific purposes, enacted under Spanish law 1201/2005.

Hepatic peroxidation

Liver extracts were prepared by sonication (15 cycles) in cytoplasmic lysis buffer [25 mM Tris–HCl (pH 7.5), 10 mM NaCl, 1 mM EDTA, 100 mM $MgCl_2$, 1% NP-40, 0.1 mM phenylmethylsulfonyl fluoride, and 10 μg/ml aprotinin and leupeptin]. Malondialdehyde and hydrogen peroxide were assayed with the TBARS Assay kit (Cayman) and the Amplex Red Hydrogen Peroxide/Peroxidase Assay Kit (Invitrogen).

Glucose tolerance test

Glucose tolerance test was performed as described (Mora *et al*, 2005).

Isolation of liver-infiltrating mononuclear leukocytes

Mouse livers were collected, and a single-cell suspension was obtained and passed through a 70-μm strainer. Leukocytes were collected from the interphase of centrifuged Ficoll gradients.

Flow cytometry

Isolated liver-infiltrating leukocytes were counted with a CASY Cell Counter (57) and then labeled by surface staining (Streptavidin-PERCP/biotin-conjugated anti-CD11b and APC-conjugated anti-Gr-1; Invitrogen). Flow cytometry was performed with a FACScan cytofluorometer (FACS Canto BD), and data were collected and analyzed with FlowJo software.

Intravital microscopy

Intravital microscopy of the cremaster muscle after TNF-α injection (0.5 μg, intrascrotal injection) was performed as reported (Sreeramkumar *et al*, 2013) using an Axio Examiner Z.1 workstation (Zeiss, Germany). Fluorescently conjugated anti-Ly6G (1 mg/mouse) was injected immediately before acquisition to specifically identify neutrophils. Recorded videos were analyzed using Slidebook software (Intelligent Imaging Innovations). At least 30 venules were analyzed from 3 mice per group.

Competitive cell migration assay

Lyzs-Cre and $p38\gamma/\delta^{Lyzs\text{-}KO}$ neutrophils were isolated from bone marrow by labeling with biotin-conjugated anti-Ly6C/G antibody (BD Pharmigen) and magnetic streptavidin microbeads (Miltenyi Biotec) and then separating them on MACS MS columns (Miltenyi Biotec). Isolated Lyzs-Cre neutrophils were stained with DiO and $p38\gamma/\delta^{Lyzs\text{-}KO}$ neutrophils were stained with DiD (Vybrant Cell-Labeling Solution, Molecular Probes). Cell viability was checked by DAPI staining followed by FACS. The labeled cells were then mixed at a 1:1 ratio and injected (6×10^6 cells) into MCD-diet WT mice. After 1 h, liver-infiltrating mononuclear leukocytes were isolated and directly detected by FACS. Fluorescent neutrophils were also detected by confocal microscopy in OCT-cryopreserved liver sections.

Statistical analysis

Differences between experimental groups were examined for statistical significance by two-tailed Student's *t*-test or one-way ANOVA coupled to Bonferroni's and Newman–Keuls post-test. Characteristics of patients and controls were compared by means of Mann–Whitney *U*-test for quantitative variables and χ^2 or Fisher's tests for qualitative variables.

For more Materials and Methods, see the Appendix.

Expanded View for this article is available online.

Acknowledgements
We thank S. Bartlett for English editing, L. Manzanedo, A. Mateos, and O. Rozo for help with sample and data collection, and A. Molina for histological analysis. We are grateful to R.J. Davis for critical reading of the manuscript, R. González-Sarmiento for help with clinical study design. We thank the staff at the CNIC Genomics, Cellomics, and Bioinformatics units for technical support and help with data analysis. G.S. is an investigator of the Ramón y Cajal Program. B.G.T. is a fellow of FPI Severo Ochoa CNIC Program (SVP-2013-067639). I.G.N. is supported by a CNIC IPP FP7 Marie Curie Programme (PCOFUND-2012-600396). M.A.V. is a recipient of a Madrid Regional Government Fellowship. This work was funded by the following grants to G.S.: ERC 260464, EFSD 2030, MICINN SAF2010-19347, and Comunidad de Madrid S2010/BMD-2326; to M.M.: ISCIII and FEDER, PI10/01692, and I3SNS-INT12/049; to L.H.C.: Junta de Castilla y León GRS 681/A/11; to A.H.: SAF 2012-31142; to R.N.: MICINN BFU2012-35255, Xunta de Galicia EM 2012/039 and 2012-CP069; and to A.C.: MICINN SAF2010-19734. The CNIC is supported by the Ministerio de Economía y Competitividad and the Pro-CNIC Foundation.

Author contributions
BG-T, NM, IGN, and GS designed the study; BG-T, NM, IGN, MAV, VS, AM, GC, MLS, EB, LL-V, ER, VB, and GS performed experimental analysis; metabolic cages were performed by RN and SP-S; intravital microscopy was performed by VS and AH; *in vitro* neutrophil migration was performed by MLS and FS-M; MM designed and coordinated human study; MM, LH-C, JLT, and LO recruited subjects and were responsible for sample and data collection; AC provided reagents and BG-T, NM, IGN, and GS wrote the manuscript. All authors contributed to the revision of the manuscript and approved the final version.

Conflict of interest
The authors declare that they have no conflict of interest.

© 2016 The Authors

References

Abbassi O, Kishimoto TK, McIntire LV, Anderson DC, Smith CW (1993) E-selectin supports neutrophil rolling *in vitro* under conditions of flow. *J Clin Invest* 92: 2719 – 2730

Adams RH, Porras A, Alonso G, Jones M, Vintersten K, Panelli S, Valladares A, Perez L, Klein R, Nebreda AR (2000) Essential role of p38alpha MAP kinase in placental but not embryonic cardiovascular development. *Mol Cell* 6: 109 – 116

Allen M, Svensson L, Roach M, Hambor J, McNeish J, Gabel CA (2000) Deficiency of the stress kinase p38alpha results in embryonic lethality: characterization of the kinase dependence of stress responses of enzyme-deficient embryonic stem cells. *J Exp Med* 191: 859 – 870

Anstee QM, Goldin RD (2006) Mouse models in non-alcoholic fatty liver disease and steatohepatitis research. *Int J Exp Pathol* 87: 1 – 16

Beardmore VA, Hinton HJ, Eftychi C, Apostolaki M, Armaka M, Darragh J, McIlrath J, Carr JM, Armit LJ, Clacher C, Malone L, Kollias G, Arthur JS (2005) Generation and characterization of p38beta (MAPK11) gene-targeted mice. *Mol Cell Biol* 25: 10454 – 10464

Bertola A, Park O, Gao B (2013) Chronic plus binge ethanol feeding synergistically induces neutrophil infiltration and liver injury in mice: a critical role for E-selectin. *Hepatology* 58: 1814 – 1823

Charlton M, Krishnan A, Viker K, Sanderson S, Cazanave S, McConico A, Masuoko H, Gores G (2011) Fast food diet mouse: novel small animal model of NASH with ballooning, progressive fibrosis, and high physiological fidelity to the human condition. *Am J Physiol Gastrointest Liver Physiol* 301: G825 – G834

Criado G, Risco A, Alsina-Beauchamp D, Perez-Lorenzo MJ, Escos A, Cuenda A (2014) Alternative p38 MAPKs are essential for collagen-induced arthritis. *Arthritis Rheumatol* 66: 1208 – 1217

Fabbrini E, Sullivan S, Klein S (2010) Obesity and nonalcoholic fatty liver disease: biochemical, metabolic, and clinical implications. *Hepatology* 51: 679 – 689

Farrell GC, Larter CZ (2006) Nonalcoholic fatty liver disease: from steatosis to cirrhosis. *Hepatology* 43: S99 – S112

Gonzalez-Teran B, Cortes JR, Manieri E, Matesanz N, Verdugo A, Rodriguez ME, Gonzalez-Rodriguez A, Valverde A, Martin P, Davis RJ, Sabio G (2013) Eukaryotic elongation factor 2 controls TNF-alpha translation in LPS-induced hepatitis. *J Clin Invest* 123: 164 – 178

Han MS, Jung DY, Morel C, Lakhani SA, Kim JK, Flavell RA, Davis RJ (2013) JNK expression by macrophages promotes obesity-induced insulin resistance and inflammation. *Science* 339: 218 – 222

Ittner A, Block H, Reichel CA, Varjosalo M, Gehart H, Sumara G, Gstaiger M, Krombach F, Zarbock A, Ricci R (2012) Regulation of PTEN activity by p38delta-PKD1 signaling in neutrophils confers inflammatory responses in the lung. *J Exp Med* 209: 2229 – 2246

Kleiner DE, Brunt EM, Van Natta M, Behling C, Contos MJ, Cummings OW, Ferrell LD, Liu YC, Torbenson MS, Unalp-Arida A, Yeh M, McCullough AJ, Sanyal AJ (2005) Design and validation of a histological scoring system for nonalcoholic fatty liver disease. *Hepatology* 41: 1313 – 1321

Mansuy-Aubert V, Zhou QL, Xie X, Gong Z, Huang JY, Khan AR, Aubert G, Candelaria K, Thomas S, Shin DJ, Booth S, Baig SM, Bilal A, Hwang D, Zhang H, Lovell-Badge R, Smith SR, Awan FR, Jiang ZY (2013) Imbalance between neutrophil elastase and its inhibitor alpha1-antitrypsin in obesity alters insulin sensitivity, inflammation, and energy expenditure. *Cell Metab* 17: 534 – 548

Mantovani A, Cassatella MA, Costantini C, Jaillon S (2011) Neutrophils in the activation and regulation of innate and adaptive immunity. *Nat Rev Immunol* 11: 519 – 531

Marchesini G, Bugianesi E, Forlani G, Cerrelli F, Lenzi M, Manini R, Natale S, Vanni E, Villanova N, Melchionda N, Rizzetto M (2003) Nonalcoholic fatty liver, steatohepatitis, and the metabolic syndrome. *Hepatology* 37: 917 – 923

Mora A, Lipina C, Tronche F, Sutherland C, Alessi DR (2005) Deficiency of PDK1 in liver results in glucose intolerance, impairment of insulin-regulated gene expression and liver failure. *Biochem J* 385: 639 – 648

Nathan C (2006) Neutrophils and immunity: challenges and opportunities. *Nat Rev Immunol* 6: 173 – 182

Passegue E, Wagner EF, Weissman IL (2004) JunB deficiency leads to a myeloproliferative disorder arising from hematopoietic stem cells. *Cell* 119: 431 – 443

Risco A, del Fresno C, Mambol A, Alsina-Beauchamp D, MacKenzie KF, Yang HT, Barber DF, Morcelle C, Arthur JS, Ley SC, Ardavin C, Cuenda A (2012) p38gamma and p38delta kinases regulate the Toll-like receptor 4 (TLR4)-induced cytokine production by controlling ERK1/2 protein kinase pathway activation. *Proc Natl Acad Sci USA* 109: 11200 – 11205

Sabio G, Arthur JS, Kuma Y, Peggie M, Carr J, Murray-Tait V, Centeno F, Goedert M, Morrice NA, Cuenda A (2005) p38gamma regulates the localisation of SAP97 in the cytoskeleton by modulating its interaction with GKAP. *EMBO J* 24: 1134 – 1145

Sabio G, Das M, Mora A, Zhang Z, Jun JY, Ko HJ, Barrett T, Kim JK, Davis RJ (2008) A stress signaling pathway in adipose tissue regulates hepatic insulin resistance. *Science* 322: 1539 – 1543

Sabio G, Cavanagh-Kyros J, Ko HJ, Jung DY, Gray S, Jun JY, Barrett T, Mora A, Kim JK, Davis RJ (2009) Prevention of steatosis by hepatic JNK1. *Cell Metab* 10: 491 – 498

Sabio G, Davis RJ (2010) cJun NH2-terminal kinase 1 (JNK1): roles in metabolic regulation of insulin resistance. *Trends Biochem Sci* 35: 490 – 496

Sabio G, Kennedy NJ, Cavanagh-Kyros J, Jung DY, Ko HJ, Ong H, Barrett T, Kim JK, Davis RJ (2010) Role of muscle c-Jun NH2-terminal kinase 1 in obesity-induced insulin resistance. *Mol Cell Biol* 30: 106 – 115

Sabio G, Davis RJ (2014) TNF and MAP kinase signalling pathways. *Semin Immunol* 26: 237 – 245

Savill JS, Wyllie AH, Henson JE, Walport MJ, Henson PM, Haslett C (1989) Macrophage phagocytosis of aging neutrophils in inflammation. Programmed cell death in the neutrophil leads to its recognition by macrophages. *J Clin Invest* 83: 865 – 875

Sreeramkumar V, Leiva M, Stadtmann A, Pitaval C, Ortega-Rodriguez I, Wild MK, Lee B, Zarbock A, Hidalgo A (2013) Coordinated and unique functions of the E-selectin ligand ESL-1 during inflammatory and hematopoietic recruitment in mice. *Blood* 122: 3993 – 4001

Talukdar S, da Oh Y, Bandyopadhyay G, Li D, Xu J, McNelis J, Lu M, Li P, Yan Q, Zhu Y, Ofrecio J, Lin M, Brenner MB, Olefsky JM (2012) Neutrophils mediate insulin resistance in mice fed a high-fat diet through secreted elastase. *Nat Med* 18: 1407 – 1412

Tamura K, Sudo T, Senftleben U, Dadak AM, Johnson R, Karin M (2000) Requirement for p38alpha in erythropoietin expression: a role for stress kinases in erythropoiesis. *Cell* 102: 221 – 231

Tiniakos DG, Vos MB, Brunt EM (2010) Nonalcoholic fatty liver disease: pathology and pathogenesis. *Annu Rev Pathol* 5: 145 – 171

Vernon G, Baranova A, Younossi ZM (2011) Systematic review: the epidemiology and natural history of non-alcoholic fatty liver disease and non-alcoholic steatohepatitis in adults. *Aliment Pharmacol Ther* 34: 274 – 285

© 2016 The Authors

APPENDIX

p38γ and p38δ reprogram liver metabolism by modulating neutrophil infiltration

Bárbara González-Terán[1#], Nuria Matesanz[1#], Ivana G. Nikolic[1#], María Angeles Verdugo[2, 1], Vinatha Sreeramkumar[1], Lourdes Hernández-Cosido[3], Alfonso Mora[1], Georgiana Crainiciuc[1], María Laura Sáiz[1], Edgar Bernardo[1], Luis Leiva-Vega[1], Elena Rodríguez[1], Victor Bondía[1], Jorge L. Torres[4], Sonia Perez-Sieira[5, 6], Luis Ortega[3], Ana Cuenda[2], Francisco Sanchez-Madrid[1], Rubén Nogueiras[5, 6], Andrés Hidalgo[1], Miguel Marcos[4], Guadalupe Sabio[1*].

Contents

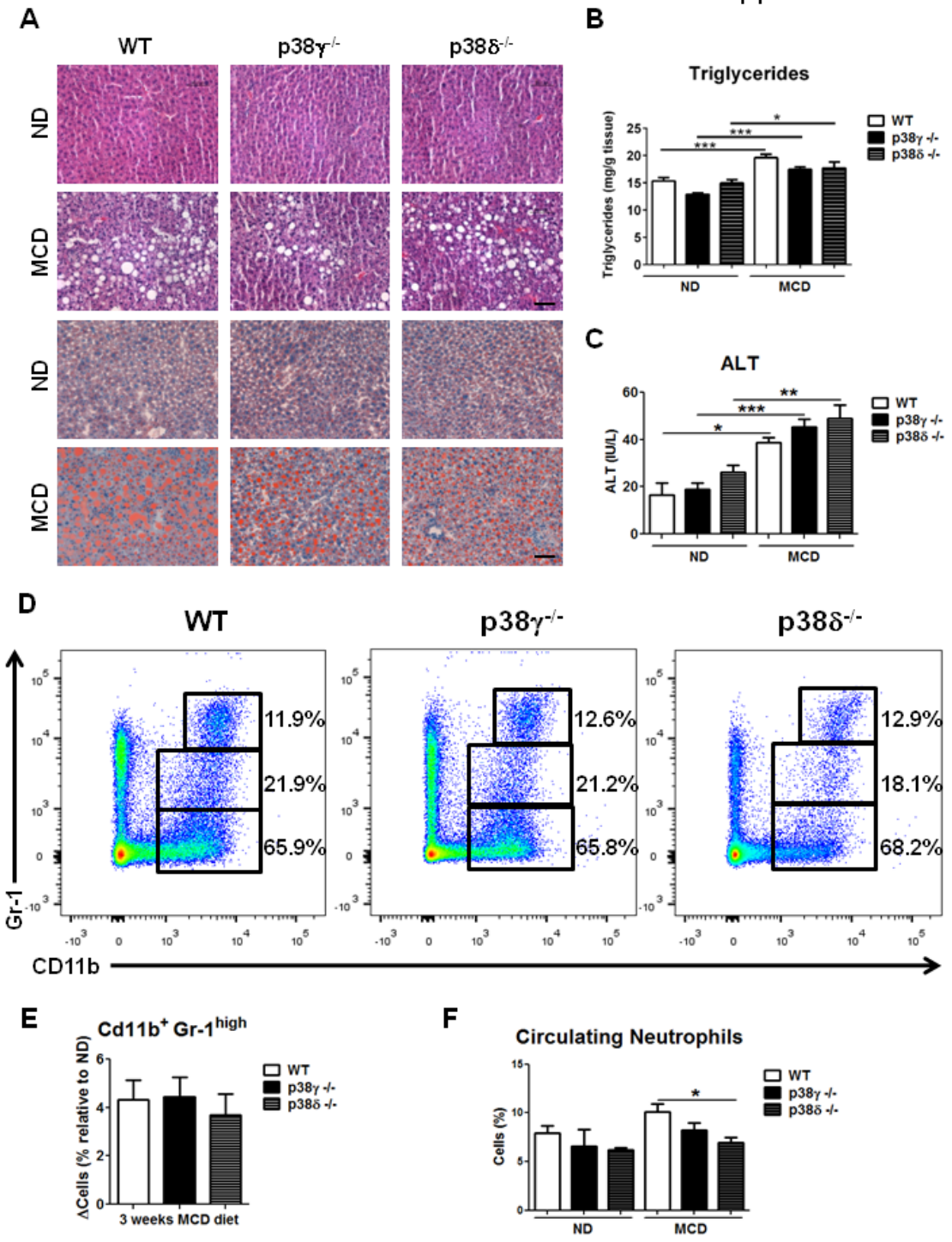

Appendix Fig. S1. p38γ$^{-/-}$ and p38δ$^{-/-}$ mice are partially protected against steatohepatitis.

WT, p38$\gamma^{-/-}$ and p38$\delta^{-/-}$ mice were fed a control diet (ND) or a diet deficient in methionine and choline (MCD) for 3 weeks. (**A**) Representative H&E and oil red stained liver sections. Scale Bar: 50μm. (**B**) Liver triglyceride and (**C**) plasma transaminase activity (ALT) at the end of the diet period. (**D-E**) Flow cytometry analysis of liver myeloid subsets (CD11b^{+} Gr-1^{high}, CD11b^{+} Gr-1^{intermediate}, CD11b^{+} Gr-1^{-}) isolated from WT, p38$\gamma^{-/-}$ and p38$\delta^{-/-}$ mice fed the MCD diet for 3 weeks. Representative dot plots are shown (**D**), and bar charts (**E**) show the diet-induced increase in each population relative to controls fed a ND as a percentage of the total intra-hepatic CD11b^{+} leukocyte population. (**F**) Neutrophils as a percentage of circulating leukocytes, measured in total blood in animals fed a MCD diet for 3 weeks. Data are means ± SEM. (n=5-10). *P<0.05; **P< 0.01; ***P< 0.001 (1-way ANOVA coupled to Bonferroni's post tests).

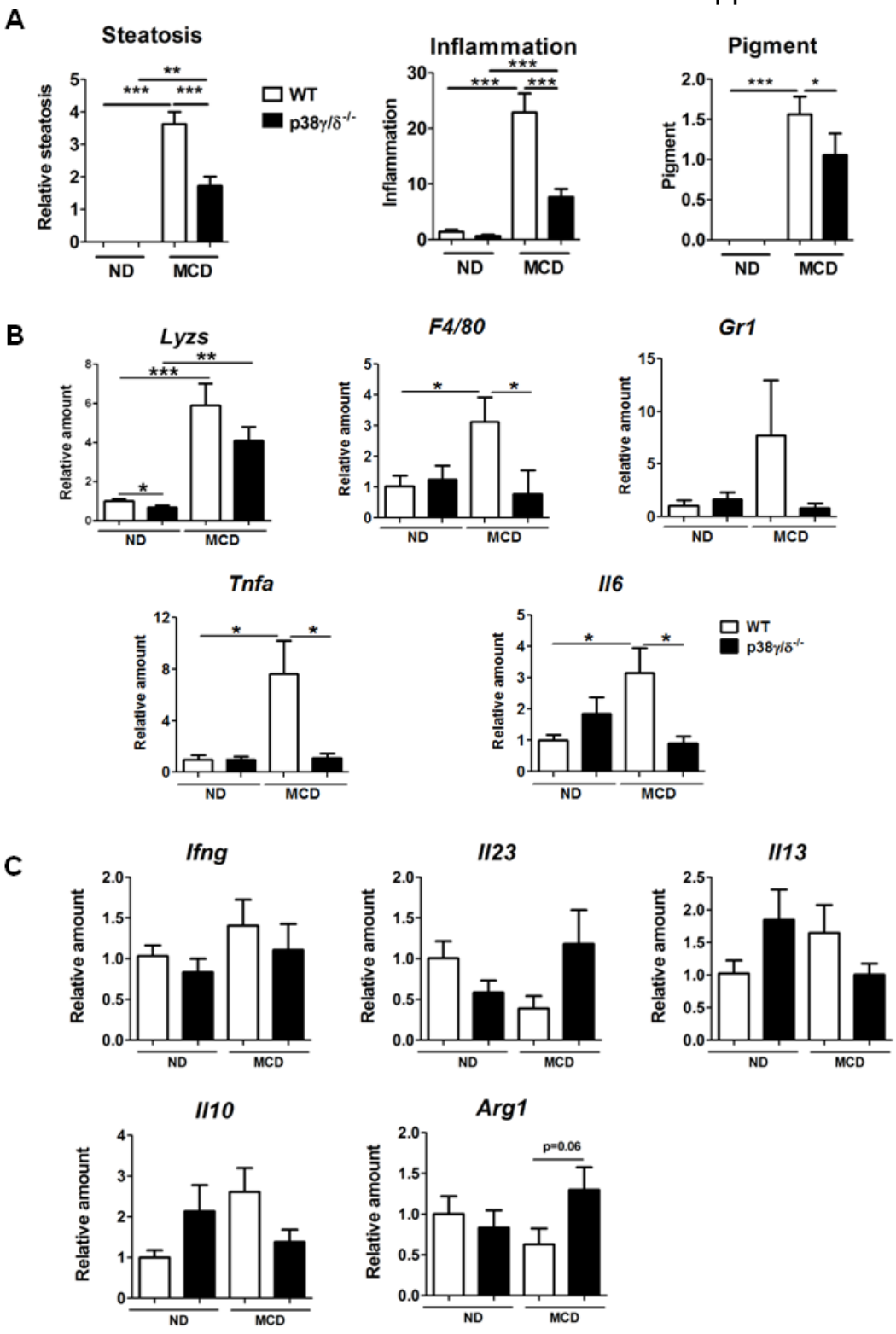
A
Steatosis
Relative steatosis
WT
p38γ/δ-/-
ND
MCD
Inflammation
Inflammation
Pigment
Pigment
B
Lyzs
F4/80
Gr1
Tnfa
Il6
Relative amount
C
Ifng
Il23
Il13
Il10
Arg1
p=0.06

Appendix Fig. S2. p38γ/δ$^{-/-}$ mice are protected against liver inflammation induced by MCD diet. WT, p38γ/δ$^{-/-}$ mice were fed a ND or the MCD diet for 3 weeks. (**A**) Quantification of liver H&E stained sections from WT and p38γ/δ$^{-/-}$ mice for steatosis, inflammation and pigment. Total RNA was extracted from livers, and (**B**) myeloid cell markers and cytokine mRNA levels and (**C**) M1 and M2 macrophages markers determined by qRT-PCR; mRNA expression was normalized to the amount of *Gapdh* mRNA. Data are means ± SEM. (n=5-10). *P<0.05; **P<0.01; ***P<0.001 (1-way ANOVA coupled to Bonferroni's post tests).

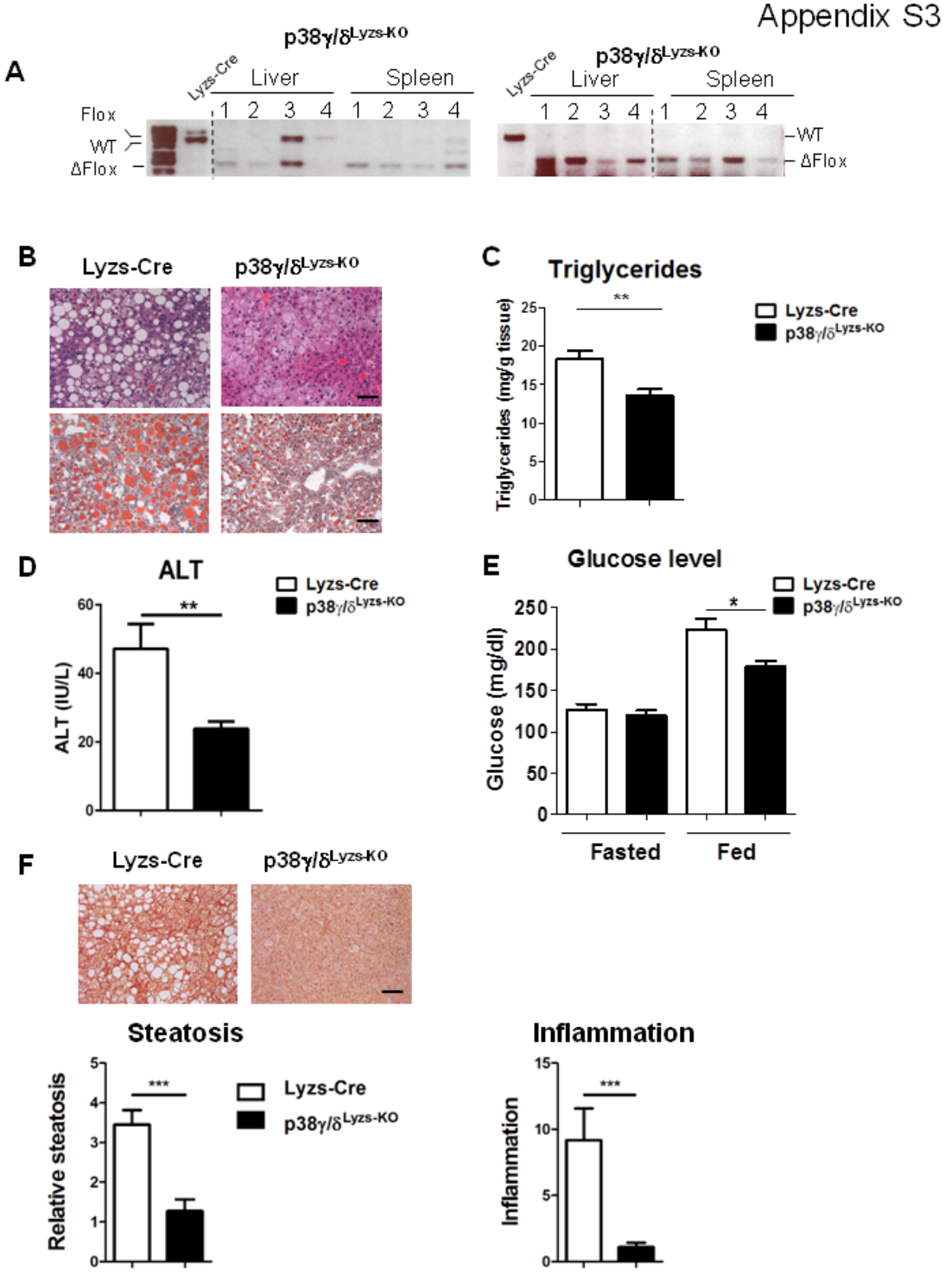

Appendix Fig. S3. p38γ/δ$^{Lyzs\text{-}KO}$ mice are protected against steatohepatitis induced by HFF. (A) PCR analysis of p38δ (left) and p38γ (right) deletion in macrophages (1), neutrophils (2), and dentritic cells (3, 4) infiltrated in liver and spleen from p38γ/δ$^{Lyzs\text{-}KO}$. **(B-F)** Lyzs-Cre and p38γ/δ$^{Lyzs\text{-}KO}$ mice were fed a high cholesterol, high saturated

fat, and high fructose (HFF) diet for 10 weeks. (**B**) Representative H&E and oil red stained liver sections (Scale Bar: 50μm) and (**C**) liver triglycerides (n=5-10). (**D**) Plasma ALT at the end of the diet period. (**E**) Basal blood glucose in overnight-fasted and fed Lyzs-Cre and p38γ/$\delta^{Lyzs\text{-}KO}$ mice (n=5-10). (**F**) Representative picrosirius red stained liver sections (Scale Bar: 50μm) and quantification of H&E stained liver sections for steatosis and inflammation. Data are means ± SEM. (n=5-10) *P<0.05; **P<0.01; ***P<0.001 refers to p38γ/$\delta^{Lyzs\text{-}KO}$ versus Lyzs-Cre; ##P<0.01; ###P<0.001 refers to ND versus HFD (1-way ANOVA coupled to Bonferroni's post tests or *t-test*).

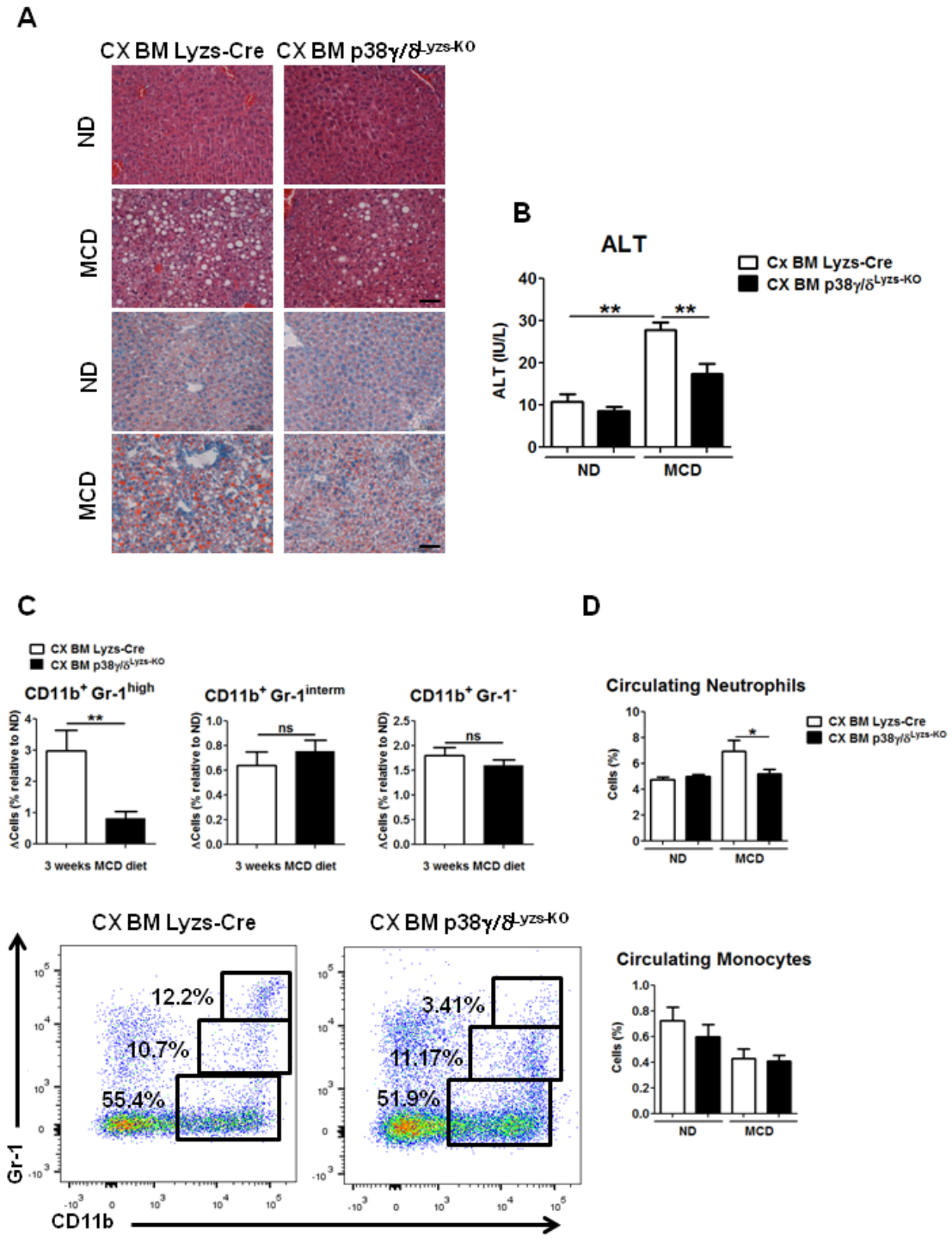

Appendix Fig. S4. Lyzs-Cre hematopoietic cells protect mice against MCD-diet–induced steatosis. Lethally irradiated WT mice were reconstituted with BM from Lyzs-

Cre (Cx BM Lyzs-Cre) or p38γ/$\delta^{Lyzs\text{-}KO}$ mice (Cx BM p38γ/$\delta^{Lyzs\text{-}KO}$). Two months after the transplant, mice were fed the MCD diet for 3 weeks. (**A**) Representative H&E and oil red-stained liver sections. Scale bar: 50 μm. (**B**) Serum transaminase ALT activity after MCD diet. (**C**) Flow cytometry analysis of liver myeloid subsets ($CD11b^+$ $Gr\text{-}1^{high}$, $CD11b^+$ $Gr\text{-}1^{intermediate}$, and $CD11b^+$ $Gr\text{-}1^-$) isolated from Cx BM Lyzs-Cre and Cx BM p38γ/$\delta^{Lyzs\text{-}KO}$ mice fed the MCD diet for 3 weeks. Representative dot plots are shown, and bar charts show the diet-induced increase in each population relative to controls fed a ND as a percentage of the total intra-hepatic $CD11b^+$ leukocyte population. (**D**) Neutrophils and monocytes as a percentage of circulating leukocytes, measured in total blood in animals fed a MCD diet for 3 weeks. Data are means ± SEM. (n=5-10) *P<0.05; **P<0.01 (1-way ANOVA coupled to Bonferroni's post tests or *t-test*).

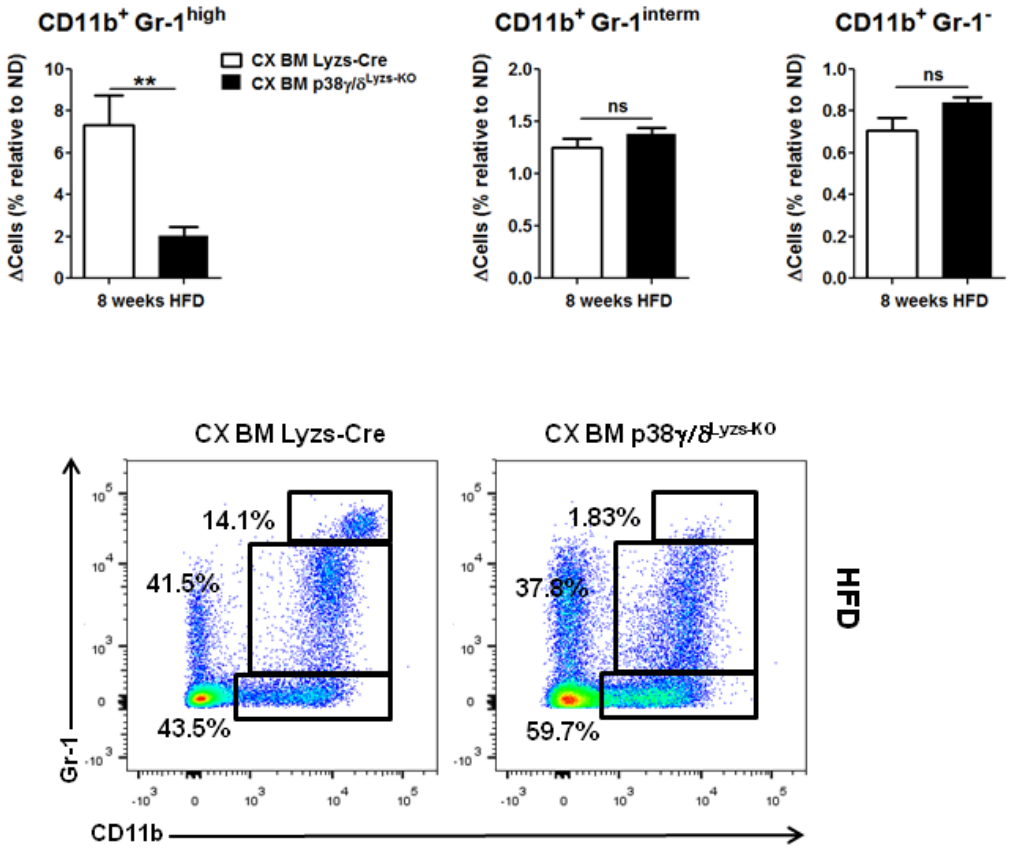

Appendix Fig. S5. Lyzs-Cre hematopoietic cells protect mice against HFD-induced liver neutrophil infiltration. Lethally irradiated WT mice were reconstituted with BM from Lyzs-Cre (Cx BM Lyzs-Cre) or p38γ/$\delta^{Lyzs\text{-}KO}$ mice (Cx BM p38γ/$\delta^{Lyzs\text{-}KO}$). Two

months after the transplant, mice were fed the HFD for 10 weeks. Flow cytometry analysis of liver myeloid subsets ($CD11b^+$ $Gr\text{-}1^{high}$, $CD11b^+$ $Gr\text{-}1^{intermediate}$, and $CD11b^+$ $Gr\text{-}1^-$) isolated from Cx BM Lyzs-Cre and Cx BM $p38\gamma/\delta^{Lyzs\text{-}KO}$ mice fed the HFD for 10 weeks. Representative dot plots are shown, and the bar charts show the diet-induced increase in each population relative to controls fed a ND as a percentage of the total intra-hepatic $CD11b^+$ leukocyte population. Data are means ± SEM. (n=5-10) **P<0.01 (*t-test*).

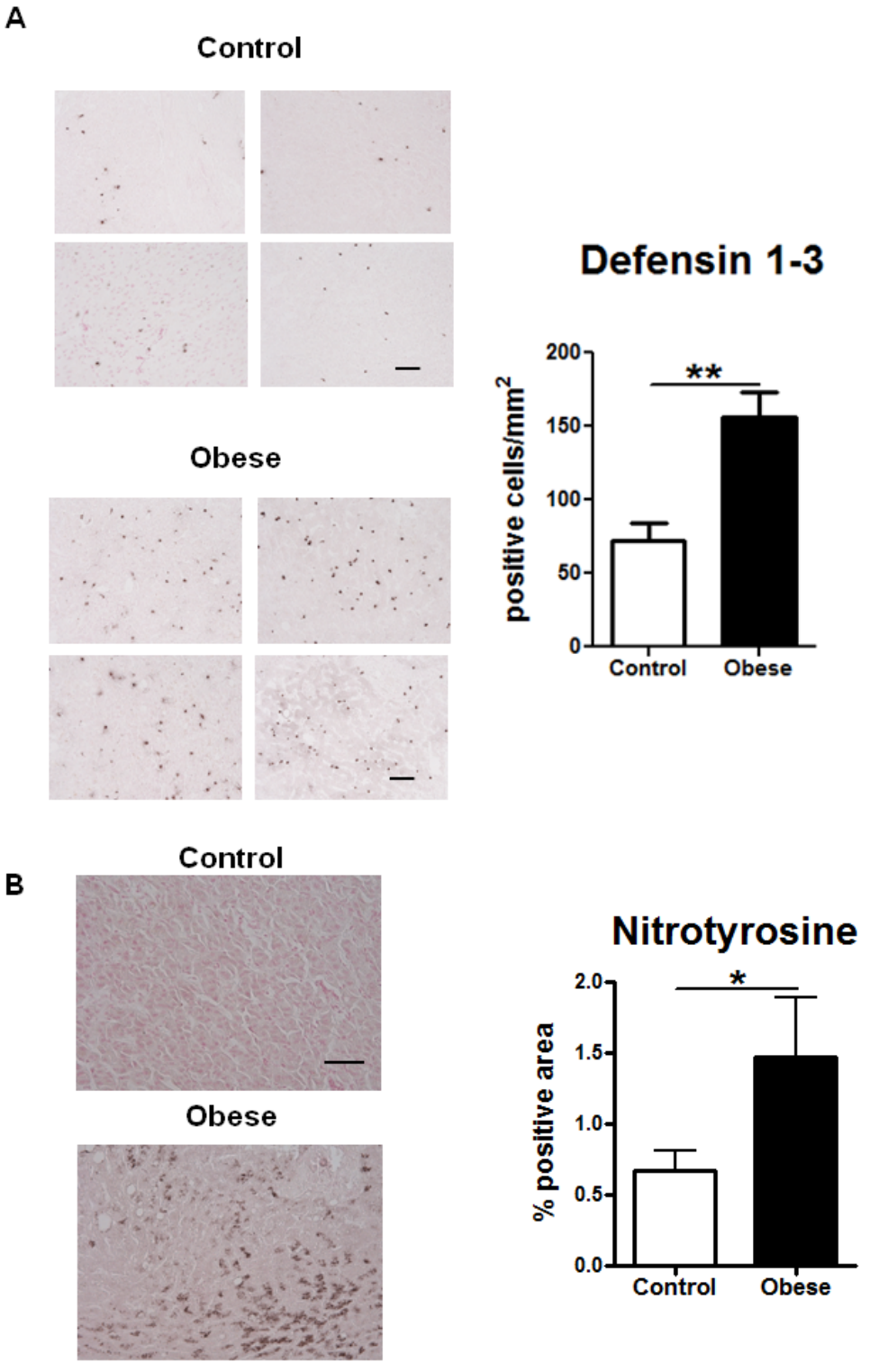

Appendix Fig. S6. Neutrophil infiltration during steatosis development. Liver biopsies from obese patients with NAFLD and from control patient without NAFLD

were stained (**A**) anti-human neutrophil defensin 1-3 (scale bar: 100 μm) and quantification of neutrophil infiltration by mm^2 of liver parenchyma. (**B**) Representative slides of liver biopsies stained with anti-nitrotyrosine antibody and quantification of neutrophil infiltration by mm^2 of liver parenchyma. Scale bar: 50 μm. Data are means ± SEM. (n=5-10) *P<0.05, **P<0.01 (*t-test*).

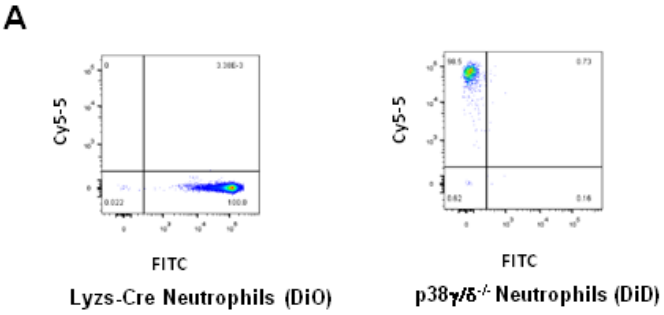

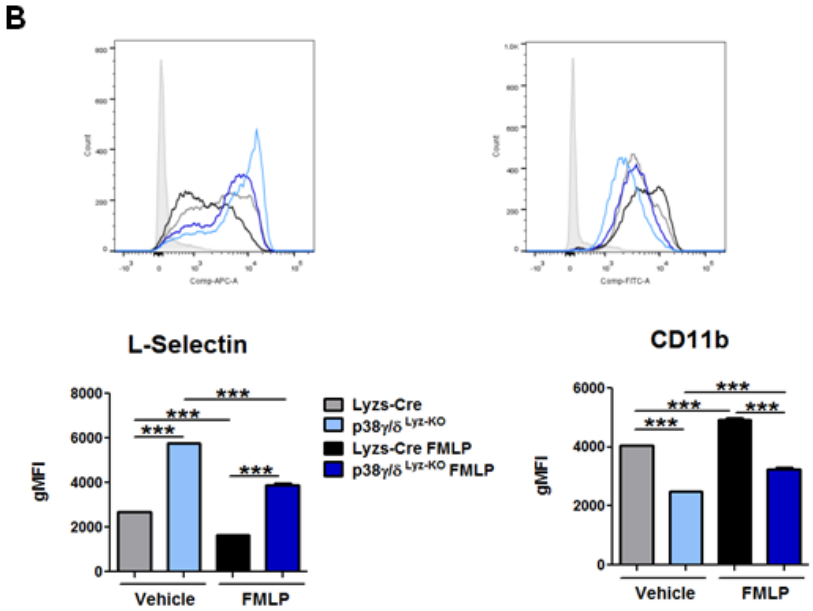

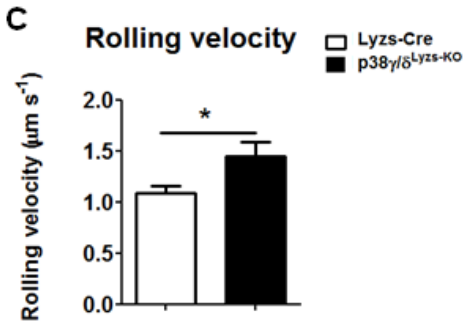

Appendix Fig. S7. Myeloid p38γ/δ deletion affects expression of L-Selectin and CD11b. (**A**) BM-isolated neutrophils isolated from Lysz-Cre mice and p38γ/δ$^{Lyz\text{-}KO}$ transgenic mice labeled with DiO (Lyzs-Cre neutrophils) and DiD (p38γ/δ$^{Lyzs\text{-}KO}$ neutrophils) were stained with DAPI and their survival were analyzed by flow

cytometry. Representative dot plots of DAPI-negative cell population were shown. (**B**) BM-isolated neutrophils isolated from Lysz-Cre mice and p38γ/$\delta^{Lyz\text{-}KO}$ transgenic mice were stimulated with FMLP 1μM or vehicle for 30 min. After stimulation, cells were stained with anti-L-selectin APC and anti-CD11b FITC. Signal was detected by flow cytometry. Histograms depict basal L-Selectin (left) or CD11b (right) membrane expression in Lysz-cre neutrophils (grey) and in p38γ/$\delta^{Lyz\text{-}KO}$ neutrophils (light blue) or fmlp induced L-Selectin (left) or CD11b (right) membrane expression in Lysz-Cre neutrophils (black) and in p38γ/$\delta^{Lyz\text{-}KO}$ neutrophils (dark blue). The shaded light grey line represents the isotype control. (**C**) Microscopy quantification of the rolling velocities of neutrophils recruited to slides covered with E-Selectin and ICAM-1. Data are means ± SEM. *P<0.05; ***P<0.001 (1-way ANOVA coupled to Bonferroni's post tests or *t-test*).

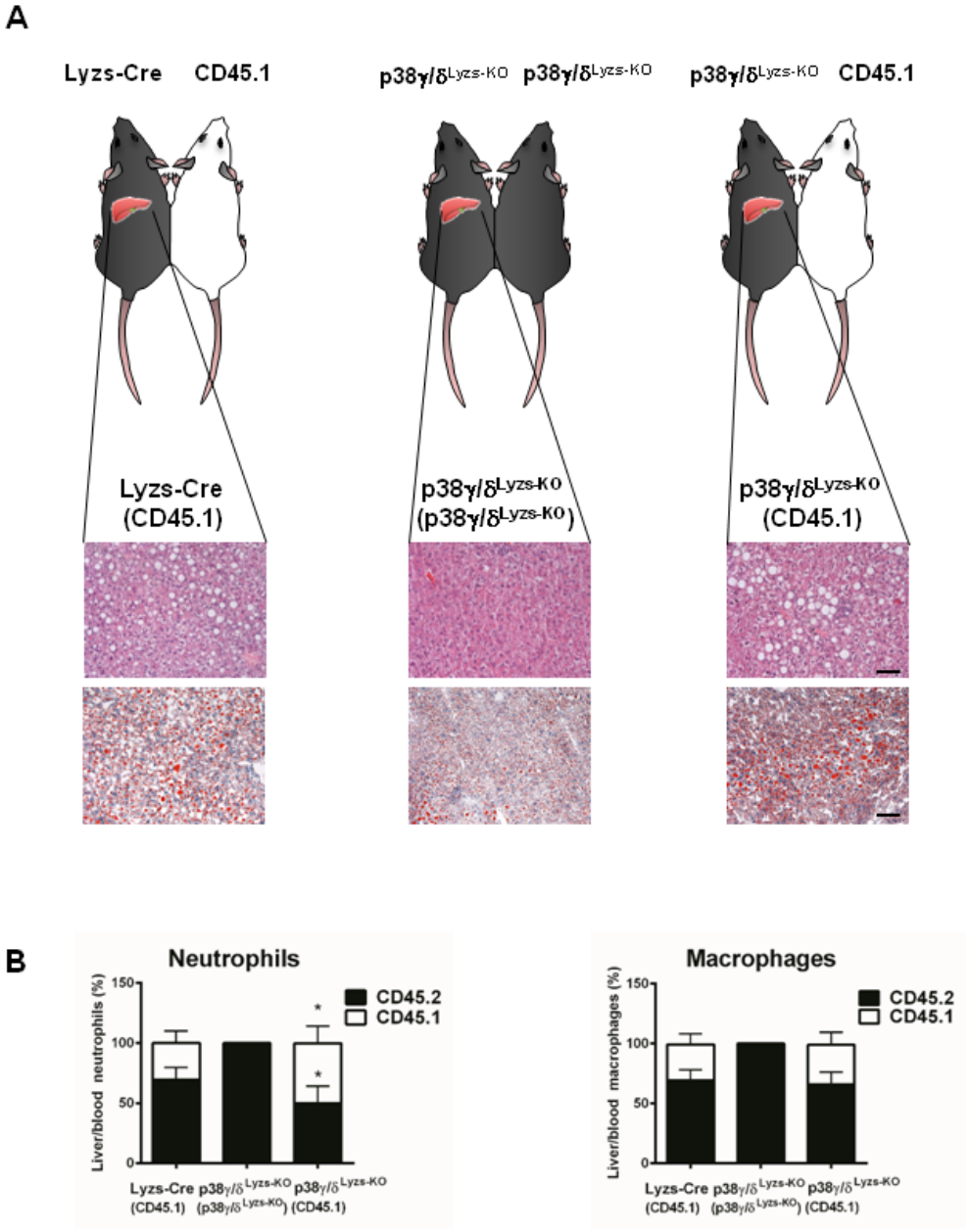

Appendix Fig. S8. Parabiosis assay, in which the circulation of a p38γ/δ$^{Lyzs\text{-}KO}$ mouse is shared with that of a WT partner mouse. CD45.1+ WT mice were sutured

to either CD45.2+ Lyzs-Cre or p38γ/δ$^{Lyzs\text{-}KO}$ mice by parabiosis surgery. Two weeks after surgery mice were fed a MCD diet for 3 weeks. (**A**) *Up*: Illustration of parabiotic couples. *Bottom*: Representative H&E stained liver sections from Lyzs-Cre (CD45.1), p38γ/δ$^{Lyzs\text{-}KO}$ (p38γ/δ$^{Lyzs\text{-}KO}$) and p38γ/δ$^{Lyzs\text{-}KO}$ (CD45.1) parabiotic mice. Scale bar: 50 μm. (**B**) Quantification of flow cytometry analysis of liver myeloid subsets (CD11b^{+} Gr-1^{high} (neutrophils) and CD11b^{+} Gr-1^{intermediate} (macrophages)) isolated from Lyzs-Cre (CD45.1), p38γ/δ$^{Lyzs\text{-}KO}$ (p38γ/δ$^{Lyzs\text{-}KO}$) and p38γ/δ$^{Lyzs\text{-}KO}$ (CD45.1) parabiotic mice. Bar charts show the diet-induced increase in each population relative to percentage of each subsets found in the blood of Lyzs-Cre (CD45.1), p38γ/δ$^{Lyzs\text{-}KO}$ (p38γ/δ$^{Lyzs\text{-}KO}$) and p38γ/δ$^{Lyzs\text{-}KO}$ (CD45.1) parabiotic mice. Data are means ± SEM. (n=5-10) **P<0.01 (1-way ANOVA coupled to Bonferroni's post tests).

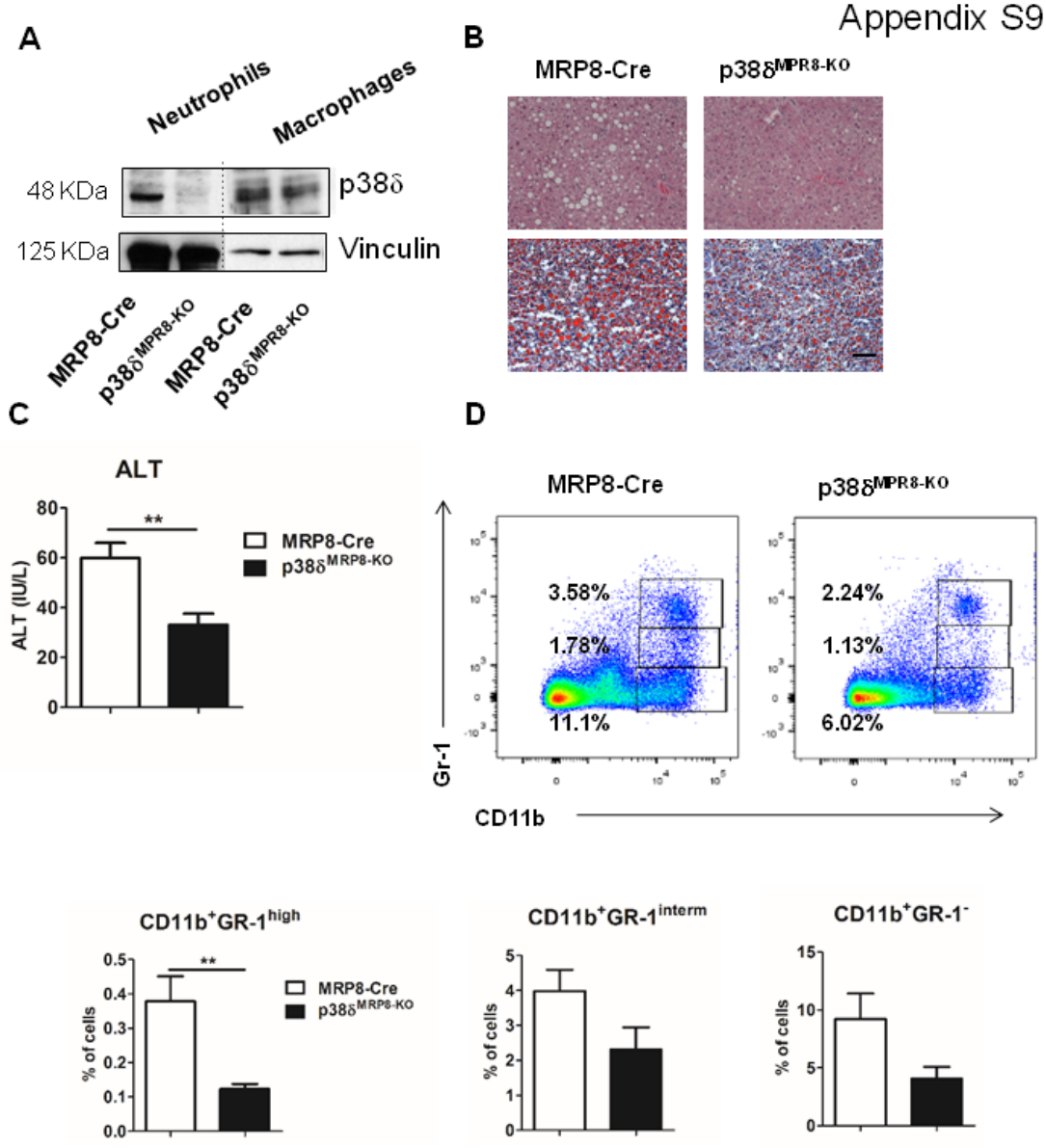

Appendix Fig. S9. Neutrophil-specific p38δ deficiency protects against MCD-induced steatosis. (**A**) Immunoblot analysis of p38δ expression in bone marrow

neutrophils (10μg) and bone marrow-derived macrophages isolated (100 μg) from MRP8-Cre and p38δ$^{MRP8\text{-}KO}$ mice. MRP8-Cre and p38δ$^{MRP8\text{-}KO}$ mice were fed a MCD diet for 3 weeks. (**B**) Representative H&E and oil red stained liver sections. Scale Bar: 50μm. (n=5-10). (**C**) Plasma ALT at the end of the diet period.(**D**) Flow cytometry analysis of liver myeloid subsets (CD11b^{+} Gr-1^{high}, CD11b^{+} Gr-1^{intermediate}, CD11b^{+} Gr-1^{-}) isolated from MRP8-Cre and p38δ$^{MRP8\text{-}KO}$ mice after the diet. Representative dot plots are shown and bar charts of each population relative as a percentage of the total intra-hepatic CD11b^{+} leukocyte population. Data are means ± SEM (n=5-10). **P<0.01 (*t-test*).

Appendix Table S1. Characteristics of patients and controls

Variable	Obese patients with NAFLD (n = 73)	Controls without NAFLD (n = 11)	Controls with NAFLD (n= 9)
Age (years)	44.6 (10.2)	42.1 (10.8)	66.2 (12.8)**
Female:male ratio	52:21	7:4	2:7***
Hypertension (n)	36 (49.3)*	0	4 (44.4)
Diabetes mellitus (n)	22 (30.1)	0	1 (11.1)
BMI (kg/m^2)	49.1 (7.9)*	26.8 (5.0)	26.1 (2.8)
Fasting blood sugar (mg/dL)	108.7 (41.1)	89.8 (11.3)	101.8 (12.8)
AST (IU/L)	23.2 (11.7)	22.4 (4.7)	30.1 (18.,9)
ALT (IU/L)	30.4 (17.4)	25.3 (12.8)	46.3 (37.5)
Bilirubin (mg/dL)	0.4 (0.1)	0.6 (0.6)	0.7 (0.3)***
Albumin (mg/dL)	4.3 (0.3)	4.4 (0.3)	4.5 (0.6)***
Total cholesterol (mg/dL)	191.4 (36.6)	186.5 (36.1)	190.5 (50.4)
Triglycerides (mg/dL)	144.7 (80.6)	108.5 (51.9)	100.5 (32.5)
LDL-cholesterol (mg/dL)	112.2 (35.2)	105.1 (35.5)	125.7 (44.3)
HDL-cholesterol (mg/dL)	48.9 (16.1)	58.6 (19.0)	44.7 (13.1)
NAS score	5.1 (1.6)*	0	2.4 (2.1)**
Steatosis	2.2 (0.8)*	0	1.2 (1.2)**
Lobular inflammation	1.4 (0.9)*	0	0.6 (0.7)**
Hepatocyte ballooning	1.4 (0.6)*	0	0.8 (0.9)**

Variables are presented as mean (standard deviation) or absolute frequency (percentage) and are compared by means of Mann-Whitney U test or χ^2 test. NAFLD: non alcoholic fatty liver disease. BMI: body mass index. AST: aspartate aminotransferase. ALT: alanine aminotransferase. NAS: NAFLD Activity Score.

* Significantly different from other groups
**Significantly different from other groups
***Significantly different from obese with NAFLD group

APPENDIX MATERIALS & METHODS

Reagent

Anti-Ly6C/G antibody (BD Pharmigen), magnetic streptavidin microbeads (Miltenyi Biotec), DiD and DiO (Vybrant Cell-Labeling Solution, Molecular Probes), TNFα, aprotinin and leupeptin (Sigma), Ficoll (GE healthcare), haematoxylin and eosin (American Master Tech Scientific), protein-G-Sepharose (Amersham), OCT (Tissue-Tek), Red oil (American Master Tech Scientific), Fast sybr green (Applied Biosystems).

Parabiosis

CD45.1+ WT mice were sutured to either CD45.2+ Lyzs-Cre or p38γ/$\delta^{Lyzs\text{-}KO}$ mice and parabiosis surgery was performed as previously described (Casanova-Acebes et al, 2013). Briefly, mice were anesthetized with isofluorane, shaved at the corresponding lateral aspects and a longitudinal incision of skin was made along one side of each mouse. The olecranon and knee joints were attached by a single 5-0 polypropylene suture and tie, and the dorsal and ventral skins were approximated by continuous suture. After surgery, mice recieved a single dose of flunixin meglumine (1 mg/kg, Schering-Plough, Segré, France). Two weeks after parabiotic surgery, mice were fed a MCD diet for 3 weeks.

Immunoblot analysis

Tissue extracts were prepared in Triton lysis buffer [20 mM Tris (pH 7.4), 1% Triton X-100, 10% glycerol, 137 mM NaCl, 2 mM EDTA, 25 mM β-glycerophosphate, 1 mM sodium orthovanadate, 1 mM phenylmethylsulfonyl fluoride, and 10 μg/mL of aprotinin and leupeptin]. Extracts (20-50 μg protein) and immunoprecipitates (prepared from 2-10 mg protein) were examined by immunoblot. For the immunoprecipitation assay,

liver extracts were incubated with 4 μg of anti-p38 delta or anti-p38 gamma coupled to protein-G-Sepharose. After incubation for 4 hours at 4°C, the captured proteins were centrifuged at 10,000 g, the supernatants discarded and the beads washed four times in lysis buffer. Beads were boiled for 5 minutes 95°C in 10μl sample buffer. The antibodies employed were anti-phospho p38 and anti-human p38δ (Cell Signaling); anti-p38γ and anti-p38δ (Gonzalez-Teran et al, 2013; Han et al, 2013); and anti-vinculin (Sigma). Immunecomplexes were detected by enhanced chemiluminescence (NEN).

Histology

Tissue samples were fixed in 10% formalin for 48h, dehydrated and embedded in paraffin. Sections (8μm) were cut and stained with haematoxylin and eosin (American Master Tech Scientific), picrosirius red (Sigma) and Masson trichromic (Merck). Tissue sections were sequentially stained with a biotinylated antibody to marker neutrophil activator nitrotyrosine (Hycultbiotech), streptavidin-conjugated horseradish peroxidase (Abcam), and the substrate 3,3'-diaminobenzidene (Vector Laboratories), followed by brief counterstaining with Mayer's haematoxylin (Sigma). Sections (8 μm) prepared from tissue frozen in OCT compound (Tissue-Tek) were stained with Red oil (American Master Tech Scientific).

Measurement of hepatic triglyceride

Hepatic triglyceride content was measured in livers from mice starved overnight. Total lipids were extracted from liver samples (25 mg) in an 8:1 mixture of chloroform and methanol (4 h). The extracts were mixed with 1N sulfuric acid and centrifuged (10 min). Triglycerides were measured with a commercial kit (Sigma).

Metabolic cages

Mice were housed under controlled temperature and lighting with free access to food and water. Food and water intake, energy expenditure, respiratory exchange ratio, and physical activity were monitored (3 days) in metabolic cages (TSE Systems, Bad Homburg, Germany). Fat and lean masses were detected by magnetic resonance imaging.

RNA-Seq Library Preparation, Sequencing, and Analysis

RNA-seq experiments were performed on biological quadruplicates. A total of 10 μg of total RNA was used for each RNA-seq library preparation according to the manufacturer's instructions (Illumina). RNA quality was verified using Bioanalyzer (Agilent); only RNA with a RIN of >9 was used. Libraries were prepared and sequenced (Illumina; GAII) in a pair-end, 36 bp format, except for the concentrated samples, which were sequenced by Hi-seq in a single-end, 50 bp format. Reads from each sample were aligned to the mouse genome (mm9 build) using TopHat (version 1.1.0). Differential expression was quantified using Cuffdiff (Trapnell et al., 2010) (version 1.0.3). Differentially expressed genes are those that have a log2 fold change of >0.58 or <0.58 and a q value of <0.05 compared with the control condition. We also required that the differentially expressed genes used for downstream analysis have a FPKM greater than 0.1 in the control condition. The raw data for the RNA-seq experiment were deposited in Gene Expression Omnibus, with the accession GSE58174.

RNA analysis

Expression of mRNA was examined by qRT-PCR using a 7900 Fast Real Time thermocycler and FAST SYBR GREEN assays (Applied Biosystems). Relative mRNA

expression was normalized to *Gapdh* mRNA measured in each sample. Primers used were as follows: *Mapk12* (Fw: AAGGGCTTTTACCGCCAGG; Rv: GGCGCAACTCTCTGTAGGC); *Mapk13* (Fw: ATGAGCCTCACTCGGAAAAGG; Rv: GCATGTGCTTCAAGAGCAGAA); *Lyzs* (Fw: ATGGAATGGCTGGCTACTATG; Rv: ACCAGTATCGG CTATTGATCT); *F4/80* (Fw: CCCCAGTGTCCTTACAGAGTG; Rv: GTGCCCAGA GTGGATGTCT); *Gr1* (Fw: GACTTCCTGCAACACAACTAC; Rv: ACAGCATTAC CAGTGATCTCA); *Tnfa* (Fw: CCCTCACACTCAGATCATCTT; Rv: GCTACGAC GTGGGCTACAG); *Il6* (Fw:TAGTCCTTCCTACCCCAATTT; Rv: TTGGTCCTTA GCCACTCCTTC); *Kc* (Fw: CTGGGATTCACCTCAAGAACA; Rv: CAGGGTCAA GGCAAGCCTC); *Ifng* (Fw: ATGAACGCTACACACTGCATC; Rv: CCATCCTTTTGCCAGTTCCTC); *Il10* (Fw: GCTCTTACTGACTGGCATGAG; Rv: CGCAGCTCTAGGAGCATGTG); *Il13* (Fw: CCTGGCTCTTGCTTGCCTT; Rv: GGTCTTGTGTGATGTTGCTCA); *Il23* (Fw: ATGCTGGATTGCAGAGCAGTA; Rv: ACGGGGCACATTATTTTTAGTCT); *Arg1* (Fw: CTCCAAGCCAAAGTCCTTAGAG; Rv: AGGAGCTGTCATTAGGGACATC); *Timp1* (Fw:GCAACTCGGACCTGGTCATAA; Rv: CGGCCCGTGATGAGAAACT); *Col1a1* (Fw: GCTCCTCTTAGGGGCCACT; Rv: CCACGTCTCACCATTGGGG); *Acta2* (Fw: GTCCCAGACATCAGGGAGTAA; Rv: TCGGATACTTCAGCGTCAGGA); *Csf1* (Fw: GGCTTGGCTTGGGATGATCCT; Rv: GAGGGTCTGGCAGGTACTC); *Cd68* (Fw: TGTCTGATCTTGCTAGGACCG; Rv: GAGAGTAACGGCCTTTTTGTG); *Ym1* (Fw: CAGGTCTGGCAATTCTTCTGA; Rv: GTCTTGCTCATGTGTGTAAGT); *Gapdh* (Fw: TGAAGCAGGCATCTGAGGG; Rv: CGAAGGTGGAAGAGTGGGA) (all mouse). Human primers used were as follows: *MAPK12* (Fw: CATGAGAAGCTAGGCGAGGAC; Rv: GCATCTGGTACACGAGGAACT);

MAPK13 (Fw: AAAAGGGCTTCTACAAGCAGG; Rv: TCGGGGACACGTAGGTCTT); *GAPDH* (Fw: CCATGAGAAGTATGACAACAGCC; Rv: GGGTGCTAAGCAGTTGGTG).

Neutrophils FACS analysis

Lyzs-Cre and p38γ/$\delta^{Lyzs\text{-}KO}$ neutrophils were isolated from bone marrow by labelling with biotin-conjugated anti-Ly6C/G antibody (BD Pharmigen) and magnetic streptavidin microbeads (Miltenyi Biotec), and then separating them on MACS columns (Miltenyi Biotec). Isolated Lyzs-Cre neutrophils were stimulated for 30 minutes with FMLP (1μM) or vehicle. Cells were stained with 1:100 anti–L-selectin APC and anti-CD11b FITC antibodies (BD Biosciences). For Lyzs-Cre and p38γ/$\delta^{Lyzs\text{-}KO}$ neutrophils isolation from the blood of parabiotic couples, mice were bled from cheeks, followed by red blood cells lysis and isolated neutrophils were stained with 1:100 anti-CD45.2 PerCP-Cy5.5 (eBioscience), anti-CD45.1 PE-Cy7, anti-Gr1 APC, anti-CD11b FITC and 1:5000 DAPI antibodies (BD Bioscience). MRP8-Cre and p38γ/$\delta^{MRP8\text{-}KO}$ neutrophils isolated from blood or liver were stained with anti-Gr1 APC and anti-CD11b FITC and 1:5000 DAPI antibodies. Signal was detected by flow cytometry.

Myeloid cells isolated from liver of Lyzs-Cre and p38γ/$\delta^{Lyzs\text{-}KO}$ mice 3 weeks after MCD diet were stained with anti-CD45.2 PerCP-Cy5.5, anti-Gr1 APC, anti-F4/80 PE-Cy7 and anti-CD11c FITC and biotin labeled anti-CD11b followed with streptavidin-eFluor450. Cells were sorted by using BDFACSAria II cytofluorimeter. Sorted liver myeloid subsets ($CD11b^+$ $Gr\text{-}1^{high}$, $CD11b^+$ $Gr\text{-}1^{intermediate}$, and $CD11b^+$ $Gr\text{-}1^-$) were stained with H&E and analyzed by using Leica DM2500 light microscope.

Blood and plasma analyses

Alanine transaminase (ALT) activity in plasma was measured using the ALT Reagent kit (Pointe Scientific). 3-Hydroxybutyrate levels were quantified using an enzymatic kit (Autokit 3-HB R1 and R2 sets, WAKO).

Blood glucose was measured with an Ascensia Breeze 2 glucose meter (Bayer), and percentages of circulating neutrophils and monocytes were measured with a Pentra80 hematologic analyser. Serum concentrations of cytokines were measured by multiplexed ELISA with a Luminex 200 analyser (Biorad).

ARTÍCULO 3: p38γ and δ promote heart hypertrophy by targeting the mTOR-inhibitory protein DEPTOR for degradation.

Autores: González-Terán B, López JA, Rodríguez E, Leiva L, Martínez-Martínez S, Bernal JA, Jiménez-Borreguero LJ, Redondo JM, Vazquez J, Sabio G

Publicado en *Nature Communications*, 2016 Jan 22;7:10477.

doi: 10.1038/ncomms10477.

RESUMEN

Alcanzar un tamaño apropiado del corazón es esencial para mantener la homeostasis del organismo y, alteraciones en los procesos de crecimiento de este órgano puede derivar en el desarrollo de cardiomiopatías. El corazón alcanza su tamaño adecuado durante el periodo postnatal del desarrollo por hipertrofia de los cardiomiocitos. Así mismo, el corazón puede hipertrofiarse como una respuesta adaptativa en respuesta a una mayor demanda funcional. Sin embargo, los mecanismos involucrados en la regulación de este proceso no se conocen con claridad. En este trabajo se muestra que la activación de p38γ y p38δ aumenta durante el desarrollo postnatal del corazón y en respuesta a estímulos hipertróficos. p38γ/δ promueven el crecimiento hipertrófico del corazón a través de la fosforilación de la proteína inhibitoria de mTORC1 y mTORC2, DEPTOR, que induce su degradación y la subsecuente activación de mTOR. Ratones deficientes en una de éstas o ambas quinasas, presentan un corazón de menor tamaño al de ratones control, alto niveles de DEPTOR, baja actividad de la vía de señalización mTOR y una síntesis proteica reducida. Este estudio aporta nuevos conocimientos sobre los mecanismos que utilizan los cardiomiocitos para crecer y adaptarse. Además, podría facilitar el diseño de nuevas estrategias terapéuticas para el tratamiento de alteraciones cardíacas provocadas por el crecimiento anómalo del corazón.

Aportación Personal al trabajo: He participado tanto en el diseño experimental, como en la realización de los experimentos y en la escritura del artículo.

nature COMMUNICATIONS

ARTICLE

Received 17 Feb 2015 | Accepted 14 Dec 2015 | Published 22 Jan 2016

DOI: 10.1038/ncomms10477 OPEN

p38γ and δ promote heart hypertrophy by targeting the mTOR-inhibitory protein DEPTOR for degradation

Bárbara González-Terán[1], Juan Antonio López[1], Elena Rodríguez[1], Luis Leiva[1], Sara Martínez-Martínez[1], Juan Antonio Bernal[1], Luis Jesús Jiménez-Borreguero[1,2], Juan Miguel Redondo[1], Jesús Vazquez[1] & Guadalupe Sabio[1]

Disrupted organ growth leads to disease development. Hypertrophy underlies postnatal heart growth and is triggered after stress, but the molecular mechanisms involved in these processes are largely unknown. Here we show that cardiac activation of p38γ and p38δ increases during postnatal development and by hypertrophy-inducing stimuli. p38γ/δ promote cardiac hypertrophy by phosphorylating the mTORC1 and mTORC2 inhibitor DEPTOR, which leads to its degradation and mTOR activation. Hearts from mice lacking one or both kinases are below normal size, have high levels of DEPTOR, low activity of the mTOR pathway and reduced protein synthesis. The phenotype of *p38γ/δ*$^{-/-}$ mice is reverted by overactivation of mTOR with amino acids, shRNA-mediated knockdown of *Deptor*, or cardiomyocyte overexpression of active p38γ and p38δ. Moreover, in WT mice, heart weight is reduced by cardiac overexpression of DEPTOR. Our results demonstrate that p38γ/δ control heart growth by modulating mTOR pathway through DEPTOR phosphorylation and subsequent degradation.

[1] Fundación Centro Nacional de Investigaciones Cardiovasculares Carlos III, CNIC, 28029 Madrid, Spain. [2] Hospital de La Princesa, 28006 Madrid, Spain. Correspondence and requests for materials should be addressed to G.S. (email: gsabio@cnic.es).

Cardiac growth is tightly regulated to ensure that the heart reaches its appropriate size. Cardiomyocytes rapidly proliferate during fetal life, but soon after birth differentiated cardiomyocytes enter a postmitotic state and the ability to proliferate is lost. Postnatal cardiac growth is therefore mainly achieved through increases in cell size (physiological hypertrophy) associated with increased protein synthesis[1] together with the expansion of non-myocyte populations[2]. Hypertrophic growth is also the adaptive response of cardiomyocytes to stress stimuli, including cardiac pressure or volume overload, cytoskeletal abnormalities and intrinsic contractility defects. Although cardiomyocyte hypertrophy initially enhances cardiac output in stress situations, prolonged hypertrophy, known as pathological hypertrophy, is associated with an increased risk of morbidity and mortality due to cardiovascular diseases such as diastolic and systolic heart failure and arrhythmia[3]. Understanding the mechanism of cardiac growth thus has important clinical implications. The key unanswered questions are how cells perceive extracellular hypertrophic stimuli and convert them into intracellular signals, and how these signals lead to cardiac hypertrophy[4].

Several studies identified mammalian TOR (mTOR) as a key regulator of cardiac hypertrophy; for example, the mTOR inhibitor rapamycin prevents heart-weight gain in an overload model of hypertrophy[5] and blocks cardiomyocyte size increases induced by AngII[6] and phenylephrine[7], likely by inhibiting protein synthesis[7]. mTOR is a conserved serine/threonine kinase with a key regulatory function in cardiovascular physiology and pathology[8]. mTOR integrates signals from growth factors, nutrients and stresses to regulate multiple processes, including translation, cell cycle progression, autophagy and cell survival[9]. mTOR function is regulated by the formation of two multi-protein complexes: mTOR complex 1 (mTORC1) and mTOR complex 2 (mTORC2). mTORC1 is composed of the mTOR catalytic subunit and five associated proteins: Raptor, PRAS40, mLST8/GβL, DEPTOR and Tti1/Tel2. In mTORC2, the mTOR catalytic subunit is associated with six proteins: mLST8/GβL, DEPTOR, Tti1/Tel2 (in common with mTORC1) and Rictor, mSin1 and Protor[10]. The activities of the mTORC1 and mTORC2 pathways are regulated by the common inhibitory component DEPTOR[11].

Stress-inducing stimuli in the heart activate several mitogen-activated protein kinases (MAPK), which are known to participate in hypertrophy, remodelling, contractility and heart failure[12,13]. MAPKs are key regulators of cell stress responses, including cell proliferation, differentiation and apoptosis[14,15]. The MAPK family consists of the extracellular signal-regulated protein kinases (ERK), the c-Jun NH2-terminal protein kinases (JNK) and the p38 MAP kinases[16]. Several studies have proposed that ERK cascade is involved in the hypertrophic response[17]. The p38 MAPKs are activated in response to proinflammatory cytokines, hormones and stress signals. Four p38 MAPK isoforms have been identified, and can be grouped into two subsets based on sequence homology, substrate specificity and sensitivity to chemical inhibitors: p38α and p38β, and p38γ and p38δ (ref. 15). MKK3 and MKK6, the kinases acting upstream of p38 MAPKs, appear to play a role in cardiac hypertrophy[18], and susceptibility to cardiac hypertrophy is promoted by cardiac-specific overexpression of dominant-negative p38α (ref. 19). However, findings in mice lacking p38α in cardiomyocytes indicate that this effect is p38α independent[20], whereas heart development requires endogenous p38β (ref. 21). Although the p38γ isoform is highly abundant in the heart[22] and p38δ is also expressed in cardiomyocytes[23], little is known about the role of these isoforms in cardiac hypertrophy[24].

Here, we report that p38γ and the closely related kinase p38δ are activated by pathological and physiological hypertrophic stimuli and are required for cardiac physiological and pathological hypertrophy. Using p38γ/δ null mice, we show that p38γ and p38δ interact with and phosphorylate the inhibitory mTOR complex component DEPTOR, inducing its degradation and thus promoting cell growth.

Results

p38γ and p38δ modulate postnatal cardiac hypertrophic growth. Stress stimuli in the heart activate several MAPKs, which have been implicated in mechanisms of cardiomyocyte hypertrophy and survival[13]. p38γ is abundant in heart tissue, and the closely related isoform p38δ is also well expressed[23]. Stress-induced hypertrophy appears to modulate the levels of both kinases[23], but their function and activation in the heart remain unsolved. Analysis of wild-type (WT) mice showed that expression of both kinases increases during postnatal growth and that they become activated, p38γ activity peaking on postnatal week 2 coinciding with the transition to hypertrophic growth[25], and p38δ activity peaking on postnatal week 6 (Fig. 1a). To assess the role of p38γ and p38δ in cardiac growth, we used knockout mice lacking p38γ, p38δ or both kinases, confirming the deletion of these kinases in the heart by western blot (Supplementary Fig. 1a). Ventricular mass between postnatal weeks 4 and 11 was monitored relative to tibia length in WT mice and mice lacking one or both of the kinases. Ventricular mass was notably lower in p38γ$^{-/-}$, p38δ$^{-/-}$ and p38γ/δ$^{-/-}$ mice (Fig. 1b). Lower heart mass in the knockout animals correlated with the presence of cardiomyocytes of below-normal size, determined from cell cross-sectional area on histological sections, suggesting a defect in postnatal hypertrophic growth (Fig. 1c,d). Similar analysis conducted at postnatal day 1 showed no differences between genotypes in heart or body size (Supplementary Fig. 1b,c), indicating that p38γ/δ kinases modulate hypertrophic heart growth in the postnatal period, and not in the fetus.

Echocardiography of 9-week-old mice revealed a thinner diastolic inter-ventricular septum (IVS) and telediastolic left ventricular posterior wall (LVPW;d) in p38γ$^{-/-}$, p38δ$^{-/-}$ and p38γ/δ$^{-/-}$ mice than in age-matched WT mice, and this correlated with a below-normal corrected left ventricular mass (Fig. 1e). However, the knockout models had normal systolic function, with no observed differences from WT in ejection fraction or fractional shortening (Fig. 1e). Moreover, haematoxylin and eosin and Picrosirius red staining revealed no differences in fibrosis or cardiac morphology (Supplementary Fig. 1d,e).

p38γ and p38δ control pathological hypertrophy. The involvement of p38γ and p38δ in physiological postnatal hypertrophic heart growth prompted us to examine whether these kinases are activated by angiotensin (Ang) II, a stress stimulus that induces hypertrophy in the adult heart[26,27]. AngII induced phosphorylation and activation of p38γ and p38δ kinases in the heart (Fig. 2a). Osmotic minipump administration of AngII over 28 days increased systolic arterial pressure in WT and all the three knockout models (Supplementary Fig. 2a), but only WT mice showed above-baseline increases in LV mass and IVS thickness (Fig. 2b and Supplementary Fig. 2b,c). In WT mice, heart mass (measured as the ventricular-weight-to-tibia-length ratio) increased almost 2-fold after 28 days of AngII infusion, whereas p38γ/δ$^{-/-}$ mice showed no hypertrophic growth (Fig. 2c and Supplementary Fig. 2d). Analysis of heart sections showed that AngII increased cardiomyocyte cross-sectional area in WT mice by around 50%; in contrast, cardiomyocyte cross-sectional area in AngII-treated p38γ/δ$^{-/-}$, p38γ$^{-/-}$ and p38δ$^{-/-}$ mice did not differ from that observed in saline-treated mice (Fig. 2d,e and Supplementary Fig. 2e). AngII

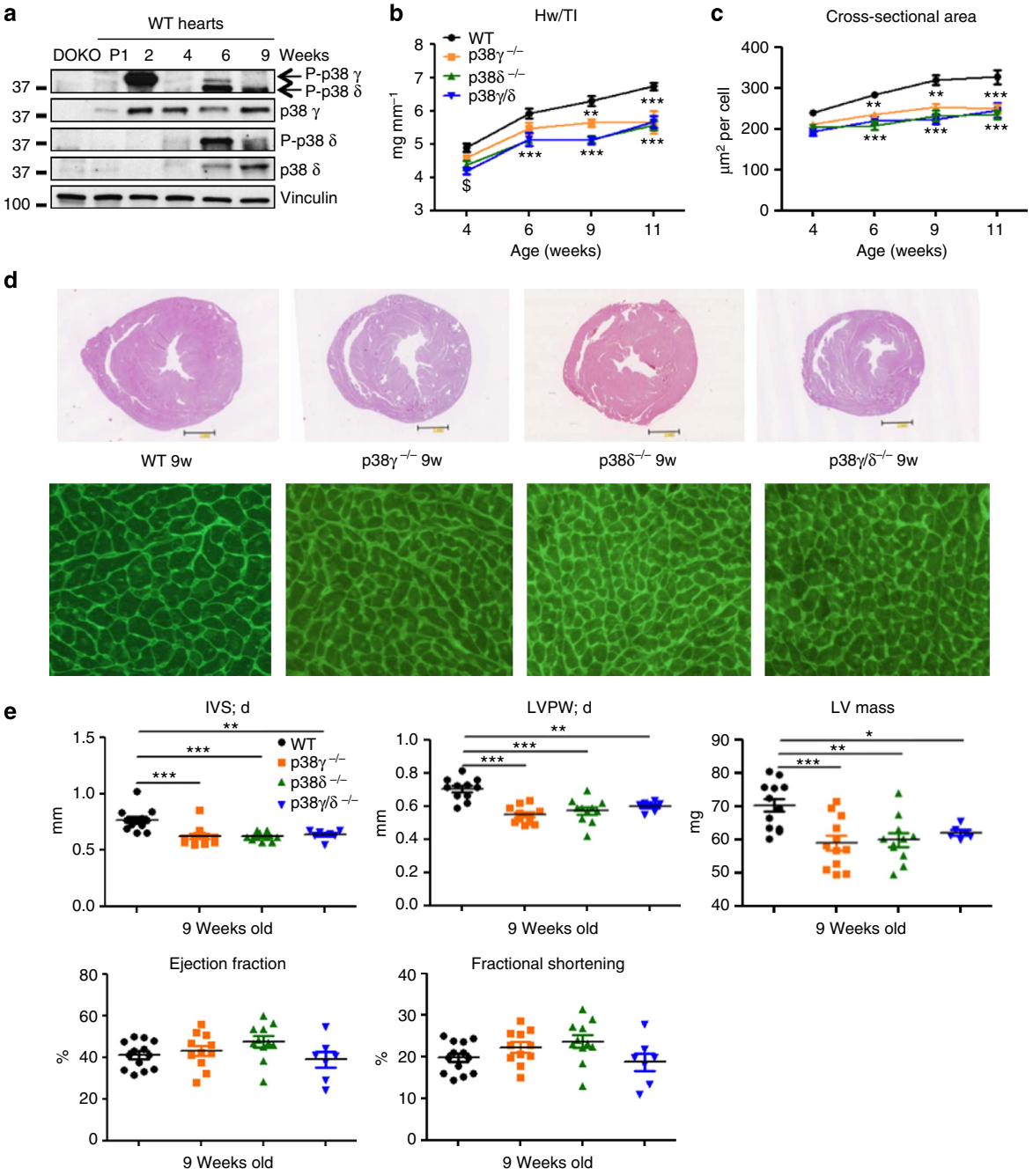

Figure 1 | p38γ and p38δ modulate postnatal cardiac hypertrophic growth. (**a**) Immunoblot analysis of p38γ and p38δ activation and expression in heart extracts prepared from wild-type (WT) mice at different ages. (**b**,**c**) WT, p38γ$^{-/-}$, p38δ$^{-/-}$ and p38γ/δ$^{-/-}$ mice were killed at 4, 6, 9 and 11 weeks. (**b**) Heart-weight-to-tibia-length ratio. (**c**) Cardiomyocyte cross-sectional area quantified in wheatgerm agglutinin (WGA)-stained hearts. Data are means ± s.e.m. ($n = 5$–13). $^{**}P < 0.01$; $^{***}P < 0.001$ (two-way analysis of variance (ANOVA) coupled to Bonferroni post tests). (**d**) Top: representative haematoxylin and eosin staining of transverse heart sections from 9-week-old WT, p38γ$^{-/-}$, p38δ$^{-/-}$ and p38γ/δ$^{-/-}$ mice. Bottom: Representative staining with FITC-WGA (green) in hearts from 9-week-old WT, p38γ$^{-/-}$, p38δ$^{-/-}$ and p38γ/δ$^{-/-}$ mice. (**e**) Echocardiography results for 9-week-old WT, p38γ$^{-/-}$, p38δ$^{-/-}$ and p38γ/δ$^{-/-}$ mice. IVS;d (inter-ventricular septum in diastole); LVPW;d (left ventricle posterior wall in diastole); LV (left ventricle). Data are means ± s.e.m. ($n = 5$–13). $^{*}P < 0.05$; $^{**}P < 0.01$; $^{***}P < 0.001$ (one-way ANOVA coupled to Bonferroni post tests).

treatment did not affect ejection fraction in WT or single or double KO mice, indicating preserved systolic ventricular function (Fig. 2f and Supplementary Fig. 2f), and the extent of fibrosis was similar in all genotypes (Supplementary Fig. 2g).

Impaired mTOR activation in hearts of p38γ or p38δ null mice. The size of mammalian cells is controlled by the mTOR pathway[28]. To assess whether mTOR signalling is altered in mice lacking p38γ and p38δ (Supplementary Fig. 3a), we analysed heart protein extracts by immunoblot. We found that cardiac activation of mTORC1 and mTORC2 was impaired in p38γ/δ$^{-/-}$, p38γ$^{-/-}$ and p38δ$^{-/-}$ mice, as assessed by the phosphorylation of the mTOR targets p70S6K, S6 and FOXO1/3a and by mTOR autophosphorylation on Ser 2481 (Fig. 3a, Supplementary Fig. 3b,c); in contrast, no changes were detected in the

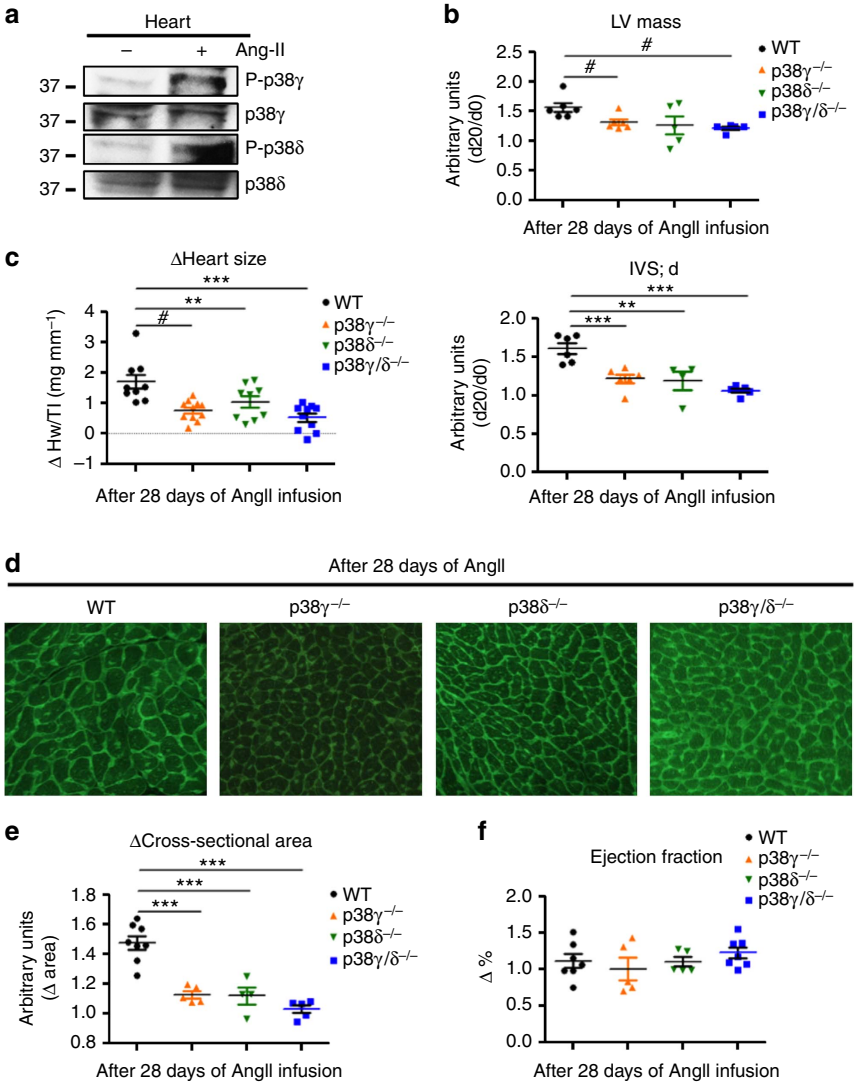

Figure 2 | p38γ and p38δ control angiotensin II-induced hypertrophy. WT, p38γ$^{-/-}$, p38δ$^{-/-}$ and p38γ/δ$^{-/-}$ mice were treated for 28 days with angiotensin II (AngII) (1 μg kg per minute) or saline, delivered by subcutaneously implanted osmotic minipumps. (**a**) Immunoprecipitation analysis of the phosphorylation and protein levels of p38γ and δ isoforms in heart extracts prepared from WT mice treated with AngII or saline. (**b**) Echocardiography results from AngII-treated WT, p38γ$^{-/-}$, p38δ$^{-/-}$ and p38γ/δ$^{-/-}$ mice shown as the change relative to saline-treated controls. (**c**) Heart-weight-to-tibia-length ratios for WT, p38γ$^{-/-}$, p38δ$^{-/-}$ and p38γ/δ$^{-/-}$ after 28 days of Ang II treatment. (**d**,**e**) Top: representative FITC-WGA staining (green) in hearts from 9-week-old WT, p38γ$^{-/-}$, p38δ$^{-/-}$ and p38γ/δ$^{-/-}$ mice after AngII treatment. (**e**) Cardiomyocyte cross-sectional area quantified in WGA-stained hearts. (**f**) Echocardiography evaluation of systolic cardiac function increment after AngII treatment. IVS;d (inter-ventricular septum in diastole); LV (left ventricle). Data are means ± s.e.m. ($n = 6$–12). $^{**}P < 0.01$; $^{***}P < 0.001$ (one-way analysis of variance coupled to Bonferroni post-tests); $^{\#}P < 0.05$ (*t*-test between indicated groups).

expression or activation of p38α (Supplementary Fig. 3d). A major function of mTORC1 is the promotion of protein synthesis[8], an essential driver of hypertrophic cardiomyocyte growth. Immunoblot analysis of translation initiation/elongation factors in the hearts of p38γ/δ$^{-/-}$ mice revealed weak phosphorylation of EIF4E, EIF4G and EIF4B and strong phosphorylation of EF2 (Fig. 3b), indicating that cardiac protein synthesis is impaired in these mice. To confirm this finding, we injected puromycin into WT and p38γ/δ$^{-/-}$ mice 30 min before heart extraction and measured its incorporation into newly synthesized proteins[29]. p38γ/δ$^{-/-}$ hearts contained fewer puromycin-labelled peptides than WT hearts, indicating a lower rate of protein synthesis (Fig. 3c). The p38γ/δ pathway thus appears to support growth induction in the heart by promoting the activation of mTOR-regulated protein synthesis.

p38γ and p38δ interact with mTOR through DEPTOR. We next investigated whether p38γ/δ isoforms interact with components of the mTOR complexes. Immunoblot analysis of immunoprecipitated p38γ from mouse embryonic fibroblasts (MEFs) surprisingly detected co-immunoprecipitation of several components of both mTORC1 and mTORC2 (Fig. 4a). To hone the search for specific interactions, we focused on mTOR and DEPTOR, components common to the mTORC1 and mTORC2 complexes. DEPTOR has an inhibitory action on the mTOR pathway and contains a PDZ domain[11], which has the potential to interact with the C-terminal of p38γ, as occurs with other PDZ-containing proteins[30,31]. To test DEPTOR–p38γ interaction, we transfected HEK-293 cells with HA-tagged p38γ, Flag-tagged DEPTOR and myc-tagged mTOR, alone and in combination. p38γ co-immunoprecipitated with DEPTOR regardless of whether the cells co-expressed mTOR (Fig. 4b);

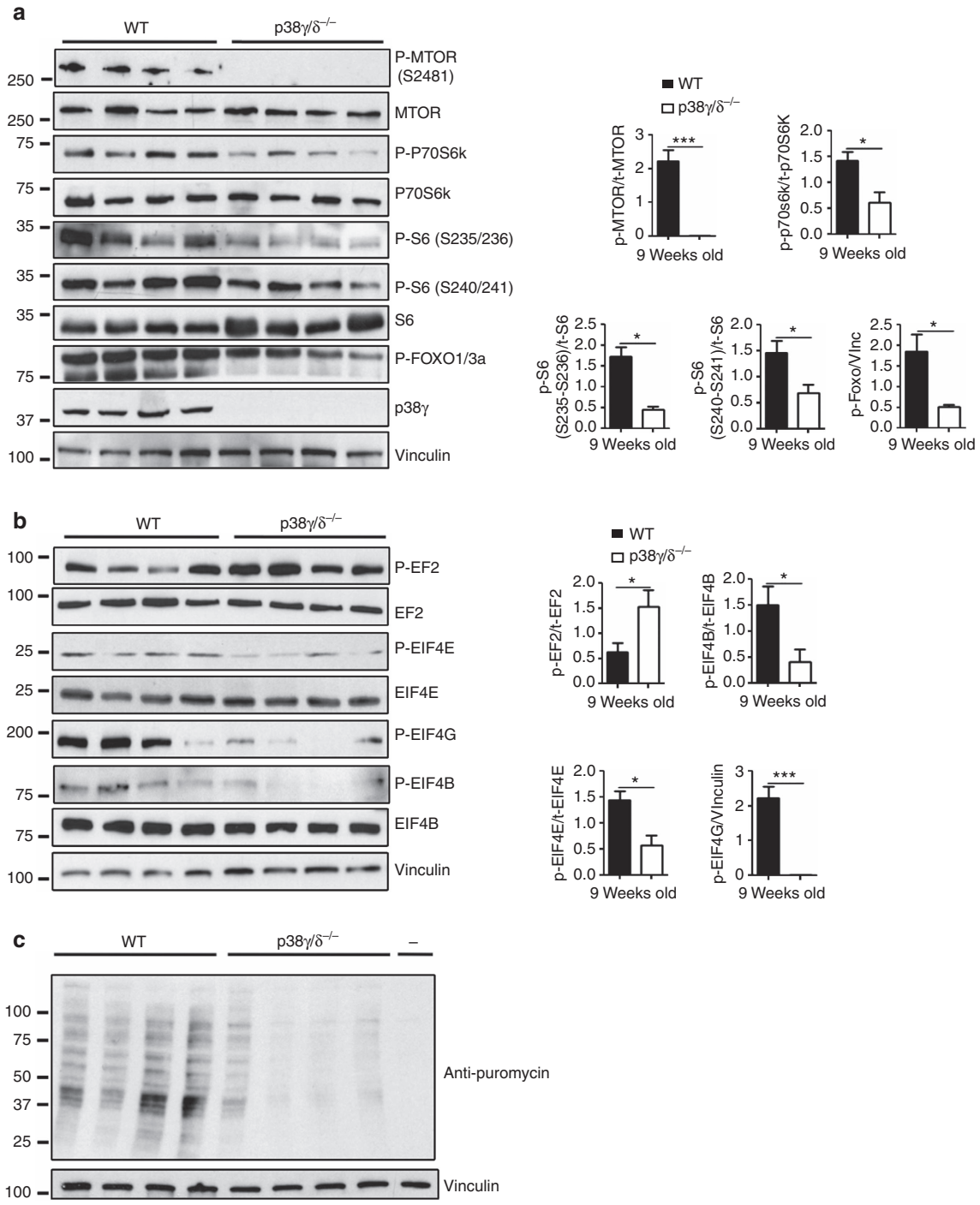

Figure 3 | Hearts from p38γ/δ$^{-/-}$ mice show reduced mTOR activation. (**a**,**b**) Immunoblot analysis of mTOR signalling pathway activity (**a**) and the activation status of translation factors (**b**) in heart lysates of 9-week-old WT and p38γ/δ$^{-/-}$ mice. Bar charts show quantification of total protein or vinculin-normalized band intensities ($n=4$). Data are means ± s.e.m. *$P<0.05$; ***$P<0.001$ (*t*-test). (**c**) *In vivo* measurement of protein synthesis. Mice were injected intraperitoneally with 0.040 μmol g^{-1} puromycin dissolved in 100 μl PBS. Exactly 30 min after injection, tissues were extracted and frozen in liquid N_2 for immunoblot analysis with anti-puromycin antibody ($n=4$).

in contrast, p38γ only co-immunoprecipitated with mTOR when it was expressed together with DEPTOR (Fig. 4c), thus indicating that p38γ is a DEPTOR-interacting protein. To determine which DEPTOR domain interacts with p38γ, we transfected HEK-293 cells with HA-tagged p38γ and Flag-tagged DEPTOR domains (the DEP domain or PDZ domain). p38γ interacted with the PDZ domain and not the DEP binding site (Supplementary Fig. 4b). To determine whether DEPTOR also interacts with p38δ, we transfected HEK-293 cells with Flag-DEPTOR and either HA-p38γ or HA-p38δ. Although both kinases co-immunoprecipitated with DEPTOR, the interaction with HA-p38γ appeared to be stronger (Fig. 4d). However in MEF, we detected co-immunoprecipitation of DEPTOR with p38δ (Supplementary Fig. 4a). Moreover, *in vitro* analysis indicated direct interaction of p38γ and p38δ with DEPTOR (Supplementary Fig. 4d). Surprisingly neither the PDZ nor DEP

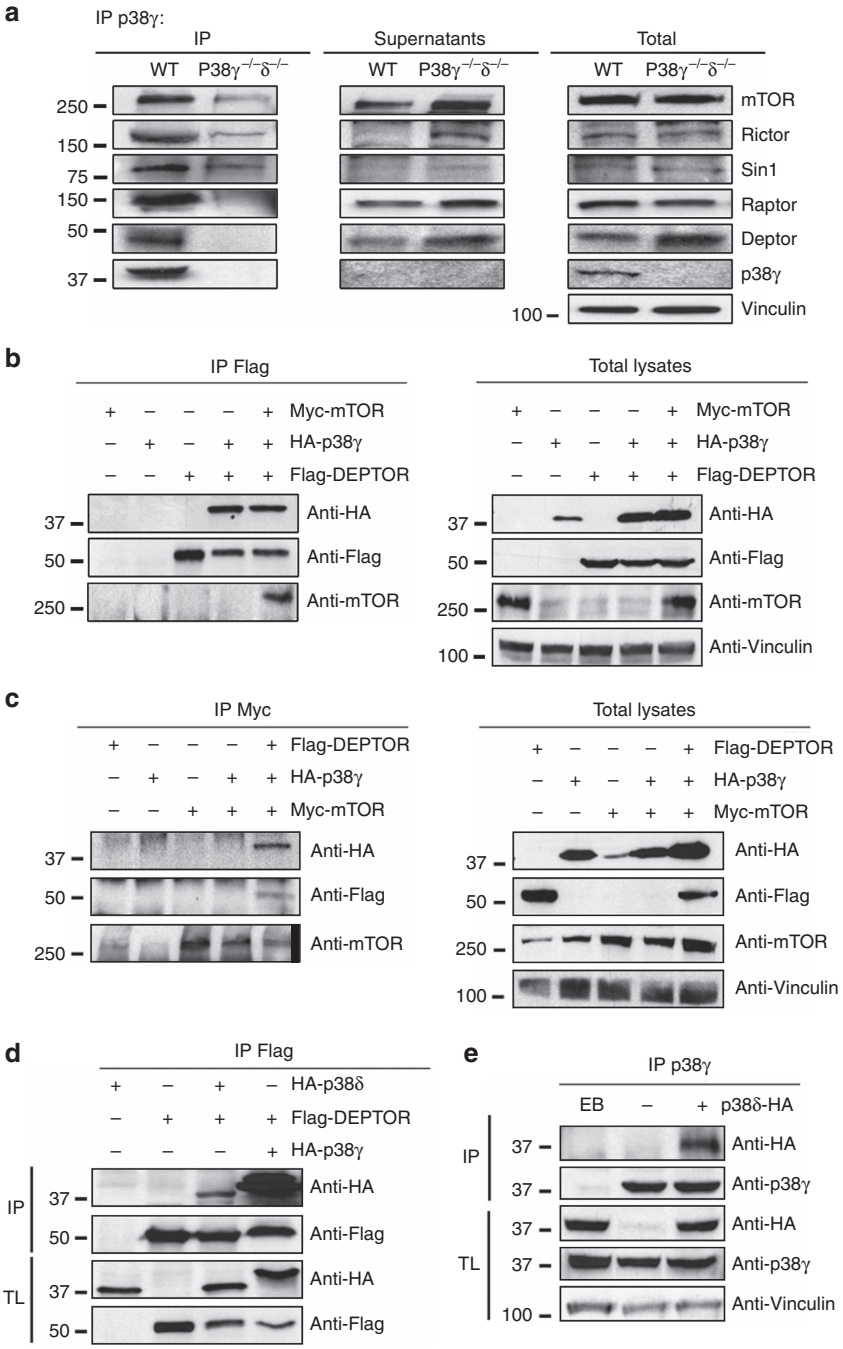

Figure 4 | p38γ and p38δ interact with mTOR through DEPTOR. (**a**) Endogenous mTOR, Raptor, Rictor, Sin-1 and DEPTOR co-immunoprecipitate with endogenous p38γ. We immunoprecipitated p38γ from WT and p38γ/δ$^{-/-}$ MEF lysates using specific antibodies; immunoprecipitates (IP), supernatants and total lysates were analysed by SDS–PAGE using the antibodies indicated. (**b**,**c**) p38γ interacts with mTOR through DEPTOR. HEK-293 cells were transfected with HA-p38γ, Flag-DEPTOR or Myc-mTOR or a combination of these and immunoprecipitated with the indicated antibodies targeting the c-myc epitope (**b**) or Flag (**c**). Immunoblots were probed with the indicated antibodies. (**d**) Co-immunoprecipitation of p38γ and p38δ with DEPTOR in HEK-293 cells. HA-p38γ or HA-p38δ expression vectors were co-expressed with Flag-DEPTOR in HEK-293T cells. Anti-Flag immunoprecipitates were analysed by SDS–PAGE. (**e**) HA- p38δ co-immunoprecipitates with endogenous p38γ. p38γ immunoprecipitates from HEK-293T cells transfected with HA-p38δ were analysed by SDS–PAGE. IP, immunoprecipitation; TL, total lysate.

domains are sufficient for this interaction, because while p38δ interacted with whole DEPTOR, it did not bind the individual DEP or PDZ domains (Supplementary Fig. 4c). Moreover, HA-p38δ co-immunoprecipitated with endogenous p38γ, indicating that p38γ and p38δ form part of the same complex (Fig. 4e).

p38γ and p38δ modulate DEPTOR protein levels. DEPTOR contains several potential MAPK phosphorylation sites (S/T-P), located outside the PDZ domain. An *in vitro* kinase assay showed p38γ-mediated phosphorylation of DEPTOR at four residues (Ser145, Ser244, 265 and Ser293) and p38δ-mediated phosphorylation at two (Ser265 and Thr321); no phosphorylation by p38α was detected (Fig. 5a, Supplementary Fig. 5a). DEPTOR phosphorylation on (S/T-P) residues in live cells was confirmed by immunoprecipitation/immunoblot analysis of HEK-293 cells transfected with DEPTOR or DEPTOR (13xS/T→A) mutant

together with constitutively active p38γ or p38δ mutants (Fig. 5b) and was confirmed by mass spectrometry to selected peptides (Supplementary Table 1 and Supplementary Fig. 5a,b).

DEPTOR levels increase in response to serum deprivation, resulting in mTOR inhibition, whereas serum stimulation leads to phosphorylation-dependent degradation of DEPTOR and enhanced mTOR activity[11,32]. To investigate whether p38γ or p38δ promote mTOR activity by triggering DEPTOR degradation, we blocked translation of new protein with cycloheximide in HEK 293 cells transfected with DEPTOR and the active p38 mutants. Active p38γ or p38δ reduced DEPTOR protein levels to a similar extent as serum stimulation (Fig. 5c,

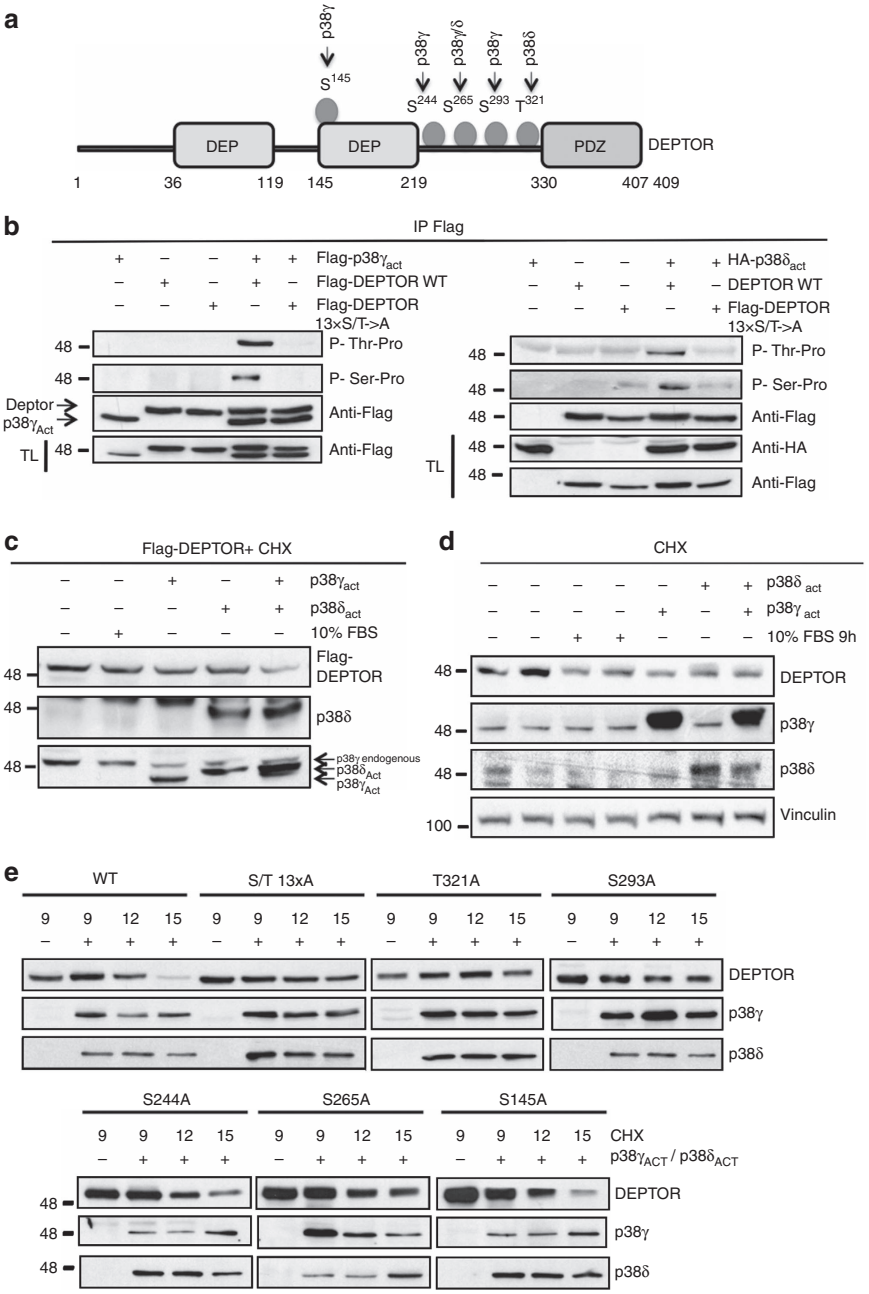

Figure 5 | p38γ and p38δ phosphorylate and downregulate DEPTOR protein levels. (**a**) Structural organization of DEPTOR, indicating p38γ and p38δ phosphorylation sites found by *in vitro* kinase assay. (**b**) p38γ and p38δ phosphorylate native DEPTOR on the canonical serine-proline MAPK phosphorylation residues *in vivo*. p38γ or p38δ active mutants were co-expressed in HEK-293T cells with Flag-DEPTOR or Flag-13xS/T→A DEPTOR (a mutated form with alanine substitutions of the S/T target residues). Flag-DEPTOR proteins were immunoprecipitated from cell lysates. Immunoprecipitates were analysed by SDS–PAGE and blotted with anti-phospho-threonine-proline and anti-phospho-serine-proline antibody; TL, total lysate. (**c**,**d**) Constitutively active p38γ and p38δ mutants induce DEPTOR degradation. (**c**) Flag-DEPTOR was expressed in HEK-293T cells alone or together with constitutively active p38γ and p38δ mutants, singly or together. HEK-293T cells starved for 30 h were incubated for 9 h with 10 μM cycloheximide (CHX) with or without 10% FBS. Cell lysates were analysed by immunoblotting with the indicated antibodies. (**d**) Endogenous DEPTOR levels are reduced when the active p38γ and p38δ mutants are overexpressed in HELA cells. HELA cells were serum-starved for 30 h and treated as in **c**. (**e**) DEPTOR phosphorylation mutants were expressed in HEK-293T alone or together with constitutively active p38γ and p38δ mutants. Fresh media without serum was added together with 10 μM cycloheximide (CHX) and cells collected at the times indicated. DEPTOR degradation was analysed by immunoblot.

Supplementary Fig. 6a), and the effect was stronger in cells co-transfected with both kinases (Fig. 5c). Similar results were obtained for endogenous DEPTOR in HeLa cells (Fig. 5d, Supplementary Fig. 6b). Moreover, the DEPTOR (13xS/T→A) mutant was not degraded, confirming that DEPTOR degradation was phosphorylation-dependent (Supplementary Fig. 6c). We next determined which phosphorylation sites in DEPTOR are necessary for its degradation by generating single-point DEPTOR mutants through the substitution of serine/threonine with alanine in codons 145, 244, 265, 293 or 321 (Supplementary Table 2). The protein half-life of two mutants (S293A and T321A) was extended to the same level as that of the mutated DEPTOR (13xS/T→A) mutant (Fig. 5e and Supplementary Fig. 6d), whereas a more moderate half-life extension was observed for S244A and S265A mutants (Fig. 5e and Supplementary Fig. 6d). These data indicate that p38γ- and p38δ-mediated phosphorylation of key residues targets DEPTOR for degradation. DEPTOR is a substrate of SCF E3 ubiquitin ligase[33], and DEPTOR poly-ubiquitination is dependant on DEPTOR phosphorylation[33]. Then we assayed whether phosphorylation *in vitro* of DEPTOR by p38γ or p38δ promote ubiquitination of DEPTOR. Our results indicate that DEPTOR presented higher ubiquitination after *in vitro* phosphorylation by p38γ and p38δ (Supplementary Fig. 6e). Moreover, we observed that in HEK293, active p38γ or p38δ significantly enhanced poly-ubiquitination of native DEPTOR but not the non-phosphorylatable DEPTOR (13xS/T→A) mutant (Supplementary Figs 6f and 7a).

To determine whether p38γ is involved in DEPTOR degradation after serum stimulation, we first verified the activation of the kinase in this setting (Supplementary Fig. 7b). MEFs lacking p38γ/δ had above-normal levels of DEPTOR and were resistant to DEPTOR degradation after serum stimulation (Fig. 6a). No changes were found in the mTOR complex components Raptor or Sin1 (Supplementary Fig. 7c). The above-normal and serum-independent DEPTOR content in p38γ/δ$^{-/-}$ cells correlated with impaired mTOR activation, measured by below-normal phosphorylation of p70S6K and its target S6 (Supplementary Fig. 7c). Moreover, the serum-independent DEPTOR content in these cells correlated with increased binding to mTOR (Supplementary Fig. 7d). Consistent with impaired mTOR pathway activation (Supplementary Fig. 7e), p38γ/δ$^{-/-}$ MEFs had lower protein synthesis activity and were smaller than WT counterparts (Fig. 6b,c).

To confirm whether p38γ/δ isoforms trigger DEPTOR degradation through a posttranscriptional mechanism, we treated MEFs with the protein synthesis inhibitor cycloheximide (CHX). DEPTOR levels in WT MEFs declined after 12 h exposure to CHX, whereas high DEPTOR levels were sustained in p38γ/δ null MEFs after 24 h (Supplementary Fig. 7f). Consistent with these results, DEPTOR levels in HeLa cells were reduced by expression of the constitutively active p38γ and p38δ mutants, and this effect was blocked by the proteasome inhibitor MG132 (ref. 34; Fig. 6d). As expected, shRNA-mediated suppression of DEPTOR in WT cells resulted in greater mTOR activation, protein synthesis and in consequence increased cell size (Supplementary Fig. 8a–c). Interestingly, treatment with DEPTOR shRNA in p38γ/δ$^{-/-}$ cells restored WT mTOR activity, protein synthesis and cell size (Fig. 6e,f, Supplementary Fig. 8d). These results thus suggest that p38γ/δ isoforms are key regulators of DEPTOR degradation by the proteasome, thereby promoting mTOR-dependent protein synthesis and cell growth.

p38γ/δ regulation of mTOR activity controls heart hypertrophy. To determine whether p38γ and p38δ interact with cardiac mTOR complexes *in vivo*, we immunoprecipitated p38γ and p38δ from heart extracts. The immunoprecipitates contained several mTORC1 and mTORC2 components, including DEPTOR (Fig. 7a,b Supplementary Fig. 9a,b). Moreover, p38γ immunoprecipitates contained p38δ and vice versa, confirming that the two kinases form part of the same complex *in vivo* (Supplementary Fig. 9c,d). Further analysis in heart extracts of p38γ$^{-/-}$ and p38δ$^{-/-}$ mice revealed that each kinase is needed for the interaction of the other in the mTOR complexes (Supplementary Fig. 9c), providing a probable explanation for the shared phenotype of p38γ and p38δ null mice.

The control of heart size by p38γ/δ-induced DEPTOR degradation in cardiomyocytes predicts that hearts from p38γ and p38δ null mice will present higher protein levels of DEPTOR, and this was confirmed by immunoblot analysis of hearts from 9-week-old animals (Fig. 7c). Interestingly, DEPTOR mRNA levels were below normal in p38γ and p38δ null hearts, indicating that the increased DEPTOR protein expression is not owing to higher DEPTOR transcription (Supplementary Fig. 9e). Moreover, DEPTOR levels were strongly reduced from P1 to 2 weeks in WT hearts, a period in which the heart switches from proliferation to hypertrophic growth. This correlated with maximal activation of p38γ and p38δ, and with the activation of mTOR (Fig. 7d). Moreover, DEPTOR phosphorylation and ubiquitination in WT mice were increased during this period, whereas phosphorylation and ubiquitination were reduced in p38γ and p38δ null mice (Fig. 7e). In WT mice, angiotensin II, which activates p38γ and p38δ (Fig. 2a), also correlated with DEPTOR degradation and mTOR activation (Fig. 7f). These results suggest that p38γ and p38δ modulate heart growth *in vivo* by controlling DEPTOR degradation and in consequence mTOR activity.

To determine whether the impaired heart growth in the p38γ/δ$^{-/-}$ animals results from an autonomous effect on postnatal cardiomyocyte growth, we generated mice lacking p38δ in striated muscle by crossing mice carrying *lox*P-flanked *p38δ* with MCK Cre mice (p38δ^{Mck-KO}), which reach peak Cre expression on postnatal day 10 (ref. 35). The cardiac phenotype of mice lacking p38δ specifically in striated muscle resembled that of p38δ$^{-/-}$ mice, suggesting that p38δ-mediated control of heart growth is cell autonomous (Fig. 7g–j and Supplementary Fig. 10a). To further confirm that the phenotype is cardiac specific, we treated p38γ/δ$^{-/-}$ mice with cardiac-specific adeno-associated viruses expressing p38γ/δ active mutants under the troponin T promoter (AAV-TnT-p38γ/δact). Cardiac-specific expression of p38γ/δ-active mutant reduced DEPTOR levels in p38γ/δ$^{-/-}$ heart to the levels of WT mice and increased mTOR activation (Fig. 8a). In consequence, reduction of heart growth was reverted in p38γ/δ$^{-/-}$ mice treated with AAV-TnT-p38γ/δact and cardiomyocyte cross-sectional area increased to WT levels (Fig. 8b,c).

To confirm whether p38-mediated modulation of the mTOR pathway is responsible for normal postnatal heart growth, we treated MCK-cre and p38δ^{Mck-KO} mice with the mTOR inhibitor rapamycin from weeks 4 to 9 after birth. Rapamycin treatment reduced the heart weight and cardiomyocyte size only in control mice (MCK-cre), equalizing with heart weight in p38δ^{Mck-KO} mice (Fig. 8e,f). Moreover, echocardiographic studies showed that rapamycin reduced diastolic IVS, LVPW and LV mass in MCK-Cre mice but not p38δ^{Mck-KO} mice (Fig. 8g), without between-genotype differences in ejection fraction (Fig. 8g). Thus the small hearts in p38δ^{Mck-KO} and p38γ/δ KO mice appear to result from the inhibition of mTOR activation in these mice.

To test whether decreased mTOR signalling could account for the weak heart growth in p38γ/δ$^{-/-}$ mice, we hyperactivated mTOR with aminoacids (aa) to restore heart growth in p38γ/δ KO mice. As expected, daily aa injection activated the mTOR pathway in p38γ/δ$^{-/-}$ hearts (Supplementary Fig. 10b).

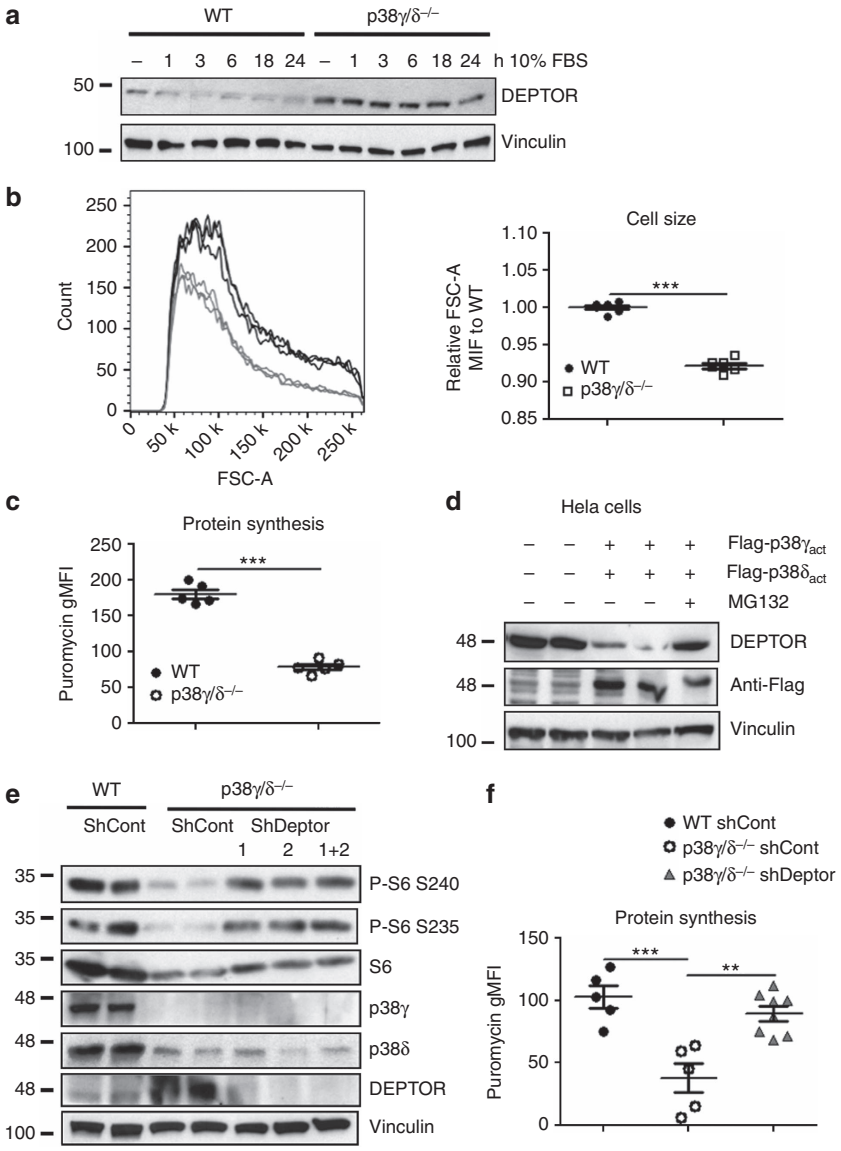

Figure 6 | p38γ/δ control cell size and protein synthesis through DEPTOR levels. (**a**) p38γ/δ$^{-/-}$ MEFs present altered serum-induced DEPTOR degradation. WT and p38γ/δ$^{-/-}$ MEFs were serum-starved for 30 h, followed by serum addition. Cells were collected at successive time points for immunoblotting with the indicated antibodies. (**b**) p38γ/δ$^{-/-}$ MEFs are of below-normal size. Cell size was measured by flow cytometry (forward scatter). Right: representative histogram. Left: quantification graph of the forward scatter mean fluourescence intensity (FSC-A MFI) relative to WT. Data are means ± s.e.m. ***$P<0.001$ (*t*-test). (**c**) p38γ/δ$^{-/-}$ MEFs have downregulated protein synthesis. SUnSET was performed by pulsing 10 min 10 μg ml^{-1} puromycin and chasing for 1 h before FACS analysis with anti-puromycin 12D10 antibody and anti-mouse IgG conjugated with PE. Data are means ± s.e.m. ***$P<0.001$ (*t*-test). (**d**) p38γ/δ-induced DEPTOR degradation by the proteasome. HELA cells co-transfected with active p38γ and p38δ mutants were serum-starved for 30 h. Cells were treated with MG132 (10 μM) or vehicle together with 10 μM cycloheximide (CHX) for 9 h, and were analysed by immunoblotting with the indicated antibodies. (**e**) Silencing DEPTOR in p38γ/δ$^{-/-}$ MEF cells restores mTOR signalling. MEFs were singly or doubly infected with two different DEPTOR lentiviral shRNA constructs for 24 h. Uninfected cells were eliminated by selection with 3 μg ml^{-1} puromycin for 1 week. The resulting cell lines were then serum-starved for 24 h before collecting. Equal amounts of whole-cell lysates were immunoblotted with the indicated antibodies. (**f**) Silencing of DEPTOR in p38γ/δ$^{-/-}$ MEFs increases protein synthesis. MEFs were infected as in **e**. In the resulting cell lines, the protein concentration per cell was measured by SUnSET assay, performed as in **b**. Data are means ± s.e.m. **$P<0.01$; ***$P<0.001$ (one-way analysis of variance coupled to Bonferroni post tests).

Compared with saline treatment, aa supplementation significantly increased heart size, LV mass and cardiomyocite cross-sectional area (Supplementary Fig. 10c–f). Consistently, cardiac-specific overexpression of DEPTOR in WT mice resulted in reduced mTOR activation and lower heart mass, correlating with the presence of cardiomyocytes of below-normal size, determined from cell cross-sectional area on histological sections (Fig. 9a–d).

To confirm that decreased DEPTOR degradation in cardiomyocytes contributes to the phenotype of p38γ/δ KO mice, we used DEPTOR-targeted shRNA under the promoter of cardiac troponin T (AAV-TnT-shDEPTOR). Cardiac-specific reduction of DEPTOR expression in p38γ/δ$^{-/-}$ mice was confirmed by western blot and was sufficient to restore mTOR activation (Fig. 9e). Furthermore, these animals showed re-established cardiac growth and increased cardiomyocyte cross-sectional area (Fig. 9f–h). Moreover, a control, AAV-Tnt or AAV-TnT-shDEPTOR did not affect cardiac growth in WT mice (Supplementary Figs 11 and 12). These results confirm that

reduction of heart growth observed in p38γ/δ$^{-/-}$ mice is driven by the accumulation of DEPTOR caused by the absence of DEPTOR phosphorylation and degradation. DEPTOR accumulation inhibits mTOR pathway and consequently growth.

Discussion

In this study, we provide evidence that two stress kinases, p38γ and p38δ, promote the activity of mTOR, a critical sensor of metabolic and nutrient stresses, by targeting the mTOR inhibitory partner DEPTOR for proteasome degradation. The finding that DEPTOR is a physiological p38γ/δ substrate is, to our knowledge, the first demonstration of DEPTOR interaction with a non-mTOR complex protein. Moreover, our results show that p38γ or p38δ are both able to phosphorylate DEPTOR and induce its subsequent proteasomal degradation, contrary to the proposal that DEPTOR phosphorylation was only mTOR dependent[11].

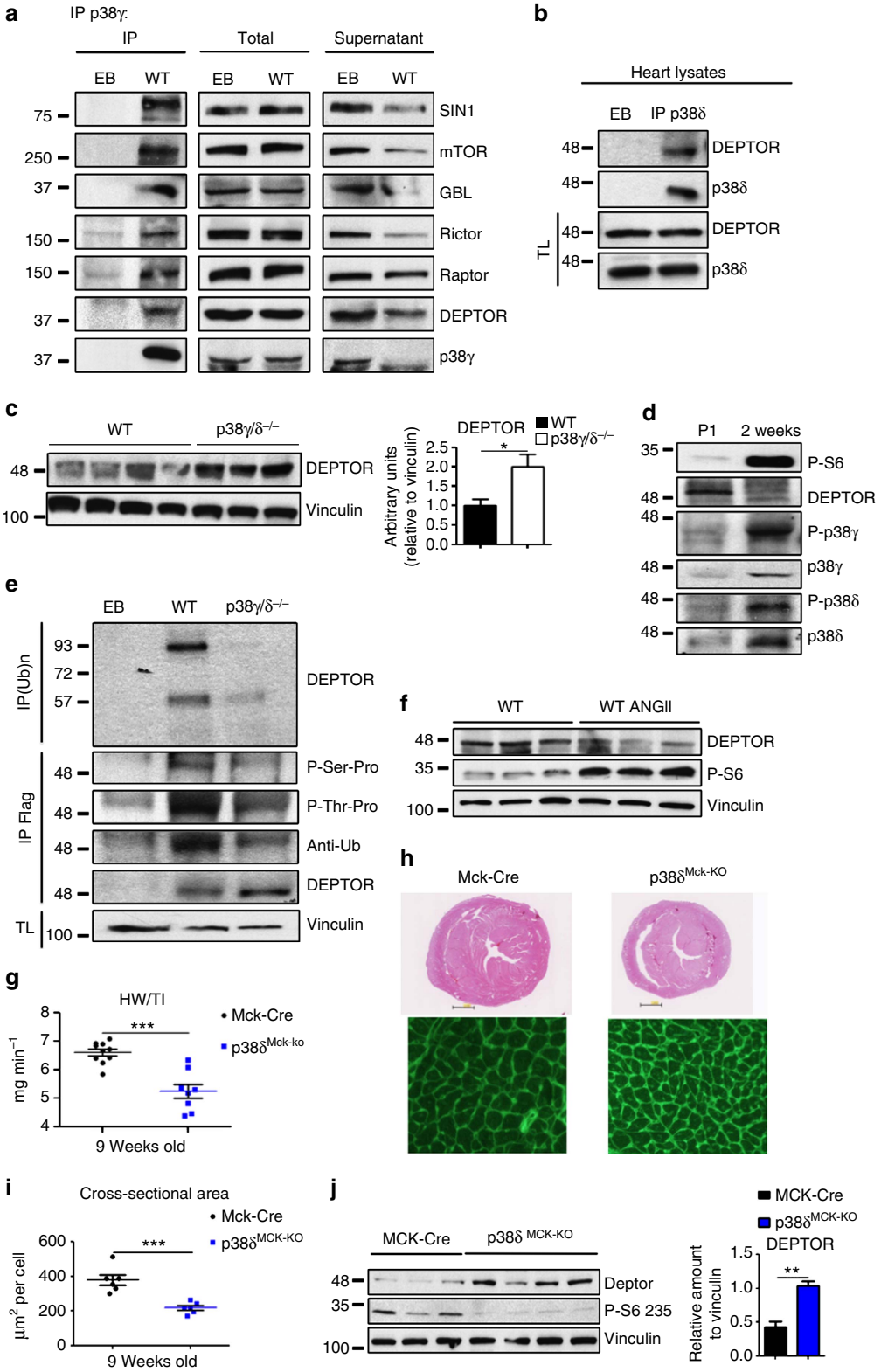

The p38γ/δ-mTOR signalling pathway controls protein synthesis and cell growth, and molecular and functional evidence indicates that this pathway plays an important physiological role in the regulation of ventricular cardiac hypertrophy.

Our conclusion is supported by several lines of evidence: (1) mTOR activity is below-normal in hearts and cells from mice deficient in p38γ and p38δ; (2) low mTOR activation in cells lacking p38γ and p38δ leads to reduced cell size and protein synthesis; (3) p38γ and p38δ co-immunoprecipitate with mTORC1 and mTORC2 complexes; (4) p38γ and p38δ bind to DEPTOR; (5) DEPTOR is phosphorylated by p38γ and p38δ; (6) DEPTOR protein half-life is shortened by active p38γ and p38δ mutants, but extended by knockout of p38γ and p38δ; (7) DEPTOR levels are elevated in hearts lacking p38δ or p38γ/δ; (8) reduction of DEPTOR levels correlates with p38γ and p38δ activation; (9) silencing of DEPTOR in cells lacking p38γ and p38δ increases their protein content and size; (10) rapamycin treatment in the postnatal period equalizes heart size in WT and KO animals; (11) mTOR activation by aa injection into p38γ/δ$^{-/-}$ mice results in heart growth; (12) cardiac-specific overexpression of active p38γ/δ reduces DEPTOR levels, increasing mTOR activity and cardiomyocyte growth; (13) cardiac overexpression of DEPTOR phenocopies the p38γ/δ$^{-/-}$ phenotype; (14) cardiac-specific silencing DEPTOR in p38γ/δ$^{-/-}$ mice increases their heart size and cardiomyocyte growth.

Despite the physiological and pathological importance of cell-size regulation, our understanding of the underlying mechanisms remains very limited. In the heart, the regulation of cell size is a key process that modulates the organ's response to external stimuli. Identifying molecular mechanisms through which hypertrophy can be suppressed without provoking circulatory insufficiency is a major challenge. Our data strongly indicate that lack of p38γ and p38δ reduces the capacity for cardiomyocyte growth without having functional implications: cardiac function remained normal in these mice even in the presence of AngII-induced hypertrophy, and they showed no increase in fibrosis with respect to WT mice.

Surprisingly, although mTOR is necessary for embryonic cardiovascular development and for the postnatal maintenance of cardiac function[8], inhibition of mTOR as a result of the lack of p38γ and p38δ does not have a deleterious effect on heart physiology in basal condition. This is likely because p38γ and p38δ act through the mTOR modulator DEPTOR, so that the lack of p38γ and p38δ results only in partial inhibition of mTOR activity. This finding is of great interest because other models in which the heart is incapable of growing display signs of cardiac pathology such as cardiac dilation or heart failure[36,37]. The fact that the modulation of these kinases results in reduced heart hypertrophy without obvious secondary effects makes p38γ and p38δ potential targets for therapeutic intervention. However, it would be interesting to further study whether modulation of these kinases could have functional implication after a stronger challenge such as myocardial infarction.

Our findings provide definition of the previously uncharacterized role of p38γ and p38δ in cardiac hypertrophy[38], demonstrating that p38γ and p38δ are activated during postnatal growth and by stress stimuli in the heart. This activation correlates with DEPTOR phosphorylation, ubiquitination and degradation, modulating cardiac growth in tissue culture and animal models. Mice deficient in these kinases presented reduced DEPTOR phosphorylation and degradation, correlating with impaired postnatal and pathologically induced cardiac hypertrophy.

The finding that lack of just one of these kinases produces the defect is quite surprising because each normally compensates the loss of the other in other biological processes. The non-redundancy of these isoforms in the induction of cardiac hypertrophy is likely explained by their interaction *in vivo*. Both kinases cooperate in the binding to the mTOR complex and in the modulation of its activity through the phosphorylation and subsequent ubiquitination and proteasomal degradation of DEPTOR. Although p38γ interacts with DEPTOR through the PDZ domain, the exact interaction between DEPTOR and p38δ remains unclear. Moreover, our experiments with single-point mutants indicated that both kinases are needed to induce DEPTOR degradation. Lack of phosphorylation on S293 or T321, residues respectively phosphorylated by p38γ and p38δ, are sufficient to abolish DEPTOR degradation, indicating a requirement for cooperation between both kinases to induce DEPTOR degradation. Moreover, mTOR induces DEPTOR phosphorylation on other residues, which are also necessary for DEPTOR ubiquitination and degradation[11,32,33]. Additional studies will be needed to clarify how these kinases cooperate to phosphorylate DEPTOR and to determine whether p38 γ and δ act as a heterodimer. Moreover it would be interesting to study whether this mechanism acts in other tissues and in response to other stimuli.

Cell autonomous control of cell hypertrophy by p38γ and p38δ was validated by several independent approaches, including the use of mice lacking p38δ in myocytes, and immortalized fibroblasts from p38γ/δ$^{-/-}$ mice. Furthermore, hearts from p38γ/δ null animals are able to grow after AAV-mediated

Figure 7 | Cardiac p38γ/δ activation correlates negatively with DEPTOR levels. (**a**) Endogenous cardiac Sin-1, mTOR, GβL, Rictor, Raptor and DEPTOR co-immunoprecipitate with endogenous p38γ. p38γ immunoprecipitates (IP), total lysates and Co-IP supernatants from WT heart lysates were analysed by SDS–PAGE. EB: beads with IgG control. (**b**) Endogenous cardiac DEPTOR co-immunoprecipitates with p38δ. Immunoblot analysis of p38δ immunoprecipitates (IP) and total lysates (TL) from the hearts of 9-week-old p38γ/δ$^{-/-}$ mice infected with AAV-TnT-p38γ$_{act}$ and AAV-TnT-p38δ$_{act}$. (**c**) p38γ/δ$^{-/-}$ hearts express above-normal levels of DEPTOR protein. Immunoblot analysis of heart lysates from WT and p38γ/δ$^{-/-}$ mice starved for 4 h and re-fed for 2h ($n=3$–4). (**d**) Cardiac DEPTOR levels during postnatal development correlate negatively with p38γ and p38δ activation and mTOR pathway activation. Heart lysates from WT p1 and 2-week-old mice were analysed by immunoblot ($n=6$). (**e**) Levels of DEPTOR phosphorylation and ubiquitination *in vivo* are reduced in p38γ/δ$^{-/-}$ hearts. Upper panel: poly-ubiquitinated proteins were IP from WT and p38γ/δ$^{-/-}$ heart lysates and immunoprecipitates were immunoblotted with anti-DEPTOR antibody. Lower panels: WT and p38γ/δ$^{-/-}$ mice were intravenously injected with AAV-TNT-Flag-DEPTOR and hearts harvested at the age of 2 weeks. Flag-DEPTOR was immunoprecipitated from heart lysates, and immunoprecipitates were analysed by immunoblotting with the indicated antibodies. ($n=5$). (**f**) Angiotensin II (ANGII) treatment induces a reduction in DEPTOR levels in WT hearts. WT mice were treated with ANGII or saline for 21 days. Heart lysates were analysed by immunoblotting. ($n=3$). (**g**–**i**) MCKdelta KO mice have small hearts. (**f**) Heart-weight-to-tibia-length ratios in WT and MCKdelta KO (p38δ^{MCK-KO}) mice killed at 9 weeks. (**g**) Top: representative haematoxylin and eosin staining of transverse heart sections from 9-week-old WT and MCKdelta KO mice. Bottom: representative staining with FITC-WGA (green) in hearts from 9-week-old WT and MCKdelta KO mice. (**h**) Cardiomyocyte cross-sectional area quantified from WGA-stained hearts. (**j**) MCKdelta KO hearts have higher protein levels of DEPTOR. MCK-Cre control mice and MCKdelta KO (p38δ^{MCK-KO}) mice were starved for 4 h before being killed and tissue was collected. Heart lysates were analysed by immunoblotting; the bar chart shows quantification of vinculin-normalized band intensities (ImageJ; $n=4$). Data are means ± s.e.m. ($n=5$). $^{**}P<0.01$; $^{***}P<0.001$ (*t*-test).

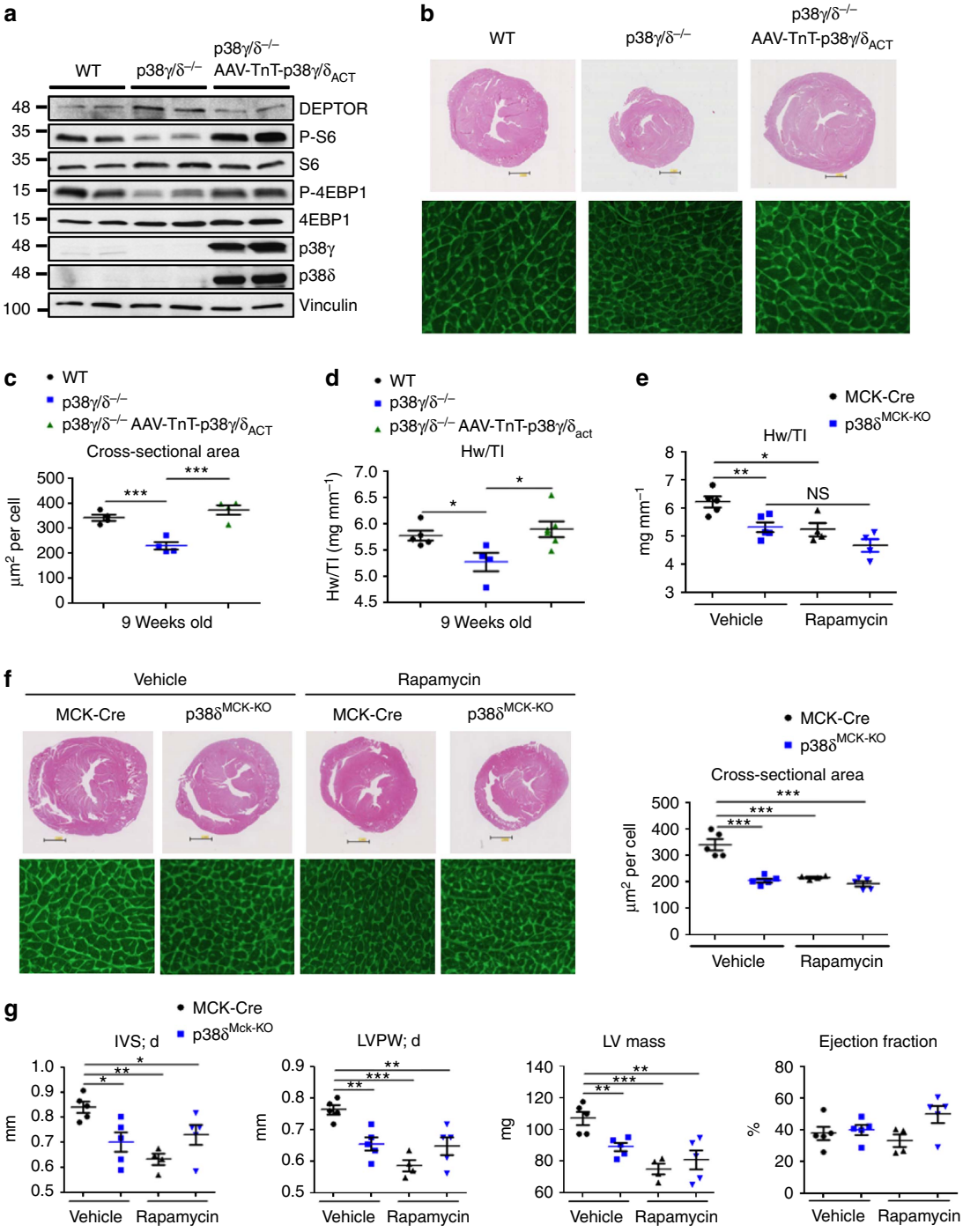

Figure 8 | Cardiac p38γ/δ control heart growth by modulating mTOR activity. (**a**–**d**) Cardiac-specific expression of active p38γ and p38δ mutant forms in p38γ/δ$^{-/-}$ hearts restores normal heart size. p38γ/δ$^{-/-}$ mice were intravenously injected at 4 weeks of age with AAV-TnT-p38γ$_{act}$ and AAV-TnT-p38δ$_{act}$, and hearts were harvested from 9-week-old WT, p38γ/δ$^{-/-}$ and p38γ/δ$^{-/-}$ AAV-TnT-p38γ/δ$_{act}$ mice. (**a**) Immunoblot analysis of heart lysates. (**b**) Top: representative haematoxylin and eosin (H&E) staining of transverse heart sections. Bottom: representative staining with FITC-WGA (green). (**c**) Cardiomyocyte cross-sectional area quantified from WGA-stained hearts. (**d**) Heart-weight-to-tibia-length ratio. (**e**–**g**) Rapamycin treatment preserves normal heart size in MCKdelta KO hearts. MCK-Cre (control) and MCKdelta KO (p38δ^{MCK-KO}) mice were intraperitoneally injected daily with rapamycin (2 mg kg^{-1} per day) from 4 to 9 weeks of age. (**e**) Heart-weight-to-tibia-length ratio. (**f**) Top: representative H&E stained transverse heart sections from 9-week-old MCK-Cre and MCKdelta KO mice after rapamycin treatment. Bottom: representative FITC-WGA staining (green) in hearts from 9-week-old MCK-Cre and MCKdelta KO mice after rapamycin treatment. (**g**) Echocardiography analysis of 9-week-old MCK-Cre and MCKdelta KO mice treated with rapamycin or vehicle. IVS;d (interventricular septum in diastole); LVPW;d (left ventricle posterior wall in diastole); LV Mass (left ventricle) and ejection fraction. Data are means ± s.e.m. ($n=5$). *$P<0.05$; **$P<0.01$; ***$P<0.001$ (one-way analysis of variance coupled to Bonferroni post test). NS, not significant.

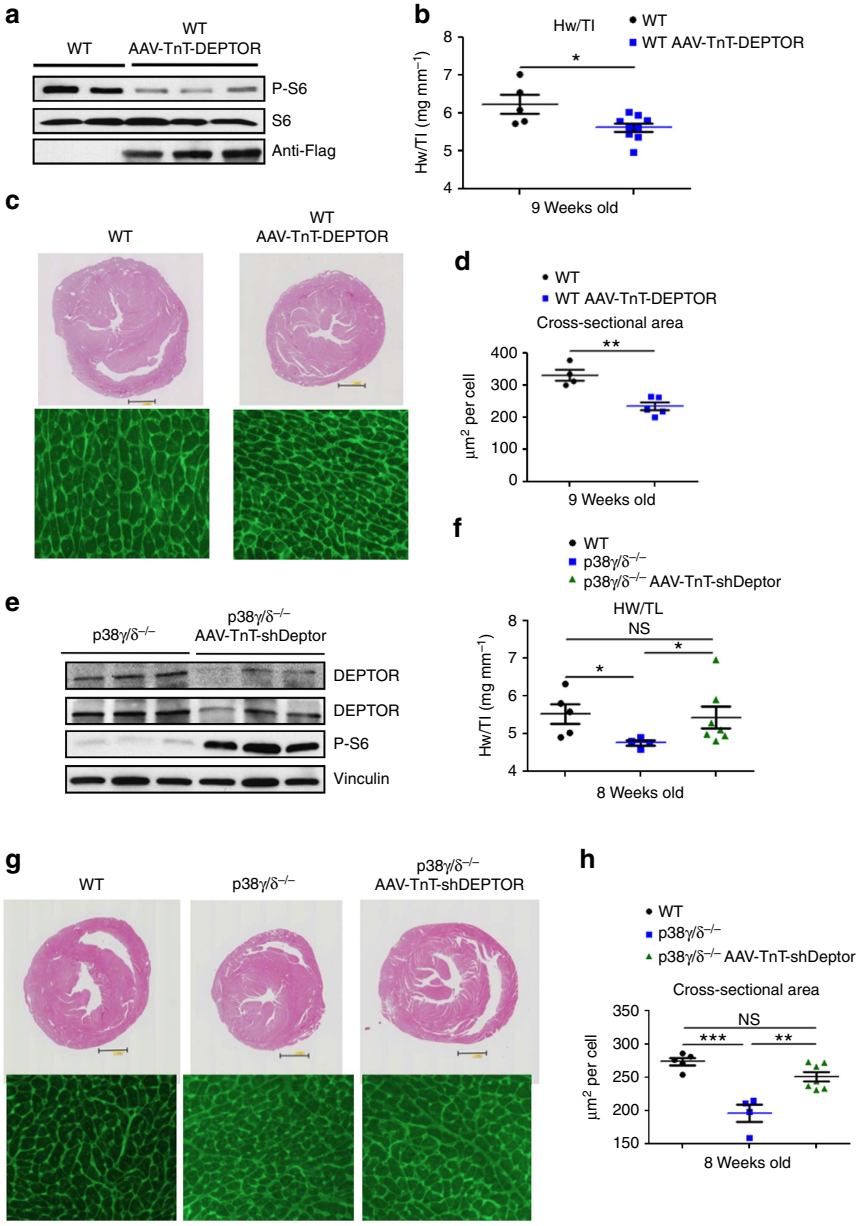

Figure 9 | Deptor cardiac specific expression reduces heart size. (**a**–**d**) Cardiac-specific expression of Flag-DEPTOR in WT hearts reduces heart size. WT mice were intravenously injected at 4 weeks of age with AAV-TnT-Flag-DEPTOR and hearts harvested at 9 weeks of age. (**a**) Immunoblot analysis of heart lysates. (**b**) Heart-weight-to-tibia-length ratio (**c**) Top: representative haematoxylin and eosin (H&E) staining of transverse heart sections from untreated (WT) and AAV-TnT-Flag-DEPTOR-injected mice. Bottom: representative staining with FITC-WGA (green). (**d**) Cardiomyocyte cross-sectional area quantified from WGA-stained heart. ($n=5$–9). Data are means ± s.e.m. ($n=5$). *$P<0.05$; **$P<0.01$ (*t*-test). (**e**–**h**) Cardiac-specific DEPTOR silencing in p38γ/δ$^{-/-}$ mice restores normal heart size. Hearts from WT, p38γ/δ$^{-/-}$ and p38γ/δ$^{-/-}$ mice intravenously injected at birth with AAV-TnT-shDeptor were harvested at 9 weeks of age. (**e**) Immunoblot analysis of heart lysates. (**f**) Heart-weight-to-tibia-length ratio (**g**) Top: representative H&E staining of transverse heart sections from untreated WT and p38γ/δ$^{-/-}$ and from AAV-TnT-shDeptor injected p38γ/δ$^{-/-}$ mice. Bottom: representative staining with FITC-WGA (green). (**h**) Cardiomyocyte cross-sectional area quantified from WGA-stained hearts. ($n=5$–7). Data are means ± s.e.m. ($n=5$). *$P<0.05$; **$P<0.01$; ***$P<0.001$ (one-way analysis of variance coupled to Bonferroni post test). NS, not significant.

cardiomyocyte overexpression of p38γ and p38δ, and AAV-mediated DEPTOR overexpression in WT hearts reduces cardiomyocyte size. Finally, reduction of DEPTOR levels in cardiomyocytes from p38γ/δ null animals increased heart growth to the level seen in WT mice, indicating that the phenotype found in p38γ/δ null animals is mediated by DEPTOR.

Our results identify p38γ and p38δ signalling as a key regulator of mTOR activity, promoting protein synthesis and cell hypertrophy by phosphorylating the mTOR inhibitor DEPTOR and inducing its ubiquitination and degradation. p38γ/δ signalling through mTOR complexes is an important mediator of cardiac hypertrophy, and this pathway may also be important in other physiological processes mediated by mTOR, such as cancer and autophagy. These results reveal a new avenue in the control of mTOR activation and open a route to the development of new treatment strategies for disease.

Methods

Mice. Mice deficient for p38γ (B6.129-Mapk12tm1) and p38δ (B6.129-Mapk13tm1) were backcrossed for 10 generations to the C57BL/6J background

(Jackson Laboratory). To generate mice lacking p38δ in striated muscle, p38δ (B6.129-Mapk13tm1) mice were crossed with the FVB-Tg(Ckmm-cre)5Khn/J line on the C57BL/6J background (Jackson Laboratory). Genotype was confirmed by PCR analysis of genomic DNA. For signalling studies, animals were killed by cervical dislocation. For AngII experiments, 9-week-old male mice were treated with AngII ($1\,\mu g\,kg^{-1}$ per minute, 28 days) via subcutaneously implanted mini-osmotic pumps (Alzet); saline was administered as a control. For rapamycin treatment, mice were daily injected intraperitoneally with rapamycin (LC Laboratories, R-5000) ($2\,mg\,kg^{-1}$ per day) or vehicle (0.25% polyethylene glycol (Sigma), 0.25% Tween-20 (Sigma) in PBS); injections started at 4 weeks of age and continued until 9 weeks of age, when heart size was analysed by echocardiography and mice were killed. Amino acid (aa) supplementation was achieved by daily intraperitoneal injections, starting at the day of birth, of aa solution at a dose of $0.1\,ml\,g^{-1}$ body weight, with a maximal dose of 2 ml per day[39]. All aa were purchased from Sigma-Aldrich. The solution contained the following aa concentrations: $6.0\,g\,l^{-1}$ isoleucine, $12.0\,g\,l^{-1}$ leucine, $7.2\,g\,l^{-1}$ valine, and $6.04\,g\,l^{-1}$ arginine (pH 7.4; Sigma). PBS (pH 7.4) was used as a control. Four-week-old mice were intravenously injected with 1×10^{12} viral particles encoding human p38γ and p38δ active mutants or wild-type human Flag-DEPTOR under the TnT promoter. Hearts were harvested from 9-week-old mice. Day-old mice were intravenously injected with 0.5×10^{12} viral particles encoding wild-type human Flag-DEPTOR under the TnT promoter and hearts were harvested for analysis of DEPTOR phosphorylarion/ubiquitination at 2 weeks of age. To avoid DEPTOR degradation, mice were injected the proteasome inhibitor MG132 (Shelleckchem; $0.1\,mg\,kg^{-1}$ per day intraperitoneally) on the 2 days before harvesting the hearts. In the cardiac-specific DEPTOR silencing experiment, 1-day-old mice were intravenously injected with 0.5×10^{12} viral particles encoding shDEPTOR and the cardiac phenotype was studied at 8 weeks of age. All animal procedures conformed to EU Directive 86/609/EEC and Recommendation 2007/526/EC regarding the protection of animals used for experimental and other scientific purposes, enacted under Spanish law 1201/2005.

Histology. Tissue samples were fixed in 10% formalin for 48 h, dehydrated and embedded in paraffin. Sections (8 μm) were cut and stained with haematoxylin and eosin (American Master Tech Scientific). Fibrosis was assessed with Picrosirius red staining (Sigma). For wheatgerm agglutinin (WGA) immunofluorescence, 8 μm heart sections were prepared, washed in PBS, incubated for 2 h in WGA-Alexa 488 lectin (Invitrogen, Carlsbad, CA, USA), and washed and mounted in anti-fade reagent. Four images (× 20) were taken from each heart, and the diameter and areas of 100–200 cross-sectionally oriented myocytes were measured and analysed with *Image J* software.

Echocardiography. Mice were anaesthetized by inhalation of isoflurane and oxygen (1.25% and 98.75%, respectively), and echocardiography was performed with a 30-MHz transthoracic echocardiography probe. Images were obtained with the Vevo 2100 micro-ultrasound imaging system (VisualSonics, Toronto, Canada). Short-axis, long-axis, B-mode and two-dimensional M-mode views were obtained. In summary, scans were conducted by two experienced researchers blinded to the mouse genotype. Measurements of left parasternal long and short axes and M-mode (left parasternal short axis) images were obtained at a heart rate of 500–550 b.p.m. LV end-diastolic diameter (LVEDD), LV end-systolic diameter (LVESD) and wall thickness were measured from M-mode tracings, and the average of three consecutive cardiac cycles is reported. The LV fractional shortening percentage was calculated as ([LVEDD − LVESD]/LVEDD) × 100 MRI of lung was performed with a 7-T Agilent scanner (Agilent, Santa Clara, CA, USA) equipped with a DD2 console and an actively shielded gradient set (205/120 insert of maximum $130\,mT\,m^{-1}$ gradient strength). For image acquisition, we used a combination of volume coil/surface coil coil to enhance signal-to-noise ratio formed by a 72-mm inner diameter quadrature birdcage TX coil (Rapid Biomedical GmBH, Germany) and an actively detuning 30-mm flexible customized surface RX coil (Neos Biotec, Pamplona, Spain). Following a tripilot gradient-echo image, a gradient-echo sequence without gating was used to acquire oblique coronal slices (one to two slices) and axial slices (7–10 slices covering the entire lung, 72-s acquisition time per slice) using the following parameters: TR/TE = 6.7/2.2 ms, flip angle = 10 degree, bandwidth = 100 kHz, field of view = 3 × 3 cm, matrix = 256 × 128, slice thickness = 1 mm (ref. 40). From these images, interventricular septum and left ventricle posterior wall thicknesses and left ventricle corrected mass were determined; the short-axis M-mode quantification was chosen as the most representative. Function was estimated from the ejection fraction and fractional shortening obtained from M-mode views by a blinded echocardiography expert. For ejection fraction measurements, a long- or short-axis view of the heart was selected to obtain an M-mode registration in a line perpendicular to the left ventricular septum and posterior wall at the level of the mitral chordae tendinea.

Immunoblot analysis. Tissue extracts were prepared in Triton lysis buffer (20 mM Tris (pH 7.4), 1% Triton X-100, 10% glycerol, 137 mM NaCl, 2 mM EDTA, 25 mM β-glycerophosphate, 1 mM sodium orthovanadate, 1 mM phenylmethylsulfonyl fluoride, and $10\,\mu g\,ml^{-1}$ of aprotinin and leupeptin), and for co-immunoprecipitation experiments, lysis buffer was supplemented with 0.3% Chaps. Extracts (20–50 μg protein) and immunoprecipitates (prepared from 2–10 mg protein) were examined by immunoblot. For the immunoprecipitation assay, heart extracts were incubated with 4 μg of a specific antibody coupled to protein-G-Sepharose. After incubation overnight at 4 °C with agitation, the captured proteins were centrifuged at 10,000*g*, the supernatants collected, and the beads washed four times in lysis buffer. Beads were boiled for 5 min 95 °C in 10 μl sample buffer. Extracts and immunoprecipitates were examined by SDS–PAGE and blotted with antibodies to the following targets: p38γ and p38δ (refs 41,42) at $1\,\mu g\,ml^{-1}$; vinculin and Flag (Sigma); puromycin (Millipore clone 12D10); HA and Myc (Bethyl Laboratories, Inc.); ubiquitin (ThermoFisher); and phospho-p38, phospho-mTOR (Ser2481), mTOR, Myc-Tag, phospho-p70S6 kinase, p70S6 kinase, phospho-S6 (Ser 235/236), phospho-S6 (Ser 240/244), S6 ribosomal protein, phospho-FOXO1/3a, phospho-eEF2, eEF2, phospho-EIF4E, EIF4E, phospho-EIF4G, EIF4G, phospho-EIF4B, EIF4B, DEPTOR, phospho-MAPK/CDK substrate (PXSP or SPXR/K) (34B2), phospho-Threonine-Proline, Raptor, Rictor, Sin1, GβL, phospho-4EBP1, 4EBP1, phospho-AKT (Ser473) and AKT (Cell Signaling) all were used at 1:1,000. Immunocomplexes were detected by enhanced chemiluminescence (GE Healthcare Lifesciences). Full scans of all blots and gels are available as Supplementary Fig. 13.

Cell lines and cell culture. HeLa and HEK-293T (American Type Culture Collection (ATCC), USA) cells and mouse embryonic fibroblasts (MEF) were cultured in DMEM supplemented with 10% heat-inactivated fetal bovine serum (FBS; Sigma), glutamine (2 mM) and penicillin/streptomycin ($100\,\mu g\,ml^{-1}$).

Lentivirus vector production and cell infection. Lentiviruses were produced by transient calcium phosphate co-transfection of HEK-293T cells was done with the pLKO mouse shRNA 1 DEPTOR (plasmid #21337 Addgene), pLKO mouse shRNA 2 DEPTOR (plasmid #21338 Addgene), together with pΔ8.9 and pVSV-G. Supernatants containing the LV particles were collected 48 and 72 h after removal of the calcium phosphate precipitate and were centrifuged at 700*g* at 4 °C for 10 min and filtered through 0.45-μm filter units (Corning). Once filtered, the virus-containing medium was added (1:1 volume) to MEF culture medium. After incubation for 24 h at 37 °C and 5% CO_2, the medium was changed, and puromycin selection ($3\,\mu g\,ml^{-1}$ puromycin) was initiated 48 h after infection. The selection medium was changed every 2 days during 1 week, and the cells were subsequently used for experiments.

Adeno-associated virus vector production and cell infection. The AAV shuttle and helper plasmids were transfected into HEK 293A cells by calcium-phosphate co-precipitation. A total of 840 μg plasmid DNA (mixed in an equimolar ratio) was used per Hyperflask (Corning) seeded with 1.2 × 108 cells the day before. Seventy-two hours after transfection, the cells were collected by centrifugation and the cell pellet was resuspended in TMS (50 mM Tris HCl, 150 mM NaCl, 2 mM $MgCl_2$) on ice before digestion with DNase I and RNaseA ($0.1\,mg\,ml^{-1}$ each; Roche) at 37 °C for 60 min. Clarified supernatant containing the viral particles was obtained by iodixanol gradient centrifugation[44]. Gradient fractions containing virus were concentrated using Amicon UltraCel columns (Millipore) and stored at − 70 °C (ref. 43).

AAV plasmids were cloned and propagated in the Stbl3 *E. coli* strain (Life Technologies). pRK5 FLAG human DEPTOR (plasmid #21334, Addgene), pCEFL Flag p38γ D129A, pCMV Flag p38δ F324S and pGIPZ mouse shRNA DEPTOR clone 1 (V3LMM_485571) were cloned into the pAcTnT AAV plasmid to generate pAAV-TnT-GFP-Luc, pAAV-TnT-p38γ_{act}, pAAV-TnT-p38δ_{act}, pAAV-TnT-Flag-DEPTOR and pAAV-TnT-shDeptor. These AAV plasmids were packaged into AAV-9 capsids with the use of pAdDF6 helper plasmids (providing the three adenoviral helper genes) and pAAV2/9 (providing rep and cap viral genes), obtained from PennVector. Shuttle vectors were generated by direct cloning (GeneScript) of synthesized NheI-SalI fragments into pAcTnT cut with the same restriction enzymes.

The AAV shuttle and helper plasmids were transfected into HEK 293A cells by calcium-phosphate co-precipitation. A total of 840 μg plasmid DNA (mixed in an equimolar ratio) was used per Hyperflask (Corning) seeded with 1.2×10^{8} cells the day before. Seventy-two hours after transfection, the cells were collected by centrifugation and the cell pellet was resuspended in TMS (50 mM Tris HCl, 150 mM NaCl, 2 mM $MgCl_2$) on ice before digestion with DNase I and RNaseA ($0.1\,mg\,ml^{-1}$ each; Roche) at 37 °C for 60 min. Clarified supernatant containing the viral particles was obtained by iodixanol gradient centrifugation[44]. Gradient fractions containing virus were concentrated using Amicon UltraCel columns (Millipore) and stored at − 70 °C.

Standard curves were constructed using known copy numbers (10^5–10^8) of the respective plasmid (pAAV-TnT-GFP-Luc, pAAV-TnT-p38γ_{act}, pAAV-TnT-p38δ_{act}, pAAV-TNT-Flag-DEPTOR and pAAV-TNT-shDeptor) carrying the appropriate complementary DNA.

***In vivo* protein synthesis assay.** For all *in vivo* measurements of protein synthesis, mice were injected intraperitoneally with $0.040\,\mu mol\,g^{-1}$ puromycin dissolved in 100 μl PBS. Exactly 30 min after injection, tissues were extracted and

frozen in liquid N_2 for subsequent immunoblot analysis of protein-incorporated puromycin.

Measurement of *in vitro* protein synthesis by SUnSET assay. All the experiments were performed following the protocol described in ref. 45 with some modifications. MEFs were seeded in six-well plates with 10^6 cells per well in 1 ml complete DEMEM, and treated with 1 μg ml^{-1} puromycin solution (Sigma) for 10 min at 37 °C and 5% CO_2 (=pulse). The cells were washed twice with pre-warmed complete medium, resuspended in 1 ml of the same medium and incubated for 50 min at 37 °C and 5% CO_2 (=chase). The cells were washed twice with cold PBS, and harvested. They were then washed once more by centrifugation at 4 °C in cold PBS/0.1% BSA, and pellets were incubated in 30 μl of staining mix (mouse IgG2 anti-puromycin antibody (12D10) diluted 1/50 in PBS/BSA) for 30 min. The cells were washed twice with PBS/BSA and incubated in 30 μl of PE-labelled anti-mouse IgG (Invitrogen) diluted 1/100 in PBS/BSA. The cells were washed and resuspended in 200 μl PBS/BSA and analysed by FACS (fluorescence-activated cell sorting).

cDNA transfection-based experiments. Cells were plated at 60% confluence in DMEM/10%FBS 12–15 h before transfection. The cells were transfected using the calcium phosphate method[30] with the pRK5-based cDNA expression plasmids indicated in the figures. The culture medium was replaced 12 h after transfection with fresh complete medium, and cells were collected 48 h later. For DEPTOR degradation experiments in HEK 293T or HELA cells, the medium was changed after 24 h for medium lacking serum, and after a further 24 h, the cells were incubated in medium with 10% FBS or no FBS together with 10 μM cycloheximide. At the times indicated, the cells were collected and analysed by western blot. To block DEPTOR degradation induced by the constitutionally active p38γ/δ mutants, cells were preincubated with the proteasome inhibitor MG132 (Shelleckchem) at a final concentration of 10 μM.

The plasmids used in the different experiments were pRK5 myc Rat mTOR (plasmid #1861, Addgene); pRK5 FLAG human DEPTOR (plasmid #21334, Addgene); pRK5 FLAG human DEPTOR (13xS/T→A; plasmid #21702, Addgene); pRK5 FLAG DEPTOR (PDZ domain; plasmid #21701, Addgene); pRK5 FLAG DEPTOR (DEP domains; plasmid #21700, Addgene); pcDNA3-myc3-CUL1 (plasmid #19896, Addgene); pcDNA3-myc3-bTrCP (plasmid #20718, Addgene); HA-Ubiquitin (plasmid #18712); pcDNA3 HA human p38γ and pcDNA3 HA human p38δ, kindly provided by Roger Davis (University of Massachusetts Medical School, Worcester, USA); and pCEFL Flag p38γ^{D129A} and pCMV Flag p38δ^{F324S}, kindly provided by David Engelberg (The Hebrew University of Jerusalem, Israel).

***In vitro* kinase assay.** One microgram of human GST-DEPTOR protein (H00064798, Novus Biologicals) was incubated for 30 min with 1 μg of active recombinant p38γ, p38γ or p38α kinases (provided by MRC Protein Phosphorylation and Ubiquitylation Unit, Dundee, UK) in the presence of 200 μM cold ATP. The reaction was stopped by adding SDS-containing sample buffer, and proteins were resolved by SDS–PAGE and visualized by staining with colloidal Coomassie Blue. The band containing GST-DEPTOR was excised and treated with DTT to reduce disulfide bonds and with iodoacetamide to derivatize cysteine residues. The protein was in-gel digested with trypsin, and the resulting peptides were extracted from the gel and analysed by nanoscale-microcapillary reversed phase liquid chromatography tandem mass spectrometry[46,47].

Flow cytometry cell size analysis. MEFs were trypsinized, washed and analysed by FACS to determine cell size based on the mean forward scattered light intensity.

Blood pressure measurement. Blood pressure in mice was measured using the noninvasive tail-cuff method[48].

Statistical analysis. Differences between groups were examined for statistical significance by two-tailed Student's *t*-test, one-way or two-way analysis of variance coupled to the Bonferroni post test.

The rest of the materials and methods are found in the Supplementary Methods.

References

1. Akazawa, H. & Komuro, I. Roles of cardiac transcription factors in cardiac hypertrophy. *Circ. Res.* **92,** 1079–1088 (2003).
2. Maillet, M., van Berlo, J. H. & Molkentin, J. D. Molecular basis of physiological heart growth: fundamental concepts and new players. *Nat. Rev. Mol. Cell Biol.* **14,** 38–48 (2013).
3. Heineke, J. & Molkentin, J. D. Regulation of cardiac hypertrophy by intracellular signalling pathways. *Nat. Rev. Mol. Cell Biol.* **7,** 589–600 (2006).
4. Frey, N. & Olson, E. N. Cardiac hypertrophy: the good, the bad, and the ugly. *Annu. Rev. Physiol.* **65,** 45–79 (2003).
5. Shioi, T. *et al.* Rapamycin attenuates load-induced cardiac hypertrophy in mice. *Circulation* **107,** 1664–1670 (2003).
6. Sadoshima, J. & Izumo, S. Rapamycin selectively inhibits angiotensin II-induced increase in protein synthesis in cardiac myocytes *in vitro*. Potential role of 70-kD S6 kinase in angiotensin II-induced cardiac hypertrophy. *Circ. Res.* **77,** 1040–1052 (1995).
7. Boluyt, M. O. *et al.* Rapamycin inhibits alpha 1-adrenergic receptor-stimulated cardiac myocyte hypertrophy but not activation of hypertrophy-associated genes. Evidence for involvement of p70 S6 kinase. *Circ. Res.* **81,** 176–186 (1997).
8. Sciarretta, S., Volpe, M. & Sadoshima, J. Mammalian target of rapamycin signaling in cardiac physiology and disease. *Circ. Res.* **114,** 549–564 (2014).
9. Sarbassov, D. D., Ali, S. M. & Sabatini, D. M. Growing roles for the mTOR pathway. *Curr. Opin. Cell. Biol.* **17,** 596–603 (2005).
10. Guertin, D. A. & Sabatini, D. M. Defining the role of mTOR in cancer. *Cancer Cell* **12,** 9–22 (2007).
11. Peterson, T. R. *et al.* DEPTOR is an mTOR inhibitor frequently overexpressed in multiple myeloma cells and required for their survival. *Cell* **137,** 873–886 (2009).
12. Auger-Messier, M. *et al.* Unrestrained p38 MAPK activation in Dusp1/4 double-null mice induces cardiomyopathy. *Circ. Res.* **112,** 48–56 (2013).
13. Rose, B. A., Force, T. & Wang, Y. Mitogen-activated protein kinase signaling in the heart: angels versus demons in a heart-breaking tale. *Physiol. Rev.* **90,** 1507–1546 (2010).
14. Manieri, E. & Sabio, G. Stress kinases in the modulation of metabolism and energy balance. *J. Mol. Endocrinol.* **55,** R11–R22 (2015).
15. Sabio, G. & Davis, R. J. TNF and MAP kinase signalling pathways. *Semin. Immunol.* **26,** 237–245 (2014).
16. Kyriakis, J. M. & Avruch, J. Mammalian MAPK signal transduction pathways activated by stress and inflammation: a 10-year update. *Physiol. Rev.* **92,** 689–737 (2012).
17. Yue, T. L. *et al.* Extracellular signal-regulated kinase plays an essential role in hypertrophic agonists, endothelin-1 and phenylephrine-induced cardiomyocyte hypertrophy. *J. Biol. Chem.* **275,** 37895–37901 (2000).
18. Liao, P. *et al.* The *in vivo* role of p38 MAP kinases in cardiac remodeling and restrictive cardiomyopathy. *Proc. Natl Acad. Sci. USA* **98,** 12283–12288 (2001).
19. Braz, J. C. *et al.* Targeted inhibition of p38 MAPK promotes hypertrophic cardiomyopathy through upregulation of calcineurin-NFAT signaling. *J. Clin. Invest.* **111,** 1475–1486 (2003).
20. Nishida, K. *et al.* p38alpha mitogen-activated protein kinase plays a critical role in cardiomyocyte survival but not in cardiac hypertrophic growth in response to pressure overload. *Mol. Cell. Biol.* **24,** 10611–10620 (2004).
21. del Barco Barrantes, I., Coya, J. M., Maina, F., Arthur, J. S. & Nebreda, A. R. Genetic analysis of specific and redundant roles for p38alpha and p38beta MAPKs during mouse development. *Proc. Natl Acad. Sci. USA* **108,** 12764–12769 (2011).
22. Beardmore, V. A. *et al.* Generation and characterization of p38beta (MAPK11) gene-targeted mice. *Mol. Cell. Biol.* **25,** 10454–10464 (2005).
23. Dingar, D. *et al.* Effect of pressure overload-induced hypertrophy on the expression and localization of p38 MAP kinase isoforms in the mouse heart. *Cell. Signal.* **22,** 1634–1644 (2010).
24. Marber, M. S., Rose, B. & Wang, Y. The p38 mitogen-activated protein kinase pathway—a potential target for intervention in infarction, hypertrophy, and heart failure. *J. Mol. Cell. Cardiol.* **51,** 485–490 (2011).
25. Li, F., Wang, X., Capasso, J. M. & Gerdes, A. M. Rapid transition of cardiac myocytes from hyperplasia to hypertrophy during postnatal development. *J. Mol. Cell. Cardiol.* **28,** 1737–1746 (1996).
26. Schluter, K. D. & Wenzel, S. Angiotensin II: a hormone involved in and contributing to pro-hypertrophic cardiac networks and target of anti-hypertrophic cross-talks. *Pharmacol. Ther.* **119,** 311–325 (2008).
27. Patrick, D. M. *et al.* Stress-dependent cardiac remodeling occurs in the absence of microRNA-21 in mice. *J. Clin. Invest.* **120,** 3912–3916 (2010).
28. Fingar, D. C., Salama, S., Tsou, C., Harlow, E. & Blenis, J. Mammalian cell size is controlled by mTOR and its downstream targets S6K1 and 4EBP1/eIF4E. *Genes Dev.* **16,** 1472–1487 (2002).
29. Goodman, C. A. *et al.* Novel insights into the regulation of skeletal muscle protein synthesis as revealed by a new nonradioactive in vivo technique. *FASEB J.* **25,** 1028–1039 (2011).
30. Sabio, G. *et al.* Stress- and mitogen-induced phosphorylation of the synapse-associated protein SAP90/PSD-95 by activation of SAPK3/p38gamma and ERK1/ERK2. *Biochem. J.* **380,** 19–30 (2004).
31. Sabio, G. *et al.* p38gamma regulates the localisation of SAP97 in the cytoskeleton by modulating its interaction with GKAP. *EMBO J.* **24,** 1134–1145 (2005).
32. Zhao, Y., Xiong, X. & Sun, Y. DEPTOR, an mTOR inhibitor, is a physiological substrate of SCF(betaTrCP) E3 ubiquitin ligase and regulates survival and autophagy. *Mol. Cell.* **44,** 304–316 (2011).

33. Gao, D. *et al.* mTOR drives its own activation via SCF(betaTrCP)-dependent degradation of the mTOR inhibitor DEPTOR. *Mol. Cell* **44,** 290–303 (2011).
34. Tsubuki, S. *et al.* Purification and characterization of a Z-Leu-Leu-Leu-MCA degrading protease expected to regulate neurite formation: a novel catalytic activity in proteasome. *Biochem. Biophys. Res. Commun.* **196,** 1195–1201 (1993).
35. Bruning, J. C. *et al.* A muscle-specific insulin receptor knockout exhibits features of the metabolic syndrome of NIDDM without altering glucose tolerance. *Mol. Cell* **2,** 559–569 (1998).
36. Mora, A. *et al.* Deficiency of PDK1 in cardiac muscle results in heart failure and increased sensitivity to hypoxia. *EMBO J.* **22,** 4666–4676 (2003).
37. Frey, N., Katus, H. A., Olson, E. N. & Hill, J. A. Hypertrophy of the heart: a new therapeutic target? *Circulation* **109,** 1580–1589 (2004).
38. Liang, Q. & Molkentin, J. D. Redefining the roles of p38 and JNK signaling in cardiac hypertrophy: dichotomy between cultured myocytes and animal models. *J. Mol. Cell. Cardiol.* **35,** 1385–1394 (2003).
39. Riehle, C. *et al.* Insulin receptor substrate signaling suppresses neonatal autophagy in the heart. *J. Clin. Invest.* **123,** 5319–5333 (2013).
40. Cruz-Adalia, A. *et al.* CD69 limits the severity of cardiomyopathy after autoimmune myocarditis. *Circulation* **122,** 1396–1404 (2010).
41. Han, M. S. *et al.* JNK expression by macrophages promotes obesity-induced insulin resistance and inflammation. *Science* **339,** 218–222 (2013).
42. Gonzalez-Teran, B. *et al.* Eukaryotic elongation factor 2 controls TNF-alpha translation in LPS-induced hepatitis. *J. Clin. Invest.* **123,** 164–178 (2013).
43. Cruz, F. M. *et al.* Exercise triggers ARVC phenotype in mice expressing a disease-causing mutated version of human plakophilin-2. *J. Am. Coll. Cardiol.* **65,** 1438–1450 (2015).
44. Hauswirth, W. W., Lewin, A. S., Zolotukhin, S. & Muzyczka, N. Production and purification of recombinant adeno-associated virus. *Methods Enzymol.* **316,** 743–761 (2000).
45. Schmidt, E. K., Clavarino, G., Ceppi, M. & Pierre, P. SUnSET, a nonradioactive method to monitor protein synthesis. *Nat. Methods* **6,** 275–277 (2009).
46. Inuzuka, H. *et al.* Phosphorylation by casein kinase I promotes the turnover of the Mdm2 oncoprotein via the SCF(beta-TRCP) ubiquitin ligase. *Cancer Cell* **18,** 147–159 (2010).
47. Dibble, C. C., Asara, J. M. & Manning, B. D. Characterization of Rictor phosphorylation sites reveals direct regulation of mTOR complex 2 by S6K1. *Mol. Cell. Biol.* **29,** 5657–5670 (2009).
48. Kubota, Y. *et al.* Evaluation of blood pressure measured by tail-cuff methods (without heating) in spontaneously hypertensive rats. *Biol. Pharm. Bull.* **29,** 1756–1758 (2006).

Acknowledgements

We thank S. Bartlett for English editing. We are grateful to Dr R.J. Davis for providing the mammalian expression plasmids for p38γ and p38δ, and to Dr D. Engelberg for providing the constitutively active mutants. We thank Dr D. Sabatini for the mTOR and DEPTOR plasmids, Dr Yeh for the HA-Ubiquitin plasmid and Dr Xiong for the bTrCP and Cul1. Recombinant active p38 proteins were provided by the Division of Signal Transduction Therapy (DSTT), University of Dundee, UK. We are grateful to A.R. Nebreda for his critical reading of the manuscript. We thank the staff at the CNIC Imaging and viral vectors Unit for technical support. G.S. and J.A.B. are investigators of the Ramón y Cajal Program. B.G.-T. is a fellow of the FPI Severo Ochoa CNIC program (SVP-2013-067639). This work was funded by the following grants to G.S.: ERC 260464, EFSD 2030, MICINN SAF2013-43506-R and Comunidad de Madrid S2010/BMD-2326; J.M.R., J.V. and JMR are supported by the Spanish Ministry of Health (Ministerio de Sanidad y Consumo) Red de Investigación Cardiovascular (RIC) cofounded by FEDER (grants RD06/0042/0022 to J.M.R. and RD12/0042/0056 to J.V.). S.M.-M. is supported by the Fundación La Marató TV3 (122532). The Centro Nacional de Investigaciones Cardiovasculares (CNIC) is supported by the Spanish Ministry of Economy and Competitiveness and the Pro-CNIC Foundation.

Author contributions

B.G.-T. and G.S. designed the study; B.G.-T., J.A.L., E.R., L.L., S.M.-M., J.A.B., L.J.J.-B., J.M.R., J.V. and G.S. performed the experimental analysis; B.G.-T. and G.S. wrote the manuscript. All the authors contributed to the revision of the manuscript and approved the final version.

Additional information

Supplementary Information accompanies this paper at http://www.nature.com/naturecommunications

Competing financial interests: The authors declare no competing financial interests.

Reprints and permission information is available online at http://npg.nature.com/reprintsandpermissions/

How to cite this article: González-Terán, B. *et al.* p38γ and δ promote heart hypertrophy by targeting the mTOR-inhibitory protein DEPTOR for degradation. *Nat. Commun.* 7:10477 doi: 10.1038/ncomms10477 (2016).

This work is licensed under a Creative Commons Attribution 4.0 International License. The images or other third party material in this article are included in the article's Creative Commons license, unless indicated otherwise in the credit line; if the material is not included under the Creative Commons license, users will need to obtain permission from the license holder to reproduce the material. To view a copy of this license, visit http://creativecommons.org/licenses/by/4.0/

SUPPLEMENTARY INFORMATION

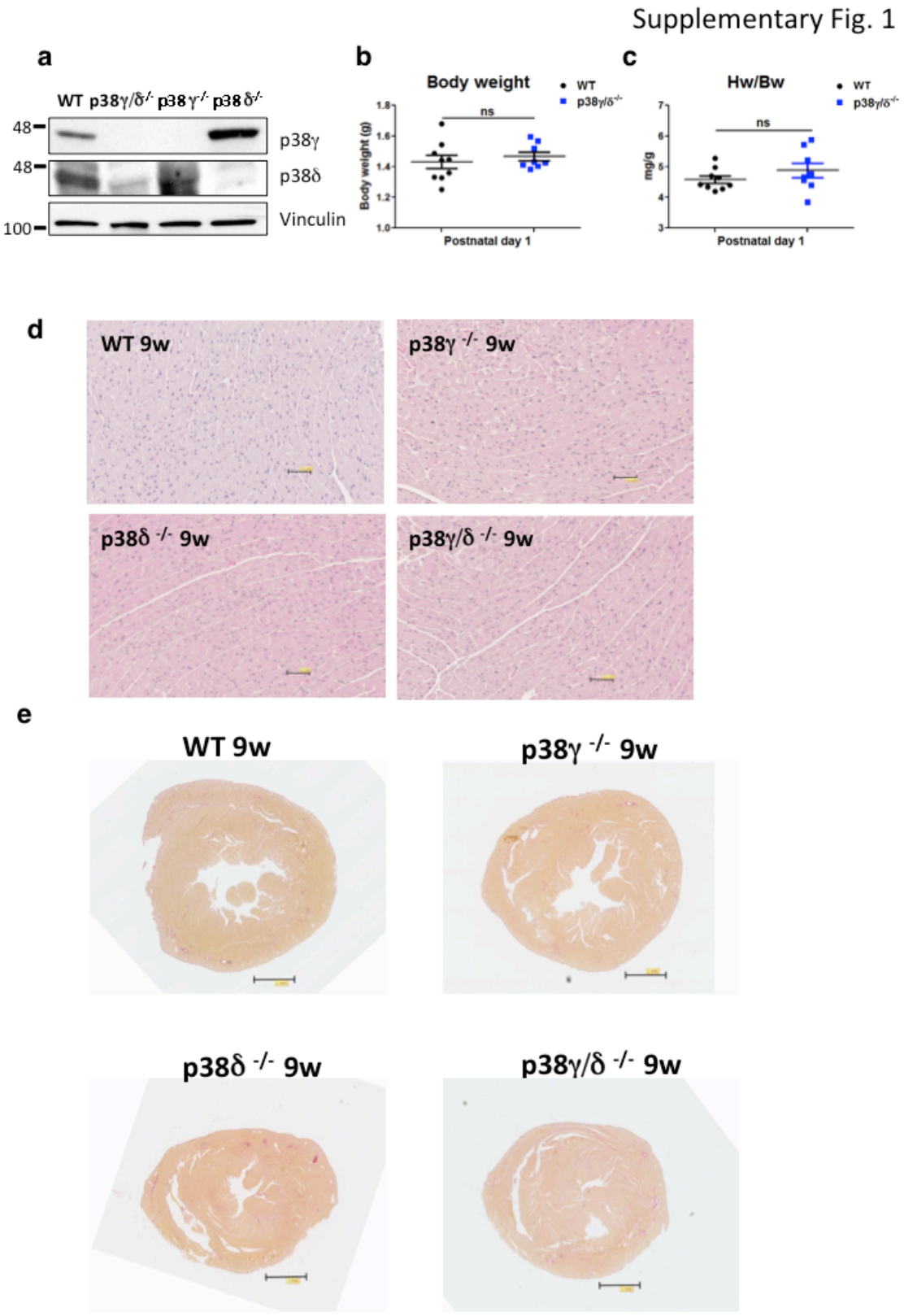

Supplementary Figure 1. p38γ and δ deficiency results in small hearts without fibrosis development.

(a) WT, p38γ/δ$^{-/-}$, p38γ$^{-/-}$, p38δ$^{-/-}$ mice were sacrificed at 9 weeks of age and cardiac p38γ and p38δ expression was analysed in heat lysates.

(b & c) Wild type (WT) and p38γ/δ$^{-/-}$ male mice were sacrificed at postnatal day one and body weight (**b**) and heart weight:tibia length ratio (**c**) were measured (n=8-9). Data are means ± SEM (n=5-13). Ns, P>0.05 (*t*-test).

(d) Representative H&E heart micrographs from 9-week-old WT, p38γ$^{-/-}$, p38δ$^{-/-}$ and p38γ/δ$^{-/-}$ mice. Scale bar, 50.2μm (n=8-10).

(e) Representative picrosirius red stained transverse heart sections from 9-week-old WT, p38γ$^{-/-}$, p38δ-/- and p38γ/δ-/- mice. Scale bar, 1mm, (n=8-10).

Data are means ± SEM. (*t*-test).

Supplementary Fig. 2

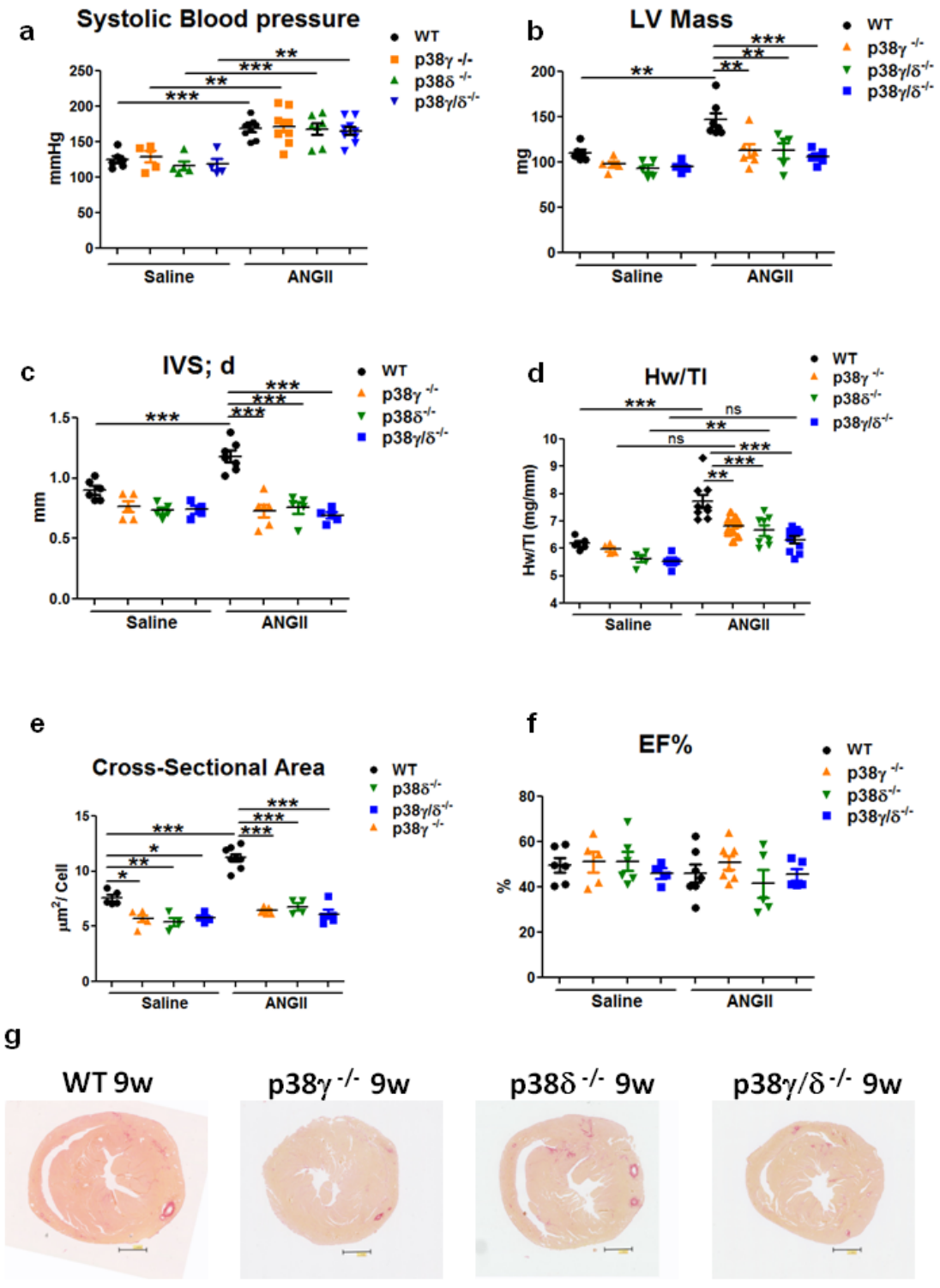

Supplementary Figure 2. p38γ and δ are involved in angiotensin-II -induced hypertrophy in vivo.

WT, p38γ$^{-/-}$, p38δ$^{-/-}$ and p38γ/δ$^{-/-}$ mice were treated for 28 days with angiotensin II (AngII) (1µg/kg/min) or saline, delivered by subcutaneously implanted osmotic minipumps.

(a, b, c & d) p38γ$^{-/-}$, p38δ$^{-/-}$ and p38γ/δ$^{-/-}$ are protected against angiotensin II-induced cardiac hypertrophy. **(a)** WT, p38γ$^{-/-}$, p38δ$^{-/-}$ and p38γ/δ$^{-/-}$ mice treated for 28 days with AngII or Saline show no differences in systolic blood pressure development. **(b & c)** Echocardiography evaluation of LV Mass and IVS;d after AngII or Saline treatment. **(d)** Heart weight to tibia length ratios for WT, p38γ$^{-/-}$, p38δ$^{-/-}$ and p38γ/δ$^{-/-}$ after 28 days of Ang II or saline treatment. (n=4-7). (**e**) Cardiomyocyte cross-sectional area quantified in WGA-stained hearts. **(f)** Echocardiography evaluation of systolic cardiac function after AngII or Saline treatment. IVS;d (inter-ventricular septum in diastole); LV (left ventricle).

(g) WT, p38γ$^{-/-}$, p38δ$^{-/-}$ and p38γ/δ$^{-/-}$ mice treated for 28 days with AngII show no differences in fibrosis development. Representative picrosirius red stained transverse heart sections from 9-week-old WT, p38γ$^{-/-}$, p38δ$^{-/-}$ and p38γ/δ$^{-/-}$ mice treated for 28 days with AngII. Scale bar, 1mm (n=6-12).

Data are means ± SEM. *P<0.05; **P<0.01; ***P<0.001 (1-way ANOVA coupled to Bonferroni's post test).

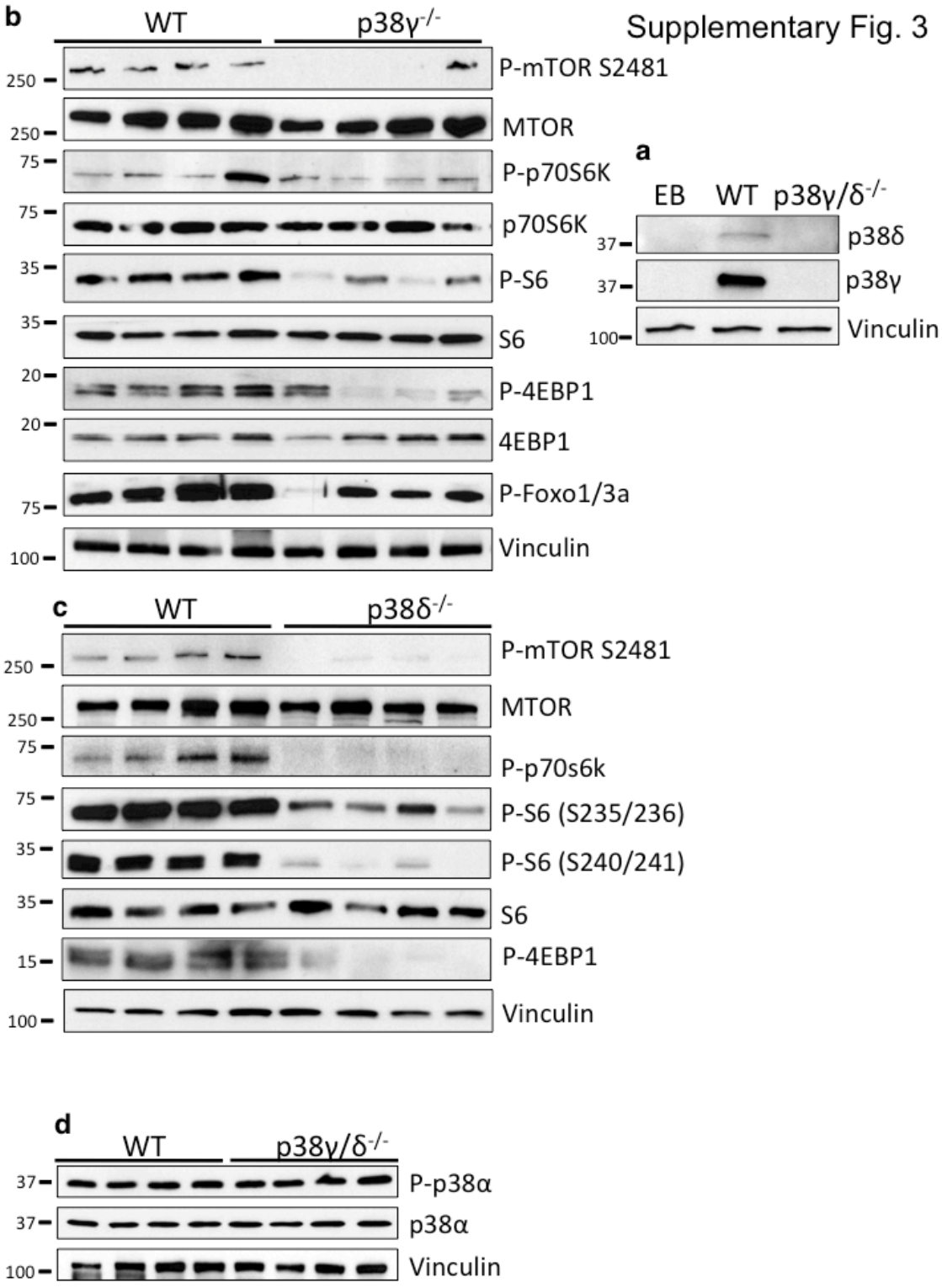

Supplementary Figure 3. Hearts of p38γ$^{-/-}$ or p38δ$^{-/-}$ mice show below-normal mTOR activation.

(**a**) p38γ or p38δ were immunoprecipited from WT and p38γ/δ$^{-/-}$ heart lysates and analyzed by immunoblot. (n=4)

(b & c) WT and p38$\gamma^{-/-}$ or p38$\delta^{-/-}$ heart lysates from 9-week-old male mice were analyzed by immunoblot for mTOR signalling pathway components. (n=4).

(d) WT and p38$\gamma/\delta^{-/-}$ heart lysates from 9-week-old male mice were analyzed by immunoblot for p38 alpha activation and protein levels. (n=4).

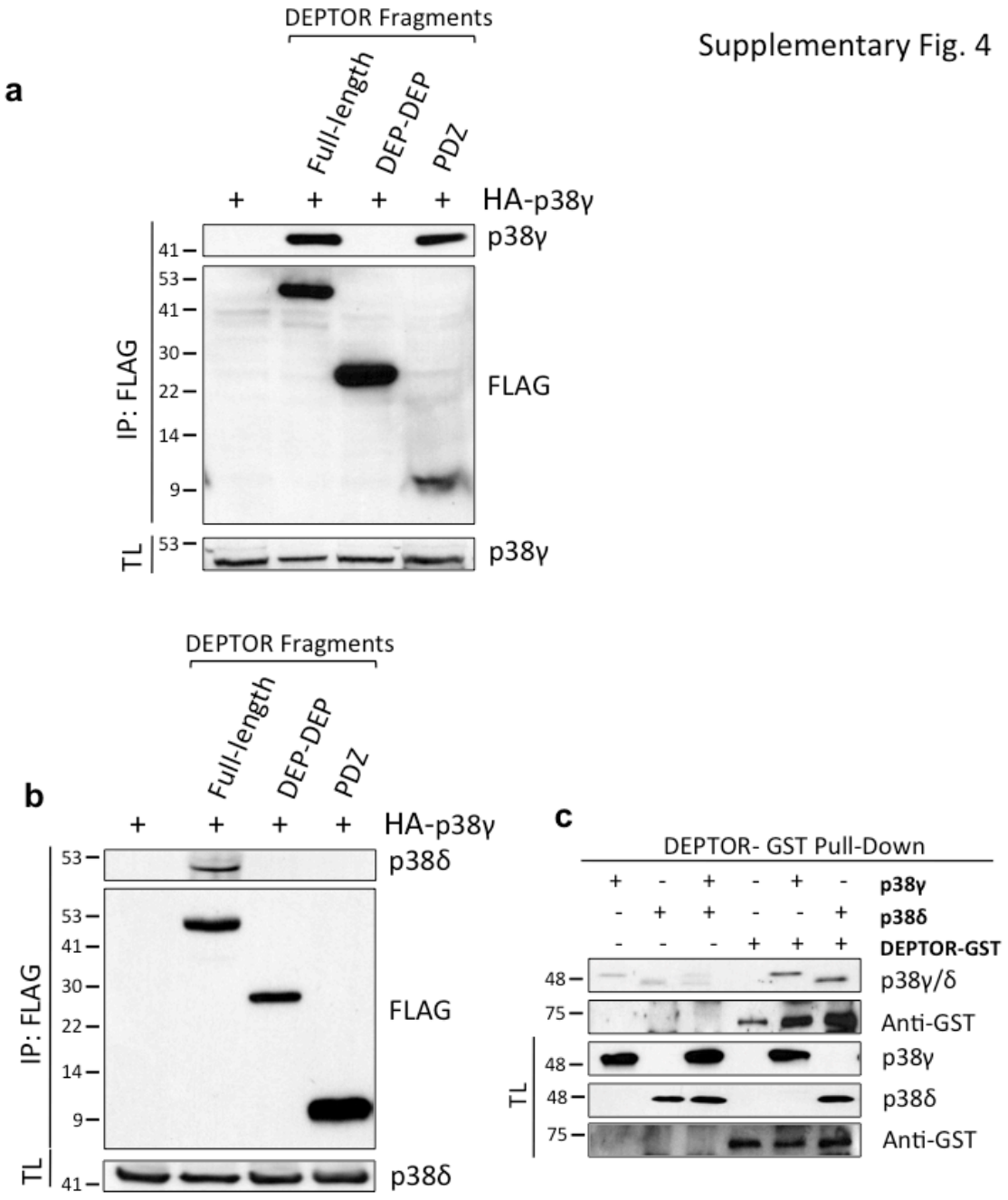

Supplementary Figure 4. p38γ directly interacts with DEPTOR through its PDZ domain.

(a) p38γ interacts with DEPTOR through its PDZ domain**.** Full length Flag-DEPTOR, Flag-DEP DOM and Flag-PDZ DOM were expressed in HEK-293T cells together with HA-p38γ or HA-p38γ alone. Anti-Flag co- immunoprecipitates or total lysates were analyzed by SDS-PAGE.

(b) p38δ interacts with DEPTOR through un unkown domain**.** Full length Flag-DEPTOR, Flag-DEP DOM and Flag-PDZ DOM were expressed in HEK-293T cells together with HA-p38δ or HA-p38δ alone. Anti-Flag co- immunoprecipitates or total lysates were analyzed by SDS-PAGE.

(**c**) p38γ and p38δ directly interact with DEPTOR. GST Pull down experiment. GST-DEPTOR was used to precipitate untagged p38γ and p38δ recombinant proteins.

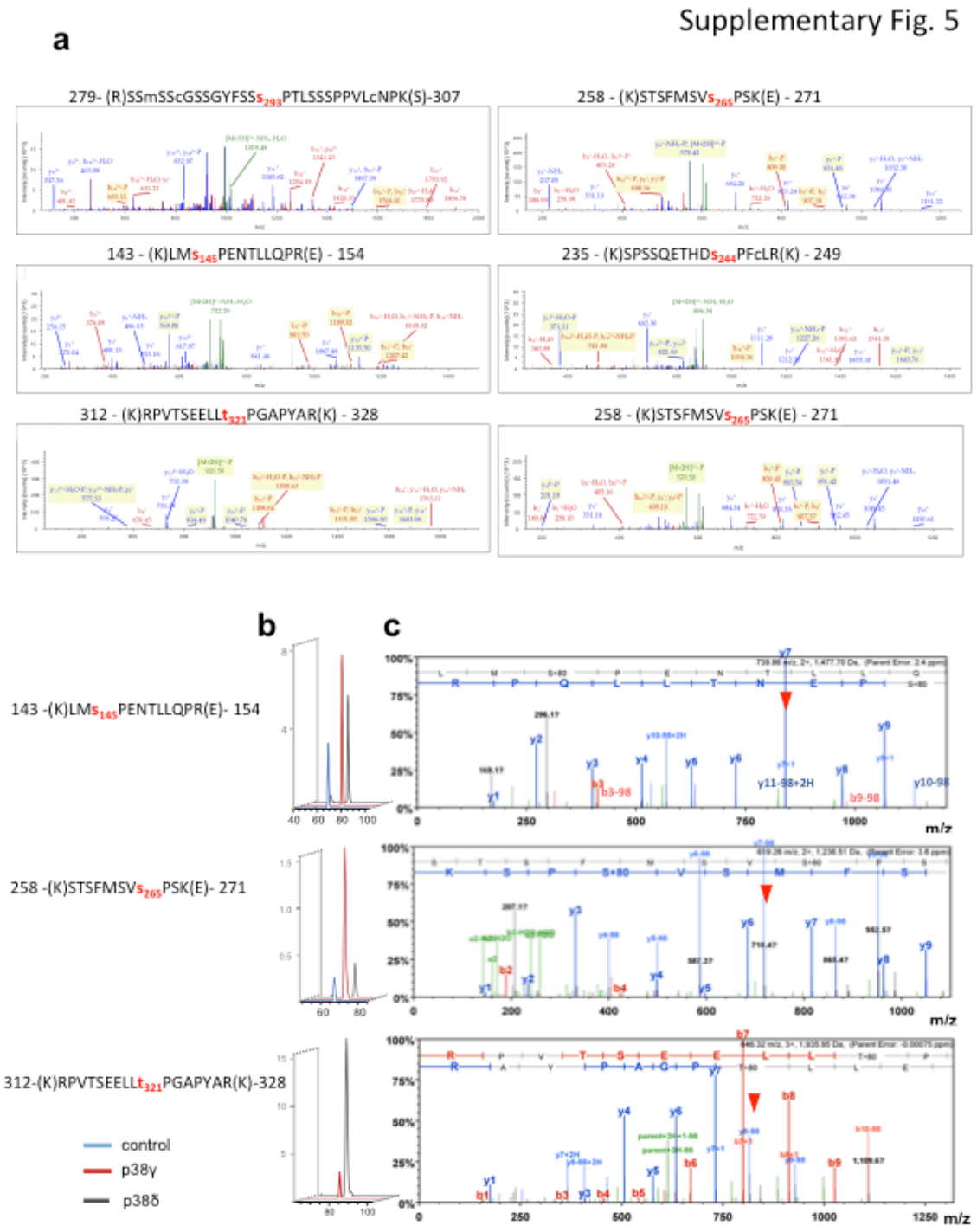

Supplementary Figure 5. DEPTOR is specifically phosphorylated by p38γ and p38δ in vitro and in vivo.

(a) ESI-MS analysis of DEPTOR phosphorylation by constitutively active p38γ or p38δ mutants. In an in vitro kinase assay, recombinant human DEPTOR protein (1μg) was incubated

alone or in the presence of p38γ or p38δ kinases (1µg) and 0.2mM of cold ATP.

(b-c) ESI-MS analysis of DEPTOR phosphorylation by constitutively active p38γ or p38δ mutants. In an in vivo kinase assay, human Flag-DEPTOR was expressed in HEK-293T cells alone or together with constitutively active p38γ or p38δ mutants. HEK-293T cells starved for 30h. DEPTOR phosphorylation was analyzed from Flag immunoprecipitates by mass spectrometry. After trypsin digestion, phosphopeptides previously detected in the *in vitro* experiments and their non-phosphorylated counterparts were monitored using the parallel reaction monitoring (PRM) mode in a Q Exactive hybrid quadrupole-orbitrap mass spectrometer (Thermo Scientific). **(b)** Extracted ion chromatogram traces (XIC) of the fragments indicated with a red triangle in **(c)**. The relative intensity of DEPTOR-derived phosphopeptides in each experiment is expressed as percentage, taking the intensity of the corresponding unmodified peptide as a reference. **(c)** MS/MS spectra interpreted using Scaffold at the peak apex of each phosphorylated peptide. Note that the MS/MS spectra confirm peptide phosphorylation at Ser and Thr residues in the consensus sequences SP and TP, respectively. For peptide (K)STSFMSVsPSK(E), treatment with MG132 was necessary to prevent their proteolysis.

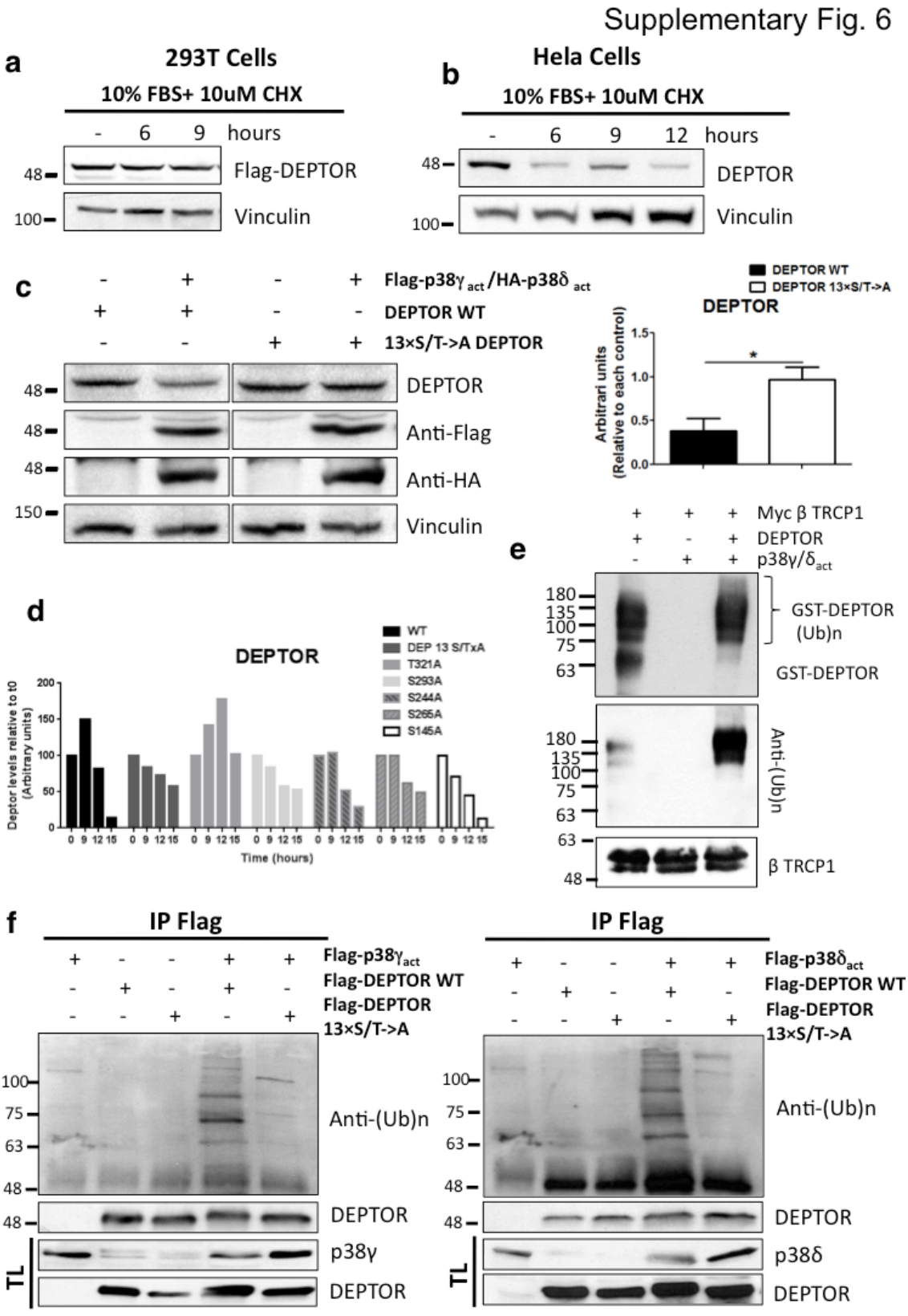

Supplementary Figure 6. DEPTOR degradation is dependent of p38γ and p38δ phosphorylation.

(a) Flag-DEPTOR was expressed in HEK-293T cells, which were serum starved for 30 hr. Fresh serum-free or 10% FBS medium was then added together with 10μM cycloheximide (CHX) for the times indicated. Flag-DEPTOR levels were analyzed by immunoblotting with the indicated antibodies.

(b) HeLa cells were serum starved for 30 hr and fresh serum-free or 10% FBS medium was then added together with 10μM cycloheximide (CHX) for the times indicated. Endogenous DEPTOR levels were then analyzed by immunoblotting with the indicated antibodies.

(c) Constitutively active p38γ and p38δ mutants induce DEPTOR degradation but not 13xS/T→A DEPTOR mutant degradation. Blots were quantified with ImageJ relative to vinculin levels. Data are means ± SEM. *P<0.05 (*t*-test).

(d) Quantification of DEPTOR protein levels from immunoblot assay. DEPTOR phosphorylation mutants were expressed in HEK-293T alone or together with constitutively active p38γ and p38δ mutants. Fresh media without serum was added together with 10μM cycloheximide (CHX) and cells harvested at the times indicated. DEPTOR degradation was analyzed by immunoblot.

(e) SCF E3 was prepared by FLAG beads IP using 293 cells transfected with βTrCP. Recombinant GST-DEPTOR was in vitro phosphorylated or not with active p38γ and p38δ. SCF E3, and DEPTOR as the substrate, were added into a reaction mixture containing ATP, ubiquitin, E1 and E2, followed by constant mixing for 60 min. The reaction mixture was then loaded onto PAGE gel for IB with the indicated antibodies.

(f) Constitutively active p38γ and p38δ mutants induce ubiquitination of DEPTOR but not the 13xS/T→A DEPTOR mutant. Flag-DEPTOR or Flag- 13xS/T→A DEPTOR was expressed in HEK-293T cells alone or together with constitutively active p38γ and p38δ mutants. HEK-293T cells starved for 30 hr and were incubated for 12 hr with 10μM MG132. DEPTOR was inmunoprecipitated using anti-Flag antibody. Inmunoprecipitates and cell lysates were analyzed by immunoblotting with the indicated antibodies.

Data are means ± SEM (n=3). *P<0.05 (*t*-test).

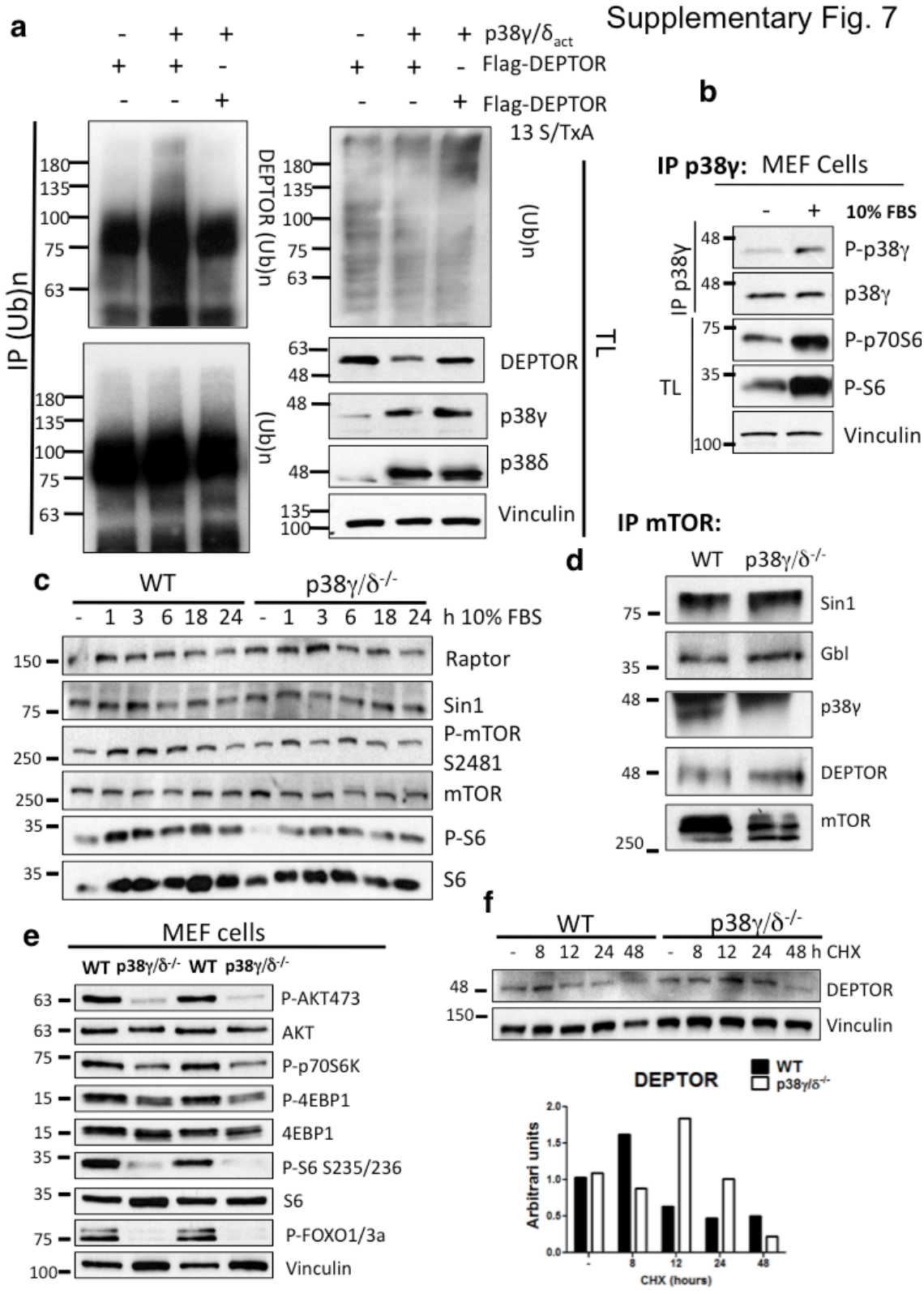

Supplementary Figure 7. p38γ and p38δ control mTOR pathway through the regulation of DEPTOR degradation.

(a) Constitutively active p38γ and p38δ mutants induce ubiquitination of DEPTOR but not the 13xS/T→A DEPTOR mutant. Flag-DEPTOR or Flag- 13xS/T→A DEPTOR was expressed in

HEK-293T cells alone or together with constitutively active p38γ and p38δ mutants and HA-Ub. Cells were serum starved and incubated for 12 hr with 10μM MG132. Poly-Ubiquitinated proteins were IP from cell lysates with bead-conjugated anti-HA Ab and immunoprecipitates were analyzed by immunoblotting with the indicated antibodies.

(b) p38γ is activated upon serum stimulation. MEF cells were stimulated with 10% FBS during 30 min. Then cells were harvested and p38γ immunoprecipitated. Total lysates (TL) and p38γ immunoprecipitates analyzed by immunoblot.

(c) p38γ/δ$^{-/-}$ MEFs have below-normal serum-induced mTOR activation. WT and p38γ/δ$^{-/-}$ MEFs were serum-starved for 30 hr, followed by serum addition. Cells were harvested at the indicated time points for immunoblotting with the indicated antibodies.

(d) p38γ/δ$^{-/-}$ MEFs have below-normal activation of the mTOR pathway in starvation conditions. Confluent WT and p38γ/δ$^{-/-}$ MEFs were serum-starved for 16 hr and harvested for immunoblotting with the indicated antibodies.

(e) Higher amounts of endogenous DEPTOR co-immunoprecipitate with mTOR in p38γ/δ$^{-/-}$ MEFs. Endogenous mTOR was immunoprecipitated from WT and p38γ/δ$^{-/-}$ MEFs and immunoprecipitates were analyzed by SDS-PAGE.

(f) DEPTOR degradation is impaired in p38γ/δ$^{-/-}$ MEF cells. WT and p38γ/δ$^{-/-}$ MEFs were treated with 10μM cycloheximide (CHX), harvested at the times indicated, and endogenous DEPTOR levels were analyzed by immunoblotting. Western blot was quantified.

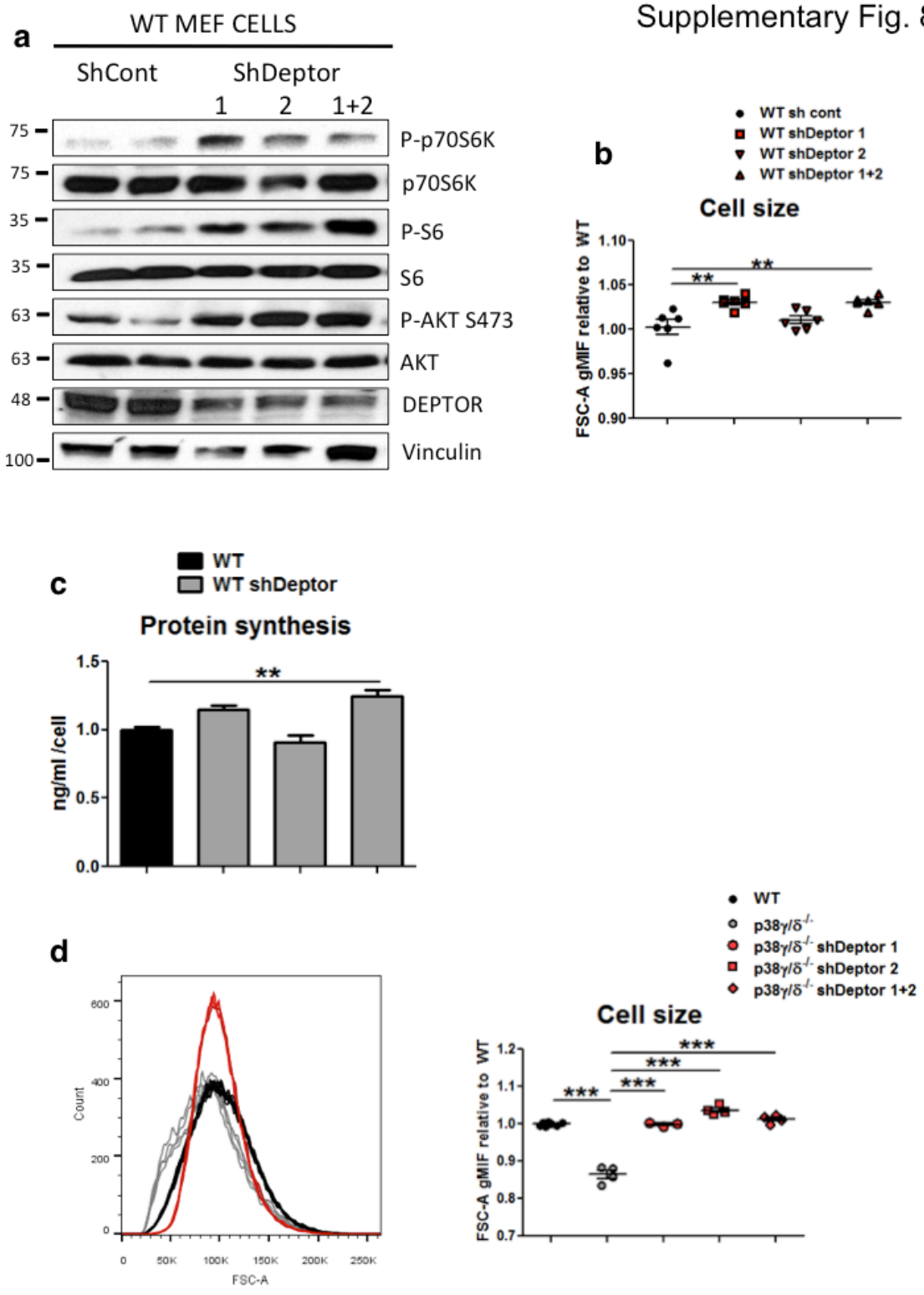

Supplementary Figure 8. Deptor silencing leads to mTOR pathway hyperactivation and

reverts p38γ/δ$^{-/-}$ reduced cell size.

(a, b & c) Silencing DEPTOR in WT MEFs results in mTOR hyperactivation and a slight increase in protein syinthesis. MEFs were singly or doubly infected with two different DEPTOR lentiviral shRNA constructs for 24 hr. Uninfected cells were eliminated by selection with 3 μg/ml puromycin for 1 week. (**a**) The resulting cell lines were then serum-starved for 24 hr before harvesting. Equal amounts of whole cell lysates were immunoblotted with the indicated antibodies. (**c**) Cell size was measured by flow cytometry (forward scatter). *Left*: Representative histogram. *Right*: Quantification graph of the forward scatter mean fluourescence intensity (FSC-A MFI) relative to WT. (**c**) In the resulting cell lines the protein concentration per cell was measured by Bradford method. (n=4-6)

(d) Silencing DEPTOR in p38γ/δ$^{-/-}$ MEFs rescues normal cell size. MEFs were infected with two DEPTOR lentiviral shRNA constructs alone or in combination for 24 hr. Uninfected cells were eliminated by selection with 3 μg/ml puromycin for 1 week. In the resulting cell lines cell size was measured by flow cytometry (forward scatter). *Top*: Representative histogram. *Bottom*: Quantification of forward scatter mean fluorescence intensity (FSC-A MIF) relative to WT cells. (n=4)

Data are means ± SEM (n=6). **P<0.01; ***P<0.001 (1-way ANOVA coupled to Bonferroni's post test).

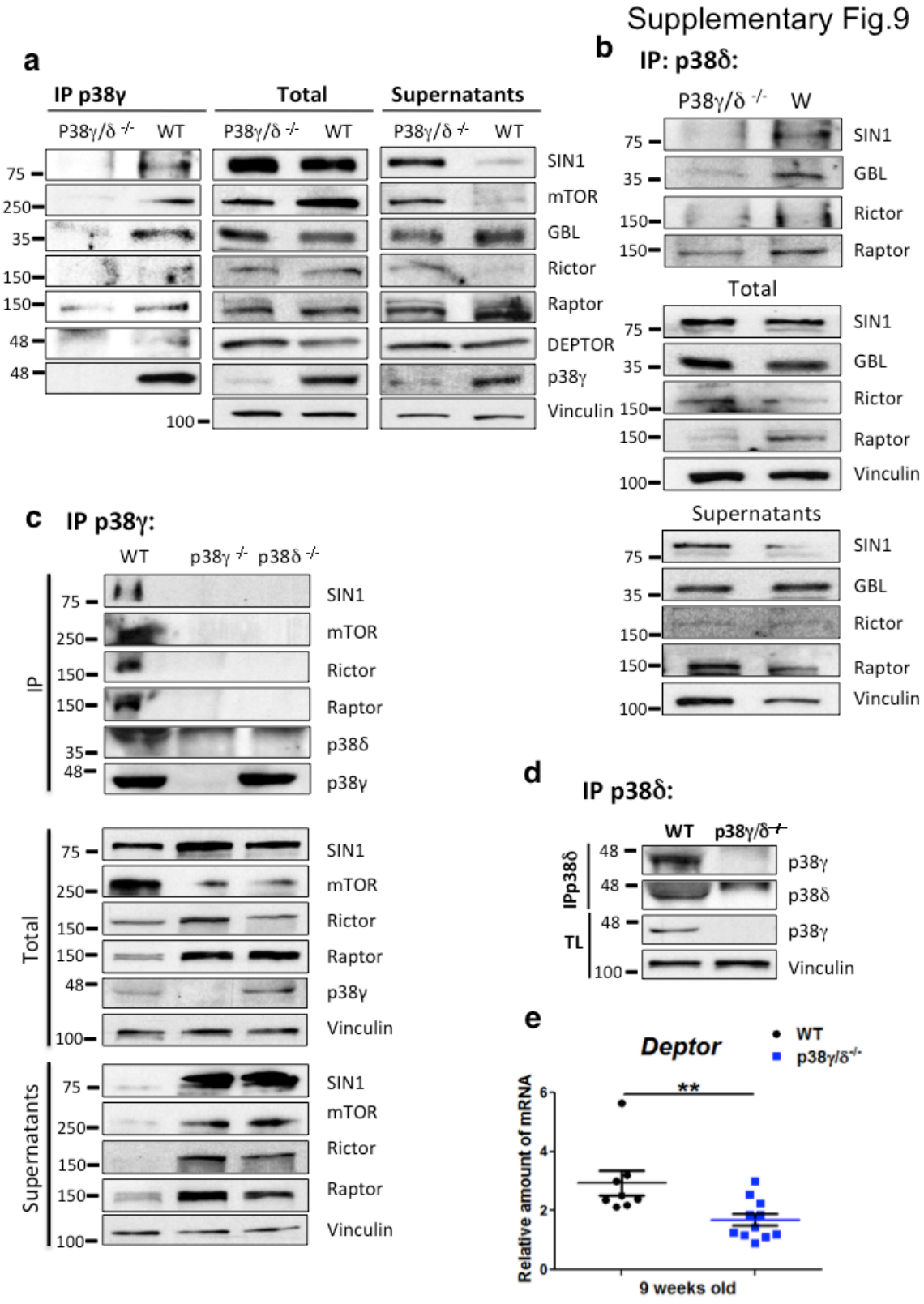

Supplementary Figure 9. p38γ and δ are mutually necessary for their interaction with mTOR complexes in heart tissue.

(a) Endogenous cardiac mTOR, GβL, Raptor, Rictor and Sin-1 co-immunoprecipitate with endogenous p38γ. p38γ immunoprecipitates (IP), total lysates (Total) and supernatants from WT and p38γ/$\delta^{-/-}$ heart lysates were analyzed by SDS-PAGE.

(b) Endogenous cardiac mTOR, GβL, Raptor, Rictor and Sin-1 co-immunoprecipitate with endogenous p38δ. p38δ immunoprecipitates (IP), total lysates and Co-IP supernatants from WT and p38γ/$\delta^{-/-}$ heart lysates were analyzed by SDS-PAGE.

(c) Endogenous cardiac mTOR, Raptor, Rictor, Sin-1 and p38δ co-immunoprecipitate with endogenous p38γ only when both p38γ and p38δ are present. p38γ immunoprecipitates (IP), total lysates and Co-IP supernatants from WT, p38$\gamma^{-/-}$ and p38$\delta^{-/-}$ heart lysates were analyzed by SDS-PAGE.

(d) Endogenous p38γ co-immunoprecipitates with endogenous p38δ in heart lysates. p38δ immunoprecipitates (IP) and total lysates (TL) from WT and p38γ/δ-/- heart lysates were analyzed by SDS-PAGE.

(e) p38γ/$\delta^{-/-}$ hearts present reduced DEPTOR mRNA levels. DEPTOR mRNA was measured by qRT-PCR and normalized to GADPH mRNA levels. (n=7-11).

Data are means ± SEM (n=7-10). **P<0.01 (*t*-test).

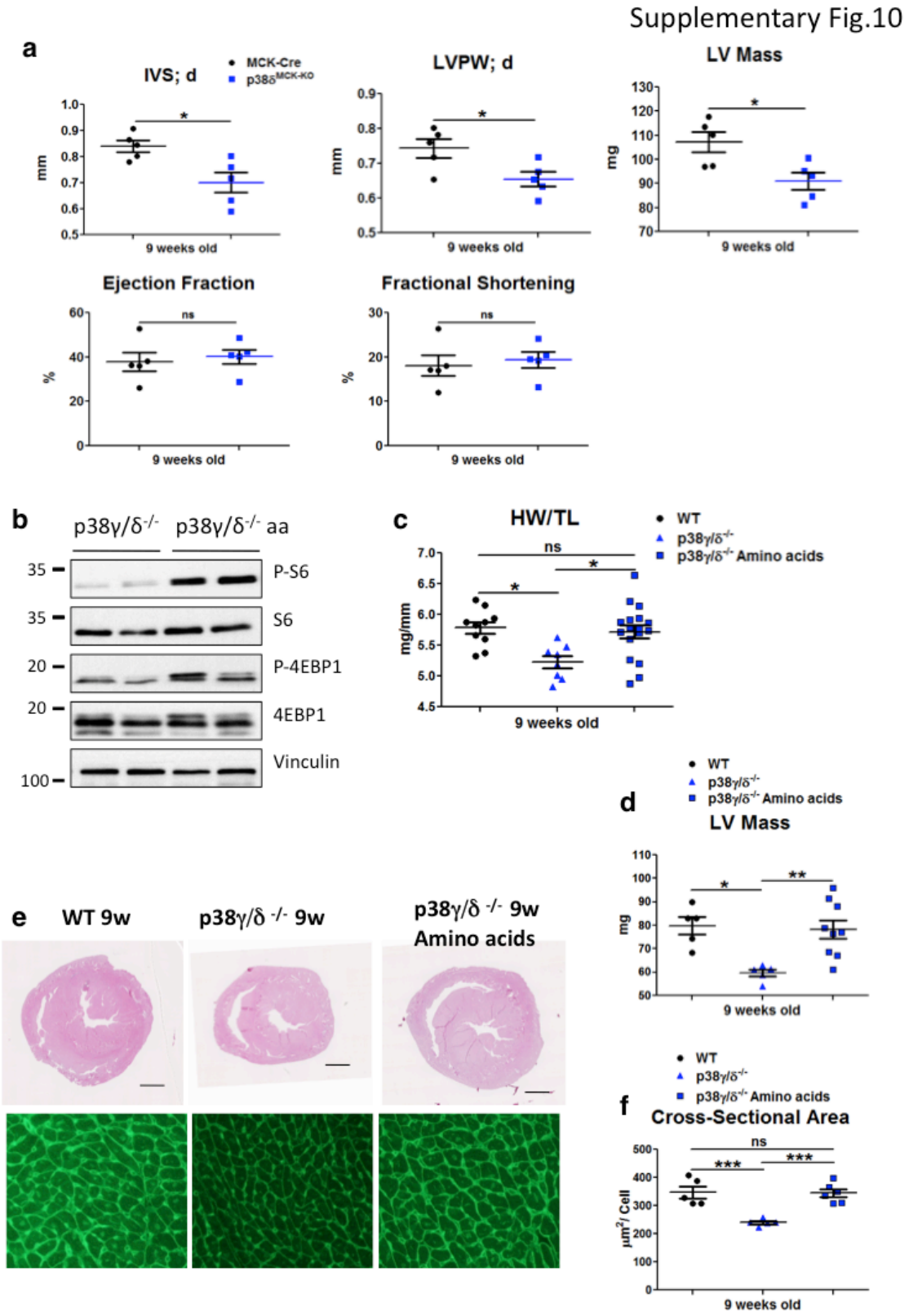

Supplementary Figure 10. Amino acid induced mTOR activation in mice deficient in p38γ and δ is sufficient to revert its small heart phenotype.

(a) Echocardiography results for 9-week-old MCK-Cre and MCK p38δ KO (p38δ^{MCK-KO}) mice. IVS;d (inter-ventricular septum in diastole); LVPW;d (left ventricle posterior wall in diastole); LV (left ventricle). (n=5).

(b, c, d & e) Amino acids (aa) treatment reverts reduced heart size in p38γ/δ$^{-/-}$ mice. WT and p38γ/δ$^{-/-}$ mice were injected daily with a mixture of amino acids i.p or Saline until 9 weeks of age. **(b)** Amino acid treatment activated mTOR pathway in p38γ/δ$^{-/-}$ 9 weeks old hearts. Heart lysates were analyzed by immunoblot for mTOR pathway activation. **(c)** Heart weight to tibia length ratio. **(g)** Echocardiography analysis LV Mass at 9 weeks of age in saline or amino acid treated mice. **(e)** *Top*: Representative H&E stained transverse heart sections from 9-week-old WT and p38γ/δ$^{-/-}$ mice after amino acid or saline treatment. Scale bar, 1mm. *Bottom*: Representative FITC-WGA staining (green) in hearts from 9-week-old 9-week-old WT and p38γ/δ$^{-/-}$ mice after amino acid or saline treatment. **(f)** Cardiomyocyte cross-sectional area quantification from the FITC-WGA staining (green) in hearts from 9-week-old

Data are means ± SEM (n=5). *P<0.05; **P<0.01; ***P<0.001 (2-way ANOVA coupled to Bonferroni's post test or *t*-test).

Supplementary Fig. 11

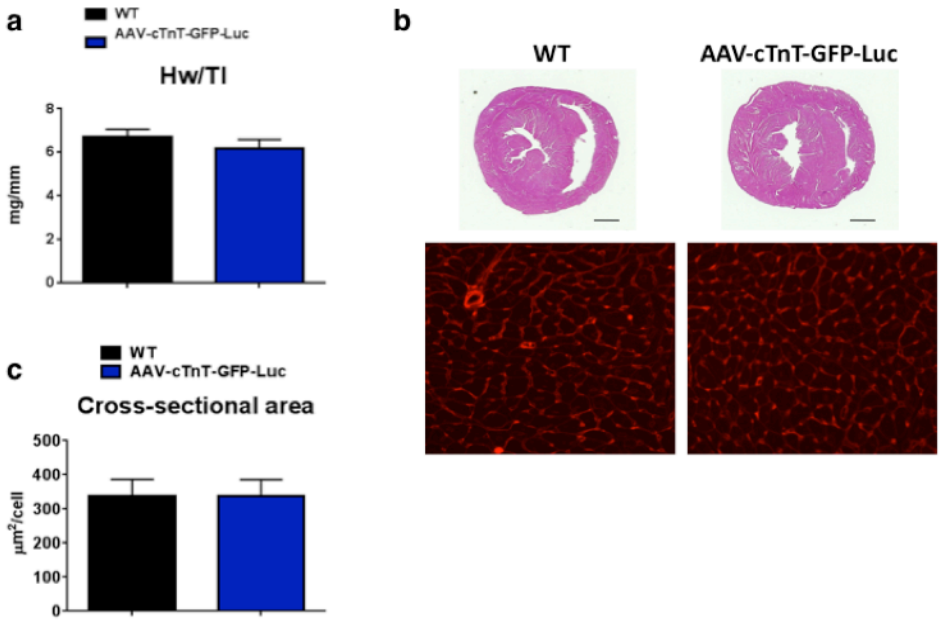

Supplementary Figure 11. Adeno-associated control virus injection does not affect cardiac growth.

(a, b & c) Adeno-associated serotype 9-virus control injection does not affect cardiac growth. WT mice were injected or not at 4 weeks old with AAV-cTnT-GFP-Luc virus and heart phenotype analyzed at 9 weeks of age. **(a)** Heart weight to tibia length ratio. **(b)** *Top*: Representative H&E stained transverse heart sections from WT and AAV-cTnT-GFP-Luc injected mice. Scale bar, 1mm. *Bottom*: Representative WGA (red) and dapi (blue) staining in hearts from WT and AAV-cTnT-GFP-Luc injected mice. **(c)** Cardiomyocyte cross-sectional area quantification from the WGA staining (red) in heart sections.

Data are means ± SEM (n=5), (*t*-test).

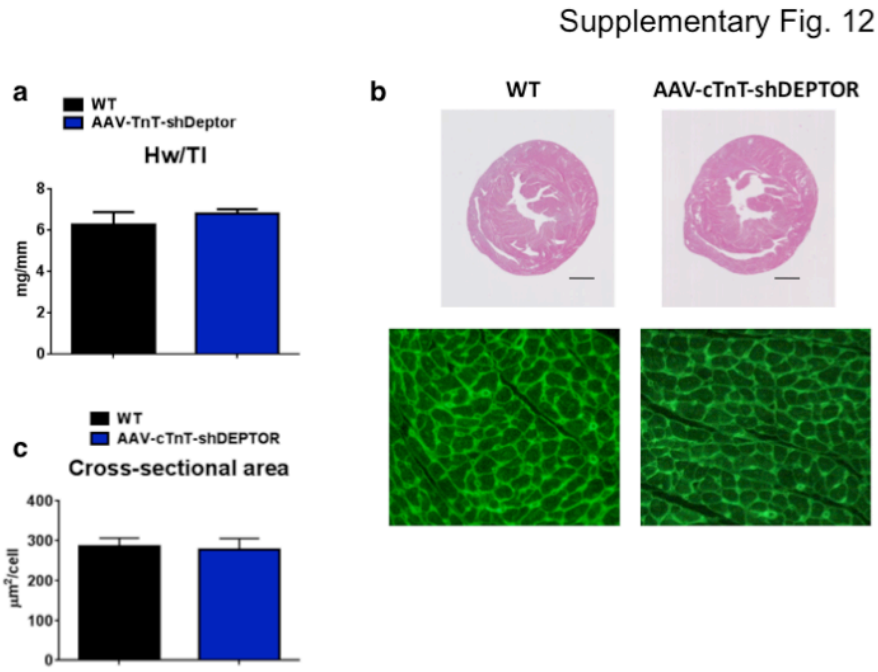

-

Supplementary Figure 12. Adeno-associated shDEPTOR virus injection in WT mice does not affect cardiac growth.

(a, b & c) Adeno-associated serotype 9-virus shDEPTOR was injected to 4 weeks-old mice and heart phenotype analyzed at 8 weeks-old. **(a)** Heart weight to tibia length ratio. **(b)** *Top*: Representative H&E stained transverse heart sections from 8-week-old WT and AAV-cTnT-shDEPTOR injected mice. Scale bar, 1mm. *Bottom*: Representative FITC-WGA staining (green) in hearts from 8-weeks-old WT and AAV-cTnT-shDEPTOR injected mice. **(c)** Cardiomyocyte cross-sectional area quantification from the FITC-WGA staining (green) in hearts from 8-week-old.

Data are means ± SEM (n=5), (*t*-test).

Supplementary Figure 13. Western blots full scans.

m/z (mi)	MH+2(mi)	MH+3(mi)	Mods	Start	End	Miss	Sequence	length
1494.7022	747.8547	498.9056	1Oxidation 1Phospho	143	154	0	(K)LMSPENTLLQPR(E)	12
1398.741	699.8741	466.9185		143	154	0	(K)LMSPENTLLQPR(E)	12
1414.7359	707.8716	472.2501	1Oxidation	143	154	0	(K)LMSPENTLLQPR(E)	12
1478.7073	739.8573	493.5739	1Phospho	143	154	0	(K)LMSPENTLLQPR(E)	12
2070.0536	1035.5304	690.6894		143	160	1	(K)LMSPENTLLQPREEEGVK(Y)	18
2086.0485	1043.5279	696.021	1Oxidation	143	160	1	(K)LMSPENTLLQPREEEGVK(Y)	18
2166.0148	1083.5111	722.6765	1Oxidation 1Phospho	143	160	1	(K)LMSPENTLLQPREEEGVK(Y)	18
2150.0199	1075.5136	717.3448	1Phospho	143	160	1	(K)LMSPENTLLQPREEEGVK(Y)	18
1936.9528	968.98	646.3225	1Phospho	312	328	0	(K)RPVTSEELLTPGAPYAR(K)	17
1856.9865	928.9969	619.667		312	328	0	(K)RPVTSEELLTPGAPYAR(K)	17
2065.0478	1033.0275	689.0208	1Phospho	312	329	1	(K)RPVTSEELLTPGAPYARK(T)	18
1985.0815	993.0444	662.3653		312	329	1	(K)RPVTSEELLTPGAPYARK(T)	18
1157.5507	579.279	386.5218		258	268	0	(K)STSFMSVSPSK(E)	11
1253.5119	627.2596	418.5088	1Oxidation 1Phospho	258	268	0	(K)STSFMSVSPSK(E)	11
1173.5456	587.2764	391.8534	1Oxidation	258	268	0	(K)STSFMSVSPSK(E)	11
1237.517	619.2622	413.1772	1Phospho	258	268	0	(K)STSFMSVSPSK(E)	11
1527.7723	764.3898	509.929		258	271	1	(K)STSFMSVSPSKEIK(I)	14
1623.7336	812.3704	541.916	1Oxidation 1Phospho	258	271	1	(K)STSFMSVSPSKEIK(I)	14
1543.7672	772.3873	515.2606	1Oxidation	258	271	1	(K)STSFMSVSPSKEIK(I)	14
1607.7387	804.373	536.5844	1Phospho	258	271	1	(K)STSFMSVSPSKEIK(I)	14
2364.2323	1182.6198	788.7489	1Phospho	308	328	1	(K)SVLKRPVTSEELLTPGAPYAR(K)	21
2284.266	1142.6366	762.0935		308	328	1	(K)SVLKRPVTSEELLTPGAPYAR(K)	21
1285.6457	643.3265	429.2201		257	268	1	(R)KSTSFMSVSPSK(E)	12
1381.6069	691.3071	461.2072	1Oxidation 1Phospho	257	268	1	(R)KSTSFMSVSPSK(E)	12
1301.6406	651.3239	434.5517	1Oxidation	257	268	1	(R)KSTSFMSVSPSK(E)	12
1365.612	683.3096	455.8755	1Phospho	257	268	1	(R)KSTSFMSVSPSK(E)	12
2011.9922	1006.4998	671.3356	1Phospho	139	154	1	(R)LYEKLMSPENTLLQPR(E)	16
2027.9872	1014.4972	676.6672	1Oxidation 1Phospho	139	154	1	(R)LYEKLMSPENTLLQPR(E)	16
1932.0259	966.5166	644.6802		139	154	1	(R)LYEKLMSPENTLLQPR(E)	16
1948.0208	974.5141	650.0118	1Oxidation	139	154	1	(R)LYEKLMSPENTLLQPR(E)	16

Supplementary table 1. Peptides selected in this study for the in vitro and in vivo analysis of p38γ and p38δ phosphorylation of human DEPTOR by PRM

Monoisotopic masses for singly (m/z), doubly (MH+2) or triply (MH+3) charged ions from trypsin-digested peptides of human DEPTOR (Uniprot entry Q8TB45 - DPTOR_HUMAN), containing SP or TP consensus phosphorylation motifs of p38γ and p38δ, and their unmodified or Met-oxidized counterparts. In red, selected masses for each sequence. Parent and fragment masses for later analyses were generated using the ProteinProspector Tools (http://prospector.ucsf.edu/prospector/mshome.htm).

Gene	Primer	Sequence
Deptor	Fw	ATAGACGGCACCATCTCAA
	Rev	GTCGGCTAATTTCTGCATG
S145A mutation	Fw	GGCTATATGAAAAGCTGATG**GC**CCCTGAAAACACACTCCTGC
	Rev	GCAGGAGTGTGTTTTCAGGGGCCATCAGCTTTTCATATAGCC
S244A mutation	Fw	CCAGGAAACTCATGAC**GC**TCCCTTCTGCCTGAGG
	Rev	CCTCAGGCAGAAGGGAGCGTCATGAGTTTCCTGG
S265A mutation	Fw	CCAGCTTTATGTCAGTG**GC**CCCCAGCAAGGAGATC
	Rev	GATCTCCTTGCTGGGGGCCACTGACATAAAGCTGG
S293A mutation	Fw	GCTACTTCAGCAGC**GC**CCCCACCCTCAGC
	Rev	GCTGAGGGTGGGGGCGCTGCTGAAGTAGC
T321A mutation	Fw	**CC**TCTGAGGAACTCCTT**G**CTCCCGGGGCTCCG
	Rev	CGGAGCCCCGGGAGCAAGGAGTTCCTCAGAGG

Supplementary Table 2. Primers sequences.

SUPPLEMENTARY METHODS

Detection of DEPTOR Phosphorylation Sites *In Vivo*

HEK-293T cells were transfected with FLAG-DEPTOR using the calcium phosphate method. At 30 hr post-transfection, 293T cells were treated with 10 μM MG132 for 16 hr to block the 26S proteasome pathway prior to collecting the whole cell lysates for FLAG-immunoprecipitation. After extensive washing with PBS 1x buffer, 10μl of sample buffer was added to FLAG-immunoprecipitates, which were boiled for 5 minutes at 95ºC. The samples were reduced, alkylated, digested with trypsin, and desalted on C18 reverse phase microcolumns as before [1,2]. Analyses were performed on a nano HPLC system coupled with a hybrid quadrupole orbitrap mass spectrometer (QExactive, Thermo Scientific). For LC analysis, each sample was loaded in Buffer A (0.1% formic acid) and on-line desalted on a 2 cm packed pre-column (Thermo Acclaim

PepMap 100). Analytical separation was performed over a 50 cm column (Thermo Acclaim PepMap 100, 75 μm ID x 500 mm) at 200 nL/min with a 180 min gradient from 8 to 31% of Buffer B (0.1% formic acid / 90 % acetonitrile) using an EASY-nLC 1000 HPLC (Thermo Scientific). Samples were analysed randomly with an extensive column wash between each sample to minimize carry-over. Phosphorylated peptides detected in the *in vitro* experiments, and their non-phosphorylated counterparts, were monitored using the parallel reaction monitoring (PRM) mode. In all experiments, a full mass spectrum with 2 microscans at 140.000 resolution relative to m/z 200 (AGC target 1×10^6, 20 ms maximum injection time, m/z 400–1200) was followed by PRM scans at 17.500 resolution (AGC target 2×10^5, 120 ms maximum injection time, isolation width of ±2 Th) and triggered by a scheduled inclusion list of the selected peptide ions (Supplementary Table 1). Fragmentation was performed in the HCD collision cell using anormalized collision energy of 27%. Quantification was carried out post-acquisition using the extracted ion chromatograms (XICs) using a ±3 ppm mass tolerance, unless otherwise noted. Detection of the targeted peptide was based on the presence of the intact monoisotopic precursor signal, mass error within ±3 ppm, and manual verification of the MS/MS spectra. Proteome Discoverer 1.4.0.288 (Thermo Scientific) was also used together with Scaffold (version Scaffold_4.4.1, Proteome Software Inc., Portland, OR) to validate MS/MS based peptide identifications and fragment assignments.

Site-Directed Mutagenesis

The DEPTOR cDNA in pRK5 (plasmid #21334, Addgene) was mutagenized with the QuikChange II XL Site-Directed Mutagenesis Kit (Agilent Technologies). The primers used are specified in the Supplementary table 2.

qRT-PCR

The expression of mRNA was examined by qRT-PCR using a 7900 Fast Real Time thermocycler and FAST SYBR GREEN assays (Applied Biosystems). Relative mRNA expression was normalized to *Gapdh* mRNA measured in each sample. *Deptor* was amplified using the primers shown in Supplemental Table 2.

In vitro ubiquitin assay

Cullin-βTrCP E3 complex was precipitated from 293 cells overexpressing both proteins with myc. GST-DEPTOR protein (H00064798, Novus biologicals) was incubated ofor 30 minutes with 1 μg of active recombinant p38g and p38d or without kinases (provided by MRC Protein Phosphorylation and Ubiquitylation Unit, Dundee, UK) in the presence of 200 μM cold ATP followed by incubation with Cullin-βTrCP E3 complex in the presence of E1 and E2 in a ubiquitin reaction buffer (Abcam). Polyubiquitinated DEPTOR was resolved by SDS-PAGE and detected by IB with anti-DEPTOR Ab and antiubiquitin.

SUPPLEMENTARY REFERENCES

1 Inuzuka, H. *et al.* Phosphorylation by casein kinase I promotes the turnover of the Mdm2 oncoprotein via the SCF(beta-TRCP) ubiquitin ligase. *Cancer Cell* **18**, 147-159 (2010).

2 Dibble, C. C., Asara, J. M. & Manning, B. D. Characterization of Rictor phosphorylation sites reveals direct regulation of mTOR complex 2 by S6K1. *Mol Cell Biol* **29**, 5657-5670 (2009).

ARTÍCULO 4: Physiologic Cardiac hypertrophy but Increased Sudden Cardiac Death predisposition in mice deficient in MKK6

Autores: Bárbara González-Terán, Elisa Manieri, Laura Sanz, Ivana Nicholik, Maria Elena Rodriguez, Luis Guillermo Francisco Leiva, Víctor Buendía, David Filgueiras, Luis Jesús Jiménez Borreguero & Guadalupe Sabio.

Datos no publicados/ Unpublished data

RESUMEN

La muerte súbita es una muerte inesperada que resulta de una enfermedad cardíaca cuya presencia es conocida o desconocida. Aunque se trata de un evento poco frecuente en los deportistas jóvenes, tiene un gran impacto en la sociedad actual. Numerosos estudios se han realizado para conocer cómo prevenir la muerte súbita y poder detectar los sujetos con mayor susceptibilidad. No obstante, el diagnóstico diferencial entre hipertrófia fisiológica o "corazón de atleta" y la cardiomiopatía hipertrófica aún no se ha podido establecer con claridad. Además, poco se conoce sobre las mutaciones genéticas y vías de señalización asociadas a un mayor riesgo de sufrir muerte súbita cardiaca. Previamente p38γ y p38δ han sido involucradas en el crecimiento hiperttrófico cardiaco. En este estudio mostramos que MKK3 es el principal activador de p38γ y p38δ en el corazón, mientras que MKK6 regula la actividad de p38α. De esta forma, la falta de activación de la vía MKK6-p38α lleva a la hiperactivación de MKK3-p38γ/δ y a una actividad aumentada de la vía de señalización de mTOR que deriva en el desarrollo de hipertrófia cardiaca fisiológica. Sin embargo, cuando los ratones deficientes en MKK6 son sometidos a un entrenamiento crónico de ejercicio de resistencia, su función sistólica cardiaca disminuye, muestran un mayor prolongamiento del intervalo QT y presentan susceptibilidad incrementada de muerte súbita. Este estudio identifica que alteraciones en la vía de señalización MKK3/6-p38γ/δ pueden llevar al desarrollo de hipertrófia fisiológica pero con un mayor riesgo de desarrollo de un intervalo QT prolongado y de muerte súbita asociada al ejercicio.

Aportación Personal al trabajo: He participado tanto en el diseño experimental, como en la realización de los experimentos y en la escritura del artículo.

Physiologic Cardiac hypertrophy but Increased Sudden Cardiac Death predisposition in mice deficient in MKK6

Bárbara González-Terán[1], Elisa Manieri[1], Laura Sanz[1], Ivana Nicholik[1], Maria Elena Rodriguez[1], Luis Guillermo Francisco Leiva[1], Víctor Buendía[1], David Filgueiras[1], Luis Jesús Jiménez Borreguero[1] & Guadalupe Sabio[1]*

1. Fundación Centro Nacional de Investigaciones Cardiovasculares Carlos III, 28029 Madrid, Spain.

*To whom correspondence should be addressed.

Key words: MKK6, MKK3, p38MAPK, cardiac hypertrophy, mTOR, sudden death,

ABSTRACT

Sudden cardiac deaths are rare events in athletics but are highly visible with substantial impact on our society. Many attempts have been made to detect those at risk for sudden cardiac death, but the differential diagnosis between physiological hypertrophy and hypertrophic cardiomyopathy is not yet clearly established. Moreover little is known about the genetic traits and signaling pathways associated to an increase risk of sudden cardiac death. Mitogen activated protein Kinases Kinases 3 and 6 (MKK) have been suggested to be implicated in the control of cardiac growth, however, the cardiac phenotype of animals lacking these kinases remains to be explored. Moreover it is not clear how these kinases control the activation of the different p38MAPK isoforms in cardiomyocytes. Here we show that, in the heart, MKK3 is the main activator of p38γ and p38δ while MKK6 activates cardiac p38α. Furthermore, the deficiency in MKK3 causes decreased postnatal cardiac growth due to reduced p38γ and p38δ activation. Likewise, the lack of MKK6-p38α activation, leads to MKK3-p38γ/δ hyperactivation, increased mTOR signaling and causes physiological cardiac hypertrophy. However, when MKK6 deficient mice are challenged with chronic endurance training, the QT interval is prolonged in these mice and show increase risk of sudden cardiac death. The cardiac hypertrophy observed in *Mkk6*$^{-/-}$ mice can be reverted by knocking out either p38γ or p38δ, as well as inhibiting mTOR pathway with Rapamycin. In conclusion, we have identified that alterations in MKK3/6-p38γ/δ pathway in cardiomyocytes are associated with physiological cardiac hypertrophy and predispose to Long QT development and sudden cardiac death.

INTRODUCTION

An enormous amount of research has been generated during the past 10 years evaluating the causes and events surrounding sudden cardiac death (SCD) and potential screening mechanisms for identifying those at risk. Although there is not a universally accepted definition, SCD can be considered a non-traumatic, non-violent, unexpected death due to cardiac causes within 1 hour of the onset of symptoms [16].

Intensive endurance training is able to cause a distinct pattern of functional and structural changes within normal myocardial tissue [18]. During intense aerobic exercise, the oxygen consumption of muscle tissue increases markedly, and cardiac output must rise to meet the demands. Over time, endurance training, leads to the development of physiological cardiac hypertrophy called "athlete's heart", which is characterized by a proportional increased in left ventricular mass, with wall thicknesses under 15 mm and a moderated dilated left ventricle, increased heart rate during exercise and decreased resting heart rate, increased ventricular stroke volume, and increased cardiac output, without fibrosis development [13]. However, there is an overlap between this type of physiologic cardiac hypertrophy and mild forms of hypertrophic cardiomyopathy (HCM), the most common genetic disorder of the cardiovascular system. HCM is commonly characterized by asymmetric left ventricular hypertrophy with a reduced LV-diameter and fibrosis development. Hypertrophic cardiomyopathy is a common cause of sudden deaths among athletes, therefore differentiating this condition from the non-pathological "athlete's heart" presents an important challenge. Several mutations have been associated to HCM, the most common and better characterized are mutations of genes encoding critical contractile myofilament proteins. Besides, with a low frequency of occurrence, mutations in genes encoding calcium-sensitive and calcium-handling proteins have been recently implicated in the pathogenesis of HCM. However, a 50% of patients diagnosed with HCM worldwide do not host known gene mutations, highlighting the need to identify novel genes responsible for HCM [19].

Long QT Syndrome has been also associated with cardiac sudden death. It is associated with specific mutations in genes that encode cardiac ion channels. Besides, cardiac hypertrophy is a risk factor for QT-prolongation and cardiac sudden death. Recent

studies in human patients and animal models have demonstrated that cardiac hypertrophy significantly affects myocardial electrotonic cell-to-cell coupling, leading to disturbance in action potential duration and potential malignant arrhythmia and cardiac sudden death [12, 17, 38].

In response to hemodynamic overload, cardiac myocytes are subjected to mechanical stretch, and autocrine and paracrine humoral factors are released. These factors bind to different receptors on cardiomyocytes, and activate intracellular signaling pathways that lead to cell growth. A great number of signaling cascades and proteins are involved in the regulation of cardiac growth and hypertrophy. Besides, it is now clear that several signaling molecules play unique roles in the regulation of pathological and physiological cardiac hypertrophy [24]. The production of cardiac IGF1 and activation of the PI3K pathway has been described during postnatal development and upon exercise training in humans and animal models [28, 32]. In contrast, pressure overload and heart failure is associated with elevated levels of angiotensin-II, catecholamines and ET-1 and the activation of GPCR specific receptors [1, 28, 31, 33, 42, 43].

However, it has been shown, that some pathways that were believed to promote physiologic hypertrophic growth, are involved in pathological hypertrophy as well. IGF transgenic mice, present proportionally enlarge hearts with normal cardiac function, but when prolonged on time, it progresses to pathological hypertrophy with decreased cardiac function [25]. An essential feature of both physiological and pathological hypertrophy is increased protein synthesis. mTOR pathway is the critical regulator of protein synthesis mainly through the phosphorylation of its downstream substrates. Activation of mTOR pathway is increased during postnatal cardiac development [14], also in hearts from transgenic mouse models of physiological hypertrophy (IGF-PI3K pathway) [25, 26, 34, 35]. Moreover, rapamycin, a specific mTOR inhibitor, attenuated and regressed pathological hypertrophy induced by cardiac overload. [35]. Likewise, p38γ and p38δ MAPKs, have been recently involved in the control of postnatal cardiac hypertrophic growth as well as Angiotensin-II induced cardiac hypertrophy, through the control of mTOR pathway activation [14]. This suggests that physiological hypertrophied hearts, due to genetic causes or endurance training, depending on the type, duration and potency of the environmental signals could progress into pathological conditions.

The p38-MAPK signaling pathway is an important mediator of numerous biological functions including cell growth, cell proliferation, cell cycle and cell death, and is considered a critical component of stress response pathways [9, 15, 22]. In the heart, the four p38 MAPKs (p38α/β/γ/δ) are expressed, but p38α and p38γ gamma protein levels are higher. p38α and p38β play redundant roles in the regulation of cardiac proliferation during embryonic development, and their deficiency leads to septal defects [10]. However, mice lacking p38α or p38β alone in the heart, display a normal cardiac structure and function in basal condition. In response to cardiac overload, p38α MAPK has been implicated in the regulation of myocyte apoptosis [29], whereas p38β has a predominant role in the regulation of the hypertrophic response [2, 4, 20, 30, 40]. Additionally, we have previously reported that mice deficient in p38γ and p38δ present reduced postnatal hypertrophic growth associated to a decreased activation of the mTOR pathway. Besides, p38γ and p38δ deficiency protects against cardiac overload induced pathological hypertrophy [14].

MKK3 and MKK6, the main up-stream activators of the p38 isoforms, are highly selective for p38 MAPKs and do not activate JNKs or ERK1/2 [7, 8, 11]. Mice lacking both MKK3 and MKK6 are not viable, dying in mid-gestation with defects in the placenta and the development of the embryonic vasculature [3]. This observation indicates that MKK3 and MKK6 have partial redundant roles, because loss of either gene alone yields healthy mice [21, 37, 41]. Both MKKs are expressed in cardiac tissue and have been previously involved in cardiac hypertrophy. Nevertheless, all the studies have been performed by overexpressing the dominant negatives or by constitutively active mutants of MKK3 and MKK6, non-physiological models that could account for artefactual phenotypes associated [4, 27]. Moreover, is not known which is the major MKK required for the activation of the different p38 MAPK isoforms in the regulation of heart growth during postnatal cardiac development nor upon other hypertrophic stimuli. Thus, further experiments are needed taking advantage of MKK single knockout mice and cardiac-specific conditional knockouts.

The purpose of the study reported here was to examine the role of the MAPK Kinases MKK3 and MKK6 in the activation of the different p38 MAPK isoforms in the heart, and their implication in the regulation of physiological and pathological cardiac hypertrophy. Here we show that MKK3 is the main activator of p38γ and p38δ isoforms, whereas MKK6 activates p38α in the heart. Furthermore MKK6 exerts a

feedback loop upstream the signaling pathway, and its deficiency leads to MKK3-p38γ/δ hyperactivation, and an enhance physiological-type of cardiac hypertrophic growth. Accordingly, mice lacking MKK3 present reduced postnatal cardiac hypertrophy. *Mkk6*$^{-/-}$ physiological hypertrophy progresses into pathological hypertrophy when mice undergo chronic endurance training, with prolong QT interval and increase risk of sudden death.

RESULTS

Several studies have been done to address the role of p38 MAPK pathway in the cardiac homeostasis and disease. The four p38 isoforms are expressed in the heart and have been involved in the regulation of cardiac growth at different levels and stages during development [10, 14], as well as in the pathogenesis of cardiac diseases [40]. However, it is not yet clear the importance of the p38 up-stream kinases, MKK3 and MKK6, in this context. To study the role of MKK3 and MKK6, in the heart, we used mice deficient in either of the MKKs. At First, we studied the cardiac phenotype of *Mkk6*$^{-/-}$ mice during the postnatal stages of cardiac development. MKK6 deficient hearts were proportionally bigger than control hearts at 9 weeks of age (Figure 1A). Ventricular mass between postnatal weeks 4 and 15 was monitored in WT and *Mkk6*$^{-/-}$ mice. At 4 weeks after birth, heart size was similar between genotypes, but from this moment onwards, an enhanced cardiac growth was observed (Figure 1B). The cardiac increase in size can be due to proliferation or hypertrophy. Therefore, we studied the cardiomyocyte cross-sectional area at the same time points. Surprisingly, at 4 weeks cardiomyocytes from MKK6 deficient hearts showed reduced cardiomyocyte area compared to control mice, although their heart size at this time was similar to control hearts (Figure 1C). This suggets that *Mkk6*$^{-/-}$ hearts present an increased number of cardiomyocytes at this developmental stage, which could be indicative of enhance cardiomyocyte proliferation. Accordingly, *Mkk6*$^{-/-}$ hearts showed a strong reduction in *p21* and *Rb* expression at 4 weeks (Supplementary Figure 1A), two important tumor suppressors involved in maintaining cell cycle arrest in adult cardiomyocytes [39], and increased levels of Ki67 stainning (Supplementary Figure 1B). Nevertheless, the latter augmentation in heart size observed in *Mkk6*$^{-/-}$ mice correlates with a greater increase in cardiomyocyte cross-sectional area compared to WT cardiomyocytes, indicative of an enhance hypertrophic growth (Figure 1D). Hypertension is one of the main causes of cardiac hypertrophy. To rule out this possibility, systolic blood pressure was measured

at different time points during postnatal cardiac development. Contrary, systolic blood pressure was lower in *Mkk6*$^{-/-}$ mice indicating that differences in blood pressure could not explain the cardiac hypertrophy observed in these mice (Supplementary Figure 1C).

There are two types of cardiac hypertrophic growth, the physiological hypertrophy that occurs during cardiac postnatal development or in trained athletes, and the pathological hypertrophy associated to pressure load in a disease setting (hypertension, aortic constriction, etc.) or to cardiomyopathy (familial, viral, toxic or metabolic). Physiological cardiac hypertrophy is characterized by a proportional increased heart size, without fibrosis development that leads to normal or enhanced cardiac function, without re-expression of fetal genes. Whereas pathological hypertrophy leads to fibrosis development with the up-regulation of fetal genes, reduced cardiac function and is associated with increased mortality [24]. Analysis of these parameters was performed in order to distinguish the type of hypertrophy observed in *Mkk6*$^{-/-}$ mice. Echocardiography of 9-week-old mice reinforced the outcome that *Mkk6*$^{-/-}$ mice have significantly bigger hearts, measured as an increased left ventricle corrected mass. Moreover, *Mkk6*$^{-/-}$ hearts showed thicker diastolic interventricular septum (IVS; d) and telediastolic left ventricle posterior wall (LVPW; d), together with a wider left ventricle internal diameter in diastole compared to WT mice (Figure 1D). This indicated a proportional increase in heart size in mice lacking MKK6. The cardiac systolic function was normal in mice deficient in MKK6, but the E/A ratio, a diastolic function parameter; the stroke volume and cardiac output were increased in these mice (Figure 1E).

Moreover, the level of cardiac fibrosis in 9-week-old hearts was measured by picrosirius red staining and its posterior quantification, showed no differences in fibrosis levels between genotypes (Supplementary Figure 1C). In correlation, the expression levels of different genes markers of fibrosis were similar in WT and *Mkk6*$^{-/-}$ hearts during postnatal cardiac development and in adulthood (Supplementary Figure 1D). Another parameter used to distinguish between the two types of cardiac hypertrophy is the re-expression of fetal genes in the pathological one. Several cardiac stress gene markers were analyzed between postnatal weeks 4 and 9 and showed that although there was a cardiac stress-like expression pattern at 4 weeks of age in *Mkk6*$^{-/-}$ hearts, this stress seemed to be compensated because from there on, no changes in the fetal gene expression levels were observed (Supplementary Figure 1E). Altogether this data indicates that *Mkk6*$^{-/-}$ mice are developing physiological cardiac hypertrophy.

MKK6 is one of the main up-stream activators of p38 MAPKs, however, it is not well established the specificity of this MAPK kinase towards the different p38 isoforms in the heart. Therefore we analyzed the p38s phosphorylation levels in heart lysates from WT and MKK6 deficient hearts. Surprisingly, immunoprecipitation assays for p38γ and p38δ showed that these two alternative p38 isoforms were hyperphosphorylated in *Mkk6*$^{-/-}$ hearts (Figure 2A&B). In contrast, p38α activation was strongly reduced compared to control hearts (Figure 2C). Therefore, other MKK may be responsible of the increased p38γ and p38δ phosphorylation. Being MKK3 the other main p38 up-stream activator, its phosphorylation levels were analyzed by immunoblot. MKK3 phosphorylation was strongly increased in cardiac lysates from *Mkk6*$^{-/-}$ mice (Figure 2D). This suggested that while cardiac p38α activation was mainly mediated by MKK6, cardiac p38γ and p38δ hyperphosphorylation was probably mediated by MKK3. Accordingly, the phosphorylation of the cardiac p38γ and p38δ was strongly decreased in mice deficient in MKK3, without affecting p38α activation (Figure 2 E). These results indicate that in the heart, in homeostatic conditions, MKK3 is the dominant activator of p38γ and p38δ isoforms, whereas MKK6 is the main p38α activator. We have previously reported that p38γ and p38δ control postnatal cardiac hypertrophic growth. Consequently, the reduced activation of p38γ and p38δ in *Mkk3*$^{-/-}$ hearts correlated with a reduction in postnatal cardiac growth (Figure 2F). In the same way, the hyperactivation of p38γ and p38δ in *Mkk6*$^{-/-}$ hearts was associated with the development of physiological cardiac hypertrophy.

p38γ and p38δ promote cardiac hypertrophic growth through the activation of mTOR pathway. Correspondingly, mice deficient in MKK6 presented an increase activation of the cardiac mTOR pathway, addressed by the augmented phosphorylation of its down-stream targets (Figure 3A). It is well established that mTOR is a key regulator of protein synthesis and that protein synthesis is an essential factor in cardiomyocyte hypertrophic growth. Thus, the activation of different eukaryotic initiation/elongation translation factors in heart lysates was analyzed. Immunoblot assays showed an increase activation of translation signaling in hearts lacking MKK6 compared to WT hearts (Figure 3B). To corroborate whether protein synthesis was enhanced in *Mkk6*$^{-/-}$ hearts, puromycin was injected in WT and *Mkk6*$^{-/-}$ mice and, 30 minutes after the injection, hearts were harvested and puromycin incorporation into newly synthesized peptides was studied. *Mkk6*$^{-/-}$ hearts showed an increase in puromycin-labelled peptides compared to control

mice, indicating an enhance protein synthesis *in vivo* in hearts lacking MKK6 (Figure 3C).

To understand whether the specificity observed in the activation of the different p38 isoforms by the MKKs also occurs in other cell types, the p38γ phosphorylation was studied in MEFs WT, *Mkk3*$^{-/-}$ and *Mkk6*$^{-/-}$. In agreement with the outcomes observed in cardiac lysates, MKK6 deficiency led to p38γ hyperphosphorylation and subsequently, increase mTOR pathway activation and bigger cell size. Besides, *Mkk3*$^{-/-}$ MEFs presented reduced mTOR pathway activation and smaller cell size associated to the reduction in p38γ phosphorylation (Supplementary Figure 2).

To determine whether the enhance heart growth of *Mkk6*$^{-/-}$ was due to an autonomous effect in postnatal cardiomyocyte development, we generated mice carrying *lox*P-flanked gene *Mkk6*$^{LoxP/LoxP}$ (Figure 4A). To deplete *Mkk6* in striated muscle, these mice were crossed with MCK Cre mice (MKK6 $^{MCK-KO}$), which reach peak Cre expression on postnatal day 10 [5]. Specific deletion of *Mkk6* was achieved in these mice in muscle and heart (Figure 4A, B and Supplementary Figure 2D). The cardiac phenotype of MKK6 $^{MCK-KO}$ at 9 weeks of age resembled the one observed in MKK6 whole-body knockout mice. This suggests that MKK6 controls heart growth in a cell-autonomous manner (Figure 4C-F). To further corroborate that is MKK6 in cardiomyocytes the responsible of the increased hypertrophic growth; mice lacking MKK6 specifically in cardiomyocytes were used. With that aim *Mkk6*$^{LoxP/LoxP}$ mice were crossed with MHC Cre mice (MKK6 $^{\alpha MHC-KO}$), which starts to be expressed at embryonic day E10.5 [23]. Cardiac specific deletion of *Mkk6* rendered a phenotype very similar to the *Mkk6*$^{-/-}$ full knockout and MKK6 $^{MCK-KO}$ mice, corroborating that MKK6-mediated control of heart growth is cell autonomous (Figure 5 A-E).

Then, we confirmed that the MKK6-mediated modulation of p38γ/δ activation is responsible for the enhanced postnatal cardiac hypertrophic growth using different mouse models. *Mkk6*$^{-/-}$ mice were crossed with mice lacking p38γ in the whole body and mice with the double deficiency in *Mkk6*$^{-/-}$ *Mapk12*$^{-/-}$ were generated, and their cardiac phenotypes studied at 9 weeks after birth. p38γ deletion reverted the enhanced cardiac growth to the WT levels, rendering similar heart size and cardiomyocyte cross-sectional area to control mice (Figure 6). Besides, the cardiac phenotype of *Mkk6*$^{-/-}$ p38δ^{MCK-KO} was analyzed, showing that the deletion of p38δ specifically in striated muscle in *Mkk6*$^{-}$

$^{-/-}$ mice reduced the MKK6 enhance hypertrophy to the p38δ^{MCK-KO} heart size, which is smaller that control hearts, indicating that p38δ is downstream MKK6 in the regulation of cardiac growth (Figure 7). Altogether this data demonstrates that MKK6 enhanced cardiac hypertrophic growth is mediated by the hyperactivation of the MKK3-p38γ/δ pathway in the striated muscle.

To test whether increased mTOR signaling could account for the enhanced heart growth in *Mkk6*$^{-/-}$ mice, we inhibited mTOR activation by a daily injection of Rapamycin, a specific mTOR inhibitor, from 3 weeks until 9 weeks after birth. mTOR inhibition was enough to reduce the heart size of WT and *Mkk6*$^{-/-}$ mice to the same level, with a strong reduction in their cardiomyocyte cross-sectional area. Thus, the *Mkk6*$^{-/-}$ bigger hearts appear to result from the hyperactivation of mTOR pathway in these mice (Figure 8).

Physiological cardiac hypertrophy is understood an adaptive response that causes an increased ventricle mass but with normal or enhanced cardiac function with no increase mortality risk [18]. However, several studies suggest that physiological hypertrophy could progress into pathological, which is strongly associated with sudden cardiac death. Therefore we decided to challenge adult MKK6 deficient mice that already have developed a physiological hypertrophy with exercise training, a stimulus that changes the cardiac functional load and triggers a hypertrophic response to counterbalance the increase in wall stress.

After 3 weeks of swimming training, a significant increase in ventricular mass was observed in both genotypes. Wheat germ agglutinin (WGA) immunostaining indicated that it was due to an enlargement in the cardiomyocyte cross-sectional area (Figure 9A-C). Echocardiography studies reinforce the outcome that swimming training increased heart size in both genotypes. After 3 weeks of endurance exercise training, the systolic function did not change in control mice, but it was significantly reduced in mice lacking MKK6 to the level of the WT mice (Figure 9D). No fibrosis development was observed at the end of the training. Interestingly, swimming reduced fibrosis levels in both genotypes (Supplementary Figure 3). Although the cardiac function was similar in the swimming-trained *Mkk6*$^{-/-}$ and WT mice, the *Mkk6*$^{-/-}$ mice mortality due to chronic endurance training was increased. All mice died suddenly in the swimming training or just after the exercise (Figure 9E).

In order to understand the increased predisposition to sudden cardiac death observed in *Mkk6*$^{-/-}$ mice, an RNASeq was perform comparing WT and *Mkk6*$^{-/-}$ cardiac gene expression at 9 weeks of age. The principal Top Tox Function identified was Cardiac Arrhythmia, and within Cardiac Arrhythmia, Long QT syndrome was the most significant (Figure 10A&B). Moreover Long QT Syndrome has been associated with increased predisposition to sudden cardiac death and is known to be cause by mutations in cardiac ion channels [18]. Then, we confirmed that the mRNA expression of several cardiac ion channels involved in Long QT Syndrome was altered in *Mkk6*$^{-/-}$ hearts compared with control hearts in basal condition (Figure 10C). ECG studies showed no differences between genotypes in basal condition. After the endurance exercise training, a similar increase in the PR segment length was observed in WT and *Mkk6*$^{-/-}$ trained mice. However, the interbeat in terval and QT interval were significantly longer in mice lacking MKK6 compared to control mice after the 3 weeks of swimming training (Figure 11). This indicates that MKK6 deficiency leads to bradichardia and predisposes to the prolongation of the Long QT interval and cardiac sudden death upon endurance exercise training.

DISCUSION

A proper heart size is critical to maintain body homeostasis, therefore, derangements in cardiac growth can lead to the development of different cardiomyopathies. The heart needs to grow during development to meet the demand of blood flow to the growing body, and this growth is achieved through proliferation during the fetal stages. But soon after birth, cardiomyocytes withdraw from cell cycle and the rest of the postnatal cardiac increase in size is through cardiomyocyte hypertrophy. Furthermore, cardiac hypertrophy is also an adaptive response that occurs throughout life in response to changes in blood pressure and circulatory resistance. However, when the hypertrophic stimuli are sustained in time, it can become pathological. Chronic hypertension associated to cardiovascular diseases can lead to pathological hypertrophy and heart failure. On the other hand, exercise training is the only chronic stimulus that in most cases leads to physiological hypertrophy characterized by normal or increased cardiac function. However, a low percentage of athletes that undergo high-intensity exercise training, progress into heart disease or suffer sudden cardiac death.

The present study provides several independent lines of evidence to support a critical role of the MKK3/6–p38γ/δ signaling pathway in the development of physiological cardiac hypertrophy with increased predisposition to sudden cardiac death upon endurance exercise training. As documented via using different knockout mouse models, in the absence of MKK6 the MKK3- p38γ/δ kinases become hyperactivated, which induce enhanced postnatal hypertrophic growth through the mTOR pathway. The hypertrophy developed is physiological, with normal or even increased cardiac function in basal condition, but associated to altered expression of cardiac ion channels. Under stress conditions such as endurance exercise training, these mice develop long QT syndrome and show increased sudden cardiac death. Moreover, we have described that the two main p38 up-stream activators present a strong specificity towards the activation of the different p38 MAPK isoforms in the heart, being p38γ/δ mainly regulated by MKK3, and p38α by MKK6 at least in homeostatic conditions.

The p38 MAPK pathway has been previously associated with the regulation of cardiac hypertrophic growth. While p38α and p38β have been involved in pathological cardiac hypertrophy in different disease models, p38γ and p38δ seem to be involved in the regulation of physiological cardiac growth during development but also pathological hypertrophy in response to angiotensin-II treatment. However, how the activation of the different p38 MAPK isoforms is regulated in this context has not been previously addressed. Likewise, the involvement of MKK3 and MKK6 in cardiac hypertrophy was still controversial. On the one hand, several studies reported that the overexpression of the constitutive active form of MKK3 and MKK6 in cardiomyocytes *in vitro* leads to hypertrophic growth [36, 44]. On the other hand, it has been also shown that the overexpression of the MKK3 and MKK6 dominant negatives drives cardiac hypertrophy [4]. Our data agrees with the idea that MKK3 promotes hypertrophic growth. We show that the hyperactivation of MKK3 leads to cardiac hypertrophy, and its deficiency alters the hypertrophic growth process. Furthermore, our studies also support the fact that both, the hyperactivation and deficiency of MKK6 in cardiomyocytes, could lead to cardiac hypertrophy. This can be explained by the involvement of MKK6 in the promotion of cardiac hypertrophy at the same time that exerts a negative feedback up-stream the signaling pathway. The negative feedback could be done directly by MKK6, or by p38α, whose phosphorylation levels are strongly decreased in *Mkk6*$^{-/-}$ hearts. Negative regulation of the MAP3K TAK1 by p38α

has been reported in other cell types, but the fact that cardiac-specific p38α conditional mice do not have cardiac basal phenotype does not support this hypothesis [29]. The negative feedback would also explain why in the absence of MKK6, MKK3 becomes hyperphosphorylated. Although this hypothesis could explain as well how the dnMKK6 overexpression causes cardiac hypertrophy, it does not clarify the reasons why dnMKK3 causes hypertrophy. It is true that the overexpression of dominant negative forms does not inhibit the scaffold functions of the kinase. Besides, it is an indirect form to inhibit the endogenous kinase function that could affect other signaling molecules. The activation of the different p38 MAPK cardiac isoforms has not been characterized in these models, and no studies have been performed to this date in the specificity of the MKK3 and MKK6 towards the p38 MAPKs in the heart. We show that MKK3 preferentially regulates p38γ and p38δ activation, while MKK6 is responsible for p38α regulation.

MKK6 mice present hyperactive p38γ/δ and reduced p38α activation, therefore any of these isoforms could be involved in the phenotype observed. It has been shown that p38α cardiac-specific knockout mice do not present a basal cardiac phenotype. Furthermore, p38α has been involved in the regulation of apoptosis, but does not control hypertrophy in an aortic constriction model [29]. We demonstrate that hyperphosphorylated MKK3 promotes cardiac hypertrophic growth through the activation p38γ and p38δ, which in turn increase mTOR signaling in the heart. This agrees with the previous reports from our group that point out an essential role of p38γ and p38δ in the promotion of physiological and pathological cardiac hypertrophy, through the mTOR pathway [14]. We further corroborate this conclusion, firstly by showing that the double deficiency in MKK6 and p38γ or p38δ in the heart reverts the cardiac hypertrophy observed in MKK6 deficient mice. Secondly, the treatment with Rapamycin, an mTOR specific inhibitor, in MKK6 mice during the early postnatal cardiac development leads to a strong reduction in heart size to the same level that control hearts. In correlation, MKK3 deficient mice show decreased p38γ and p38δ activation and reduced postnatal hypertrophic growth.

p38γ and p38δ control of cardiac hypertrophy during postnatal cardiac development is cell autonomous [14]. Accordingly, the lack of MKK6 in skeletal striated muscle or in cardiomyocytes renders a similar phenotype to the full knockout mice. Furthermore, the lack of p38δ specifically in the striated muscle is sufficient to revert the enhanced

cardiac hypertrophic growth to the same size as the p38δ^{MCK-KO} mice, indicating that cardiac p38δ is downstream MKK6 in the signaling pathway controlling the hypertrophic growth. Notably, p38δ reversion of MKK6 phenotype is stronger than the reversion achieved with p38γ. This agrees with the already reported dominant role of p38δ in the regulation of cardiac hypertrophic growth [14].

The hypertrophic response can broadly be classified as either physiological or pathological. The *Mkk6*$^{-/-}$ hearts develop a physiological hypertrophy based on the distinctive characteristics of both types of hypertrophic growth. The increase in heart size is proportional, left ventricle walls are thicker, but at the same time the left ventricle internal diameter is wider, therefore the normal cardiac structure is maintained. Moreover, the cardiac function is normal with increased cardiac output and stroke volume. Finally, no fibrosis development or fetal gene up-regulation is observed. Although the expression level of several cardiac ion channels is altered in *Mkk6*$^{-/-}$ hearts, in basal condition the ECG in these mice is normal and no arrhythmias are detected. However, after endurance exercise training during 3 weeks, *Mkk6*$^{-/-}$ mice develop long QT syndrome and show increased sudden cardiac death. It is known that pathologic cardiac hypertrophy alters ion channel coupling and is a risk factor for QT-prolongation and cardiac sudden death [12, 17, 38], however it is thought that physiological hypertrophy is benign and is not associated with increased mortality. Although is not frequent, a small percentage of elite athletes die from cardiac sudden death. Some of them suffered from mild congenital hypertrophic cardiomyopathies that are wrongly diagnosed as Athlete's heart. It would be of interest to study whether there is an association in athletes between the initial physiologic heart size, and the probability to die from sudden cardiac death when they have already become athletes and whether they carry mutations in the MKK3/6-p38γ/δ pathway.

Our results identified the MKK3/6- p38γ/δ as new genetic pathway involved in physiological cardiac hypertrophy. However, the cardiac hyperactivation of MKK3 and p38γ and p38δ is associated with an increased risk to develop long QT syndrome and to suffer sudden cardiac death upon chronic exercise training.

MATERIALS AND METHODS

Mice

Mkk3$^{-/-}$ (B6.129-*Map2k3*^{tm1Flv}) [21, 41] and *Mkk6*$^{-/-}$ (B6.129-*Map2k6*^{tm1Flv}) mice [37] were as previously described [3]. Mice with a germ-line mutation in the *Map2k6* gene with *LoxP* elements inserted into two different introns (*Map2k6*^{LoxP}) were constructed by using homologous recombination in ES cells. ES cells were electroporated with this vector (Figure 4A) and selected with 200 μg/ml G418 and 2 μM gangcyclovir. Several correctly targeted ES cell clones were identified by Southern blot analysis and PCR analysis. These ES cell clones were injected into C57BL/6J blastocysts to create chimeric mice that transmitted the mutated *Map2k6* allele through the germ line. The Flp *Neo*^{R} cassette was excised by crossing these mice with ACTB:FLPe B6;SJL that expresses a *FLP1* recombinase gene under the direction of the human *ACTB* promoter. The *Map2k6*^{LoxP} mice were maintained on a C57BL/6J mouse strain background (back-crossed 10 generations). To generate mice lacking MKK6 or p38δ in striated muscle, *Map2k6*^{LoxP} or p38δ (B6.129-Mapk13tm1) mice were crossed with the FVB-Tg(Ckmm-cre)5Khn/J line on the C57BL/6J background (Jackson Laboratory). Mice lacking MKK6 in cardiomyocytes were generated by crossing *Map2k6*^{LoxP} mice with the Tg(Myh6-cre)2182Mds line on the C57BL/6J background (Jackson Laboratory). p38γ (B6.129-Mapk12tm1) line was crossed with the *Mkk6*$^{-/-}$ (B6.129-*Map2k6*^{tm1Flv}) line to generate double knockout mice. Likewise, mice lacking p38δ in striated muscle were crossed with the *Mkk6*$^{-/-}$ (B6.129-*Map2k6*^{tm1Flv}) line. Genotype was confirmed by PCR analysis of genomic DNA. For signaling studies, animals were killed by cervical dislocation. For rapamycin treatment, mice were daily injected intraperitoneally with rapamycin (LC Laboratories, R-5000) (2 mg kg−1 per day) or vehicle (0.25% polyethylene glycol (Sigma), 0.25% Tween-20 (Sigma) in PBS); injections started at 4 weeks of age and continued until 9 weeks of age, when heart size was analyzed by echocardiography and mice were killed. All animal procedures conformed to EU Directive 86/609/EEC and Recommendation 2007/526/EC regarding the protection of animals used for experimental and other scientific purposes, enacted under Spanish law 1201/2005.

Histology

Tissue samples were fixed in 10% formalin for 48 h, dehydrated and embedded in paraffin. Sections (8 μm) were cut and stained with haematoxylin and eosin (American

Master Tech Scientific). Fibrosis was assessed with Picrosirius red staining (Sigma). For wheat germ agglutinin (WGA) immunofluorescence, 8 μm heart sections were prepared, washed in PBS, incubated over-night in WGA-Alexa 488 lectin (Invitrogen, Carlsbad, CA, USA), and washed and mounted in anti-fade reagent. Four images (× 20) were taken from each heart, and the diameter and areas of 100–200 cross-sectionally oriented myocytes were measured and analysed with Image J software.

Echocardiography

Mice were anaesthetized by inhalation of isoflurane and oxygen (1.25% and 98.75%, respectively), and echocardiography was performed with a 30-MHz transthoracic echocardiography probe. Images were obtained with the Vevo 2100 micro-ultrasound imaging system (VisualSonics, Toronto, Canada). Short-axis, long-axis, B-mode and two-dimensional M-mode views were obtained. In summary, scans were conducted by two experienced researchers blinded to the mouse genotype. Measurements of left parasternal long and short axes and M-mode (left parasternal short axis) images were obtained at a heart rate of 500–550 b.p.m. LV end-diastolic diameter (LVEDD), LV end-systolic diameter (LVESD) and wall thickness were measured from M-mode tracings, and the average of three consecutive cardiac cycles is reported. The LV fractional shortening percentage was calculated as ([LVEDD−LVESD]/LVEDD) × 100 MRI of lung was performed with a 7-T Agilent scanner (Agilent, Santa Clara, CA, USA) equipped with a DD2 console and an actively shielded gradient set (205/120 insert of maximum 130 mT m−1 gradient strength). For image acquisition, we used a combination of volume coil/surface coil coil to enhance signal-to-noise ratio formed by a 72-mm inner diameter quadrature birdcage TX coil (Rapid Biomedical GmBH, Germany) and an actively detuning 30-mm flexible customized surface RX coil (Neos Biotec, Pamplona, Spain). Following a tripilot gradient-echo image, a gradient-echo sequence without gating was used to acquire oblique coronal slices (one to two slices) and axial slices (7–10 slices covering the entire lung, 72-s acquisition time per slice) using the following parameters: TR/TE=6.7/2.2 ms, flip angle=10 degree, bandwidth=100 kHz, field of view=3 × 3 cm, matrix=256 × 128, slice thickness=1 mm (ref. 40). From these images, interventricular septum and left ventricle posterior wall thicknesses and left ventricle corrected mass were determined; the short-axis M-mode quantification was chosen as the most representative. Function was estimated from the ejection fraction and fractional shortening obtained from M-mode views by a blinded

echocardiography expert. For ejection fraction measurements, a long- or short-axis view of the heart was selected to obtain an M-mode registration in a line perpendicular to the left ventricular septum and posterior wall at the level of the mitral chordae tendinea.

Immunoblot analysis

Tissue extracts were prepared in Triton lysis buffer (20 mM Tris (pH 7.4), 1% Triton X-100, 10% glycerol, 137 mM NaCl, 2 mM EDTA, 25 mM β -glycerophosphate, 1 mM sodium orthovanadate, 1 mM phenylmethylsulfonyl fluoride, and 10 μg ml−1 of aprotinin and leupeptin). Extracts (20–50 μg protein) and immunoprecipitates (prepared from 0,5-2mg) were examined by immunoblot. For the immunoprecipitation assay, heart extracts were incubated with 4 μg of a specific antibody coupled to protein-G-Sepharose. After incubation overnight at 4 °C with agitation, the captured proteins were centrifuged at 10,000g, the supernatants collected, and the beads washed four times in lysis buffer. Beads were boiled for 5 min 95 °C in 10 μl sample buffer. Extracts and immunoprecipitates were examined by SDS–PAGE and blotted with antibodies to the following targets: p38γ and p38δ (refs 41, 42) at 1 μg ml−1; vinculin (Sigma); puromycin (Millipore clone 12D10); and phospho-MKK3/6, MKK3, MKK6, phospho-p38, phospho-mTOR (Ser2481), mTOR, phospho-p70S6 kinase, p70S6 kinase, phospho-S6 (Ser 235/236), phospho-S6 (Ser 240/244), S6 ribosomal protein, phospho-FOXO1/3a, phospho-eEF2, eEF2, phospho-EIF4E, EIF4E, phospho-EIF4G, EIF4G, phospho-EIF4B, EIF4B, phospho-4EBP1, 4EBP1 (Cell Signaling) all were used at 1:1,000. Immunocomplexes were detected by enhanced chemiluminescence (GE Healthcare Lifesciences).

Cell lines and cell culture

Immortalized mouse embryonic fibroblasts from WT mice, *Mkk3*$^{-/-}$ and *Mkk6*$^{-/-}$ mice (were cultured in DMEM supplemented with 10% heat-inactivated fetal bovine serum (FBS; Sigma), glutamine (2 mM) and penicillin/streptomycin (100 μg ml−1).

***In vivo* protein synthesis assay**

For all *in vivo* measurements of protein synthesis, mice were injected intraperitoneally with 0.040 μmol g−1 puromycin dissolved in 100 μl PBS. Exactly 30 min after injection, tissues were extracted and frozen in liquid nitrogen for subsequent immunoblot analysis of protein-incorporated puromycin.

Blood pressure measurement

Blood pressure in mice was measured using the non-invasive tail-cuff method48.

qRT-PCR

The expression of mRNA was examined by qRT-PCR using a 7900 Fast Real Time thermocycler and FAST SYBR GREEN assays (Applied Biosystems). Relative mRNA expression was normalized to *Gapdh* mRNA measured in each sample. *p21* Fw: CCTGGTGATGTCCGACCTG, Rev: CCATGAGCGCATCGCAATC , *Rb* Fw: TGCATCTTTATCGCAGCAGTT, Rev: GTTCACACGTCCGTTCTAATTTG *Fn1* Fw: ATGTGGACCCCTCCTGATAGT, Rev: GCCCAGTGATTTCAGCAAAGG;, *Col1a1* Fw: GCTCCTCTTAGGGGCCACT, Rev: CCACGTCTCACCATTGGGG;, *Col3a1* Fw: CTGTAACATGGAAACTGGGGAAA, Rev: CCATAGCTGAACTGAAAACCACC;, *Nppa* Fw: GCTTCCAGGCCATATTGGAG, Rev: GGGGGCATGACCTCATCTT , *Nppb* Fw: GAGGTCACTCCTATCCTCTGG, Rev: GCCATTTCCTCCGACTTTTCTC, *Acta-2* Fw: CCCAAAGCTAACCGGGAGAAG, Rev: CCAGAATCCAACACGATGCC;, *Myh7* Fw: ACTGTCAACACTAAGAGGGTCA, Rev: TTGGATGATTTGATCTTCCAGGG; , *Kcnh2* Fw: GTGCTGCCTGAGTATAAGCTG; Rev: CCGAGTACGGTGTGAAGACT; *Scn5a* Fw: ATGGCAAACTTCCTGTTACCTC, Rev: CCACGGGCTTGTTTTTCAGC; *Ank2* Fw: AGATTACTGTGCAGCATAACAGG, Rev: TGGTTGTAAAGGAAACACACTCA;, *Cav3* Fw: GGATCTGGAAGCTCGGATCAT, Rev: TCCGCAATCACGTCTTCAAAAT; *Kcnj2* Fw: ATGGGCAGTGTGAGAACCAAC, Rev: TGGACTTTACTCTTGCCATTCC.

Endurance exercise training

Swimming training was performed as previously described [6] with some modifications. Mice swam in water at a depth of 25 cm in a glass container (60×30×45 cm) at 30 to 32ºC. The animals were progressively familiarized with swimming during the first 2 weeks by increasing each swimming session time by 10 min per day, and held at 90 min per session until the end of the training. The first swimming session started at 12.30 pm and four hours of rest were left between sessions. Mice were allowed to swim at their

own pace, and the water was gently bubbled to ensure that mice swam rather than floating.

	Time (min)						
Week 1	10'+10'	20'+20'	30'+30'	40'+40'	50'+50'	0	0
Week 2	60'+60'	70'+70'	80'+80'	90'+90'	90'+90'	90'+90'	90'+90'
Week 3	90'+90'	90'+90'	90'+90'	90'+90'	90'+90'	90'+90'	90'+90'
Week 4	90'+90'	90	90	90	90	90'+90'	90'+90'
Week 5	90	90	90	90'+90'	END		

Electrocardiographic Recordings

Mice were lightly anaesthetized using 1.5% isoflurane in 95% oxygen. Baseline ECG was recorded for 5 min and at the end of the endurance training protocol. Response to toe-pinch reflex was examined to ensure the proper level of anesthesia.

Statistical analysis

Differences between groups were examined for statistical significance by two-tailed Student's t-test, one-way or two-way analysis of variance coupled to the Bonferroni post-test. Survival was analyzed with Kruskal-Wallis test.

ACKNOWLEDGEMENTS

We thank S. Bartlett for English editing, F. Cruz and J.A. Bernal for their help with swimming training protocol, A. Molina for histological analysis. We are grateful to R.J. Davis for critical reading of the manuscript. We thank the staff at the CNIC Genomics and Bioinformatics units for technical support and help with data analysis. G.S. is an investigator of the Ramón y Cajal Program. B.G.T. is a fellow of FPI Severo Ochoa CNIC Program (SVP-2013-067639). This work was funded by the following grants to G.S.: ERC 260464, EFSD 2030, MICINN SAF2010-19347, and Comunidad de Madrid S2010/BMD-2326. The CNIC is supported by the Ministerio de Economía y Competitividad and the Pro-CNIC Foundation.

FIGURE LEDGENDS

Figure 1. *Mkk6*$^{-/-}$ hearts are hypertrophic.

Cardiac phenotype from WT and *Mkk6*$^{-/-}$ was studied at 9 weeks. (**a**) Hearts and hematoxylin and eosin-stained cardiac longitudinal sections of wild-type (WT) and *Mkk6*$^{-/-}$ mice. (**b**) Heart-weight-to-tibia-length ratio at the indicated time points. (**c**) Bottom. Hematoxylin and eosin-stained sections from 9 weeks-old WT and *Mkk6*$^{-/-}$ mice. Top: Cardiomyocyte cross-sectional area quantified in FITC wheat germ agglutinin (FITC-WGA)-stained hearts. (**d**) Echocardiography results for 9-week-old WT and MKK6$^{-/-}$ mice. LV Mass (Left ventricle mass), LVID;d (Left ventricle internal diameter in diastole), LVPW;d (left ventricle posterior wall in diastole); IVS;d (inter-ventricular septum in diastole). (**e**) Cardiac function measured by echocardiography. Data are means±s.e.m. (n=5–13). *P<0.05; **P<0.01; ***P<0.001 (one-way ANOVA coupled to Bonferroni post tests or t-test).

Figure 2. MKK6 is necessary for p38α activation and MKK3 for p38γ and p38δ in the heart.

(**a-d**) p38 MAPK signaling pathway in WT and *Mkk6*$^{-/-}$ heart lisates was analyzed at 9 weeks. (**a, b**) Immunoprecipitation analysis of the phosphorylation and protein levels of p38γ and δ isoforms respectively in heart extracts. (**c**) Immunoblot analysis of the p38α phosphorylation and protein levels. (**d**) Phosphorylation and protein levels of MKK3 and MKK6 in cardiac lysates. (**e**) Heart-weight-to-tibia-length ratio at the indicated time

points from WT and *Mkk3*$^{-/-}$ mice. (f) Immunoprecipitation analysis of the phosphorylation and protein levels of p38α, p38γ and p38δ isoforms in heart extracts from 9 week-old WT and *Mkk3*$^{-/-}$ Data are means±s.e.m. (n=4–6). *P<0.05; (one-way ANOVA coupled to Bonferroni post tests).

Figure 3. Hearts from *Mkk6*$^{-/-}$ mice show increased mTOR activation.

(**a**,**b**) Immunoblot analysis of mTOR signaling pathway activity (**a**) and the activation status of translation factors (**b**) in heart lysates of 9-week-old WT and *Mkk6*$^{-/-}$ mice. (**c**) Protein content from WT and *Mkk6*$^{-/-}$ hearts measured as the protein-DNA ratio. (**d**) *In vivo* measurement of protein synthesis. Mice were injected intraperitoneally with 0.040 µmol g^{-1} puromycin dissolved in 100 µl PBS. Exactly 30 min after injection, tissues were extracted and frozen in liquid nitrogen for immunoblot analysis with anti-puromycin antibody (n=3-4).

Figure 4. Striated Muscle MKK6 controls postnatal heart growth.

The cardiac phenotype from MCK-Cre and MKK6^{MCK-KO} mice was studied at 9 weeks. (**a**) Schematic view of the generation of the MKK6^{MCK-KO} conditional knockout mice. (**b**) Deletion of MKK6 in tissue lysates from MCK-Cre and MKK6^{MCK-KO} (K) mice in quadriceps (Q), gastronemius (G), Soleus (S) and Heart (H). (**c**) Heart-weight-to-tibia-length ratio. (**d**) Hematoxylin and eosin-stained cardiac transversal sections of wild-type (WT) and MKK6$^{-/-}$ mice. (**e**) Cardiomyocyte cross-sectional area quantified in FITC wheat germ agglutinin (FITC-WGA)-stained hearts. (**f**) Fibrosis development analyzed with picrosirius red staining. Data are means±s.e.m. (n=4-8). *P<0.05 (t-test).

Figure 5. Cardiomyocyte MKK6 controls postnatal heart growth.

The cardiac phenotype from αMHC-Cre and MKK6$^{αMHC-KO}$ mice was studied at 9 weeks. (**a**) Specific deletion of MKK6 in tissue lysates from αMHC-Cre (C) and MKK6$^{αMHC-KO}$ (K) mice in heart (H), muscle (M), kidney (K), spleen (S), brain (B), liver (L), white fat (WF) and brown fat (BF). (**b**) Heart-weight-to-tibia-length ratio. (**c**) Hematoxylin and eosin-stained cardiac transversal sections. (**d**) Cardiomyocyte cross-sectional area quantified in FITC wheat germ agglutinin (FITC-WGA)-stained hearts. (**e**) Fibrosis development analyzed with picrosirius red staining. Data are means±s.e.m. (n=3-7). *P<0.05 (t-test).

Figure 6. p38γ is downstream MKK6 in the regulation of cardiac hypertrophy.

The cardiac phenotype from WT and *Mkk6*$^{-/-}$ p38γ$^{-/-}$ mice was studied at 9 weeks. **(a)** Heart-weight-to-tibia-length ratio from WT, *Mkk6*$^{-/-}$ and *Mkk6*$^{-/-}$ p38γ$^{-/-}$ mice. (**b**) Hematoxylin and eosin-stained cardiac transversal sections. (**c**) Cardiomyocyte cross-sectional area quantified in FITC wheat germ agglutinin (FITC-WGA)-stained hearts. Data are means±s.e.m. (n=5-10). **P<0.01 (t-test).

Figure 7. p38δ is downstream MKK6 in the regulation of cardiac hypertrophy.

The cardiac phenotype from MCK-Cre and *Mkk6*$^{-/-}$, p38δ$^{MCK\text{-}KO}$ and *Mkk6*$^{-/-}$ p38δ$^{MCK\text{-}KO}$ mice was studied at 9 weeks. **(a)** Heart-weight-to-tibia-length ratio. (**b**) Hematoxylin and eosin-stained cardiac transversal sections. (**c**) Cardiomyocyte cross-sectional area quantified in FITC wheat germ agglutinin (FITC-WGA)-stained hearts. Data are means±s.e.m. (n=5-10). *P<0.05; ***P<0.001 (one-way ANOVA coupled to Bonferroni post tests).

Figure 8. *Mkk6*$^{-/-}$ control heart growth by modulating mTOR activity.

(a-c) WT and *Mkk6*$^{-/-}$ mice were intraperitoneally injected daily with rapamycin (2 mg kg^{-1} per day) or vehicle from 4 to 9 weeks of age. (**a**) Heart-weight-to-tibia-length ratio. (**b**) Representative H&E stained transverse heart sections after treatment. (**c**) Cardiomyocyte cross-sectional area quantified in FITC wheat germ agglutinin (FITC-WGA)-stained hearts. Data are means±s.e.m. (n=5). *P<0.05; **P<0.01; ***P<0.001 (one-way analysis of variance coupled to Bonferroni post test).

Figure 9. *Mkk6*$^{-/-}$ mice show increased susceptibility to sudden cardiac death upon endurance training.

WT and *Mkk6*$^{-/-}$ mice were swimming trained during 3 weeks and a sedentary group was used as control. (**a**) Heart-weight-to-tibia-length ratio. (**b**) Representative H&E stained transverse heart sections after treatment. (**c**) Cardiomyocyte cross-sectional area quantified in FITC wheat germ agglutinin (FITC-WGA)-stained hearts. (**d**) Echocardiography results for 9-week-old WT and *Mkk6*$^{-/-}$ after the training program. LV Mass (Left ventricle mass). (**e**) Percentage of survival during the training program. Data are means±s.e.m. (n=5). *P<0.05; **P<0.01; ***P<0.001 (one-way analysis of variance coupled to Bonferroni post test or Kapplan-Meier survival analysis).

Figure 10. *Mkk6*$^{-/-}$ mice resent altered cardiac ions channels expression associated with Long QT Syndrome.

(**a-b**) Genes differentially expressed between WT and *Mkk6*$^{-/-}$ -9 week-old mice involved in (**a**) Top Tox Functions, and specifically in (**b**) Arrythmia. (**c**) Cardiac Ion Channel gene expression from WT and *Mkk6*$^{-/-}$ -9 week-old mice. Data are means±s.e.m. (n=4). **P*<0.05; ***P*<0.01; ****P*<0.001 (t-test analysis).

Figure 11. Endurance training caused a greater increase in the QT interval from *Mkk6*$^{-/-}$ mice.

Electrocardiograms were recorded from WT and *Mkk6*$^{-/-}$ sedentary and trained groups after the training program was completed**.** Data are means±s.e.m. (n=8-5). ***P*<0.01; (one-way analysis of variance coupled to Bonferroni post test).

REFERENCES

1. Arai, M., et al., *Endothelin-1 and its binding sites are upregulated in pressure overload cardiac hypertrophy.* Am J Physiol, 1995. **268**(5 Pt 2): p. H2084-91.
2. Baines, C.P. and J.D. Molkentin, *STRESS signaling pathways that modulate cardiac myocyte apoptosis.* J Mol Cell Cardiol, 2005. **38**(1): p. 47-62.
3. Brancho, D., et al., *Mechanism of p38 MAP kinase activation in vivo.* Genes Dev, 2003. **17**(16): p. 1969-78.
4. Braz, J.C., et al., *Targeted inhibition of p38 MAPK promotes hypertrophic cardiomyopathy through upregulation of calcineurin-NFAT signaling.* J Clin Invest, 2003. **111**(10): p. 1475-86.
5. Bruning, J.C., et al., *A muscle-specific insulin receptor knockout exhibits features of the metabolic syndrome of NIDDM without altering glucose tolerance.* Mol Cell, 1998. **2**(5): p. 559-69.
6. Cruz, F.M., et al., *Exercise triggers ARVC phenotype in mice expressing a disease-causing mutated version of human plakophilin-2.* J Am Coll Cardiol, 2015. **65**(14): p. 1438-50.
7. Cuenda, A., et al., *Purification and cDNA cloning of SAPKK3, the major activator of RK/p38 in stress- and cytokine-stimulated monocytes and epithelial cells.* EMBO J, 1996. **15**(16): p. 4156-64.
8. Cuenda, A., et al., *Activation of stress-activated protein kinase-3 (SAPK3) by cytokines and cellular stresses is mediated via SAPKK3 (MKK6); comparison of the specificities of SAPK3 and SAPK2 (RK/p38).* EMBO J, 1997. **16**(2): p. 295-305.
9. Cuenda, A. and S. Rousseau, *p38 MAP-kinases pathway regulation, function and role in human diseases.* Biochim Biophys Acta, 2007. **1773**(8): p. 1358-75.
10. del Barco Barrantes, I., et al., *Genetic analysis of specific and redundant roles for p38alpha and p38beta MAPKs during mouse development.* Proc Natl Acad Sci U S A, 2011. **108**(31): p. 12764-9.
11. Derijard, B., et al., *Independent human MAP-kinase signal transduction pathways defined by MEK and MKK isoforms.* Science, 1995. **267**(5198): p. 682-5.

12. Frenneaux, M.P., *Assessing the risk of sudden cardiac death in a patient with hypertrophic cardiomyopathy.* Heart, 2004. **90**(5): p. 570-5.
13. Futterman, L.G. and R. Myerburg, *Sudden death in athletes: an update.* Sports Med, 1998. **26**(5): p. 335-50.
14. Gonzalez-Teran, B., et al., *p38gamma and delta promote heart hypertrophy by targeting the mTOR-inhibitory protein DEPTOR for degradation.* Nat Commun, 2016. **7**: p. 10477.
15. Gupta, J. and A.R. Nebreda, *Roles of p38alpha mitogen-activated protein kinase in mouse models of inflammatory diseases and cancer.* FEBS J, 2015. **282**(10): p. 1841-57.
16. Huikuri, H.V., A. Castellanos, and R.J. Myerburg, *Sudden death due to cardiac arrhythmias.* N Engl J Med, 2001. **345**(20): p. 1473-82.
17. Kahan, T. and L. Bergfeldt, *Left ventricular hypertrophy in hypertension: its arrhythmogenic potential.* Heart, 2005. **91**(2): p. 250-6.
18. Kang, Y.J., *Cardiac hypertrophy: a risk factor for QT-prolongation and cardiac sudden death.* Toxicol Pathol, 2006. **34**(1): p. 58-66.
19. Landstrom, A.P. and M.J. Ackerman, *Beyond the cardiac myofilament: hypertrophic cardiomyopathy- associated mutations in genes that encode calcium-handling proteins.* Curr Mol Med. **12**(5): p. 507-18.
20. Liao, P., et al., *The in vivo role of p38 MAP kinases in cardiac remodeling and restrictive cardiomyopathy.* Proc Natl Acad Sci U S A, 2001. **98**(21): p. 12283-8.
21. Lu, H.T., et al., *Defective IL-12 production in mitogen-activated protein (MAP) kinase kinase 3 (Mkk3)-deficient mice.* EMBO J, 1999. **18**(7): p. 1845-57.
22. Manieri, E. and G. Sabio, *Stress kinases in the modulation of metabolism and energy balance.* J Mol Endocrinol, 2015. **55**(2): p. R11-22.
23. McFadden, D.G., et al., *The Hand1 and Hand2 transcription factors regulate expansion of the embryonic cardiac ventricles in a gene dosage-dependent manner.* Development, 2005. **132**(1): p. 189-201.
24. McMullen, J.R. and G.L. Jennings, *Differences between pathological and physiological cardiac hypertrophy: novel therapeutic strategies to treat heart failure.* Clin Exp Pharmacol Physiol, 2007. **34**(4): p. 255-62.

25. McMullen, J.R., et al., *The insulin-like growth factor 1 receptor induces physiological heart growth via the phosphoinositide 3-kinase(p110alpha) pathway.* J Biol Chem, 2004. **279**(6): p. 4782-93.
26. McMullen, J.R., et al., *Deletion of ribosomal S6 kinases does not attenuate pathological, physiological, or insulin-like growth factor 1 receptor-phosphoinositide 3-kinase-induced cardiac hypertrophy.* Mol Cell Biol, 2004. **24**(14): p. 6231-40.
27. Muslin, A.J., *MAPK signalling in cardiovascular health and disease: molecular mechanisms and therapeutic targets.* Clin Sci (Lond), 2008. **115**(7): p. 203-18.
28. Neri Serneri, G.G., et al., *Increased cardiac sympathetic activity and insulin-like growth factor-I formation are associated with physiological hypertrophy in athletes.* Circ Res, 2001. **89**(11): p. 977-82.
29. Nishida, K., et al., *p38alpha mitogen-activated protein kinase plays a critical role in cardiomyocyte survival but not in cardiac hypertrophic growth in response to pressure overload.* Mol Cell Biol, 2004. **24**(24): p. 10611-20.
30. Petrich, B.G. and Y. Wang, *Stress-activated MAP kinases in cardiac remodeling and heart failure; new insights from transgenic studies.* Trends Cardiovasc Med, 2004. **14**(2): p. 50-5.
31. Rapacciuolo, A., et al., *Important role of endogenous norepinephrine and epinephrine in the development of in vivo pressure-overload cardiac hypertrophy.* J Am Coll Cardiol, 2001. **38**(3): p. 876-82.
32. Scheinowitz, M., et al., *Short- and long-term swimming exercise training increases myocardial insulin-like growth factor-I gene expression.* Growth Horm IGF Res, 2003. **13**(1): p. 19-25.
33. Schunkert, H., et al., *Increased rat cardiac angiotensin converting enzyme activity and mRNA expression in pressure overload left ventricular hypertrophy. Effects on coronary resistance, contractility, and relaxation.* J Clin Invest, 1990. **86**(6): p. 1913-20.
34. Shioi, T., et al., *The conserved phosphoinositide 3-kinase pathway determines heart size in mice.* EMBO J, 2000. **19**(11): p. 2537-48.
35. Shioi, T., et al., *Rapamycin attenuates load-induced cardiac hypertrophy in mice.* Circulation, 2003. **107**(12): p. 1664-70.
36. Streicher, J.M., et al., *MAPK-activated protein kinase-2 in cardiac hypertrophy and cyclooxygenase-2 regulation in heart.* Circ Res, 2010. **106**(8): p. 1434-43.

37. Tanaka, N., et al., *Differential involvement of p38 mitogen-activated protein kinase kinases MKK3 and MKK6 in T-cell apoptosis.* EMBO Rep, 2002. **3**(8): p. 785-91.
38. ten Eick, R.E., D.W. Whalley, and H.H. Rasmussen, *Connections: heart disease, cellular electrophysiology, and ion channels.* FASEB J, 1992. **6**(8): p. 2568-80.
39. von Harsdorf, R., et al., *E2F-1 overexpression in cardiomyocytes induces downregulation of p21CIP1 and p27KIP1 and release of active cyclin-dependent kinases in the presence of insulin-like growth factor I.* Circ Res, 1999. **85**(2): p. 128-36.
40. Wang, Y., *Mitogen-activated protein kinases in heart development and diseases.* Circulation, 2007. **116**(12): p. 1413-23.
41. Wysk, M., et al., *Requirement of mitogen-activated protein kinase kinase 3 (MKK3) for tumor necrosis factor-induced cytokine expression.* Proc Natl Acad Sci U S A, 1999. **96**(7): p. 3763-8.
42. Yamazaki, T., I. Komuro, and Y. Yazaki, *Role of the renin-angiotensin system in cardiac hypertrophy.* Am J Cardiol, 1999. **83**(12A): p. 53H-57H.
43. Yayama, K., et al., *Up-regulation of angiotensin II type 2 receptor in rat thoracic aorta by pressure-overload.* J Pharmacol Exp Ther, 2004. **308**(2): p. 736-43.
44. Zechner, D., et al., *A role for the p38 mitogen-activated protein kinase pathway in myocardial cell growth, sarcomeric organization, and cardiac-specific gene expression.* J Cell Biol, 1997. **139**(1): p. 115-27.

FIGURES

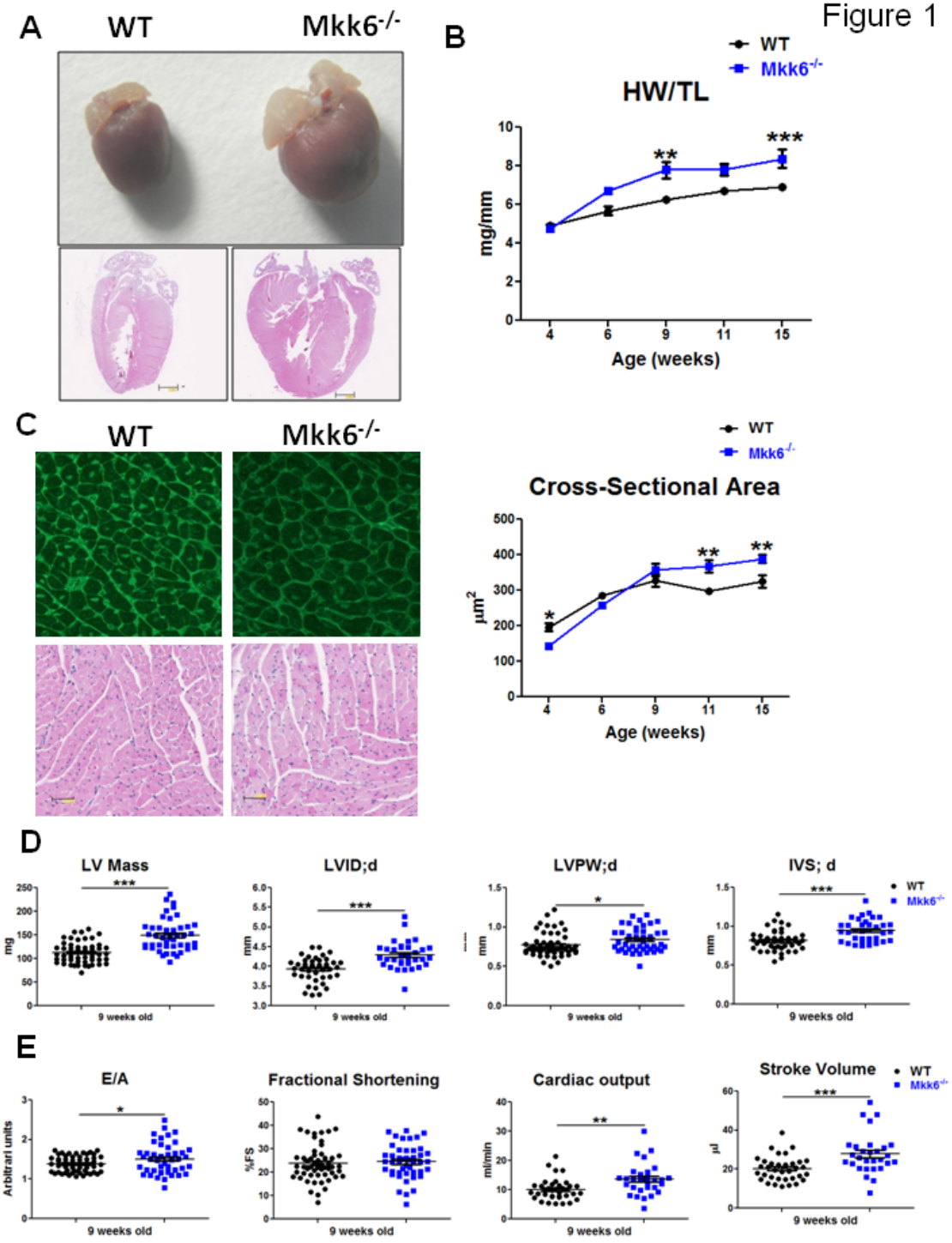
Figure 1
A
WT
Mkk6-/-
B
WT
Mkk6-/-
HW/TL
mg/mm
Age (weeks)
C
WT
Mkk6-/-
Cross-Sectional Area
µm2
Age (weeks)
D
LV Mass
mg
LVID;d
mm
LVPW;d
mm
IVS; d
mm
9 weeks old
E
E/A
Arbitrari units
Fractional Shortening
%FS
Cardiac output
ml/min
Stroke Volume
µl

Figure 2

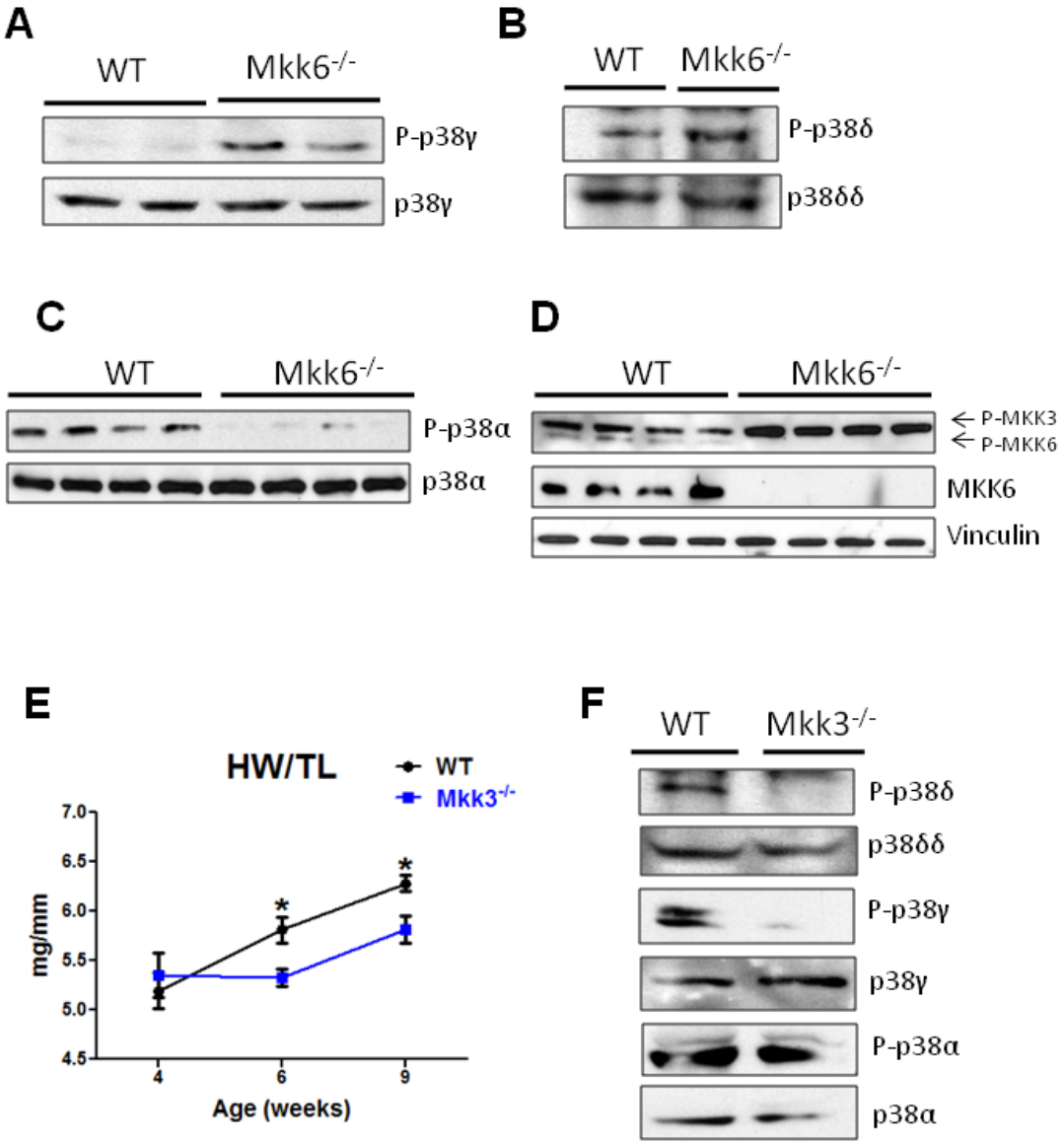
A
WT
Mkk6-/-
P-p38γ
p38γ
B
WT
Mkk6-/-
P-p38δ
p38δδ
C
WT
Mkk6-/-
P-p38α
p38α
D
WT
Mkk6-/-
P-MKK3
P-MKK6
MKK6
Vinculin
E
HW/TL
WT
Mkk3-/-
mg/mm
7.0
6.5
6.0
5.5
5.0
4.5
4
6
9
Age (weeks)
F
WT
Mkk3-/-
P-p38δ
p38δδ
P-p38γ
p38γ
P-p38α
p38α

Figure 3

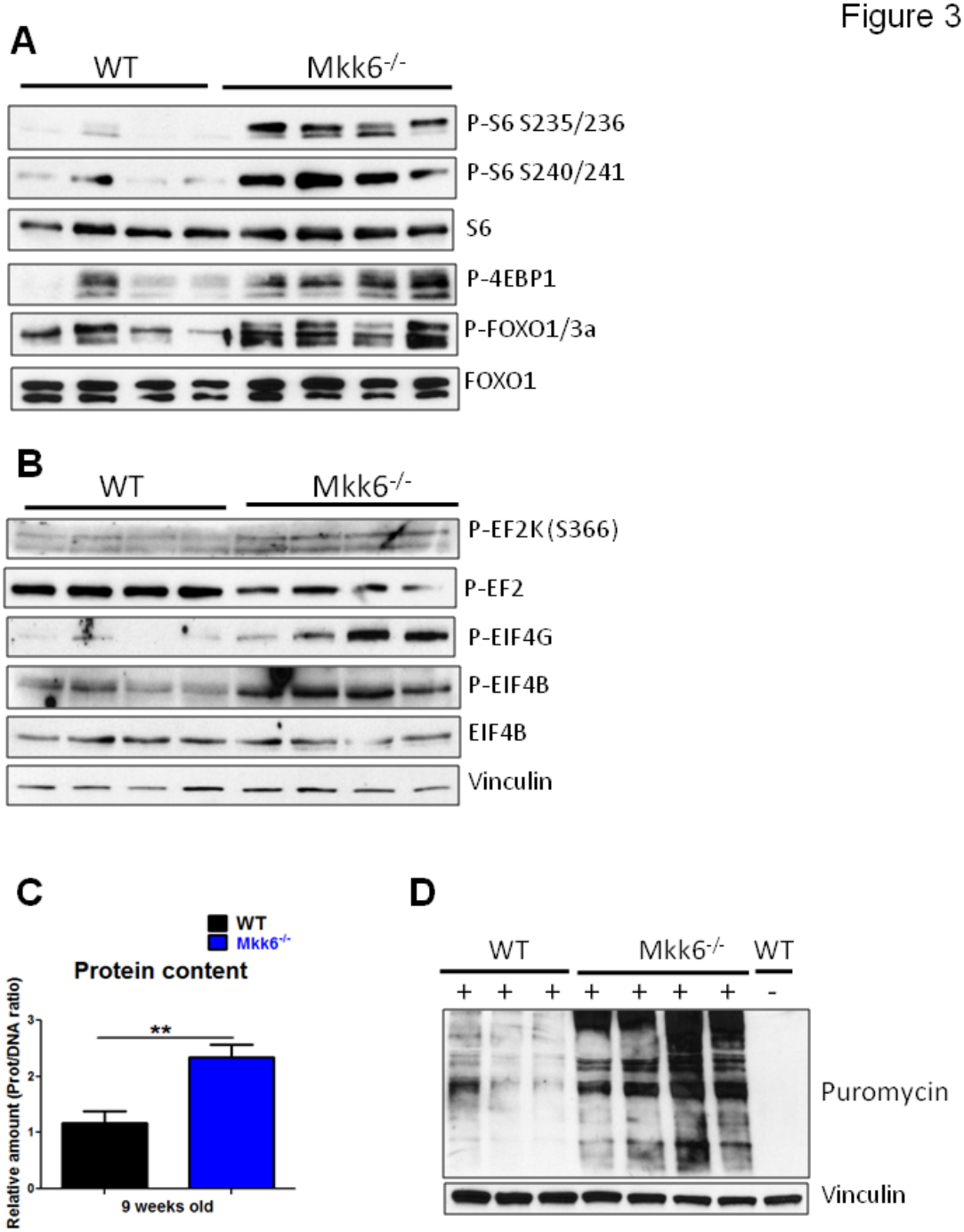
A
WT
Mkk6-/-
P-S6 S235/236
P-S6 S240/241
S6
P-4EBP1
P-FOXO1/3a
FOXO1
B
WT
Mkk6-/-
P-EF2K (S366)
P-EF2
P-EIF4G
P-EIF4B
EIF4B
Vinculin
C
WT
Mkk6-/-
Protein content
Relative amount (Prot/DNA ratio)
**
9 weeks old
D
WT
Mkk6-/-
WT
+ + + + + + + -
Puromycin
Vinculin

Figure 4

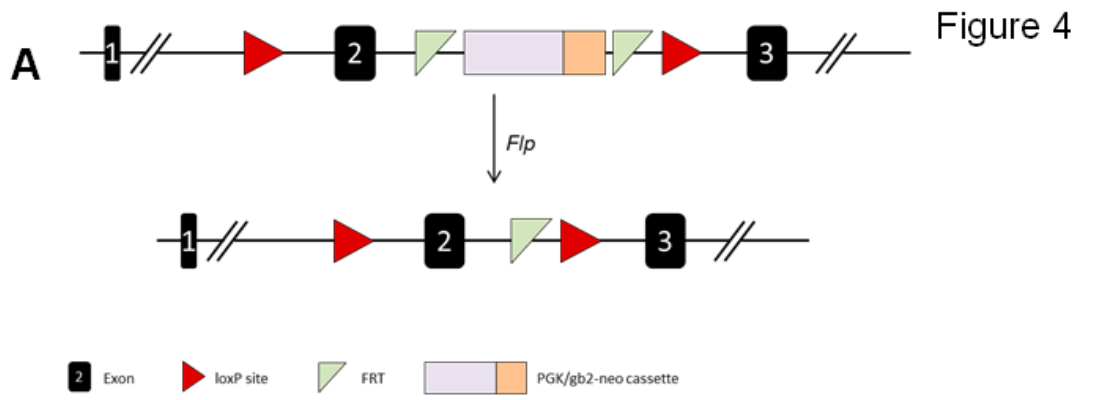
A
1
2
3
Flp
1
2
3
2 Exon
loxP site
FRT
PGK/gb2-neo cassette

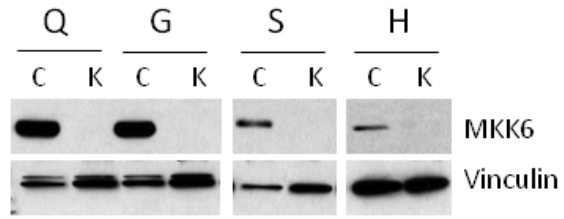
B
Q
G
S
H
C K C K C K C K
MKK6
Vinculin

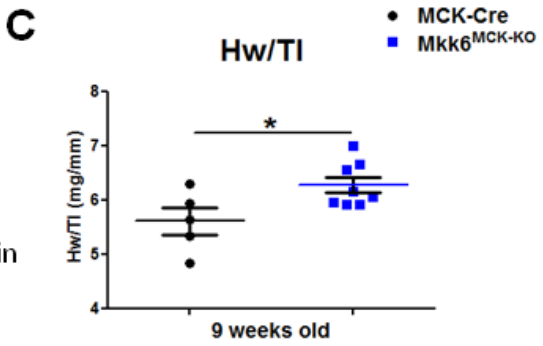
C
Hw/Tl
MCK-Cre
Mkk6MCK-KO
Hw/Tl (mg/mm)
8
7
6
5
4
*
9 weeks old

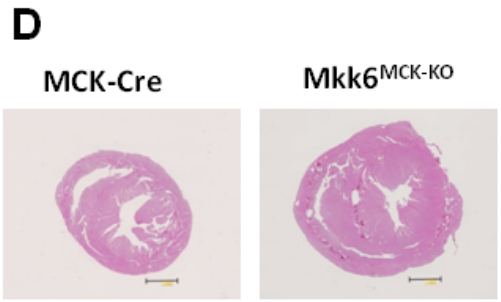
D
MCK-Cre
Mkk6MCK-KO

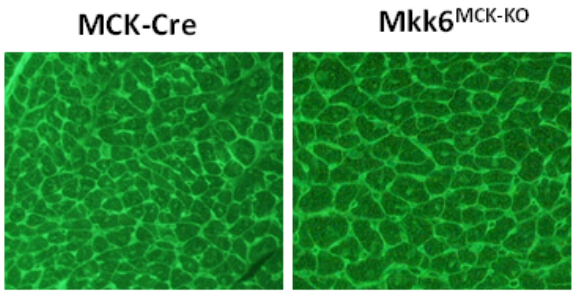
E
MCK-Cre
Mkk6MCK-KO

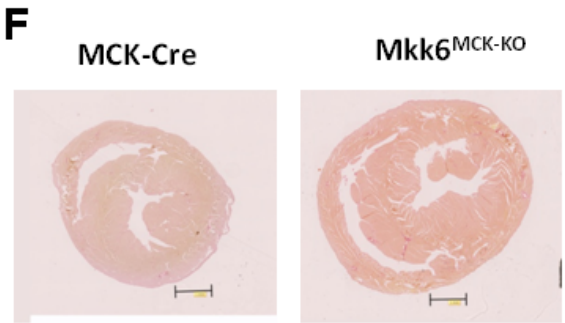
F
MCK-Cre
Mkk6MCK-KO

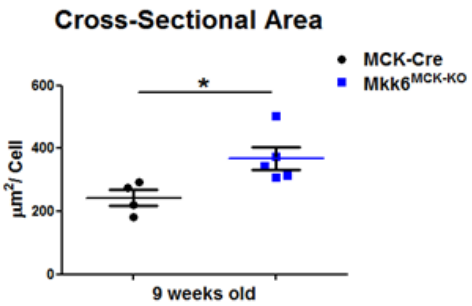
Cross-Sectional Area
MCK-Cre
Mkk6MCK-KO
μm2/ Cell
600
400
200
0
*
9 weeks old

Figure 5

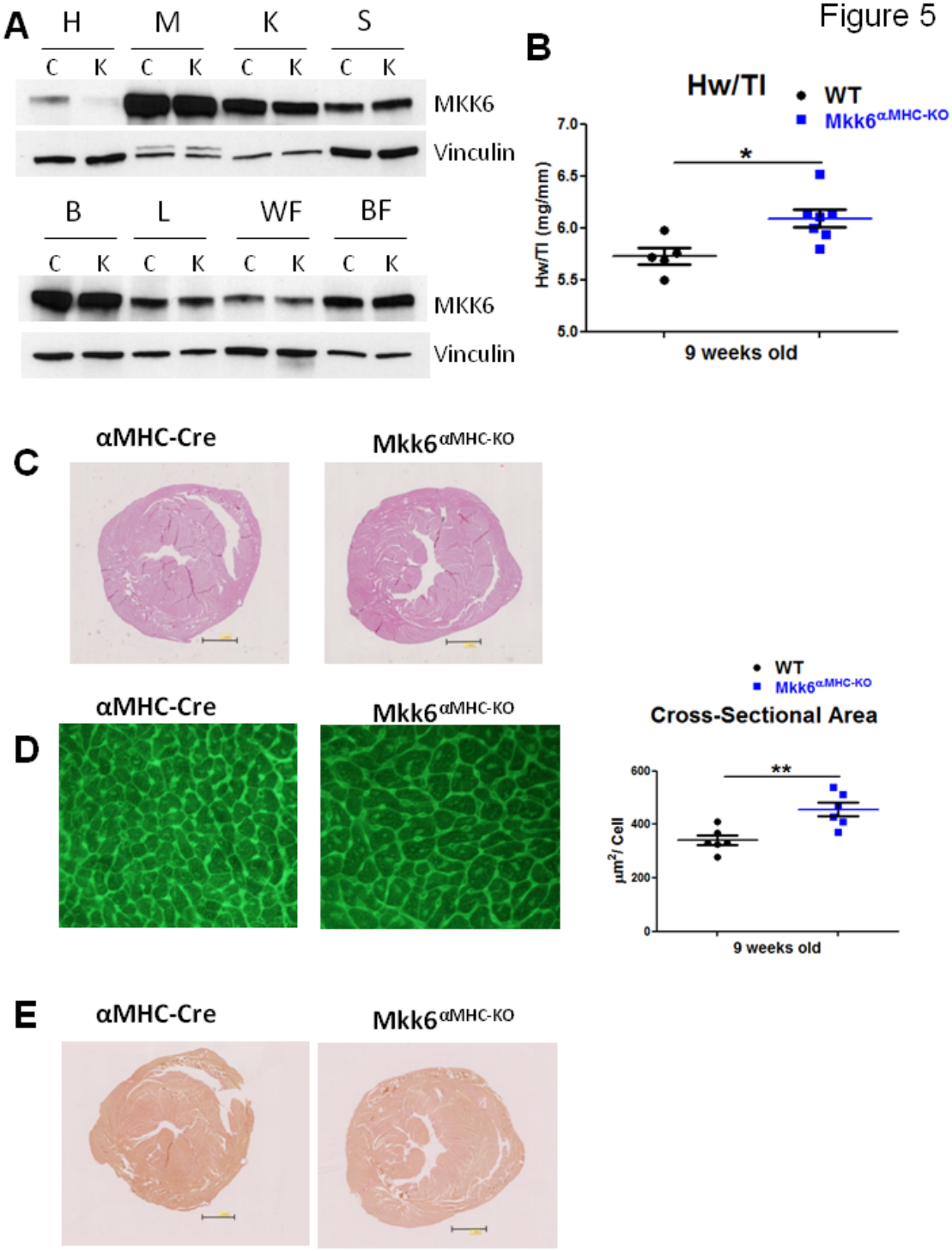
A
H
M
K
S
C K C K C K C K
MKK6
Vinculin
B
L
WF
BF
C K C K C K C K
MKK6
Vinculin
B
Hw/Tl
WT
Mkk6αMHC-KO
Hw/Tl (mg/mm)
7.0
6.5
6.0
5.5
5.0
*
9 weeks old
C
αMHC-Cre
Mkk6αMHC-KO
D
αMHC-Cre
Mkk6αMHC-KO
WT
Mkk6αMHC-KO
Cross-Sectional Area
μm2/ Cell
600
400
200
0
**
9 weeks old
E
αMHC-Cre
Mkk6αMHC-KO

Figure 6

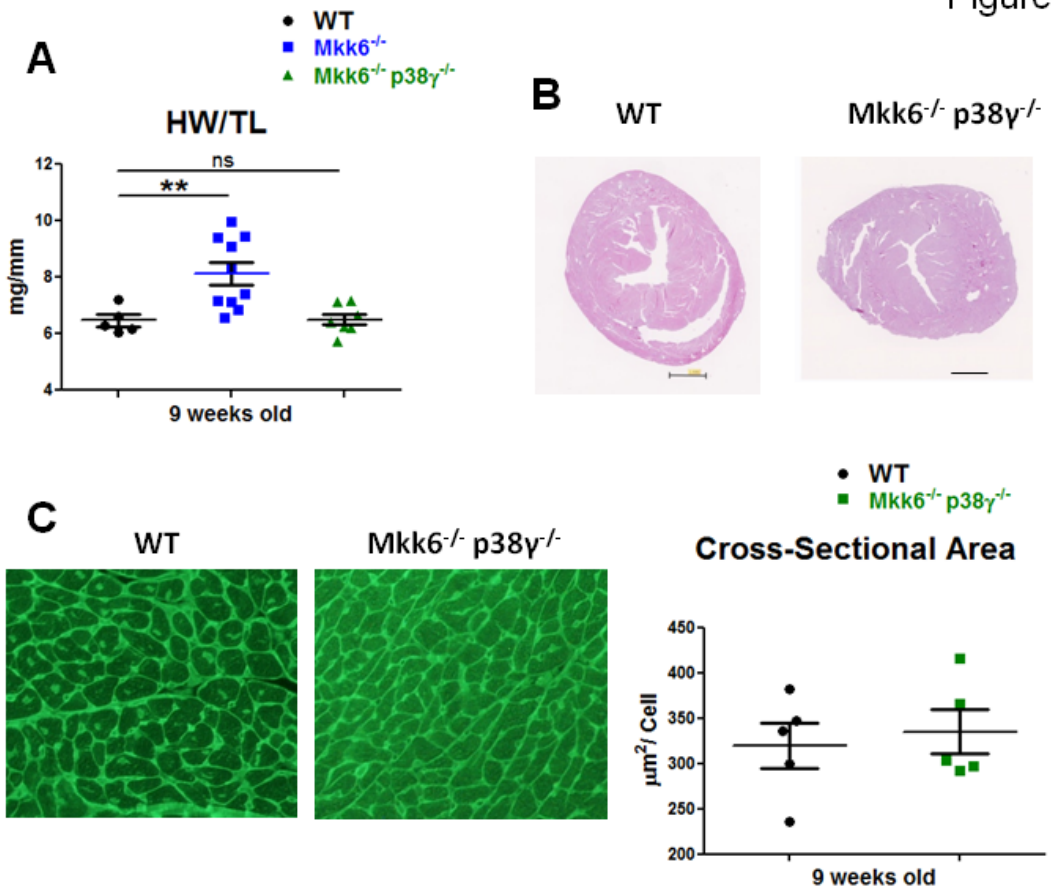
A
WT
Mkk6-/-
Mkk6-/- p38γ-/-
HW/TL
ns
**
mg/mm
12
10
8
6
4
9 weeks old
B
WT
Mkk6-/- p38γ-/-
C
WT
Mkk6-/- p38γ-/-
WT
Mkk6-/- p38γ-/-
Cross-Sectional Area
μm2/ Cell
450
400
350
300
250
200
9 weeks old

Figure 7

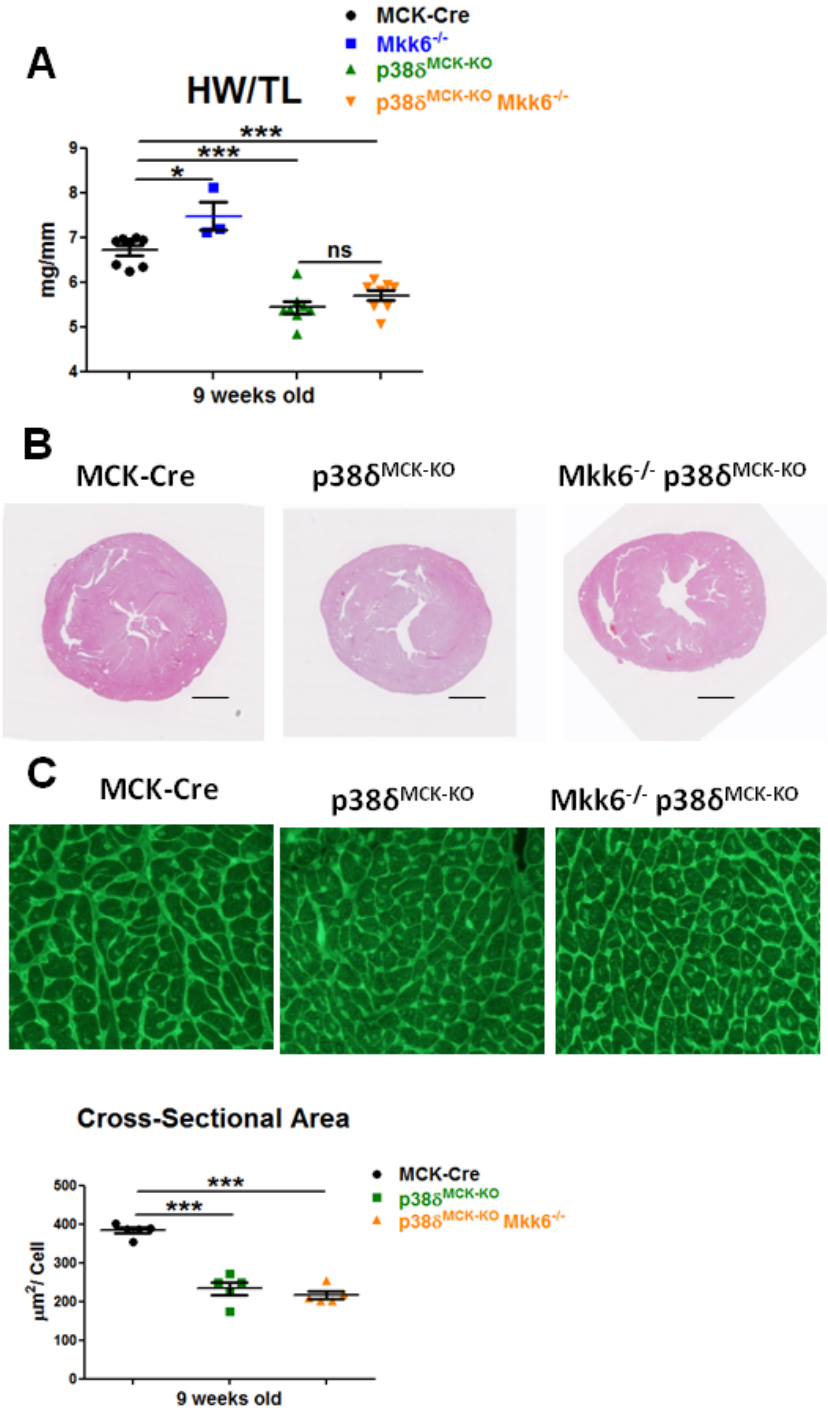
A
HW/TL
MCK-Cre
Mkk6-/-
p38δMCK-KO
p38δMCK-KO Mkk6-/-
***
***
*
ns
mg/mm
9 weeks old
B
MCK-Cre
p38δMCK-KO
Mkk6-/- p38δMCK-KO
C
MCK-Cre
p38δMCK-KO
Mkk6-/- p38δMCK-KO
Cross-Sectional Area
***
***
MCK-Cre
p38δMCK-KO
p38δMCK-KO Mkk6-/-
μm2/ Cell
9 weeks old

Figure 8

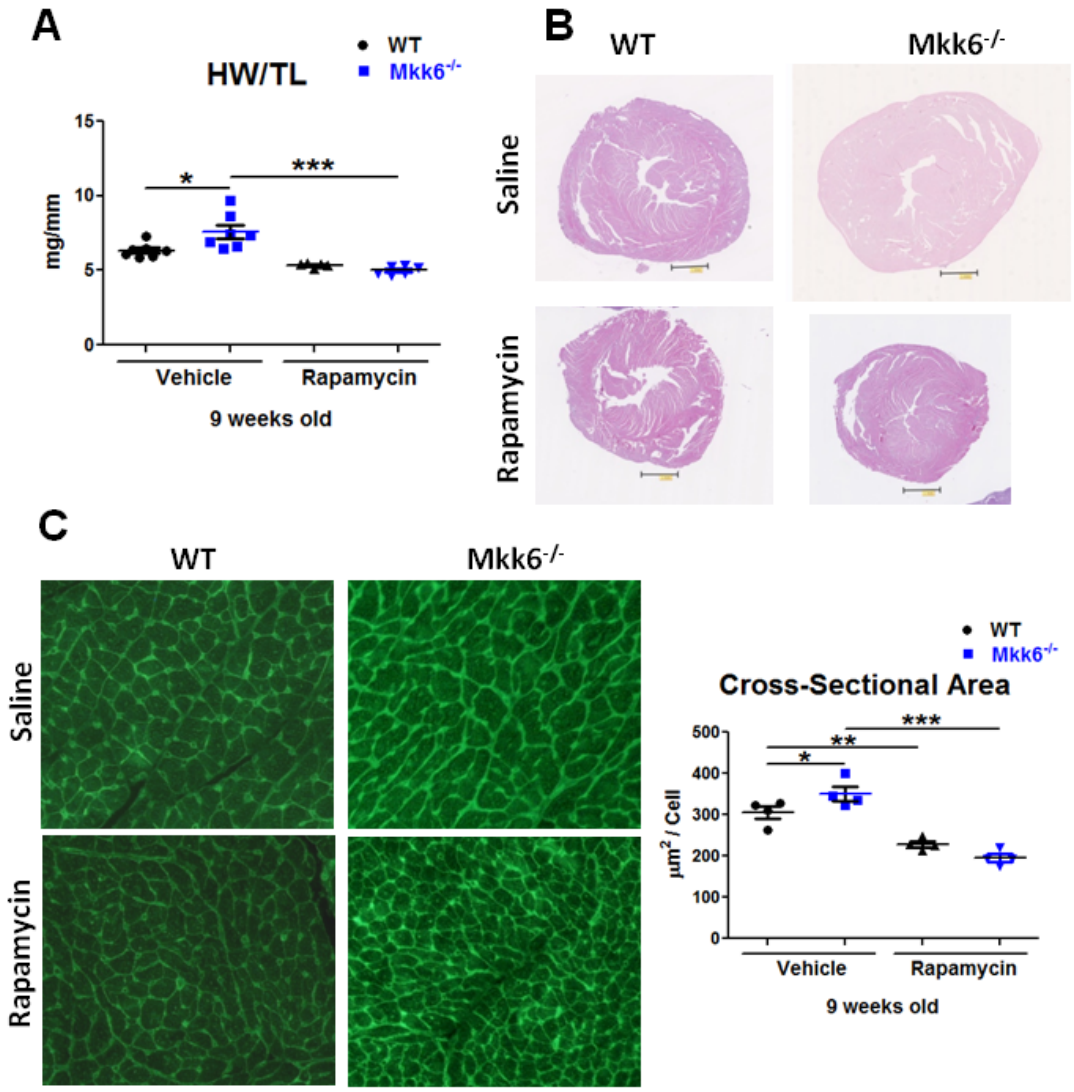
A
HW/TL
WT
Mkk6-/-
mg/mm
15
10
5
0
*
***
Vehicle
Rapamycin
9 weeks old
B
WT
Mkk6-/-
Saline
Rapamycin
C
WT
Mkk6-/-
Saline
Rapamycin
WT
Mkk6-/-
Cross-Sectional Area
μm2 / Cell
500
400
300
200
100
0
*
**
***
Vehicle
Rapamycin
9 weeks old

Figure 9

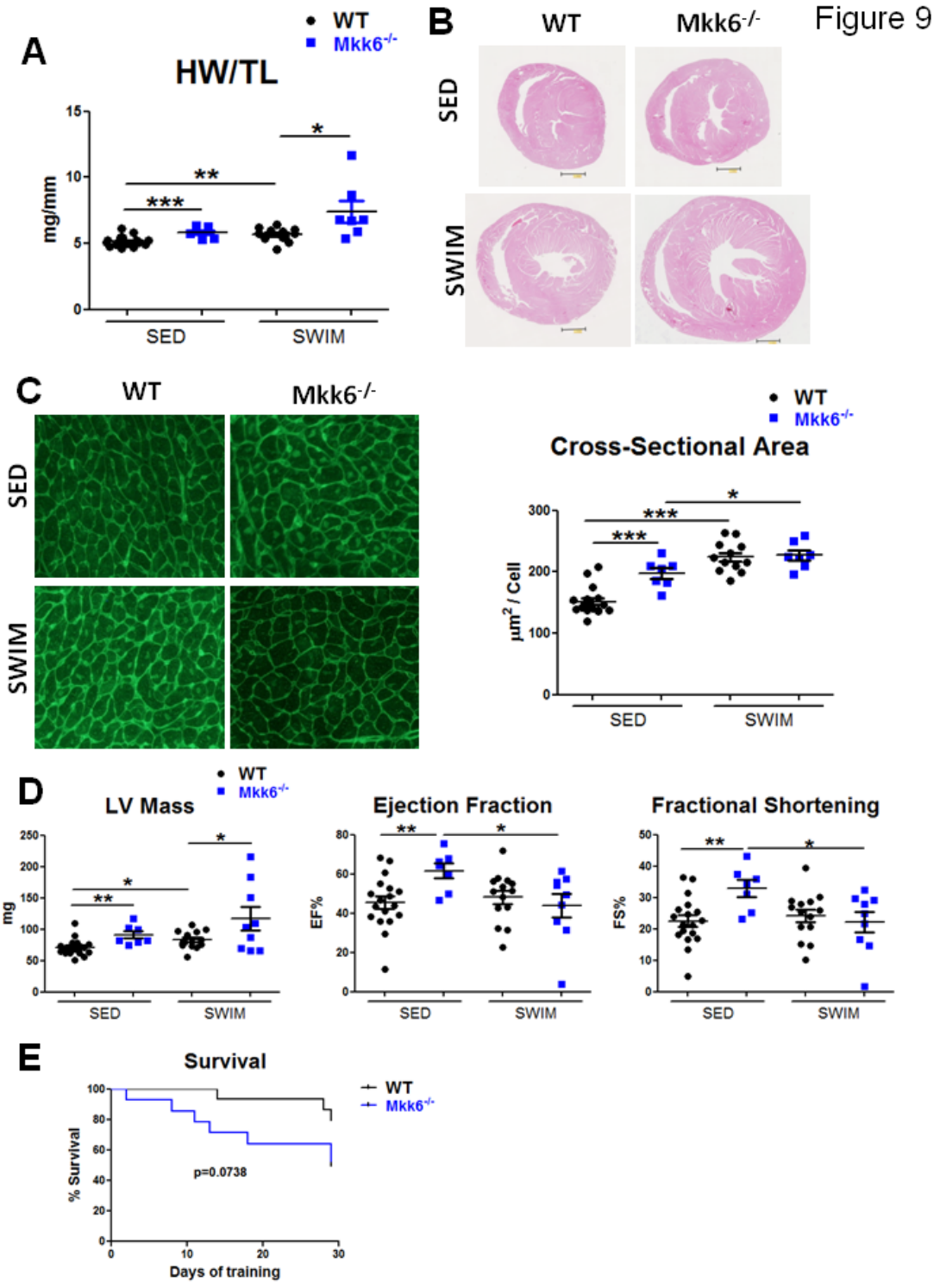
A
WT
Mkk6-/-
HW/TL
mg/mm
15
10
5
0
*
**
***
SED
SWIM
B
WT
Mkk6-/-
SED
SWIM
C
WT
Mkk6-/-
SED
SWIM
WT
Mkk6-/-
Cross-Sectional Area
µm2 / Cell
300
200
100
0
*
***
***
SED
SWIM
D
WT
Mkk6-/-
LV Mass
mg
250
200
150
100
50
0
*
**
*
SED
SWIM
Ejection Fraction
EF%
80
60
40
20
0
**
*
SED
SWIM
Fractional Shortening
FS%
50
40
30
20
10
0
**
*
SED
SWIM
E
Survival
% Survival
100
80
60
40
20
0
p=0.0738
0
10
20
30
Days of training
WT
Mkk6-/-

Figure 10

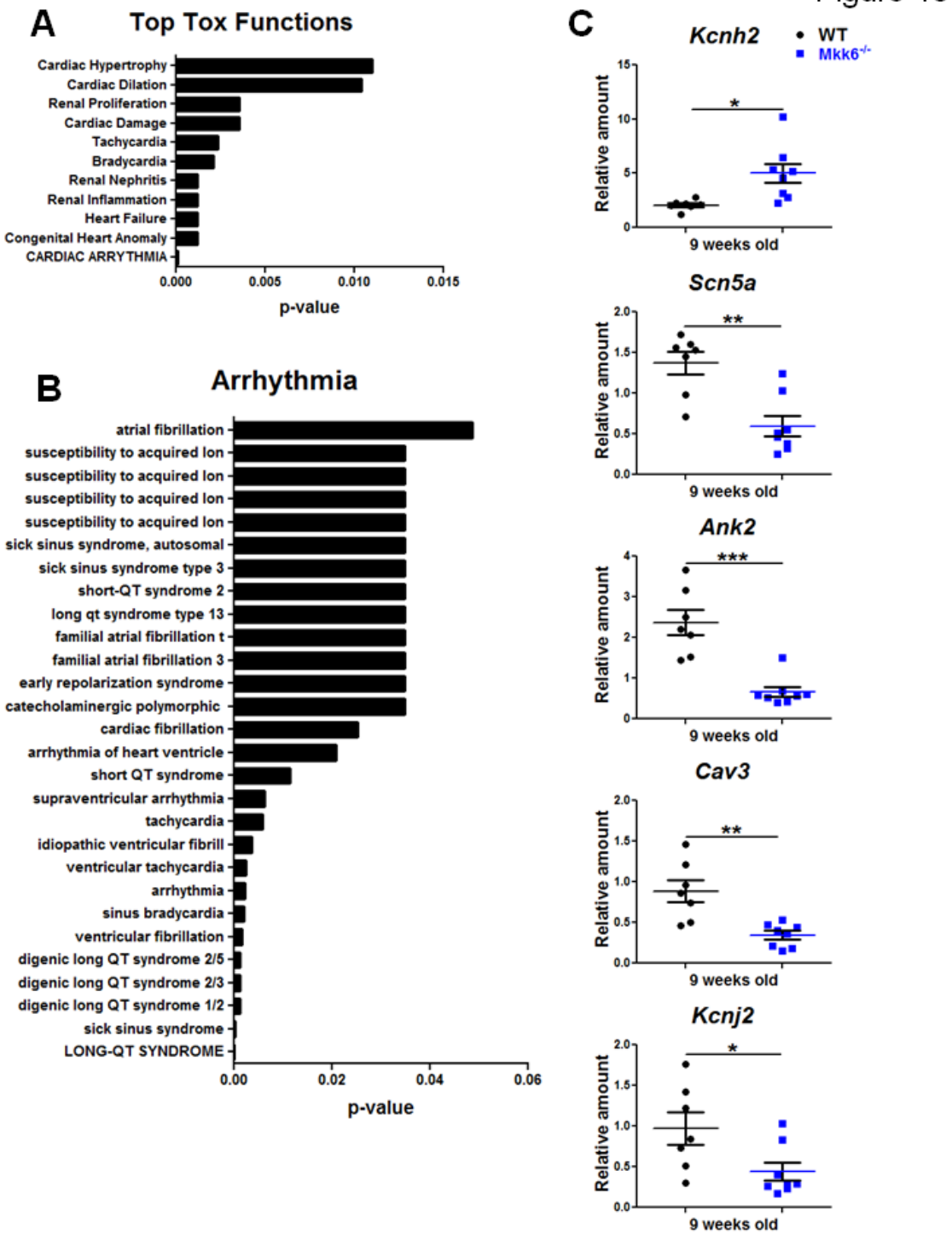
A
Top Tox Functions
Cardiac Hypertrophy
Cardiac Dilation
Renal Proliferation
Cardiac Damage
Tachycardia
Bradycardia
Renal Nephritis
Renal Inflammation
Heart Failure
Congenital Heart Anomaly
CARDIAC ARRYTHMIA
0.000
0.005
0.010
0.015
p-value
B
Arrhythmia
atrial fibrillation
susceptibility to acquired lon
susceptibility to acquired lon
susceptibility to acquired lon
susceptibility to acquired lon
sick sinus syndrome, autosomal
sick sinus syndrome type 3
short-QT syndrome 2
long qt syndrome type 13
familial atrial fibrillation t
familial atrial fibrillation 3
early repolarization syndrome
catecholaminergic polymorphic
cardiac fibrillation
arrhythmia of heart ventricle
short QT syndrome
supraventricular arrhythmia
tachycardia
idiopathic ventricular fibrill
ventricular tachycardia
arrhythmia
sinus bradycardia
ventricular fibrillation
digenic long QT syndrome 2/5
digenic long QT syndrome 2/3
digenic long QT syndrome 1/2
sick sinus syndrome
LONG-QT SYNDROME
0.00
0.02
0.04
0.06
p-value
C
Kcnh2
WT
Mkk6-/-
Relative amount
9 weeks old
Scn5a
Ank2
Cav3
Kcnj2

Figure 11

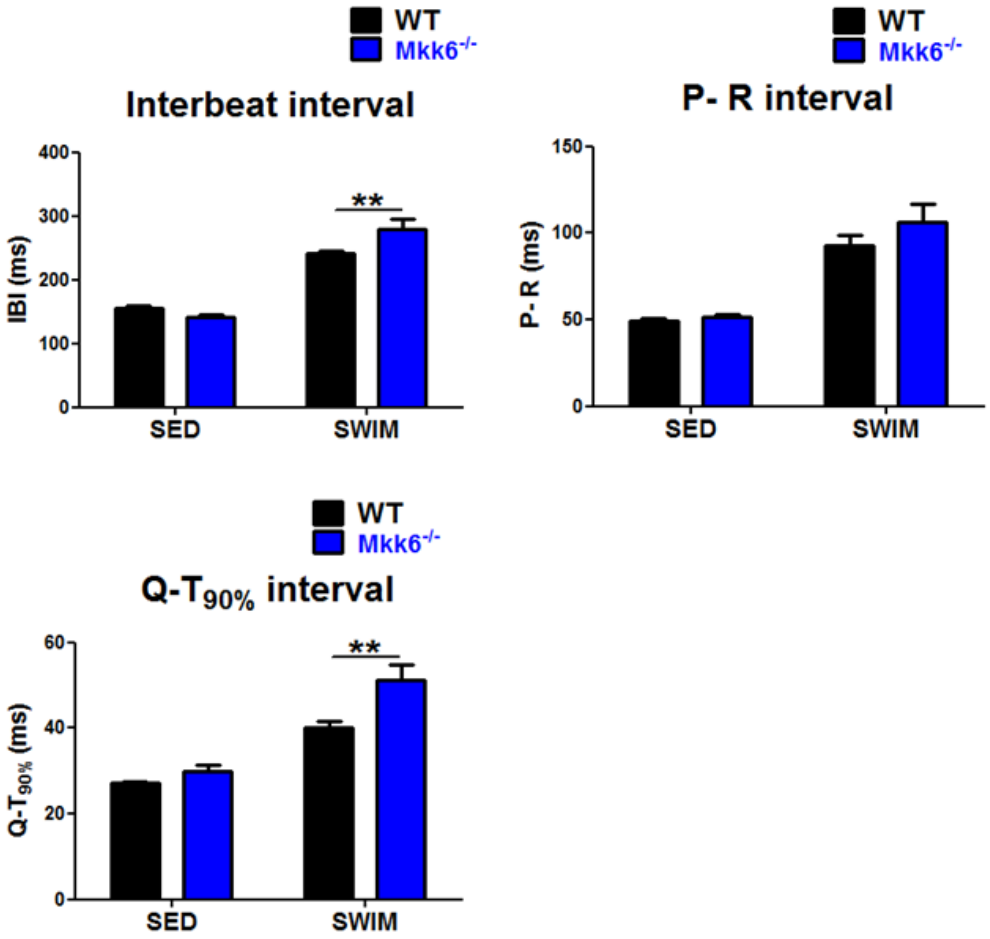
WT
Mkk6-/-
Interbeat interval
IBI (ms)
400
300
200
100
0
**
SED
SWIM
WT
Mkk6-/-
P- R interval
P- R (ms)
150
100
50
0
SED
SWIM
WT
Mkk6-/-
Q-T90% interval
Q-T90% (ms)
60
40
20
0
**
SED
SWIM

SUPPLEMENTARY INFORMATION

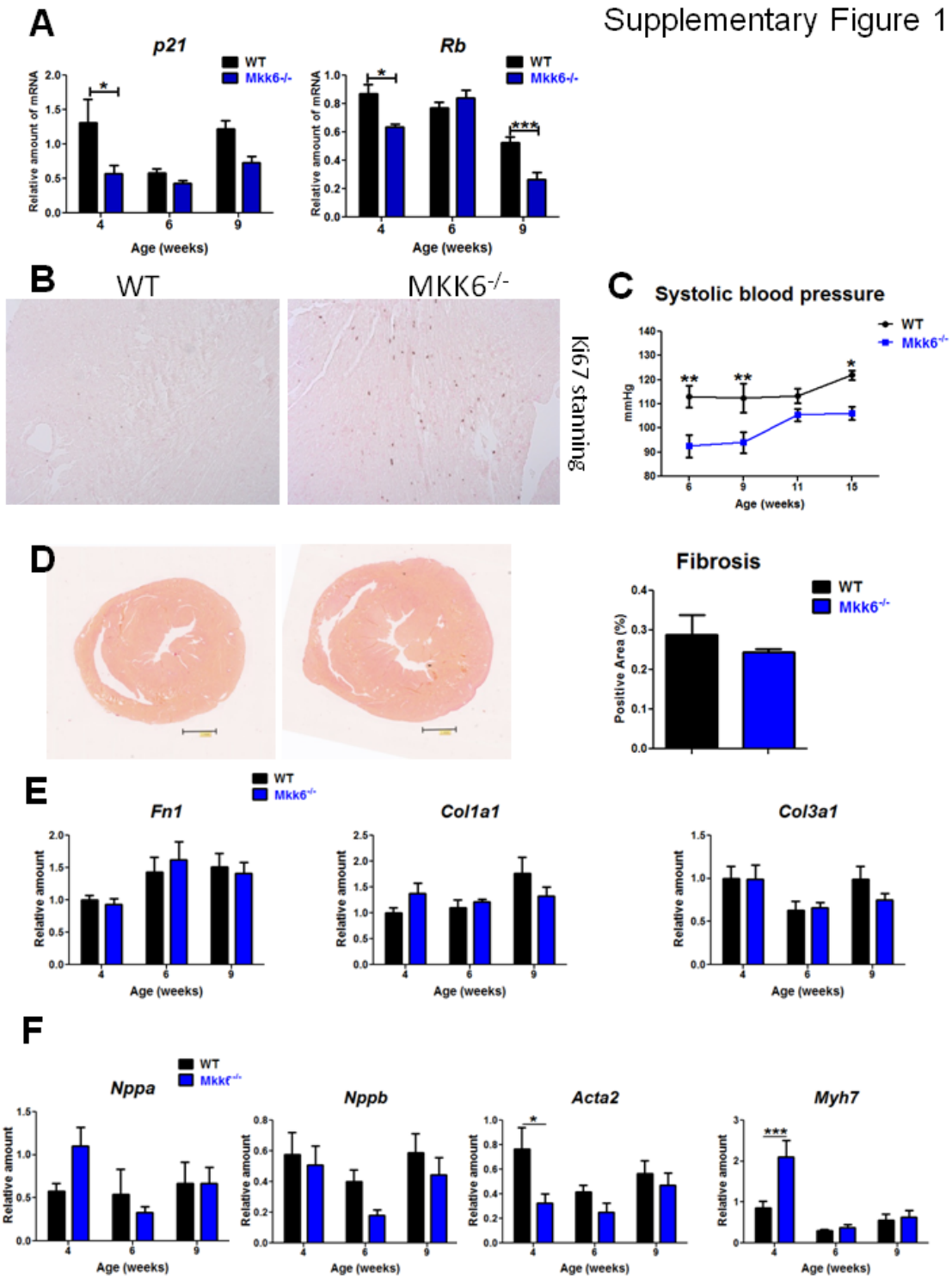

Supplemetary Figure 1. ***Mkk6*$^{-/-}$ mice develop physiological hypertrophy.**

(**a**) p21 and Rb expression levels in hearts from WT and *Mkk6*$^{-/-}$ mice at the indicated time points. (**b**) Ki67 staining of cardiac sections at 6 weeks from WT and *Mkk6*$^{-/-}$ mice. (**c**) Systolic blood pleasure measured from WT and *Mkk6*$^{-/-}$ mice. (**d**) Fibrosis quantification from picrosirius red staining of WT and *Mkk6*$^{-/-}$ hearts. (**e-f**) Gene expression of different markers of (**e**) fibrosis and (**f**) cardiac stress, from WT and *Mkk6*$^{-/-}$ hearts at the indicated time points.

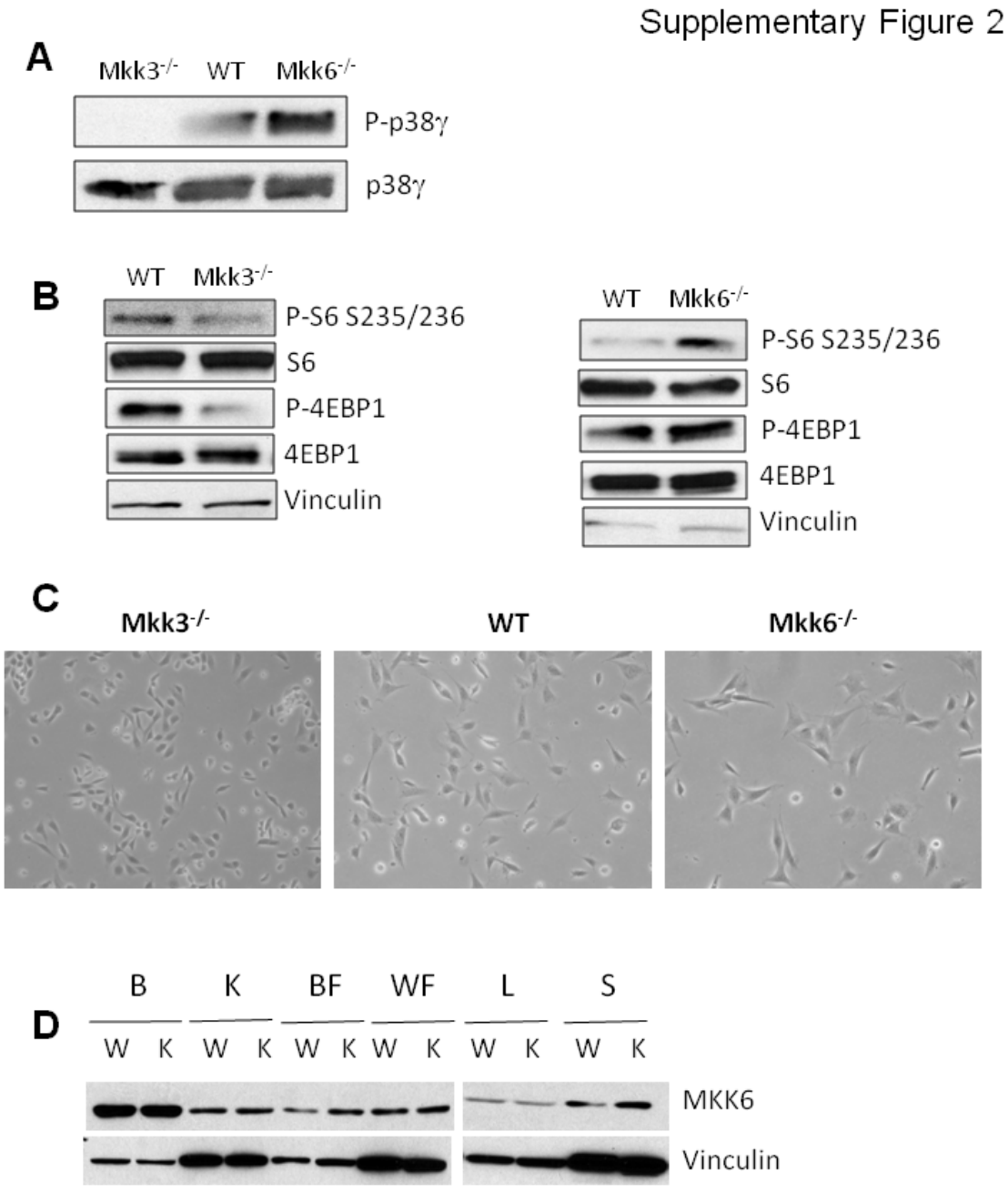

Supplementary Figure 2. MKK3/6-p38 pathway regulates mTOR activation and cell size in MEF cells.

(**a**) Analysis of p38γ activation and expression by immunoprecipitation in WT, *Mkk3*$^{-/-}$ and *Mkk6*$^{-/-}$ MEF cells. (**b**) Immunoblot analysis of mTOR signaling in WT, *Mkk3*$^{-/-}$ and *Mkk6*$^{-/-}$ MEF cells. (**c**) Micrographs from WT, *Mkk3*$^{-/-}$ and *Mkk6*$^{-/-}$ MEF cells. (**d**) MKK6 deletion specificity from MCK-Cre (C) and MKK6$^{\alpha MHC\text{-}KO}$ (K) in brain (B), kidney (K), brown fat (BF), white fat (WF), liver (L) and spleen (S) (n=3).

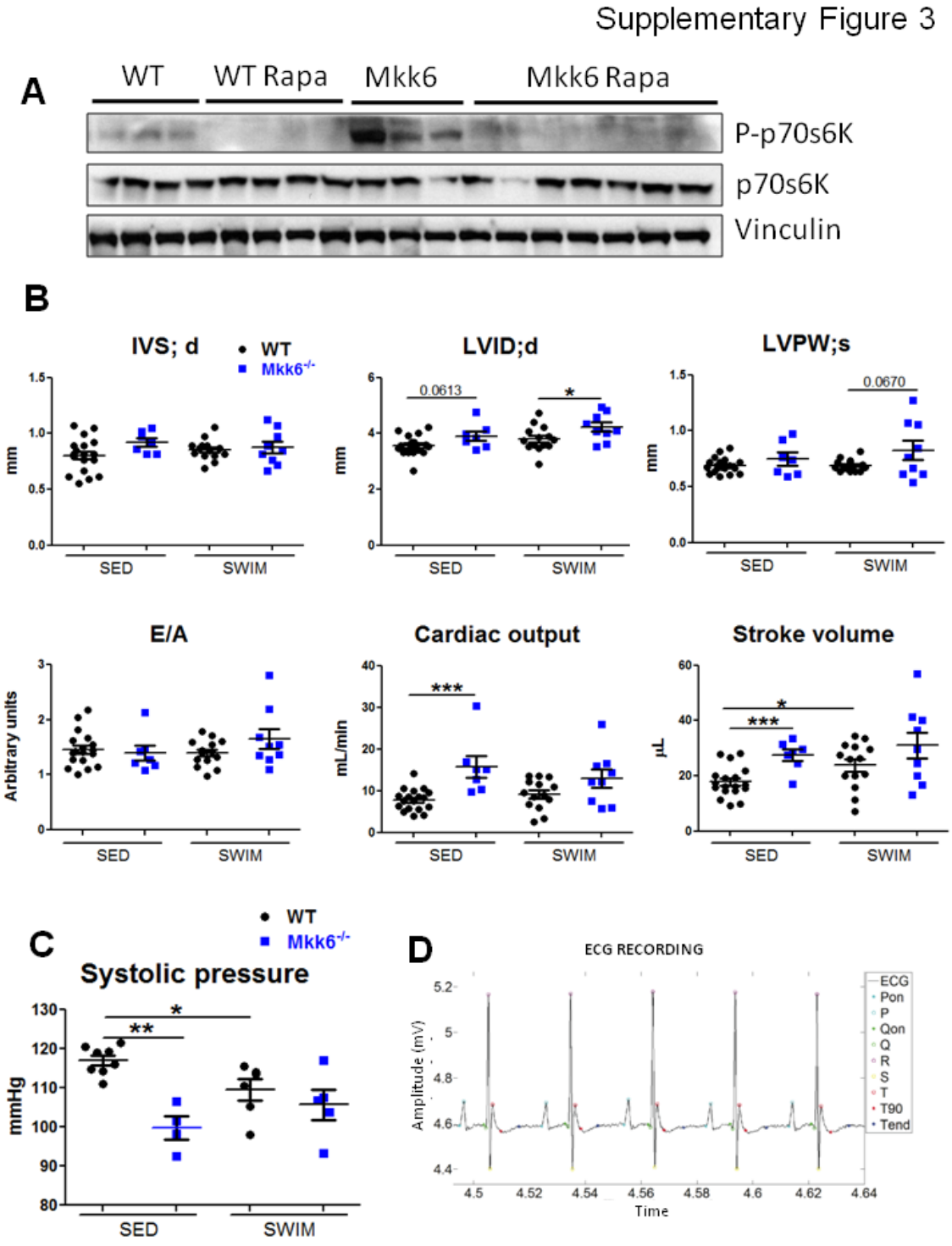

Supplementary Figure 3. *Mkk6*$^{-/-}$ mice were swimming trained.

(**a**) Immunoblot analysis of mTOR inhibition by Rapamycin in heart lysates from WT and *Mkk6*$^{-/-}$ mice. (**b**) Echocardiography results for 9-week-old WT and *Mkk6*$^{-/-}$ mice. LV Mass (Left ventricle mass), LVID;d (Left ventricle internal diameter in diastole), LVPW;d (left ventricle posterior wall in diastole); IVS;d (inter-ventricular septum in diastole). (**c**) Systolic blood pleasure measured from WT and *Mkk6*$^{-/-}$ mice at the end of the endurance training. (**d**) Electrocardiogram detection in mice. Data are means±s.e.m. (n=5–12). *P<0.05; **P<0.01; ***P<0.001 (one-way ANOVA coupled to Bonferroni post tests or t-test).

DISCUSION

To preserve the homeostasis and health of the organism, cells are constantly responding to changes in the physical and chemical properties of the environment by altering many of their cellular functions. The p38 MAPK pathway belongs to the Mitogen Activated Protein Kinases (MAPKs) family and is involved in the transduction of most extracellular signals, specifically stress signals. While the p38 MAPK family has been implicated in a wide variety of biological processes, a specific role for p38γ and p38δ MAPKs in cellular signaling and its contribution to both physiological and pathological conditions are presently lacking. In this thesis, we outline a role for p38γ and p38δ MAPK in important cellular processes such as in acute and chronic inflammatory responses and cardiac growth, as well as in pathological conditions such as inflammatory disease, steatosis, diabetes and cardiac hypertrophy.

The p38 MAPK pathway has been involved in the regulation of inflammatory responses since its discovery. p38α MAPK was first identified as the primary target of anti-inflammatory pyridinyl imidazole drugs that inhibit endotoxin-stimulated production of TNFα [105]. Thanks to the availability of specific inhibitors for p38α and p38β isoforms, nowadays we have great understanding of the essential role of p38α in inflammation and in numerous TLR4-triggered responses in macrophages and dendritic cells [62]. Furthermore, studies using whole body knockout and conditional tissue-specific knockouts of p38α and p38β allowed dissecting the contribution of each of these isoforms revealing a dominant role of p38α in the regulation of cytokine production and inflammatory responses. In contrast, p38β appears to be required neither for the acute, nor chronic inflammatory responses [13, 124]. However, the contributions of p38γ and p38δ to inflammatory responses were largely unexplored until two years ago that our group and others showed that these two kinases are key elements in the control of inflammation. Several studies have reinforced the importance of p38γ and p38δ in inflammatory responses and in diseases with a strong inflammatory component such as psoriasis, arthritis and colon cancer [35, 45, 194]. A role of the alternative p38 isoforms in inflammation was suggested first by the similarities in the activation of p38 family members. Specifically, MKK6 activates all p38 isoforms, and when overexpressed by cell transfection, each p38 can be activated in cells treated with IL-1β and TNF-α [54, 84, 90, 110, 170].

Besides, while p38α is expressed in all inflammatory cell lineages and its expression levels does not seem to change during cell differentiation or upon stimulation, in this

thesis work we have shown that p38γ and p38δ present a very distinct expression pattern in the different myeloid cell lineages. p38γ and p38δ are expressed in macrophages and monocytes, however, kupffer cells express high protein levels of p38γ isoform, but very low levels of p38δ, and on the other hand, neutrophils express high levels of p38δ but almost no p38γ. A similar expression pattern has been reported by other groups [73, 81]. The activation pattern of the p38 isoforms also differs in myeloid cell lineages. In macrophages activation of p38α and p38δ has been detected upon LPS stimulation [73], however, p38γ is the only isoform activated in Kuppfer cells, and p38α the one activated in neutrophils by LPS. All this particularities in the expression and activation of p38γ and p38δ in myeloid cells indicate that both may be regulating important processes in inflammatory responses and that their functions might be non redundant with p38α, or between each other.

In 1994 C. Manthey's lab, found that SB202190 inhibits maximally 65% of LPS-induced TNF-α production by macrophages [73]. Since SB202190 does not inhibit p38δ [84, 170] they speculated that p38δ might mediate the 35% of TNF-α production that is insensitive to SB202190 [115]. This observation correlates with our finding that p38δ, together with p38γ, phosphorylates in macrophages the eEF2K to regulate TNFα production in a model of LPS-induced acute hepatitis. In the same year, Risco et al. reported that p38γ and p38δ regulate TNFα production through the regulation of ERK activation. [138]. Nevertheless, we didn't detect changes in ERK activation upon LPS stimulation neither in bone marrow derived macrophages (BMDM) from *Mkk3*$^{-/-}$*Mkk6*$^{+/-}$ full body knockout mice or from mice lacking specifically p38γ and p38δ in myeloid cells. Although they also use LPS treatment of bone marrow derived macrophages (BMDM) the difference in LPS dosage or in mouse models (they obtain the BMDM from p38γ and p38δ full body knockout mice, whereas we isolated them from myeloid-specific conditional mice) could be responsible for the different outcome. Firstly, the lack of these kinases in other tissues could affect the bone marrow cells in an independent manner from the autonomous p38γ and p38δ deficiency. Secondly, the moment in which the deletion occurs during the mouse development and the effectiveness of the deletion may be different in both models.

Likewise, p38γ and p38δ have an essential role in chronic inflammatory responses. In this thesis we have shown that myeloid p38γ and p38δ contribute to the pathogenesis of non-alcoholic fatty liver disease (NAFLD), which refers to a wide spectrum of liver

damage, from steatosis to inflammation, fibrosis and cirrhosis. NALFD is strongly associated with obesity and type-2-diabetes and predisposes to hepatocellular carcinoma.

Lack of p38γ and p38δ specifically in myeloid cells conferred protection against three different models of steatosis: methionine-coline deficient diet (MCD), high fat diet (HF) and high fat and fructose diet (HFF), indicating that the protection observed is independent of the model used to induce the disease. This reduced liver damage and steatosis development is due to an impaired migration and infiltration of neutrophils lacking p38γ and p38δ into the liver. The defects in neutrophil migration are consistent with previous reports using global and myeloid-restricted p38δ deletion in an acute lung injury model [81]. Surprisingly, the lack of p38δ alone in the whole body is insufficient to protect against liver steatosis in our MCD model. However, the deletion of p38 specifically in neutrophils is enough to confer protection against liver neutrophil infiltration and steatosis development. Although p38γ is only expressed at very low levels, in non-stimulated or LPS-stimulated neutrophils, one possibility we did not rule out is whether in *Mapk13*$^{-/-}$ neutrophils, p38γ activation or expression is increased as a compensatory mechanism. These kind of compensatory behaviors have been previously described inside the p38 MAPK pathway [143, 145]. Another possibility is that p38γ contributes in other cell type to the regulation of liver neutrophil infiltration and steatosis progression. The fact that p38δ deficiency specifically in neutrophils confers a greater protection against steatosis development than its deletion in myeloid cells (not shown) or the whole body p38δ knockout mice might indicate that p38δ has an opposite role in other tissue.

Our studies have shed some light in the pathophisiology of LPS-induced acute liver damage and of NAFLD development. In both disease models, myeloid cells play an essential role in liver inflammation and damage, however, TNFα production by macrophages and monocytes but not neutrophil liver infiltration is determinant for LPS-hepatitis, but in NALFD pathogenesis neutrophils are the key players. Although more experiments should be done to elucidate whether there is a primary defect in neutrophil migration and liver infiltration in the LPS-induced acute hepatitis, or if the reduced liver neutrophil population it is secondary to the reduced TNFα production and reduced liver inflammation, our data indicate that neutrophils do not play a dominant role LPS–stimulated hepatic damage. Moreover, the neutrophil competitive migration experiment

demonstrates that the defective neutrophil migration in diet-induced steatosis is not secondary to a defective production of TNFα or other chemokines.

Several studies have suggested redundant functions among the p38 MAPK isoforms and its upstream activators MKK3 and MKK6 [19, 129]. Sabio G. et al (2005) clearly demonstrated that the different p38 present overlapping functions by the use of cells from knockout mice lacking multiple family members in combination with the use of specific inhibitors for the different kinases. Such redundancy may account for the failure on finding a phenotype in the different p38 knockout mice and point to the need to generate knock-in mice expressing inactive p38MAPK and mice with tissue-specific inactivation of the individual p38MAPK family members [143]. In our studies we have observed that p38γ/δ$^{Lyz\text{-}KO}$ mice present a stronger phenotype than either of the single conditional knockouts, indicating partial redundant roles for p38γ and p38δ in myeloid cells. Nevertheless, a dominant role of p38δ could be appreciated, indicating that their functions are not overlapping completely and some of them are only partially compensated by the other isoform. In the LPS-induced acute hepatitis model, p38γ and p38δ have opposite roles in the regulation of IL-10 levels in BMDM. While the lack of p38γ leads to an increase IL-10 production, the deficiency in p38δ increases its levels in response to LPS. Besides, double knockout BMDM show IL-10 levels comparable to WT cells. On the other hand, p38δ seems to be the main isoform in the regulation of IL-6 production; p38γ deficiency does not affect it. However, both are involved in the control of TNFα levels in response to LPS, although, p38δ seems to have a predominant role. This explains why in p38δ$^{Lyz\text{-}KO}$ show a stronger protection against LPS-induced liver damage than p38γ$^{Lyz\text{-}KO}$.

This redundancy is also observed between the p38s up stream kinases, MKK3 and MKK6. Whereas mice lacking both MKK3 and MKK6 are not viable, dying at mid-gestation with defects in the placenta and the development of the embryonic vasculature [19], loss of either gene alone yields healthy mice [113, 160, 179]. Likewise, in our acute hepatitis model the single deficiency in MKK3 or MKK6 partially protects against LPS-induced liver damage, but this protection is not enough to reduce the mortality. In this acute inflammatory model, MKK6 seems to have a dominant role in the regulation of hepatic apoptosis, necrosis and neutrophil infiltration. Although TNFα production by liver monocytes/macrophages is reduced in single knockout mice, BMDM deficient in either of the MKKs produce normal levels of cytokines in response to LPS. This may

reflect important differences in between the two myeloid cell populations. Moreover, it is possible as well, that the lack of MKK3 and MKK6 in other cell types could be affecting the liver monocytes/macrophages. Furthermore, the fact that only MKK6 deficient mice present reduced hepatic apoptosis and necrosis, while both single knockout mice show reduced TNFα production by liver myeloid cells, suggests that MKK6 may be playing a role in other cell type such as hepatocytes that explains the protection observed. To address this possibility, further experiments should be performed using liver-specific conditional knockout mice.

But this redundancy does not always occur, Romeo Ricci has reported specific roles of p38δ in insulin secretion and neutrophil migration that cannot be compensated by other p38 isoforms [81, 156], and the same occurs for the role in p38α in placental development. Along with this idea, we have shown that the expression of both alternative p38 MAPKs is essential in the heart for a normal postnatal cardiac growth.

Several studies have implicated the p38 MAPK pathway in cardiomyocyte proliferation and hypertrophy [20, 44, 111, 171]. It has been shown that p38α and p38β play redundant roles in the regulation of embryonic heart development. Double knockout mice die during embryonic development with septal defects associated to cardiomyocyte-reduced proliferation [44]. However, Yibin Wang et al. proposed that these kinases also have divergent roles in the heart, p38α seems to regulate cardyomyocyte apoptosis and p38β the hypertrophic response induced by the overexpression of MKK3 constitutive active mutant [171]. In contrast, no studies had been performed before in the cardiac role of p38γ and p38δ *in vivo*, despite of the fact that the four p38 isoforms are expressed in the heart, and p38γ together with p38α is one of the predominant isoforms. In this thesis work we show that the alternative p38 MAPKs cooperate to regulate postnatal cardiac hypertrophic growth, through the regulation of mTOR pathway activation in a non-redundant manner. Although, it has been described that p38δ is highly expressed in the ventricles during embryonic development [139], the cardiac size and structure of mice lacking p38γ and p38δ is normal at birth. At this moment, the expression levels of both kinases are very low, but protein levels and activation increase during the early postnatal cardiac development. Single knockout and double knockout mice present a similar reduction in heart size due to a decreased cardiomyocyte hypertrophic growth. This indicates that p38γ and p38δ cooperate in the regulation of cardiomyocyte growth and that the deficiency in one of

these isoforms cannot be compensated by other p38 MAPKs. Interestingly, p38γ and p38δ interact in the heart and this interaction seems to be necessary for the regulation of Deptor degradation. This explains why the loss of only one of these kinases produces the defect in cardiac growth. We have shown that p38γ interaction with Deptor occurs through its PDZ domain, but we do not know how p38δ interacts with Deptor. Something surprising is the stronger phenotype observed in p38δ deficient mice compared to those that lack p38γ, despite the fact p38γ interaction with Deptor is stronger, and both isoforms phosphorylate key residues involved in Deptor degradation. This could be due to the regulation of an additional substrate for p38δ involved in cardiac growth different from Deptor, or due to a role of p38δ in other cell types that contribute to regulate cardiomyocyte hypertrophy. To rule out this possibility the postnatal cardiac phenotype should be studied in cardiomyocyte-specific conditional knockout mice for p38γ and p38δ. Although p38α homodimers have been described, to date this is the first report of interaction in between different p38 isoforms to cooperate in substrate phosphorylation. It remains to be clarified whether p38γ and p38δ are acting in the heart as a heterodimer and whether this interaction occurs in other tissues.

In contrast with the MKK3 and MKK6 partial redundancy observed in the LPS-induced acute inflammatory model, in the cardiac tissue these MKKs have divergent roles in the control of heart growth. On the one hand MKK6 deficiency leads to the hyperactivation of MKK3 and the subsequent p38γ and p38δ hyperphosphorylation. However, p38α phosphorylation was strongly reduced. On the other hand, MKK3 deficiency leads to a reduction in p38γ and p38δ phosphorylation, but p38α phosphorylation is not affected. Besides, in agreement with the role of p38γ and p38δ in the promotion of hypertrophic growth, *Mkk3*$^{-/-}$ mice have a reduced heart size and *Mkk6*$^{-/-}$ hearts are bigger than control hearts. This suggests that MKK6 mainly activates cardiac p38α, whereas MKK3 is the main activator of cardiac p38γ and p38δ in postnatal cardiac homeostasis. Besides, the presence of a negative feedback from MKK6 to up-stream activators or to MKK3, could explain the hyperactivation of MKK3 observed in the absence of MKK6. Although the cardiac specific conditional knockout for p38α does not develop a hypertrophic heart as the *Mkk6*$^{-/-}$ mouse model, there is the possibility that in *Mkk6*$^{-/-}$ hearts the reduction of p38α activation could account for the MKK3 hyperactivation. This negative feedback it has been described before at the level of TAK1 activation [30]. The absence of a hypertrophic phenotype in p38α conditional mice could be due to

compensatory changes in the expression/activation of other p38 isoforms. More experiments need to be done to clarify this question.

The heart is one of the organs whose size is essential to maintain body homeostasis. A proper cardiac growth is necessary during development to meet the demand of blood flow to the growing body and organs, but also throughout life to be able to respond to changes in the patterns of blood pressure and circulatory resistance. Cardiomyocytes withdraw from the cell cycle soon after birth and postnatal cardiac increase in size in through hypertrophic growth. There are physiological hypertrophy and pathological hypertrophy of the heart. The physiological hypertrophy is considered as an adaptive response, which is accompanied by an adjustment of the cardiac function with an increased demand of cardiac output. Such an adaptive hypertrophy is observed in the increase in cardiac mass after birth and in response to exercise. It is characterized by the absence of fibrosis and leads to enhance contractility and cardiac output. In response to pathological stresses (toxins, hypertension, etc.), the heart also often increases its mass, which was viewed in the past as an adaptive response as well. However, cumulative evidence obtained from studies using more advanced technologies in human patients and animal models suggests that cardiac hypertrophy is a maladaptive process of the heart in response to intrinsic and extrinsic stresses. Although toxic stress-induced hypertrophy can normalize wall tension, it is a risk factor for malignant arrhythmia and cardiac sudden death. The lack of p38γ and p38δ leads to decrease hypertrophic growth during postnatal development, but also in response to hypertension caused by angiotensin-II treatment due to reduced mTOR activation, indicating that these kinases are involved in the control of physiologic and pathologic cardiac hypertrophy. This correlates with the finding that the PI3K pathway, which also controls mTOR activation through AKT, is also activated in both physiological and pathological hypertrophy. Furthermore, the insulin-like growth factor (IGF) that signals through PI3K, is involved in the growth of the heart after birth [152] and its overexpression induces cardiac hypertrophy [46]. IGF-I expression is sufficient to initially induce an analog of physiological cardiac hypertrophy; however, this hypertrophy progresses to a pathological condition characterized by decreased systolic performance and increased fibrosis. Likewise, the hyperactivation of endogenous p38γ and p38δ in MKK6 deficient hearts leads to the development of physiological cardiac hypertrophy, with increased cardiac output and no fibrosis development. However, when challenged with

endurance exercise training, these mice show increase sudden death probably associated to the prolongation of the QT interval and increase arrhythmias. Alterations in the function of cardiac channels or "cardiac channelopathies" occur at the cellular level in cardiac hypertrophy [88]. In correlation with this observation, MKK6 deficient mice present at baseline alter expression of different ion channels that have been previously associated with prolongation of the QT interval. However, the long QT and the arrhythmias do only appear after the heart is challenged. At baseline these alterations are no pathological, whereas with endurance training, *Mkk6*$^{-/-}$ hearts become even more hypertrophic but without fibrosis development leading to an increase rate of sudden death in these mice. Suggesting that the increase susceptibility to arrhythmias and the prolongation of the QT interval is not due to fibrosis development, but maybe due to the further increase in cardiac mass. The increase in cardiac mass induced by endurance training is very similar in both genotypes, which could indicate that endurance training is activating signaling pathways independent of p38γ and p38δ activation. It would be of interest to treat *Mkk6*$^{-/-}$ mice with stimuli that induce pathological hypertrophy, such as angiotensin-II, to study whether their hearts become further hypertrophic and if it also leads to increased sudden cardiac death susceptibility. Likewise, challenging mice deficient in p38γ and p38δ with endurance training could add significant knowledge to the signaling pathways involved in cadiac hypertrophy.

In general, these outcomes suggest that even a hypertrophic heart that seems to be physiological and with improve cardiac function could present a higher predisposition for malignant arrhythmia and cardiac sudden death when challenged. It could be hypothesized that those people who have an increased heart mass with better cardiac function due to genetic causes, could be predispose to become elite athletes. It would be of interest to study whether mutations in the MKK3/6-p38γ and p38δ pathway are enriched in this population, and whether they are associated with increased risk of arrhythmias and sudden death.

A distinction between adaptive and maladaptive hypertrophy is whether the hypertrophy is necessary for the compensatory function of the heart under physiological and pathological stress conditions. Several studies and our own work agree with the idea that cardiac hypertrophy is neither required nor necessarily compensatory in response to pathological stimuli. Mice lacking p38γ and p38δ do not develop cardiac hypertrophy in response to the hypertension induced by angiotensin-II treatment. The elimination of

hypertrophy in these animals did not cause compromised hemodynamic changes through an observation of over a period of several weeks. Similar results were obtained by forced expression of a dominant negative calcineurin mutant or by calcineurin suppression in an aortic constriction model [80, 193]. Interestingly, the absence of a hypertrophic cardiac response to aortic banding in a transgenic mouse model was accompanied by a significant slower pace of deterioration of systolic function [56]. All this suggests that cardiac hypertrophy in response to extrinsic and intrinsic stresses is not a compensatory response. It would be interesting to study whether the lack of p38γ and p38δ abolishes the hypertrophic growth induced by endurance training as well as if the lack of this hypertrophic response leads to cardiac failure. Furthermore, it remains to be addressed whether the cardiac phenotype observed in MKK6 deficient mice is only due to the lack of this kinase in cardiomyocytes or is also mediated by other cell types. Mice deficient in MKK6 specifically in striated muscle or in cardiomyocytes develop cardiac hypertrophy, although the hypertrophy is milder that the one observed in the whole body knockout mice. Moreover, the depletion of p38δ in striated muscle is enough to revert *Mkk6*$^{-/-}$ hypertrophic phenotype. Altogether suggests that at least part of the phenotype is cell autonomous. Nevertheless, the endurance training experiment should be performed in the cardiac-specific MKK6 conditional knockout to verify that the increased sudden death is due to the lack of this kinase in the heart.

Although hypertrophic growth is very important in cardiomyocytes, it also occurs in other cell types. Interestingly, immortalized mouse embryonic fibroblasts (MEFs) from *Mkk3*$^{-/-}$ mice or *Mapk12*$^{-/-}$ and *Mapk13*$^{-/-}$ mice are significantly smaller than control MEFs, whereas the deficiency in MKK6 leads to a bigger cell size. This seems to correlate with the activation status of p38γ and p38δ and mTOR pathway, indicating that p38γ and p38δ may be regulating hypertrophic growth through the regulation of mTOR pathway activation in other cell types different from cardiomyocytes.

With the increased understanding of the p38 MAPK pathway, its potential as therapeutic targets for different diseases is growing very fast during the last years. For a long time it has been known that p38α is a key component in the regulation of inflammatory mediators such as TNFα, IL-1b, IL-6 or IL-8, which are commonly implicated in the detrimental inflammatory pathogenesis of different disease models. Furthermore, in cardiovascular diseases, inflammation constitutes a key factor involved in the pathogenesis of the disease. In addition, p38α is activated in the heart upon

ischemia/ reperfusion injury and its inhibition in animal models reduces the infraction size. Several promising p38α inhibitors have progressed into clinical trials for the treatment of rheumatoid arthritis, psoriasis, Chron's disease, cancer, COPD, multiple myeloma and cardiovascular disease. However, a great number have been withdrawn due to safety issues, being hepatotoxicity the most common. This hepatotoxicity also occurs in mice as observed with the SB203580 treatment in the LPS-induced acute hepatitis model. Almost all of p38α inhibitors are ATP competitors, generated by structural modifications of the first generation of pyrinidyl imidazoles. In this regard, new strategies for the inhibition of p38α should be designed with less likelihood to cross-react with other kinases or other cellular signaling molecules than ATP competitors.

Recent results from our group and others indicate that p38γ and p38δ could be alternative targets for the treatment of inflammatory diseases and cardiovascular diseases. These kinases are also key regulators of cytokine production by macrophages and monocytes in inflammatory responses, as well as very important molecules in the regulation of neutrophil migration. Two myeloid populations involved in the pathogenesis of most of the chronic inflammatory diseases. Accordingly, it has been reported recently that *Mapk12*$^{-/-}$*Mapk13*$^{-/-}$ double knockout mice are protected against rheumatoid arthritis, acute lung injury, skin inflammation and carcinogenesis [35, 45, 81]. Besides, the blockage of neutrophil infiltration in the liver by p38γ and p38δ could protect against non-alcoholic fatty liver disease (NAFLD) a very frequent disease nowadays in developed countries, associated with obesity and insulin resistance. Moreover, our results show that p38γ and p38δ could be attractive pharmacological targets for the treatment of cardiac hypertrophy. However, selective small compound inhibitors for p38γ and p38δ isoforms are not currently available. There is one compound, BIRB796, which has a pan-isoform inhibitory activity. Although we do not observe hepatic toxicity with BIRB796 treatment in a mouse model of acute hepatitis, Boehringer Ingelheim completed phase II clinical studies in rheumatoid arthritis, Chron's disease and psoriasis with this inhibitor, and stopped developing this drug due to liver enzyme elevations. The only p38γ inhibitor approved by the FDA and the European Drug Agency is Pirfenidone (*Esbriet*) for the treatment of pulmonary idiopathic fibrosis. The recent discoveries suggest that p38γ and p38δ are also involved

in the development and progression of different human diseases and that a greater focus should be put on the generation of selective and potent p38γ and p38δ inhibitors.

As all the p38 isoforms, but p38β, have been involved in the regulation of inflammatory responses, one thing that we still don't know is whether the inhibition of a single specific isoform will be more effective than to inhibit more than one at the same time. One alternative could be to use MKK3 and MKK6 inhibitors that disrupt the formation of the complex between p38 and the MKKs. It has been shown that cAMP, through dinein light chain (DLC) inhibits the p38 MAPK activation using this mechanism. Thus, small molecules that mimic this inhibition might serve as new inhibitors of the p38 MAPK pathway. Nevertheless, p38 associated toxicities are more likely to occur with this strategy. To avoid them, an option would be to target only one upstream MKK, but more information about their functional differences and contributions in each tissue should be generated in order to be able to decide which MKK should be target in the different diseases. Likewise, it is important to study the expression pattern of the different p38 isoforms in a cell specific manner, as well as to define the particularities in the regulation of endogenous p38 MAPK isoforms in the different tissues.

CONCLUSIONES/ CONCLUSIONS

- p38γ y p38δ presentan un patrón de expresión muy característico en células mieloides. Los neutrófilos expresan altos niveles de p38δ, las células de kupffer altos niveles de p38γ. Sin embargo, los macrófagos y monocitos expresan niveles bajos de ambas isoformas.

- La vía de señalización MKK3/6- p38γ/δ en células mieloides es esencial para la progresión del daño hepático y la hepatitis aguda en respuesta a LPS. Específicamente, p38γ y p38δ regulan la producción de TNFα en macrófagos y células de kuppfer a nivel de la elongación proteica, a través de la fosforilación inhibitoria de eEF2K y la subsecuente activación de eEF2.

- En un modelo de ratón el silenciamiento de eEF2 reduce el daño hepático y retrasa significativamente la muerte por hepatitis aguda inducida por LPS, indicando que eEF2 es una potencial diana teraéutica para el tratamiento de esta enfermedad.

- p38γ y p38δ juegan un papel clave en el desarrollo de esteatosis hepática. Ratones deficientes en p38γ y p38δ en células mieloides están protegidos frente al desarrollo de esteatosis inducida por 3 modelos diferentes de ratón, la inducida por las dietas MCD, HFD y HFF. Además, la expresión de p38γ y p38δ aumenta en el hígado de pacientes con esteatosis hepática. De esta forma la inhibición de p38γ y p38δ en células mieloides contituye un potencial tratamiento frente a la esteatosis hepática.

- La infiltración neutrófilos en el hígado es un factor determinante en el inicio y desarrollo de la esteatosis hepática. Ratones deficientes en p38γ y p38δ en células mieloides están protegidos frente al desarrollo de esteatosis debido a una migración defectuosa de los neutrófilos hacia los hígados de dichos ratones. Además, modelos de ratones neutropénicos o la depleción de neutrófilos en ratones control, protegen frente a la esteatosis hepática inducida por la dieta MCD. Esto se debe a que los neutrófilos alteran el metabolismo hepático.

- Ambas quinasas, p38γ y p38δ se expresan en el corazón. Tanto su expresión como activación incrementan durante las etapas tempranas del desarrollo postnatal cardiaco.

- p38γ y p38δ en cardiomiocitos regulan el crecimiento hipertrófico tanto fisiológico postnatal como el inducido por sobrecarga del corazón causada por el tratamiento con angiotensina-II. Esta regulación la realizan a través de la fosforilación de la proteína inhibidora de mTOR, DEPTOR, que resulta en su degradación y en la subsecuente activación de la vía de mTOR, inducción de la síntesis proteica y del crecimiento celular.

- MKK3 y MKK6 son selectivas a la hora de activar las diferentes isoformas de p38MAPKs. En el corazón, MKK3 es esencial para la activación de p38γ y p38δ, mientras que MKK6 es necesaria para la activación de p38α.

- La falta de activación de MKK6-p38α lleva a la hiperactivación de MKK3-p38γ/δ y al desarrollo de hipertrofia cardiaca de tipo fisiológico. Mientras que el déficit en MKK3 lleva a un crecimiento cardiaco postnatal reducido. Ambos fenotipos son debido a alteraciones en la activación de p38γ y p38δ.

- Corazones deficientes en MKK6 muestran una expresión alterada de varios canales iónicos cardiacos, sin embargo su función cardiaca es normal o incluso mejor que ratones control en condiciones basales. Sin embargo, el entrenamiento de resistencia en ratones *Mkk6*$^{-/-}$ lleva a una bradicardia más pronunciada y una prolongación del intervalo QT mayor que en los ratones control. Esto resulta en un índice incrementado de muerte súbita cardiaca.

- p38γ and p38δ expression pattern in myeloid cells is very characteristic. Neutrophils express high levels of p38δ, kupffer cells high levels of p38γ, while macrophages and monocytes express both isoforms at low levels.

- MKK3/6-p38γ/δ signaling in myeloid cells is necessary for LPS-induced liver damage. Specifically, p38γ and p38δ in macrophages/kupffer cells regulate TNFα protein elongation through the inhibitory phosphorylation of EF2K, and the subsequent activation of eEF2.

- eEF2 silencing in an *in vivo* model protects against LPS-induced hepatitis, indicating that eEF2 is a potencial therapeutic target for acute hepatitis treatment.

- p38γ and p38δ play a key role in steatosis development. Mice lacking p38γ and p38δ in myeloid cells are protected against 3 different mouse models of diet induced steatosis and liver damage. Beides, p38γ and p38δ expression is up regulated in livers from patients with NAFLD. Therefore, p38γ and p38δ in myeloid cells are potencial therapeutic targets for the treatment of NAFLD.

- Neutrophil liver infiltration is determinant in the pathogenesis of liver steatosis. Mice lacking p38γ and p38δ in myeloid cells are protected against steatosis due to a defective migration and infiltration of *Mapk12*$^{-/-}$*Mapk13*$^{-/-}$ or *Mapk13*$^{-/-}$ neutrophils in the livers of these mice. Moreover, neutropenic mice or neutrophil depletion models protect against MCD-induced steatosis and liver damage. This is due to the fact that neutrophils alter liver metabolism.

- Both isoforms p38γ and p38δ are expressed in the heart, and their expression and activation increases during the early postnatal cardiac development.

- p38γ and p38δ in cardiomyocytes control cardiac physiological and pathological hypertrophic growth through the phosphorylation and subsequent degradation of DEPTOR, an inhibitory protein of mTOR pathway, which leads to mTOR activation, protein synthesis induction and promotion of cell growth.

- The up-stream MAP2Ks of the p38 pathway show selectivity in the activation of the different p38 isoforms in the heart. MKK3 is essential for p38γ and p38δ activation, whereas MKK6 is necessary for p38α activation.

- The deficiency in MKK6-p38α activation leads to the hyperactivation of MKK3-p38γ/δ in cardiac tissue and to the development of physiological cardiac hypertrophy. In contrast, the lack of MKK3 leads to a defective activation of the p38γ and p38δ isoforms associated with a decreased postnatal cardiac hypetrophic growth.

- Although *Mkk6*$^{-/-}$ mice show altered expression levels of different cardiac ion channels, in basal condition their cardiac function is normal or even improved. However, upon endurance exercise chronic training, *Mkk6*$^{-/-}$ mice develop longer QT intervals and show increased susceptibility to sudden cardiac death.

REFERENCES

1. Adams, R.H., et al., *Essential role of p38alpha MAP kinase in placental but not embryonic cardiovascular development.* Mol Cell, 2000. **6**(1): p. 109-16.
2. Adhikary, L., et al., *Abnormal p38 mitogen-activated protein kinase signalling in human and experimental diabetic nephropathy.* Diabetologia, 2004. **47**(7): p. 1210-22.
3. Alevy, Y.G., et al., *IL-13-induced airway mucus production is attenuated by MAPK13 inhibition.* J Clin Invest, 2012. **122**(12): p. 4555-68.
4. Amirouche, A., et al., *Activation of p38 signaling increases utrophin A expression in skeletal muscle via the RNA-binding protein KSRP and inhibition of AU-rich element-mediated mRNA decay: implications for novel DMD therapeutics.* Hum Mol Genet, 2013. **22**(15): p. 3093-111.
5. Aouadi, M., et al., *p38 mitogen-activated protein kinase activity commits embryonic stem cells to either neurogenesis or cardiomyogenesis.* Stem Cells, 2006. **24**(5): p. 1399-406.
6. Arthur, J.S. and S.C. Ley, *Mitogen-activated protein kinases in innate immunity.* Nat Rev Immunol, 2013. **13**(9): p. 679-92.
7. Askari, N., et al., *Hyperactive variants of p38alpha induce, whereas hyperactive variants of p38gamma suppress, activating protein 1-mediated transcription.* J Biol Chem, 2007. **282**(1): p. 91-9.
8. Attwood, P.V. and T. Wieland, *Nucleoside diphosphate kinase as protein histidine kinase.* Naunyn Schmiedebergs Arch Pharmacol, 2015. **388**(2): p. 153-60.
9. Avitzour, M., et al., *Intrinsically active variants of all human p38 isoforms.* FEBS J, 2007. **274**(4): p. 963-75.
10. Azuma, A., et al., *Double-blind, placebo-controlled trial of pirfenidone in patients with idiopathic pulmonary fibrosis.* Am J Respir Crit Care Med, 2005. **171**(9): p. 1040-7.
11. Balasubramanian, S., T. Efimova, and R.L. Eckert, *Green tea polyphenol stimulates a Ras, MEKK1, MEK3, and p38 cascade to increase activator protein 1 factor-dependent involucrin gene expression in normal human keratinocytes.* J Biol Chem, 2002. **277**(3): p. 1828-36.
12. Bardwell, A.J., M. Abdollahi, and L. Bardwell, *Docking sites on mitogen-activated protein kinase (MAPK) kinases, MAPK phosphatases and the Elk-1 transcription factor compete for MAPK binding and are crucial for enzymic activity.* Biochem J, 2003. **370**(Pt 3): p. 1077-85.
13. Beardmore, V.A., et al., *Generation and characterization of p38beta (MAPK11) gene-targeted mice.* Mol Cell Biol, 2005. **25**(23): p. 10454-64.
14. Ben-Levy, R., et al., *Nuclear export of the stress-activated protein kinase p38 mediated by its substrate MAPKAP kinase-2.* Curr Biol, 1998. **8**(19): p. 1049-57.
15. Biondi, R.M. and A.R. Nebreda, *Signalling specificity of Ser/Thr protein kinases through docking-site-mediated interactions.* Biochem J, 2003. **372**(Pt 1): p. 1-13.
16. Bogoyevitch, M.A., et al., *Stimulation of the stress-activated mitogen-activated protein kinase subfamilies in perfused heart. p38/RK mitogen-activated protein kinases and c-Jun N-terminal kinases are activated by ischemia/reperfusion.* Circ Res, 1996. **79**(2): p. 162-73.
17. Braconi Quintaje, S. and S. Orchard, *The annotation of both human and mouse kinomes in UniProtKB/Swiss-Prot: one small step in manual annotation, one*

giant leap for full comprehension of genomes. Mol Cell Proteomics, 2008. **7**(8): p. 1409-19.
18. Bradshaw, R.A. and E.A. Dennis, *Handbook of cell signaling*. 2004, Amsterdam ; Boston: Academic Press.
19. Brancho, D., et al., *Mechanism of p38 MAP kinase activation in vivo.* Genes Dev, 2003. **17**(16): p. 1969-78.
20. Braz, J.C., et al., *Targeted inhibition of p38 MAPK promotes hypertrophic cardiomyopathy through upregulation of calcineurin-NFAT signaling.* J Clin Invest, 2003. **111**(10): p. 1475-86.
21. Brenneisen, P., et al., *Activation of p70 ribosomal protein S6 kinase is an essential step in the DNA damage-dependent signaling pathway responsible for the ultraviolet B-mediated increase in interstitial collagenase (MMP-1) and stromelysin-1 (MMP-3) protein levels in human dermal fibroblasts.* J Biol Chem, 2000. **275**(6): p. 4336-44.
22. Bruce Alberts, A.J., Julian Lewis, Martin Raff, Keith Roberts, and Peter Walter. Molecular Biology of the Cell. 2002, New york: Garland Science.
23. Caldwell, K.K., M. Sosa, and C.T. Buckley, *Identification of mitogen-activated protein kinase docking sites in enzymes that metabolize phosphatidylinositols and inositol phosphates.* Cell Commun Signal, 2006. **4**: p. 2.
24. Cargnello, M. and P.P. Roux, *Activation and function of the MAPKs and their substrates, the MAPK-activated protein kinases.* Microbiol Mol Biol Rev, 2011. **75**(1): p. 50-83.
25. Carlson, C.J., et al., *Enhanced basal activation of mitogen-activated protein kinases in adipocytes from type 2 diabetes: potential role of p38 in the downregulation of GLUT4 expression.* Diabetes, 2003. **52**(3): p. 634-41.
26. Chang, L. and M. Karin, *Mammalian MAP kinase signalling cascades.* Nature, 2001. **410**(6824): p. 37-40.
27. Chatterjee, S., et al., *Role of lactosylceramide and MAP kinase in the proliferation of proximal tubular cells in human polycystic kidney disease.* J Lipid Res, 1996. **37**(6): p. 1334-44.
28. Chen, Z., et al., *MAP kinases.* Chem Rev, 2001. **101**(8): p. 2449-76.
29. Cheng, H.C., et al., *Regulation and function of protein kinases and phosphatases.* Enzyme Res, 2011. **2011**: p. 794089.
30. Cheung, P.C., et al., *Feedback control of the protein kinase TAK1 by SAPK2a/p38alpha.* EMBO J, 2003. **22**(21): p. 5793-805.
31. Clerk, A., A. Michael, and P.H. Sugden, *Stimulation of the p38 mitogen-activated protein kinase pathway in neonatal rat ventricular myocytes by the G protein-coupled receptor agonists, endothelin-1 and phenylephrine: a role in cardiac myocyte hypertrophy?* J Cell Biol, 1998. **142**(2): p. 523-35.
32. Cohen, P., *The role of protein phosphorylation in human health and disease. The Sir Hans Krebs Medal Lecture.* Eur J Biochem, 2001. **268**(19): p. 5001-10.
33. Cook, S.A., P.H. Sugden, and A. Clerk, *Activation of c-Jun N-terminal kinases and p38-mitogen-activated protein kinases in human heart failure secondary to ischaemic heart disease.* J Mol Cell Cardiol, 1999. **31**(8): p. 1429-34.
34. Court, N.W., et al., *Cardiac expression and subcellular localization of the p38 mitogen-activated protein kinase member, stress-activated protein kinase-3 (SAPK3).* J Mol Cell Cardiol, 2002. **34**(4): p. 413-26.
35. Criado, G., et al., *Alternative p38 MAPKs are essential for collagen-induced arthritis.* Arthritis Rheumatol, 2014. **66**(5): p. 1208-17.

36. Cuadrado, A. and A.R. Nebreda, *Mechanisms and functions of p38 MAPK signalling.* Biochem J, 2010. **429**(3): p. 403-17.
37. Cuenda, A. and P. Cohen, *Stress-activated protein kinase-2/p38 and a rapamycin-sensitive pathway are required for C2C12 myogenesis.* J Biol Chem, 1999. **274**(7): p. 4341-6.
38. Cuenda, A., et al., *Activation of stress-activated protein kinase-3 (SAPK3) by cytokines and cellular stresses is mediated via SAPKK3 (MKK6); comparison of the specificities of SAPK3 and SAPK2 (RK/p38).* EMBO J, 1997. **16**(2): p. 295-305.
39. Cuenda, A. and D.S. Dorow, *Differential activation of stress-activated protein kinase kinases SKK4/MKK7 and SKK1/MKK4 by the mixed-lineage kinase-2 and mitogen-activated protein kinase kinase (MKK) kinase-1.* Biochem J, 1998. **333 (Pt 1)**: p. 11-5.
40. Cuenda, A., et al., *SB 203580 is a specific inhibitor of a MAP kinase homologue which is stimulated by cellular stresses and interleukin-1.* FEBS Lett, 1995. **364**(2): p. 229-33.
41. Cuenda, A. and S. Rousseau, *p38 MAP-kinases pathway regulation, function and role in human diseases.* Biochim Biophys Acta, 2007. **1773**(8): p. 1358-75.
42. Cully, M., et al., *A role for p38 stress-activated protein kinase in regulation of cell growth via TORC1.* Mol Cell Biol, 2010. **30**(2): p. 481-95.
43. Deak, M., et al., *Mitogen- and stress-activated protein kinase-1 (MSK1) is directly activated by MAPK and SAPK2/p38, and may mediate activation of CREB.* EMBO J, 1998. **17**(15): p. 4426-41.
44. del Barco Barrantes, I., et al., *Genetic analysis of specific and redundant roles for p38alpha and p38beta MAPKs during mouse development.* Proc Natl Acad Sci U S A, 2011. **108**(31): p. 12764-9.
45. Del Reino, P., et al., *Pro-oncogenic role of alternative p38 mitogen-activated protein kinases p38gamma and p38delta, linking inflammation and cancer in colitis-associated colon cancer.* Cancer Res, 2014. **74**(21): p. 6150-60.
46. Delaughter, M.C., et al., *Local insulin-like growth factor I expression induces physiologic, then pathologic, cardiac hypertrophy in transgenic mice.* FASEB J, 1999. **13**(14): p. 1923-9.
47. Diehl, N.L., et al., *Activation of the p38 mitogen-activated protein kinase pathway arrests cell cycle progression and differentiation of immature thymocytes in vivo.* J Exp Med, 2000. **191**(2): p. 321-34.
48. Dinasarapu, A.R., et al., *Signaling gateway molecule pages--a data model perspective.* Bioinformatics, 2011. **27**(12): p. 1736-8.
49. Dingar, D., et al., *Effect of pressure overload-induced hypertrophy on the expression and localization of p38 MAP kinase isoforms in the mouse heart.* Cell Signal, 2010. **22**(11): p. 1634-44.
50. Eckert, R.L., et al., *p38 Mitogen-activated protein kinases on the body surface--a function for p38 delta.* J Invest Dermatol, 2003. **120**(5): p. 823-8.
51. Efimova, T., A.M. Broome, and R.L. Eckert, *A regulatory role for p38 delta MAPK in keratinocyte differentiation. Evidence for p38 delta-ERK1/2 complex formation.* J Biol Chem, 2003. **278**(36): p. 34277-85.
52. Efimova, T., A.M. Broome, and R.L. Eckert, *Protein kinase Cdelta regulates keratinocyte death and survival by regulating activity and subcellular localization of a p38delta-extracellular signal-regulated kinase 1/2 complex.* Mol Cell Biol, 2004. **24**(18): p. 8167-83.

53. Engelman, J.A., M.P. Lisanti, and P.E. Scherer, *Specific inhibitors of p38 mitogen-activated protein kinase block 3T3-L1 adipogenesis.* J Biol Chem, 1998. **273**(48): p. 32111-20.
54. Enslen, H., J. Raingeaud, and R.J. Davis, *Selective activation of p38 mitogen-activated protein (MAP) kinase isoforms by the MAP kinase kinases MKK3 and MKK6.* J Biol Chem, 1998. **273**(3): p. 1741-8.
55. Eriksson, M. and S. Leppa, *Mitogen-activated protein kinases and activator protein 1 are required for proliferation and cardiomyocyte differentiation of P19 embryonal carcinoma cells.* J Biol Chem, 2002. **277**(18): p. 15992-6001.
56. Esposito, G., et al., *Genetic alterations that inhibit in vivo pressure-overload hypertrophy prevent cardiac dysfunction despite increased wall stress.* Circulation, 2002. **105**(1): p. 85-92.
57. Eyers, P.A., et al., *Conversion of SB 203580-insensitive MAP kinase family members to drug-sensitive forms by a single amino-acid substitution.* Chem Biol, 1998. **5**(6): p. 321-8.
58. Feijoo, C., et al., *Evidence that phosphorylation of the microtubule-associated protein Tau by SAPK4/p38delta at Thr50 promotes microtubule assembly.* J Cell Sci, 2005. **118**(Pt 2): p. 397-408.
59. Ferrero-Miliani, L., et al., *Chronic inflammation: importance of NOD2 and NALP3 in interleukin-1beta generation.* Clin Exp Immunol, 2007. **147**(2): p. 227-35.
60. Franklin, C.C. and A.S. Kraft, *Conditional expression of the mitogen-activated protein kinase (MAPK) phosphatase MKP-1 preferentially inhibits p38 MAPK and stress-activated protein kinase in U937 cells.* J Biol Chem, 1997. **272**(27): p. 16917-23.
61. Freshney, N.W., et al., *Interleukin-1 activates a novel protein kinase cascade that results in the phosphorylation of Hsp27.* Cell, 1994. **78**(6): p. 1039-49.
62. Gaestel, M., A. Kotlyarov, and M. Kracht, *Targeting innate immunity protein kinase signalling in inflammation.* Nat Rev Drug Discov, 2009. **8**(6): p. 480-99.
63. Galanis, A., S.H. Yang, and A.D. Sharrocks, *Selective targeting of MAPKs to the ETS domain transcription factor SAP-1.* J Biol Chem, 2001. **276**(2): p. 965-73.
64. Gao, F., et al., *p38 MAPK inhibition reduces myocardial reperfusion injury via inhibition of endothelial adhesion molecule expression and blockade of PMN accumulation.* Cardiovasc Res, 2002. **53**(2): p. 414-22.
65. Ge, B., et al., *MAPKK-independent activation of p38alpha mediated by TAB1-dependent autophosphorylation of p38alpha.* Science, 2002. **295**(5558): p. 1291-4.
66. Gerits, N., S. Kostenko, and U. Moens, *In vivo functions of mitogen-activated protein kinases: conclusions from knock-in and knock-out mice.* Transgenic Res, 2007. **16**(3): p. 281-314.
67. Gillespie, M.A., et al., *p38-{gamma}-dependent gene silencing restricts entry into the myogenic differentiation program.* J Cell Biol, 2009. **187**(7): p. 991-1005.
68. Goedert, M., et al., *Activation of the novel stress-activated protein kinase SAPK4 by cytokines and cellular stresses is mediated by SKK3 (MKK6); comparison of its substrate specificity with that of other SAP kinases.* EMBO J, 1997. **16**(12): p. 3563-71.
69. Goedert, M., et al., *Phosphorylation of microtubule-associated protein tau by stress-activated protein kinases.* FEBS Lett, 1997. **409**(1): p. 57-62.

70. Goldsmith, E.J., et al., *Substrate and docking interactions in serine/threonine protein kinases.* Chem Rev, 2007. **107**(11): p. 5065-81.
71. Gum, R.J., et al., *Acquisition of sensitivity of stress-activated protein kinases to the p38 inhibitor, SB 203580, by alteration of one or more amino acids within the ATP binding pocket.* J Biol Chem, 1998. **273**(25): p. 15605-10.
72. Gupta, J. and A.R. Nebreda, *Roles of p38alpha mitogen-activated protein kinase in mouse models of inflammatory diseases and cancer.* FEBS J, 2015. **282**(10): p. 1841-57.
73. Hale, K.K., et al., *Differential expression and activation of p38 mitogen-activated protein kinase alpha, beta, gamma, and delta in inflammatory cell lineages.* J Immunol, 1999. **162**(7): p. 4246-52.
74. Han, J., et al., *Characterization of the structure and function of a novel MAP kinase kinase (MKK6).* J Biol Chem, 1996. **271**(6): p. 2886-91.
75. Han, J. and P. Sun, *The pathways to tumor suppression via route p38.* Trends Biochem Sci, 2007. **32**(8): p. 364-71.
76. Hanks, S.K. and T. Hunter, *Protein kinases 6. The eukaryotic protein kinase superfamily: kinase (catalytic) domain structure and classification.* FASEB J, 1995. **9**(8): p. 576-96.
77. Hasegawa, M., et al., *Stress-activated protein kinase-3 interacts with the PDZ domain of alpha1-syntrophin. A mechanism for specific substrate recognition.* J Biol Chem, 1999. **274**(18): p. 12626-31.
78. Hata, K., et al., *Differential roles of Smad1 and p38 kinase in regulation of peroxisome proliferator-activating receptor gamma during bone morphogenetic protein 2-induced adipogenesis.* Mol Biol Cell, 2003. **14**(2): p. 545-55.
79. Hernandez, G., et al., *A novel cardioprotective p38-MAPK/mTOR pathway.* Exp Cell Res, 2011. **317**(20): p. 2938-49.
80. Hill, J.A., et al., *Cardiac hypertrophy is not a required compensatory response to short-term pressure overload.* Circulation, 2000. **101**(24): p. 2863-9.
81. Ittner, A., et al., *Regulation of PTEN activity by p38delta-PKD1 signaling in neutrophils confers inflammatory responses in the lung.* J Exp Med, 2012. **209**(12): p. 2229-46.
82. Jacobs, D., et al., *Multiple docking sites on substrate proteins form a modular system that mediates recognition by ERK MAP kinase.* Genes Dev, 1999. **13**(2): p. 163-75.
83. Jiang, Y., et al., *Characterization of the structure and function of a new mitogen-activated protein kinase (p38beta).* J Biol Chem, 1996. **271**(30): p. 17920-6.
84. Jiang, Y., et al., *Characterization of the structure and function of the fourth member of p38 group mitogen-activated protein kinases, p38delta.* J Biol Chem, 1997. **272**(48): p. 30122-8.
85. Jiang, Y., et al., *Structure-function studies of p38 mitogen-activated protein kinase. Loop 12 influences substrate specificity and autophosphorylation, but not upstream kinase selection.* J Biol Chem, 1997. **272**(17): p. 11096-102.
86. Johansen, C., et al., *The mitogen-activated protein kinases p38 and ERK1/2 are increased in lesional psoriatic skin.* Br J Dermatol, 2005. **152**(1): p. 37-42.
87. Junttila, M.R., S.P. Li, and J. Westermarck, *Phosphatase-mediated crosstalk between MAPK signaling pathways in the regulation of cell survival.* FASEB J, 2008. **22**(4): p. 954-65.
88. Kang, Y.J., *Cardiac hypertrophy: a risk factor for QT-prolongation and cardiac sudden death.* Toxicol Pathol, 2006. **34**(1): p. 58-66.

89. Karrasch, T., et al., *Wound-induced p38MAPK-dependent histone H3 phosphorylation correlates with increased COX-2 expression in enterocytes.* J Cell Physiol, 2006. **207**(3): p. 809-15.
90. Keesler, G.A., et al., *Purification and activation of recombinant p38 isoforms alpha, beta, gamma, and delta.* Protein Expr Purif, 1998. **14**(2): p. 221-8.
91. Kennelly, P.J. and M. Potts, *Fancy meeting you here! A fresh look at "prokaryotic" protein phosphorylation.* J Bacteriol, 1996. **178**(16): p. 4759-64.
92. Keren, A., Y. Tamir, and E. Bengal, *The p38 MAPK signaling pathway: a major regulator of skeletal muscle development.* Mol Cell Endocrinol, 2006. **252**(1-2): p. 224-30.
93. Keyse, S.M., *Protein phosphatases and the regulation of mitogen-activated protein kinase signalling.* Curr Opin Cell Biol, 2000. **12**(2): p. 186-92.
94. Kikuchi, H., et al., *Involvement of histone H3 phosphorylation through p38 MAPK pathway activation in casticin-induced cytocidal effects against the human promyelocytic cell line HL-60.* Int J Oncol, 2013. **43**(6): p. 2046-56.
95. Knebel, A., et al., *Stress-induced regulation of eukaryotic elongation factor 2 kinase by SB 203580-sensitive and -insensitive pathways.* Biochem J, 2002. **367**(Pt 2): p. 525-32.
96. Knebel, A., N. Morrice, and P. Cohen, *A novel method to identify protein kinase substrates: eEF2 kinase is phosphorylated and inhibited by SAPK4/p38delta.* EMBO J, 2001. **20**(16): p. 4360-9.
97. Koistinen, H.A., A.V. Chibalin, and J.R. Zierath, *Aberrant p38 mitogen-activated protein kinase signalling in skeletal muscle from Type 2 diabetic patients.* Diabetologia, 2003. **46**(10): p. 1324-8.
98. Kraft, C.A., T. Efimova, and R.L. Eckert, *Activation of PKCdelta and p38delta MAPK during okadaic acid dependent keratinocyte apoptosis.* Arch Dermatol Res, 2007. **299**(2): p. 71-83.
99. Kuma, Y., D.G. Campbell, and A. Cuenda, *Identification of glycogen synthase as a new substrate for stress-activated protein kinase 2b/p38beta.* Biochem J, 2004. **379**(Pt 1): p. 133-9.
100. Kumar, S., J. Boehm, and J.C. Lee, *p38 MAP kinases: key signalling molecules as therapeutic targets for inflammatory diseases.* Nat Rev Drug Discov, 2003. **2**(9): p. 717-26.
101. Lancaster, L., et al., *Safety of pirfenidone in patients with idiopathic pulmonary fibrosis: integrated analysis of cumulative data from 5 clinical trials.* BMJ Open Respir Res. **3**(1): p. e000105.
102. Landon, A.L., et al., *MNKs act as a regulatory switch for eIF4E1 and eIF4E3 driven mRNA translation in DLBCL.* Nat Commun, 2014. **5**: p. 5413.
103. Lechner, C., et al., *ERK6, a mitogen-activated protein kinase involved in C2C12 myoblast differentiation.* Proc Natl Acad Sci U S A, 1996. **93**(9): p. 4355-9.
104. Lee, J., et al., *p38 MAPK-mediated regulation of Xbp1s is crucial for glucose homeostasis.* Nat Med, 2011. **17**(10): p. 1251-60.
105. Lee, J.C., et al., *A protein kinase involved in the regulation of inflammatory cytokine biosynthesis.* Nature, 1994. **372**(6508): p. 739-46.
106. Lee, Y.W., et al., *Interleukin-4, Oxidative Stress, Vascular Inflammation and Atherosclerosis.* Biomol Ther (Seoul), 2010. **18**(2): p. 135-144.
107. Li, J., et al., *AMP-activated protein kinase activates p38 mitogen-activated protein kinase by increasing recruitment of p38 MAPK to TAB1 in the ischemic heart.* Circ Res, 2005. **97**(9): p. 872-9.

108. Li, M., J. Liu, and C. Zhang, *Evolutionary history of the vertebrate mitogen activated protein kinases family.* PLoS One, 2011. **6**(10): p. e26999.
109. Li, Y., et al., *The p38 and MK2 kinase cascade phosphorylates tuberin, the tuberous sclerosis 2 gene product, and enhances its interaction with 14-3-3.* J Biol Chem, 2003. **278**(16): p. 13663-71.
110. Li, Z., et al., *The primary structure of p38 gamma: a new member of p38 group of MAP kinases.* Biochem Biophys Res Commun, 1996. **228**(2): p. 334-40.
111. Liang, Q. and J.D. Molkentin, *Redefining the roles of p38 and JNK signaling in cardiac hypertrophy: dichotomy between cultured myocytes and animal models.* J Mol Cell Cardiol, 2003. **35**(12): p. 1385-94.
112. Lilleholt, L.L., et al., *Role of p38 mitogen-activated protein kinase isoforms in murine skin inflammation induced by 12-O-tetradecanoylphorbol 13-acetate.* Acta Derm Venereol, 2011. **91**(3): p. 271-8.
113. Lu, H.T., et al., *Defective IL-12 production in mitogen-activated protein (MAP) kinase kinase 3 (Mkk3)-deficient mice.* EMBO J, 1999. **18**(7): p. 1845-57.
114. Manieri, E. and G. Sabio, *Stress kinases in the modulation of metabolism and energy balance.* J Mol Endocrinol, 2015. **55**(2): p. R11-22.
115. Manthey, C.L., et al., *SB202190, a selective inhibitor of p38 mitogen-activated protein kinase, is a powerful regulator of LPS-induced mRNAs in monocytes.* J Leukoc Biol, 1998. **64**(3): p. 409-17.
116. Marinissen, M.J., et al., *A network of mitogen-activated protein kinases links G protein-coupled receptors to the c-jun promoter: a role for c-Jun NH2-terminal kinase, p38s, and extracellular signal-regulated kinase 5.* Mol Cell Biol, 1999. **19**(6): p. 4289-301.
117. Milanesi, L., et al., *Systematic analysis of human kinase genes: a large number of genes and alternative splicing events result in functional and structural diversity.* BMC Bioinformatics, 2005. **6 Suppl 4**: p. S20.
118. Miller, C.J. and L.A. Davidson, *The interplay between cell signalling and mechanics in developmental processes.* Nat Rev Genet, 2013. **14**(10): p. 733-44.
119. Morrison, D.K. and R.J. Davis, *Regulation of MAP kinase signaling modules by scaffold proteins in mammals.* Annu Rev Cell Dev Biol, 2003. **19**: p. 91-118.
120. Mudgett, J.S., et al., *Essential role for p38alpha mitogen-activated protein kinase in placental angiogenesis.* Proc Natl Acad Sci U S A, 2000. **97**(19): p. 10454-9.
121. Munoz, L., et al., *Novel p38 MAPK inhibitor ML3403 has potent anti-inflammatory activity in airway smooth muscle.* Eur J Pharmacol. **635**(1-3): p. 212-8.
122. Nemoto, S., Z. Sheng, and A. Lin, *Opposing effects of Jun kinase and p38 mitogen-activated protein kinases on cardiomyocyte hypertrophy.* Mol Cell Biol, 1998. **18**(6): p. 3518-26.
123. Nishida, K., et al., *p38alpha mitogen-activated protein kinase plays a critical role in cardiomyocyte survival but not in cardiac hypertrophic growth in response to pressure overload.* Mol Cell Biol, 2004. **24**(24): p. 10611-20.
124. O'Keefe, S.J., et al., *Chemical genetics define the roles of p38alpha and p38beta in acute and chronic inflammation.* J Biol Chem, 2007. **282**(48): p. 34663-71.
125. Oku, H., et al., *Antifibrotic action of pirfenidone and prednisolone: different effects on pulmonary cytokines and growth factors in bleomycin-induced murine pulmonary fibrosis.* Eur J Pharmacol, 2008. **590**(1-3): p. 400-8.
126. Pargellis, C., et al., *Inhibition of p38 MAP kinase by utilizing a novel allosteric binding site.* Nat Struct Biol, 2002. **9**(4): p. 268-72.

127. Parker, C.G., et al., *Identification of stathmin as a novel substrate for p38 delta.* Biochem Biophys Res Commun, 1998. **249**(3): p. 791-6.
128. Peng, T., et al., *JNK1/c-fos inhibits cardiomyocyte TNF-alpha expression via a negative crosstalk with ERK and p38 MAPK in endotoxaemia.* Cardiovasc Res, 2009. **81**(4): p. 733-41.
129. Perdiguero, E., et al., *Genetic analysis of p38 MAP kinases in myogenesis: fundamental role of p38alpha in abrogating myoblast proliferation.* EMBO J, 2007. **26**(5): p. 1245-56.
130. Perez Lopez, I., et al., *A-kinase anchoring protein Lbc coordinates a p38 activating signaling complex controlling compensatory cardiac hypertrophy.* Mol Cell Biol, 2013. **33**(15): p. 2903-17.
131. Pierrat, B., et al., *RSK-B, a novel ribosomal S6 kinase family member, is a CREB kinase under dominant control of p38alpha mitogen-activated protein kinase (p38alphaMAPK).* J Biol Chem, 1998. **273**(45): p. 29661-71.
132. Pietersma, A., et al., *p38 mitogen activated protein kinase regulates endothelial VCAM-1 expression at the post-transcriptional level.* Biochem Biophys Res Commun, 1997. **230**(1): p. 44-8.
133. Pogozelski, A.R., et al., *p38gamma mitogen-activated protein kinase is a key regulator in skeletal muscle metabolic adaptation in mice.* PLoS One, 2009. **4**(11): p. e7934.
134. Popowski, M., et al., *Stress and IGF-I differentially control cell fate through mammalian target of rapamycin (mTOR) and retinoblastoma protein (pRB).* J Biol Chem, 2008. **283**(42): p. 28265-73.
135. Raingeaud, J., et al., *Pro-inflammatory cytokines and environmental stress cause p38 mitogen-activated protein kinase activation by dual phosphorylation on tyrosine and threonine.* J Biol Chem, 1995. **270**(13): p. 7420-6.
136. Remy, G., et al., *Differential activation of p38MAPK isoforms by MKK6 and MKK3.* Cell Signal, 2010. **22**(4): p. 660-7.
137. Risco, A. and A. Cuenda, *New Insights into the p38gamma and p38delta MAPK Pathways.* J Signal Transduct, 2012. **2012**: p. 520289.
138. Risco, A., et al., *p38gamma and p38delta kinases regulate the Toll-like receptor 4 (TLR4)-induced cytokine production by controlling ERK1/2 protein kinase pathway activation.* Proc Natl Acad Sci U S A, 2012. **109**(28): p. 11200-5.
139. Rose, B.A., T. Force, and Y. Wang, *Mitogen-activated protein kinase signaling in the heart: angels versus demons in a heart-breaking tale.* Physiol Rev, 2010. **90**(4): p. 1507-46.
140. Rothweiler, U., et al., *p38alpha MAP kinase dimers with swapped activation segments and a novel catalytic loop conformation.* J Mol Biol, 2011. **411**(2): p. 474-85.
141. Rouse, J., et al., *A novel kinase cascade triggered by stress and heat shock that stimulates MAPKAP kinase-2 and phosphorylation of the small heat shock proteins.* Cell, 1994. **78**(6): p. 1027-37.
142. Roux, P.P. and J. Blenis, *ERK and p38 MAPK-activated protein kinases: a family of protein kinases with diverse biological functions.* Microbiol Mol Biol Rev, 2004. **68**(2): p. 320-44.
143. Sabio, G., et al., *p38gamma regulates the localisation of SAP97 in the cytoskeleton by modulating its interaction with GKAP.* EMBO J, 2005. **24**(6): p. 1134-45.
144. Sabio, G. and R.J. Davis, *TNF and MAP kinase signalling pathways.* Semin Immunol, 2014. **26**(3): p. 237-45.

145. Sabio, G., et al., *Stress- and mitogen-induced phosphorylation of the synapse-associated protein SAP90/PSD-95 by activation of SAPK3/p38gamma and ERK1/ERK2.* Biochem J, 2004. **380**(Pt 1): p. 19-30.
146. Salvador, J.M., et al., *Alternative p38 activation pathway mediated by T cell receptor-proximal tyrosine kinases.* Nat Immunol, 2005. **6**(4): p. 390-5.
147. Schoorlemmer, J. and M. Goldfarb, *Fibroblast growth factor homologous factors are intracellular signaling proteins.* Curr Biol, 2001. **11**(10): p. 793-7.
148. Schoorlemmer, J. and M. Goldfarb, *Fibroblast growth factor homologous factors and the islet brain-2 scaffold protein regulate activation of a stress-activated protein kinase.* J Biol Chem, 2002. **277**(51): p. 49111-9.
149. Seidel, J.J. and B.J. Graves, *An ERK2 docking site in the Pointed domain distinguishes a subset of ETS transcription factors.* Genes Dev, 2002. **16**(1): p. 127-37.
150. Sheridan, D.L., et al., *Substrate discrimination among mitogen-activated protein kinases through distinct docking sequence motifs.* J Biol Chem, 2008. **283**(28): p. 19511-20.
151. Shi, Y. and M. Gaestel, *In the cellular garden of forking paths: how p38 MAPKs signal for downstream assistance.* Biol Chem, 2002. **383**(10): p. 1519-36.
152. Shioi, T., et al., *Akt/protein kinase B promotes organ growth in transgenic mice.* Mol Cell Biol, 2002. **22**(8): p. 2799-809.
153. Solinas, G., et al., *JNK1 in hematopoietically derived cells contributes to diet-induced inflammation and insulin resistance without affecting obesity.* Cell Metab, 2007. **6**(5): p. 386-97.
154. Sorensen, V., et al., *Phosphorylation of fibroblast growth factor (FGF) receptor 1 at Ser777 by p38 mitogen-activated protein kinase regulates translocation of exogenous FGF1 to the cytosol and nucleus.* Mol Cell Biol, 2008. **28**(12): p. 4129-41.
155. Stepniak, E., et al., *c-Jun/AP-1 controls liver regeneration by repressing p53/p21 and p38 MAPK activity.* Genes Dev, 2006. **20**(16): p. 2306-14.
156. Sumara, G., et al., *Regulation of PKD by the MAPK p38delta in insulin secretion and glucose homeostasis.* Cell, 2009. **136**(2): p. 235-48.
157. Swanson, R.V., L.A. Alex, and M.I. Simon, *Histidine and aspartate phosphorylation: two-component systems and the limits of homology.* Trends Biochem Sci, 1994. **19**(11): p. 485-90.
158. Takekawa, M., et al., *p53-inducible wip1 phosphatase mediates a negative feedback regulation of p38 MAPK-p53 signaling in response to UV radiation.* EMBO J, 2000. **19**(23): p. 6517-26.
159. Takekawa, M., T. Maeda, and H. Saito, *Protein phosphatase 2Calpha inhibits the human stress-responsive p38 and JNK MAPK pathways.* EMBO J, 1998. **17**(16): p. 4744-52.
160. Tanaka, N., et al., *Differential involvement of p38 mitogen-activated protein kinase kinases MKK3 and MKK6 in T-cell apoptosis.* EMBO Rep, 2002. **3**(8): p. 785-91.
161. Tanno, M., et al., *Diverse mechanisms of myocardial p38 mitogen-activated protein kinase activation: evidence for MKK-independent activation by a TAB1-associated mechanism contributing to injury during myocardial ischemia.* Circ Res, 2003. **93**(3): p. 254-61.
162. Tanoue, T. and E. Nishida, *Molecular recognitions in the MAP kinase cascades.* Cell Signal, 2003. **15**(5): p. 455-62.

163. Taylor, S.S., et al., *Evolution of the eukaryotic protein kinases as dynamic molecular switches.* Philos Trans R Soc Lond B Biol Sci, 2012. **367**(1602): p. 2517-28.
164. Tong, L., et al., *A highly specific inhibitor of human p38 MAP kinase binds in the ATP pocket.* Nat Struct Biol, 1997. **4**(4): p. 311-6.
165. Tortorella, L.L., C.B. Lin, and P.F. Pilch, *ERK6 is expressed in a developmentally regulated manner in rodent skeletal muscle.* Biochem Biophys Res Commun, 2003. **306**(1): p. 163-8.
166. Uhlen, M., et al., *Proteomics. Tissue-based map of the human proteome.* Science, 2015. **347**(6220): p. 1260419.
167. Vlahopoulos, S.A., et al., *Dynamic aberrant NF-kappaB spurs tumorigenesis: a new model encompassing the microenvironment.* Cytokine Growth Factor Rev, 2015. **26**(4): p. 389-403.
168. Wang, K., S.I. Grivennikov, and M. Karin, *Implications of anti-cytokine therapy in colorectal cancer and autoimmune diseases.* Ann Rheum Dis, 2013. **72 Suppl 2**: p. ii100-3.
169. Wang, L., et al., *Requirement of mitogen-activated protein kinase kinase 3 (MKK3) for activation of p38alpha and p38delta MAPK isoforms by TGF-beta 1 in murine mesangial cells.* J Biol Chem, 2002. **277**(49): p. 47257-62.
170. Wang, X.S., et al., *Molecular cloning and characterization of a novel p38 mitogen-activated protein kinase.* J Biol Chem, 1997. **272**(38): p. 23668-74.
171. Wang, Y., et al., *Cardiac muscle cell hypertrophy and apoptosis induced by distinct members of the p38 mitogen-activated protein kinase family.* J Biol Chem, 1998. **273**(4): p. 2161-8.
172. Wang, Y., et al., *Cardiac hypertrophy induced by mitogen-activated protein kinase kinase 7, a specific activator for c-Jun NH2-terminal kinase in ventricular muscle cells.* J Biol Chem, 1998. **273**(10): p. 5423-6.
173. Wang, Z., et al., *Structural basis of inhibitor selectivity in MAP kinases.* Structure, 1998. **6**(9): p. 1117-28.
174. Wang, Z., et al., *The structure of mitogen-activated protein kinase p38 at 2.1-A resolution.* Proc Natl Acad Sci U S A, 1997. **94**(6): p. 2327-32.
175. Wilson, K.P., et al., *Crystal structure of p38 mitogen-activated protein kinase.* J Biol Chem, 1996. **271**(44): p. 27696-700.
176. Wilson, K.P., et al., *The structural basis for the specificity of pyridinylimidazole inhibitors of p38 MAP kinase.* Chem Biol, 1997. **4**(6): p. 423-31.
177. Wood, C.D., et al., *Nuclear localization of p38 MAPK in response to DNA damage.* Int J Biol Sci, 2009. **5**(5): p. 428-37.
178. Wu, Z., et al., *p38 and extracellular signal-regulated kinases regulate the myogenic program at multiple steps.* Mol Cell Biol, 2000. **20**(11): p. 3951-64.
179. Wysk, M., et al., *Requirement of mitogen-activated protein kinase kinase 3 (MKK3) for tumor necrosis factor-induced cytokine expression.* Proc Natl Acad Sci U S A, 1999. **96**(7): p. 3763-8.
180. Wyss-Coray, T. and J. Rogers, *Inflammation in Alzheimer disease-a brief review of the basic science and clinical literature.* Cold Spring Harb Perspect Med. **2**(1): p. a006346.
181. Xiao, Y., et al., *Dynamics of protein kinases: insights from nuclear magnetic resonance.* Acc Chem Res, 2015. **48**(4): p. 1106-14.
182. Xu, P. and R. Derynck, *Direct activation of TACE-mediated ectodomain shedding by p38 MAP kinase regulates EGF receptor-dependent cell proliferation.* Mol Cell, 2014. **37**(4): p. 551-66.

183. Yang, M. and C.Z. Huang, *Mitogen-activated protein kinase signaling pathway and invasion and metastasis of gastric cancer.* World J Gastroenterol, 2015. **21**(41): p. 11673-9.
184. Yang, S.H., A. Galanis, and A.D. Sharrocks, *Targeting of p38 mitogen-activated protein kinases to MEF2 transcription factors.* Mol Cell Biol, 1999. **19**(6): p. 4028-38.
185. Yang, S.H., et al., *Differential targeting of MAP kinases to the ETS-domain transcription factor Elk-1.* EMBO J, 1998. **17**(6): p. 1740-9.
186. Yang, S.H., et al., *The Elk-1 ETS-domain transcription factor contains a mitogen-activated protein kinase targeting motif.* Mol Cell Biol, 1998. **18**(2): p. 710-20.
187. Yin, Y., et al., *PAC1 phosphatase is a transcription target of p53 in signalling apoptosis and growth suppression.* Nature, 2003. **422**(6931): p. 527-31.
188. Yoshida, H. and M. Goedert, *Sequential phosphorylation of tau protein by cAMP-dependent protein kinase and SAPK4/p38delta or JNK2 in the presence of heparin generates the AT100 epitope.* J Neurochem, 2006. **99**(1): p. 154-64.
189. Young, P.R., et al., *Pyridinyl imidazole inhibitors of p38 mitogen-activated protein kinase bind in the ATP site.* J Biol Chem, 1997. **272**(18): p. 12116-21.
190. Yurtsever, Z., et al., *The crystal structure of phosphorylated MAPK13 reveals common structural features and differences in p38 MAPK family activation.* Acta Crystallogr D Biol Crystallogr, 2015. **71**(Pt 4): p. 790-9.
191. Zechner, D., et al., *A role for the p38 mitogen-activated protein kinase pathway in myocardial cell growth, sarcomeric organization, and cardiac-specific gene expression.* J Cell Biol, 1997. **139**(1): p. 115-27.
192. Zhang, Y., et al., *Signal transduction pathways involved in phosphorylation and activation of p70S6K following exposure to UVA irradiation.* J Biol Chem, 2001. **276**(24): p. 20913-23.
193. Zou, Y., et al., *Calcineurin plays a critical role in the development of pressure overload-induced cardiac hypertrophy.* Circulation, 2001. **104**(1): p. 97-101.
194. Zur, R., et al., *Combined deletion of p38gamma and p38delta reduces skin inflammation and protects from carcinogenesis.* Oncotarget, 2015. **6**(15): p. 12920-35.